Technical Report
TR-23-10
March 2023

Post-closure safety for SFR, the final repository for short-lived radioactive waste at Forsmark

Data report, PSAR version

SVENSK KÄRNBRÄNSLEHANTERING AB

SWEDISH NUCLEAR FUEL
AND WASTE MANAGEMENT CO

Box 3091, SE-169 03 Solna
Phone +46 8 459 84 00
skb.se

ISSN 1404-0344
SKB TR-23-10
ID 1677462
March 2023

Post-closure safety for SFR, the final repository for short-lived radioactive waste at Forsmark

Data report, PSAR version

Svensk Kärnbränslehantering AB

Keywords: Post-closure safety, SFR, Final repository, Low- and intermediate-level radioactive waste, Forsmark, Safety assessment, Short-lived, Data, Parameters, Evaluation, Qualification, Quality assurance.

This report is published on www.skb.se

Summary

The final repository for short-lived radioactive waste (SFR) at Forsmark, Sweden is used for the final disposal of low- and intermediate-level operational waste from Swedish nuclear facilities. The PSAR assessment of post-closure safety is an important part of the construction license application for the extension of SFR. This report constitutes one of the main references supporting the **Post-closure safety report**.

This report presents, motivates and qualifies essential data for the post-closure safety assessment PSAR for the SFR repository. This is done using a quality assurance (QA) method created for assessing post-closure safety assessment data. Large amounts of data have been used in the safety assessment to calculate and assess the system. Therefore, the data presented here limits itself to those data connected to the safety functions.

The data presented in this report had to be qualified and motivated from several perspectives such as if there are conceptual uncertainties, spatial or temporal variabilities, or if the data differ drastically from data used for the same purpose in previous safety assessments. The general objective of this report is to present data that are fit to use in a post-closure safety assessment, with of all the possible uncertainties considered.

Sammanfattning

Slutförvaret för kortlivat radioaktivt avfall (SFR) i Forsmark, Sverige används för slutförvaring av låg- och medelaktivt driftavfall från svenska kärntekniska anläggningar. Analysen av säkerhet efter förslutning i PSAR är en viktig del av ansökan om medgivande för utbyggnaden av SFR. Denna rapport utgör en av huvudreferenserna till **Huvudrapporten säkerhet efter förslutning.**

Denna rapport motiverar och kvalificerar viktiga data för analysen av säkerheten efter förslutning för slutförvaret SFR. Detta görs med hjälp av en kvalitetssäkringsmetod (QA) som skapats för att bedöma data till säkerhetsanalyser. Stora mängder data har använts i säkerhetsanalysen för att beräkna och utvärdera systemet. Data som presenteras här begränsar sig till data som kopplar till säkerhetsfunktionerna.

De data som presenteras i denna rapport har kvalificerats och motiverats ur flera perspektiv såsom om det finns konceptuella osäkerheter, rumslig eller tidsmässig variabilitet, eller om uppgifterna skiljer sig avsevärt från data som används för samma ändamål i tidigare säkerhetsanalyser. Det övergripande målet med denna rapport är att presentera data som är lämpliga att användas i analysen av säkerheten efter förslutning med beaktade osäkerheter.

Contents

1 Introduction

This document is one of the main references to the **Post-closure safety report** that contributes to the preliminary safety analysis report (PSAR) for SFR, the repository for short-lived radioactive waste at Forsmark in Östhammar municipality, Sweden.

This chapter gives the background and a short overview of the PSAR post-closure safety assessment undertaken as part of the construction license application for the extension of SFR. Moreover, the purpose and content of this report are described.

1.1 Background

SFR is operated by the Swedish Nuclear Fuel and Waste Management Company, SKB, and is part of the Swedish system for management of waste from nuclear power plants, other nuclear activities, industry, research and medical care. In addition to SFR, the Swedish nuclear waste system also includes the repository for spent nuclear fuel and the repository for long-lived radioactive waste (SFL).

SFR consists of the existing part, SFR1 (Figure 1-1, grey part), and the extension, SFR3 (Figure 1-1, blue part). SFR1 is designed for disposal of short-lived low- and intermediate-level waste produced during operation of the Swedish nuclear power reactors, as well as waste generated during the application of radioisotopes in medicine, industry, and research. This part became operational in 1988. SFR3 is designed primarily for disposal of short-lived low- and intermediate-level waste from decommissioning of nuclear facilities in Sweden. The extension is called SFR3 since the name SFR2 was used in a previous plan to build vaults adjacent to SFR1. The repository is currently estimated to be closed by year 2075.

The SFR waste vaults are located below the Baltic Sea and are connected to the ground surface via two access tunnels. SFR1 consists of one 70-metre-high waste vault (silo) and four 160-metre-long waste vaults (1BMA, 1–2BTF and 1BLA), covered by about 60 metres of bedrock. SFR3 consists of six waste vaults (2BMA, 1BRT and 2–5BLA), varying in length from 255 to 275 m, covered by about 120 metres of bedrock.

A prerequisite for the extension of SFR is the licensing of the extended facility. The licensing follows a stepwise procedure. In December 2014, SKB submitted two licence applications to extend and continue the operation of SFR, one to the Swedish Radiation Safety Authority (SSM) for permission under the Act on Nuclear Activities (SFS 1984:3) and one to the Land and Environment Court for permissibility under the Environmental Code (SFS 1998:808). In October 2019 SSM submitted their pronouncement to the Swedish Government and recommended approval of the permission sought by SKB. In November 2019 the Court submitted its statement to the Swedish Government and recommended approval of the licence application. The Swedish Government granted permit and permissibility in December 2021.

The current step in the licensing of the extended SFR is the processing of the construction license application, submitted by SKB to SSM for review under the Act on Nuclear Activities. The licence documentation consists of an application document and a set of supporting documents. A central supporting document is the preliminary safety analysis report (PSAR), with a general part consisting of ten chapters[1]. Chapter 9 of the general part of that report addresses post-closure safety. The **Post-closure safety report** is the main reference to Chapter 9, and this report is a main reference to the **Post-closure safety report**.

[1] SKB, 2022. PSAR SFR – Allmän del kapitel 1 – Introduktion. SKBdoc 1702853 ver 3.0, Svensk Kärnbränslehantering AB. (In Swedish.) (Internal document.)

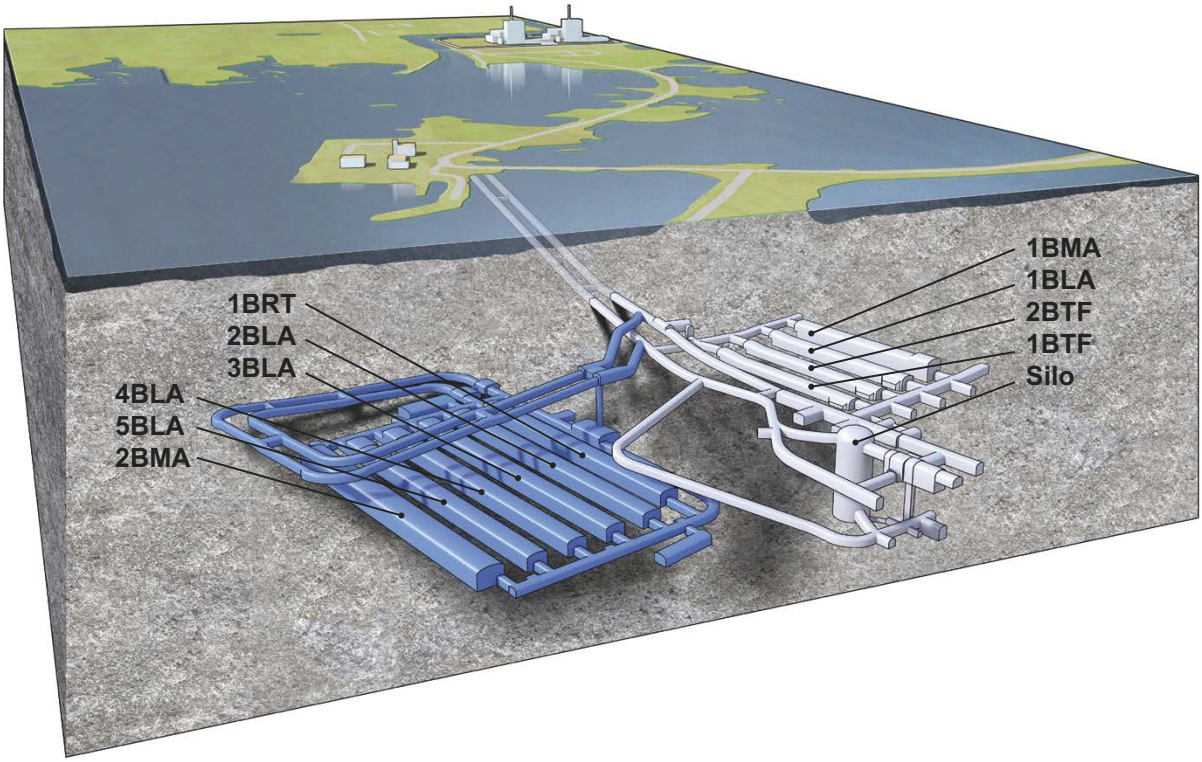

Figure 1-1. *Schematic illustration of SFR. The grey part is the existing repository (SFR1) and the blue part is the extension (SFR3). The waste vaults in the figure are the silo for intermediate-level waste, 1–2BMA vaults for intermediate-level waste, 1BRT vault for reactor pressure vessels, 1–2BTF vaults for concrete tanks and 1–5BLA vaults for low-level waste.*

1.2 Post-closure safety assessment

1.2.1 Overview

The main role of the post-closure safety assessment is to demonstrate that SFR is radiologically safe for humans and the environment after closure. This is done by evaluating compliance with respect to the Swedish Radiation Safety Authority's regulations concerning post-closure safety and the protection of human health and the environment. Furthermore, the post-closure safety assessment is being successively developed in the stepwise licensing process for the extended SFR, and thus the results from the PSAR assessment[2] provide input to the forthcoming updated assessment to be carried out before trial operation of the facility.

The overall aim in developing a geological repository for nuclear waste is to ensure that the amounts of radionuclides reaching the accessible biosphere are such that possible radiological consequences are acceptably low at all times. Important aspects of the regulations are that post-closure safety shall be maintained through a system of passive barriers. The barrier system of SFR comprises engineered and natural barriers and the function of each barrier is to, in one or several ways, contribute to the containment and prevention or retention of dispersion of radioactive substances, either directly or indirectly by protecting other barriers in the barrier system. To achieve post-closure safety, two safety principles have been defined. *Limitation of the activity of long-lived radionuclides* is achieved by only accepting waste for disposal that conforms with the waste acceptance criteria for SFR. *Retention of radionuclides* is achieved by the function of the engineered and natural barriers. The two safety principles are interlinked and applied in parallel. The engineered barrier system is designed for an inventory that contains a limited amount of long-lived radionuclides, given the conditions at the selected site and the natural barriers.

[2] For brevity, the PSAR post-closure safety assessment for SFR is also referred to as "the PSAR assessment" or "the PSAR" in the present report.

The basis for evaluating compliance is a safety assessment methodology that conforms to the regulatory requirements regarding methodology, and that supports the demonstration of regulatory compliance regarding post-closure safety and the protection of human health and the environment. The overall safety assessment methodology applied is described in the **Post-closure safety report**, Chapter 2. The methodology was developed in SR-PSU (SKB TR-14-01[3]) based on SKB's previous safety assessment for SFR1 (SAR-08, SKB R-08-130). Further, it is consistent with the methodology used for the post-closure safety assessment for the final repository for spent nuclear fuel to the extent appropriate given the different nature of the two repositories.

1.2.2 Report hierarchy

The **Post-closure safety report** and main references for the post-closure safety assessment are listed and briefly described in Table 1-1, also including the abbreviated titles (in bold) by which they are identified in the text. Furthermore, there are numerous additional references that include documents compiled either by SKB or other organisations, or that are available in the scientific literature, as indicated in Figure 1-2.

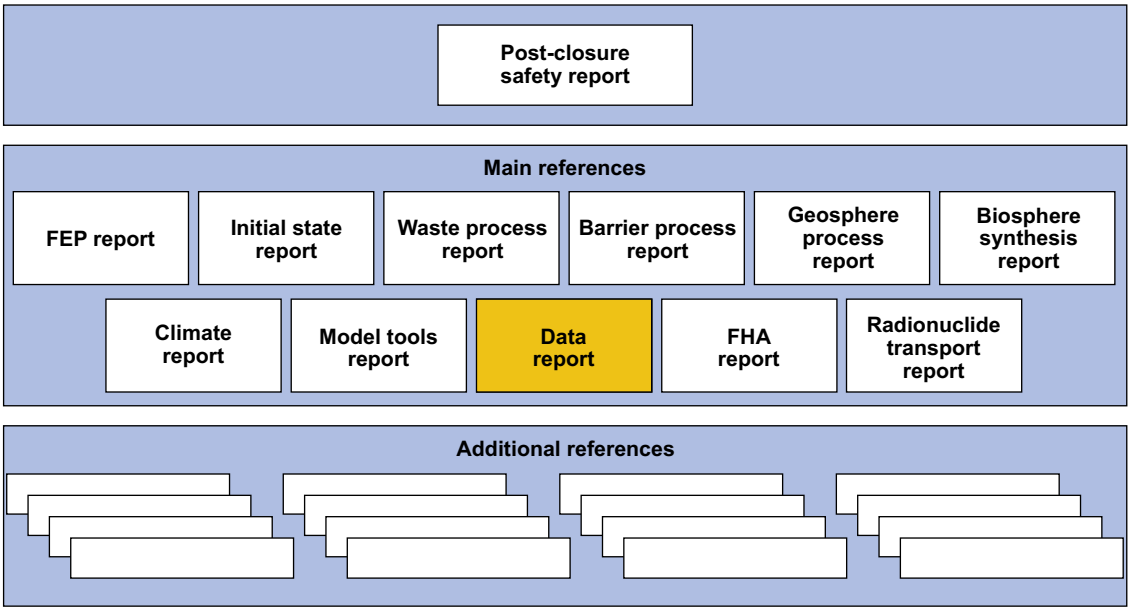

Figure 1-2. *The hierarchy of the Post-closure safety report, main references and additional references in the post-closure safety assessment.*

[3] For SKB reports without named authors, the report number is used instead of publication year when referring to them in the text.

Table 1-1. Post-closure safety report and main references for the post-closure safety assessment. The reports are available at www.skb.se.

Abbreviated title by which the reports are identified in this report and in the main references Report number	Content
Post-closure safety report SKB TR-23-01	The main report of the PSAR post-closure safety assessment for SFR.
Initial state report SKB TR-23-02	Description of the expected conditions (state) of the repository at closure. The initial state is based on verified and documented properties of the repository and an assessment of its evolution during the period up to closure.
Waste process report SKB TR-23-03	Description of the current scientific understanding of the processes in the waste form and in the packaging that have been identified in the FEP processing as potentially relevant for the post-closure safety of the repository. Reasons are given as to why each process is handled in a particular way in the safety assessment.
Barrier process report SKB TR-23-04	Description of the current scientific understanding of the processes in the engineered barriers that have been identified in the FEP processing as potentially relevant for the post-closure safety of the repository. Reasons are given as to why each process is handled in a particular way in the safety assessment.
Geosphere process report SKB TR-14-05	Description of the current scientific understanding of the processes in the geosphere that have been identified in the FEP processing as potentially relevant for the post-closure safety of the repository. Reasons are given as to why each process is handled in a particular way in the safety assessment.
Climate report SKB TR-23-05	Description of the current scientific understanding of climate and climate-related issues that have been identified in the FEP processing as potentially relevant for the post-closure safety of the repository. Description of the current scientific understanding of the future evolution of climate and climate-related issues.
Biosphere synthesis report SKB TR-23-06	Description of the present-day conditions of the surface systems at Forsmark, and natural and anthropogenic processes driving the future development of those systems. Description of the modelling performed for landscape development, radionuclide transport in the biosphere and potential exposure of humans and non-human biota.
FEP report SKB TR-14-07	Description of the establishment of a catalogue of features, events and processes (FEPs) that are potentially relevant for the post-closure safety of the repository.
FHA report SKB TR-23-08	Description of the handling of inadvertent future human actions (FHA) that are defined as actions potentially resulting in changes to the barrier system, affecting, directly or indirectly, the rate of release of radionuclides, and/or contributing to radioactive waste being brought to the surface. Description of radiological consequences of FHAs that are analysed separately from the main scenario.
Radionuclide transport report SKB TR-23-09	Description of the radionuclide transport and dose calculations carried out for the purpose of demonstrating fulfilment of compliance with the criterion regarding radiological risk criterion.
Data report SKB TR-23-10 (this report)	Description of how essential data for the post-closure safety assessment are selected, justified and qualified through traceable standardised procedures.
Model tools report SKB TR-23-11	Description of the model tool codes used in the safety assessment.

1.3 This report

1.3.1 Purpose

The purpose of this report is to describe the compilation and qualification of input data identified as essential for the post-closure safety assessment of the SFR repository and forms an important part of the reporting of the assessment. The identification of essential input data is discussed in Section 2.1. This report constitutes, together with the **Radionuclide transport report** Appendix A, **Biosphere synthesis report**, Grolander (2013) and SKB (R-23-01), the reporting of step 6 *Compilation of input data* in the overall safety assessment methodology (**Post-closure safety report** Section 2.6.6).

The data presented in this report are either compiled from supporting reports and documents, as part of previous tasks or as part of the safety assessment activities, or produced and justified in this report. Most data are compiled from background reports, such as the Site Description Model, the inventory report, reports from previous post-closure safety assessments for SFR, etc and in those cases the justification of data is mainly done in the supporting documents. In such a case, the qualifying role of this report is to ensure that the suggested data are traceable and applicable for the safety assessment, and to some extent to suggest their role in the safety assessment. For example, a set of data suggested in the site descriptions may only be valid for a certain climate domain, or under some other specified condition. Furthermore, estimates of uncertainties as well as of natural variability should be delivered in this report, so that the data can be properly used in the subsequent safety assessment modelling. It is part of the qualifying role to make sure that reasonable, quantitative, and usable uncertainty estimates are delivered.

The way of qualifying data is through traceable standardised procedures where extra effort is put into documenting the data qualification process, and to discussing uncertainties in data originating from conceptual and data uncertainty. These standardised procedures are detailed in Section 2.3.

1.3.2 Main developments since the SR-PSU

The following updates have been made since the SR-PSU Data report (SKB TR-14-01) (still following the same procedure for qualifying data):

- Chapter 3 Radionuclide decay – The chapter is updated with new information regarding the uncertainty in half-lives for Ni-59, Se-79, Mo-93, Ag-108m and Sn-126. The new recommendation is to use data from one source.
- Chapter 4 Uncertainties in the radionuclide inventory – The treatment of uncertainties in the inventory is improved in this assessment and is to a large extent described in the Inventory report (SKB R-18-07), therefore this chapter is rewritten in a simplified manner compared with the general procedure.
- Chapter 5 Metal corrosion – Due to shortcomings in the previous version, this chapter has been rewritten, and probability density functions of the corrosion rates are now provided by the supplier.
- Chapter 6 Bitumen swelling pressure – The chapter is updated with results from recent experiments and modelling, but the same data are recommended.
- Chapter 7 Concrete/Cement sorption data and Bentonite sorption and diffusivity data – New information regarding sorption on concrete and sorption reduction factors is included and the recommended sorption data on concrete for some species are changed (for example organic carbon and nickel) as well as sorption reduction factors.
- Chapter 8 Rock matrix and Crushed rock sorption data – This chapter is updated with new information. However, only the recommended data for molybdenum and selenium are changed.
- Chapter 9 Cementitious components and Crushed rock hydraulic data – The chapter is extended to also include crushed rock hydraulic data. The chapter is updated to cover the latest information as well as to give clearer motivation for the chosen hydraulic conductivities and their changes with time.
- Chapter 10 Cementitious components diffusivity data – The chapter is updated to cover the latest information as well as to give clearer motivation for the chosen diffusivities and their changes with time.
- Chapter 11 Hydraulic pressure field in the SFR local domain – Since new hydrogeological calculations have been performed, the whole chapter has been revised.
- Chapter 12 Shoreline displacement – The chapter has been rewritten based on new research.

1.3.3 Contributing experts

Project leader for the PSAR safety assessment has been Jenny Brandefelt (SKB). A number of people from various fields of expertise have been involved in the preparation of this report. The most involved are listed below in alphabetical order:

Name	Affiliation	Contribution to this report
Katrin Ahlford	SKB	Radionuclide inventory (Ch 4), co-author
Patrick Bruines	SKB	Hydraulic pressure field (Ch 11), co-author
James Crawford	Kemakta Konsult AB	Rock matrix and Crushed rock sorption data (Ch 8), co-author
Mark Elert	Kemakta Konsult AB	Bitumen swelling pressure (Ch 6), original supplier
Svante Hedström	SKB	Metal corrosion (Ch 5), Concrete/Cement sorption data and Bentonite sorption and diffusivity data (Ch 7), co-author
Lars Olof Höglund	Kemakta Konsult AB	Cementitious components hydraulic and diffusivity data (Ch 9 and 10), original supplier
Anna-Maria Jacobsson	SKB	Rock matrix and Crushed rock sorption data (Ch 8), co-author
Miranda Keith-Roach	Kemakta Konsult AB	Concrete/Cement sorption data and IRF (Ch 7), co-author, editor
Johan Liakka	SKB	Shoreline displacement (Ch 12), co-author
Maria Lindgren	Kemakta Konsult AB	Radioactive decay (Ch 3), co-author, editor
Per Mårtensson	SKB	Cementitious components hydraulic and diffusivity data and Crushed rock hydraulic data (Ch 9 and 10), co-author
Michael Ochs	BMG Engineering Ltd	Concrete/Cement sorption data and Bentonite sorption and diffusivity data (Ch 7), original supplier
Jan Rosdahl	SKB	Bitumen swelling pressure (Ch 6), co-author
Magnus Sidborn	Kemakta Konsult AB	Metal corrosion (Ch 5), co-author
Ola Wessely	SKB	Cementitious components hydraulic and diffusivity data and Crushed rock hydraulic data (Ch 9 and 10), co-author

This report has been significantly improved at different stages by adjustments in accordance with comments provided by informal and factual reviewers. The informal review has been a rather continuous process where most co-authors listed in the table have commented on texts written by other co-authors; in addition, Per-Anders Ekström (Kvot AB), Karin Andgren (SKB), Maria Rasmusson (SKB), Fredrik Bultmark (SKB), Per-Gustav Åstrand (SKB), Fredrik Vahlund (SKB), Jens-Ove Näslund (SKB), Magnus Odén (SKB) have provided feedback on various parts of the report. Factual reviewers have been; Mike Thorne (Mike Thorne and Associates Ltd.) and Jordi Bruno (Amphos 21 Consulting).

1.4 Structure of this report

This report comprises 12 chapters and one appendix. Following is a brief description of the contents:

Chapter 1 – **Introduction.** This chapter describes the background and the role of the report. Furthermore, definitions are given and explanations of the abbreviations used.

Chapter 2 – **Methodology for identifying and qualifying data.** This chapter describes how the data included in this report have been identified as well as the procedure to qualify data.

Chapter 3 – **12** Chapters describing the qualification of the selected data. Each chapter describes a group of selected data for example sorption data, diffusivity data and hydraulic data for concrete/cement. The qualified data recommended for use in the safety assessment are given in the last section in Chapters 3 to 12. In this section, clear referencing to tables in the preceding sections may substitute duplication of the data. Data that cannot be tabulated in this report, for example the coordinates of thousands of exit locations for groundwater flow paths, are stored in referenced databases.

Appendix A – **Terms and abbreviations.** To facilitate the readability of the report, selected terms and abbreviations are explained.

2 Methodology for identifying and qualifying data

2.1 Identification of essential input data

The number of input parameters for the safety assessment is very large. Some input data uncertainties will have a substantial influence on output uncertainty, which ultimately leads to uncertainty in assessed radiological risk. Other data may range over orders of magnitude but still do not influence the assessed radiological risk.

It is therefore appropriate to identify input data to which safety related output is sensitive and use these insights in the reduction of input data uncertainties. It is also important to have a high degree of confidence in the data that are used to conclude that particular processes, radionuclides, etc will never contribute significantly to radiological risk.

The overall post-closure safety principles *limitation of radioactive inventory* and *retention of radionuclides* are broken down to general safety functions directly connected to different repository system components. Identification of essential input data have been performed using the safety functions described in detail in the **Post-closure safety report**, Chapter 5.

The limited radionuclide inventory is controlled by permits from the regulatory authority, SSM, and by the waste acceptance criteria (WAC) which regulate each waste package and what the waste producers can put in them. The slow transport of radionuclides from the waste packages is governed by a low flow of water through them, by good sorption in the barriers, and by a geosphere with low permeability and hydraulic gradients.

In this safety assessment the safety functions are used to identify the essential input data which should be qualified and motivated in this report. By doing this, the amount of data is limited to a small number of highly relevant data sets. Essential data and the related safety functions are presented in Table 2-1. It should be noted that some of the safety functions and related data given in Table 2-1 are valid only for specific waste vaults.

Table 2-1. Data report chapters identified from safety function(s).

Ch	Data	Safety function(s)
3	Radionuclide decay	Limit quantity of activity
4	Uncertainties in the radionuclide inventory	Limit quantity of activity
5	Metal corrosion	Limit corrosion, Limit gas formation
6	Bitumen swelling pressure	Limit advective transport
7	Concrete/cement sorption data and Bentonite sorption and diffusivity data	Sorb radionuclides
8	Rock matrix and Crushed rock sorption data	Sorb radionuclides
9	Cementitious components and Crushed rock hydraulic data	Limit advective transport
10	Cementitious components diffusivity data	Limit advective transport
11	Hydraulic pressure field in the SFR local domain	Provide favourable hydraulic conditions
12	Shoreline displacement	Provide favourable hydraulic conditions, Avoid boreholes in the direct vicinity of the repository

2.2 Participating parties

The data recommended for use in the safety assessment are generally based on a mixture of measurements, modelling, and interpretation. Therefore, there is always a component of expert judgment involved in choosing the recommended data (as stated in Section 2.1, trivial data are not handled in this report). The work of producing much of the data, as well as of compiling the data and writing this report, has been done by experts working at, or on behalf of, SKB. Therefore, formally the expert should not be considered as independent. The experts could have their expertise in a narrow subject area, such as sorption of radionuclides in a bentonite matrix, or as generalists in the safety of radioactive waste (which indeed could also be considered as a narrow field of expertise).

The vocabulary used for separating the teams or persons supplying the data, the groups of persons within the assessment team responsible for the data, and the assessment team as a whole are:

- Supplier.
- Customer.
- The assessment team.

This vocabulary is the same as was used in the latest safety assessments for both SFR (SR-PSU Data report, SKB TR-14-10), and the repository for spent-fuel (SR-Site Data report, SKB TR-10-52) where it was first implemented as a response to the authorities' request for a more transparent data assurance process.

2.3 Qualification of input data – instructions to supplier and customer

The final objective of the **Data report** is to perform data qualification including estimates of both conceptual and data uncertainty, as well as of natural variability, for various subject areas. In addition, the traceability of the data is examined. The qualified data are intended for subsequent use as input data in the safety assessment.

The **Data report** does not concern all data used in the safety assessment, but those which are identified to be of particular significance for the safety functions (see Section 2.1 and Table 2-1). Data may comprise both measured data from the laboratory and from the field, as well as output from detailed modelling where measured data are interpreted, depending on the subject area. Even though the data may represent both parameters and entities, the word data is generally used.

It should be pointed out that in the process of qualifying and motivating data, traceability is only one aspect. Perhaps the more important aspect is the scrutinising of the scientific adequacy of the data.

Each set of data supplied in this report is categorised into one of many different subject areas. For each subject area, the data qualification process comprises a sequence of stages resulting in a text of a standard outline. The sequence of stages and the standard outline are shown in Figure 2-1.

Below the parties involved in the **Data report** and the sequence of stages shown in Figure 2-1 are discussed. The standard outline is described in Section 2.3.1 to Section 2.3.12. For each subject area, the Data report team identifies the customer and supplier of data, and assigns a customer representative and a supplier representative that co-author the subject area section[4].

The customer is in broader terms the assessment team that is responsible for performing the safety assessment. However, the entire team is generally not involved in each subject area, but it is rather represented by a group of persons with special knowledge and responsibility. The customer representative should represent the assessment team, and not rely solely upon their own opinions.

The suppliers are the teams originating the sources of data, for example the site-descriptive model reports, waste inventory reports, and other supporting documents. Again, the supplier representative should represent the team, and not rely solely upon own opinions.

[4] The terms customer and supplier come from standard quality assurance terminology.

The chronology of the writing of a subject area section is the following.

Stage A: The customer writes the first two sections defining what data are requested from the supplier, how the data will be used in the assessment, and how similar data were used in previous assessments.

Stage B: The supplier writes the following eight sections that are the core of the data qualification. This is done according to a standard outline where several issues such as traceability, data uncertainty, and natural variability should be dealt with. This section should result in sets of qualified data that are the delivery to the customer.

Stage C: The customer, representing the entire assessment team, writes the last two sections making judgments upon the delivery and recommending data for use in the assessment. The text is written in close cooperation with the supplier and other persons within the assessment team with expert knowledge in the subject area.

Upon the completion of the chapter, it undergoes a review process as part of Stage D.

Stage D: The report is reviewed according to standard procedures within the SKB quality framework.

In the following sections, the outline shown in the grey boxes in Figure 2-1 is described in detail.

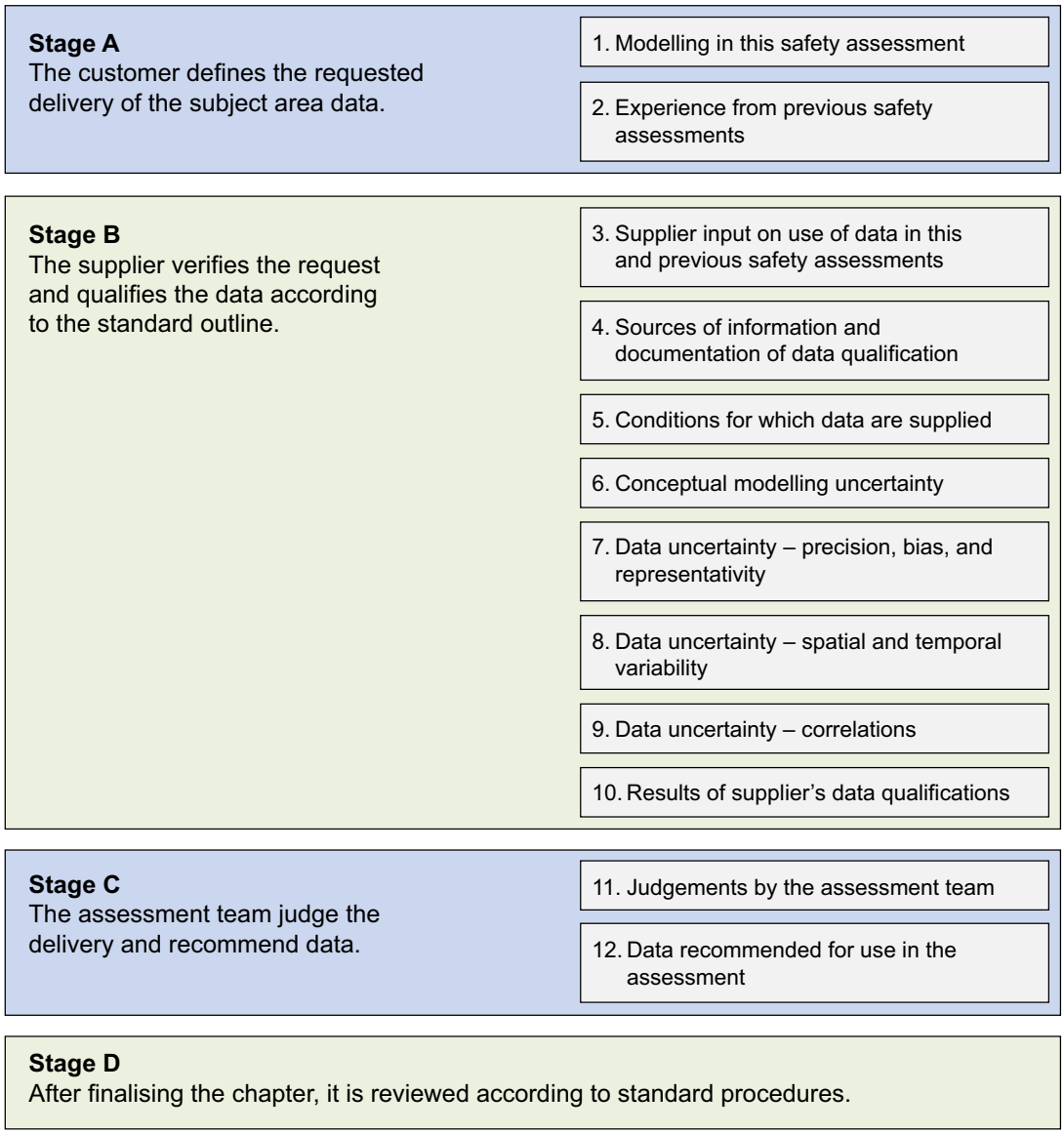

Figure 2-1. *Stages of writing and reviewing the Data report. The standard outline of a subject area is shown in the grey boxes.*

2.3.1 Modelling in this safety assessment

In this section, the customer should define what data are requested from the supplier and give a brief explanation of how the data of the subject area are intended to be used in the modelling activities.

Defining the data requested from the supplier

Here, the customer should define the data (parameters) that should be part of the supplier's delivery, in a bullet list. If applicable, the parameter symbol and unit should be provided in this list. If the supplier should focus on providing data over certain ranges, or for certain conditions, this should be specified. This text should not only facilitate the task of the supplier, but also assist the reader of the **Data report** in understanding the scope of the subject area section.

Modelling activities in which data will be used

Here the customer representative should give a brief explanation of how the data are intended to be used in different modelling activities. This explanation should cover both how the data are used in specific models, and in the model chain. Differences from the use of this type of data in previous safety assessments should be highlighted. The justification for the use of these models in the assessment is provided in other PSAR documents, such as the **Post-closure safety report** and process reports.

As a result of the extensive work that will be conducted up to near completion of the safety assessment, details of the models and the model chain may be modified. As a result, this text may have to be finalised in a late stage of the **Data report** project. Thus, only a preliminary version is provided early on to the supplier representative.

2.3.2 Experience from previous safety assessments

In this section the customer should give a brief summary on how the data of the subject area were used in previous safety assessments. The experience from these assessments should function as one of the bases for defining the input data required in the modelling. The summary of how the data were used in previous safety assessments should conform to the following outline:

- Modelling in previous safety assessments.
- Conditions for which data were used in previous safety assessments.
- Sensitivity of the assessment results to uncertainties in the data in previous safety assessments.
- Alternative modelling in previous safety assessments.
- Correlations used in previous safety assessment modelling.
- Identified limitations of the data used in previous safety assessment modelling.

More detailed guidance regarding what should be included in the summary in relation to each of these bullets is given below.

Modelling in previous safety assessments

The use of the data in previous safety assessment models, as well as in previous safety assessment model chains, should be described. Repetitions from the section "Modelling in this safety assessment" should be avoided. If there is no difference between the previous safety assessments and the current modelling approaches, it is sufficient to state this. With "previous safety assessments", SR-PSU is generally referred to but in some case information from SAR-08 as well as SAFE is also appropriate.

Conditions for which data were used in previous safety assessments

In this subsection, the relevant conditions to which the subject area data were subjected to in previous safety assessment modelling should be outlined. Relevant conditions are only those conditions that significantly influence the data, in the context of demonstrating repository safety. Different subject area data are affected by different conditions. For example, the sorption coefficient K_d may be strongly

influenced by groundwater salinity. Thus, in characterising the conditions under which K_d values were used, it is likely to be appropriate to give the salinity range during repository evolution, for example as assessed in the previous safety assessments by hydrogeochemical modelling. Other types of conditions may include gradients, boundary conditions, initial states, engineering circumstances, etc.

It is sufficient to state the relevant conditions used in previous safety assessment modelling (including those applied in sensitivity analyses, various initial states, different scenarios, and evolution within scenarios) and to refer to the previous safety assessments documents for background information. Justification as to why those conditions were studied is not required. Where appropriate, the relevant conditions should be tabulated. It should be noted that the stated conditions do not restrict qualification of data for use under other conditions, but merely underline the conditions considered appropriate within the modelling context of previous safety assessments.

Sensitivity of assessment results in previous safety assessments

Where appropriate, an account should be given of results from sensitivity analyses performed as part of the previous safety assessments. Such analyses were made in order to prioritise uncertainty assessments for those data and conditions judged to be potentially important for performance, both for overall endpoints such as risk and for conditions affecting the state of the system. If such sensitivity analysis was performed, the following issues may be outlined:

- For what ranges of the data was the impact on the previous safety assessment significant and are there ranges where the impact was negligible? If sensitivity analyses showed that only part of the range has an impact on repository safety, less effort may be given to quantifying parameter values outside this range. It should be noted that results from the sensitivity analyses may not be applicable if the assessment model have been substantially changed since the previous assessment.
- Was the impact monotonic, i.e. is there a unidirectional relationship between the data value and performance, is there an "optimal" value, or is the impact dependent in a complicated manner upon the values of other input data?
- What degree of variation in the data is needed to have an impact on safety assessment results (this answer may be different for different data ranges)?
- Were the results applicable to all conditions of interest – or only to some?

In discussing the above, the customer should consider if the cited sensitivity analyses were sufficiently general to provide definitive answers.

Alternative modelling in previous safety assessments

Whenever it applies, the customer representative should summarise alternative modelling approaches studied in previous assessments in which data of this type were used. The following issues may be reflected upon:

- What alternative models exist and what influence did they have on the safety assessment?
- Were conceptual uncertainties, related to the models in which the data were used, identified in previous safety assessments? In that case, what was the impact on assessment results?

Correlations used in previous safety assessment modelling

A correct treatment of probabilistic input data requires that any correlations between those data are identified and quantified. The correlations associated with the subject area data, as accounted for in previous safety assessments, should be briefly described. This includes internal correlations within the subject area and correlations with data of other subject areas. If the same correlations were used as will be used in this assessment, it is sufficient to state this.

Identified limitations of the data used in previous safety assessment modelling

If limitations or shortcomings of the data used in the previous safety assessments have been identified, which may significantly have affected the assessment, such should be stated. The limitations or shortcomings can be due to, for example, lack of site-specific data or lack of data obtained at conditions representative for the repository. The limitations and shortcomings may have been identified by the regulatory authorities, by SKB, or by other parties.

2.3.3 Supplier input on use of data in this and previous safety assessments

In this section the supplier has the opportunity to comment on the two above sections. The focus for the supplier should be to help the assessment team in choosing appropriate data and modelling approaches and avoid repeating errors and propagating misconceptions from previous safety assessments or from other modelling activities. Even if a single individual has the roles as both supplier and customer representative, he or she may still make comment upon the use of data in this and previous safety assessments.

2.3.4 Sources of information and documentation of data qualification

This section is devoted to presenting the most important sources of data, as well as categorising different data sets on the basis of their traceability and transparency. Sources of data may include SKB reports, SKB databases, and public domain material. Documents of importance for the data qualification may also consist of SKB internal documents. All underlying documents should be properly cited throughout the **Data report**.

Sources of information

The supplier is asked to tabulate the most prominent references used as sources of data. In addition, references to important documents describing the process of acquiring, interpreting, and refining data may be listed.

If the data qualification process is well documented in supporting documents, it is sufficient to reference these documents and to only briefly summarise the data qualification process. If not, the **Data report** gives the supplier a chance to appropriately document the data qualification process of the subject area data.

Concerning sources of information, the supplier representative should:

- Fully cite all sources of information throughout the text. It is necessary to keep in mind that the text may have readers with limited in-depth knowledge of the subject. Therefore, what normally would seem as trivial may deserve references for further reading. It is strongly recommended to make an extra effort to refer to the open literature where possible, and not only to SKB documents.
- In case of referring to a document of many pages, for example a site-descriptive model report, give detailed information on the section, figure, table, etc where the relevant information can be found.
- Properly cite databases, SKB internal documents, etc even though they may not be available to the general reader. In the case of referring to databases, the precise reference should be given to the individual data set used. For example, it is not sufficient to refer to the SKB database SICADA if not also giving detailed information, such as the activity id or data delivery note id. This is to ensure traceability.
- Fully cite advanced modelling tools that have been relied upon, where the characteristics and traceability of the underlying code may have implications for data qualification.

Categorising data sets as qualified or supporting data

The supplier representative should categorise data as either qualified data or supporting data. Qualified data have been produced within, and/or in accordance with, the current framework of data qualification, whereas supporting data has been produced outside, and/or not in conformance with, the framework. Data taken from peer-reviewed literature takes a special position in that they may be considered as qualified even though they are produced outside the SKB framework of data qualification. However, such data are not by necessity categorised as qualified, as they may be non-representative or lack in some other aspect, bearing in mind that there are substantial variations in the rigour of the peer review process.

Data produced by SKB, for example in the site investigations, should a priori be considered as qualified. However, before the data are formally categorised as qualified, several considerations need to be addressed as described below. Data produced outside the data qualification framework should a priori be considered as supporting data. This could for example be data produced by SKB prior to the implementation of its quality assurance system, or data produced by other organisations. Before formally categorising the data as supporting, a number of considerations need to be addressed, as described below.

Data taken from widespread textbooks, engineering handbooks, etc which are considered to be established facts, need not to be scrutinised. Well-known data that should be excluded from the **Data report** need not to be categorised as qualified or supporting data, although their exclusion may need to be motivated.

It is outside the scope of the **Data report** to deal with individual data. Instead, the supplier representative should characterise data sets as qualified or supporting. The supplier representative should decide to what extent various data can be included in a single data set for the specific case. The following examples of natural barrier data sets could be used for inspiration:

- Data or some of the data, obtained by a specific method at a site, rock volume, borehole, etc.
- Data or some of the data, obtained by various methods under certain conditions (e.g. saline water) at a site, rock volume, borehole, etc.
- Data or some of the data, taken from an external publication.

Qualified data

The following considerations should be addressed for data that a priori are identified as qualified, before formally categorising them as qualified. Most of the data that are delivered to the **Data report** are refinements and interpretations of observed data. Such refinements and interpretations are performed both for engineered and natural barrier data. For example, the multitudes of data acquired within the site investigation are normally refined within the site-descriptive modelling by use of more or less complex models. The supplier should judge whether data acquisition and refinement, and associated documentation, are in accordance with the implemented data qualification framework. The following considerations may form the basis for the judgement.

Considerations concerning data acquisition:

- Is the acquisition of observed data performed in conformance with a widely adopted quality management system (e.g. the ISO 9000 series or equivalent)?
- Is it possible to trace relevant quality assurance documents (for example method descriptions, field notes, etc) for the measurements? It should be noted that even though the quality assurance documents may not be available for the general reader, they are accessible for the assessment team.
- Is it possible to extract relevant information on the data quality, variability, and representativity from documents reporting the acquisition of data?
- Are concerns associated with the observed data and nonconformities of the measurements transparently described?
- Is the undertaken data acquisition programme sufficient to determine the full range of data uncertainty and natural variability, and do the acquired data appropriately characterise the intended aspect of the system (site, rock domain, concrete barrier, population, etc)?

Considerations concerning data refinement:

- Are concerns and nonconformities described in the supporting documents propagated to, and addressed in, the data refinement?
- In refining observed data by use of more or less complex modelling, is this done in accordance with documented methods?
- In the case of more complex modelling, which may have implication for data qualification, are the details of the modelling described either in a task description, planning document, or in the document reporting the modelling results? Furthermore, is the modelling tool developed in accordance with a widespread quality assurance system and/or is its quality tested in other ways?
- Has comparative/alternative modelling been performed to evaluate artefacts induced in the modelling, and to evaluate whether the modelled interpretation of the data is reasonable?

Going through these questions in detail for each data set may be a too extensive task, wherefore the sorting of data to some degree is based on expert judgement. However, in making this judgment, it may be helpful to revisit the above bullet lists.

If appropriate data qualification has been performed and documented in supporting documents or can be performed and documented as part of the delivery, the data should be formally categorised as qualified data. If the documentation of the data qualification process is inadequate in supporting documents, and appropriate data qualification cannot be performed as part of the delivery, the data must be demoted to the category supporting data.

As mentioned before, data taken from peer-reviewed literature takes a special position in that they may be considered as qualified even though they are produced outside the SKB framework of data qualification. However, before formally categorising them, one needs to judge whether they are representative for the SFR repository system and the SFR site. A prerequisite for making such a judgement is often that the documents are transparently written. If the data are not representative for SFR conditions, or their degree of representativity is difficult to evaluate, the data may be categorised as supporting data instead of as qualified data.

Supporting data

The following considerations should be made for data that a priori are identified as supporting, before formally categorising them as supporting data. Such data are produced by SKB outside the framework of data qualification, or by other organisations. The supplier representative should consider:

- How well is the method used to acquire the data described? The greater the transparency with which the method is described in the supporting document, the greater the value should be ascribed to the data.
- How well is the method used to interpret and refine the data described? The more transparently the interpretation and refinement is described in the supporting document, the greater the value should be ascribed to the data.
- Is it possible to identify and evaluate the data qualification process used in acquiring and refining the data? If it is shown that a sound data qualification process has been used, the data should be ascribed greater value.
- Judge, based on the above, whether the data can be used as part of the basis for recommending data to the safety assessment modelling, as comparative data for other qualified data, or should not be used at all. In some cases, the transparency of a document is so poor that crucial information concerning data qualification cannot be extracted. If this renders an assessment of the data's scientific adequacy and their representativity for SFR conditions impossible, the supplier representative should recommend that the data are dismissed. This can be done even if the numerical values of the data are consistent with other, qualified data.

If data that a priori are assumed to be supporting are acquired, interpreted, and refined according to a similar data qualification framework as implemented by SKB, and this is transparently described, the supplier representative can promote the data to the category qualified data.

It should be noted that data taken from peer-review literature can be categorised as supporting data. This can be done if, for example, data are only partially representative for the SFR repository concept and the SFR site.

Excluded data previously considered as important

Within the field of nuclear waste management, there are large quantities of data that are of little significance for this safety assessment, as they are less representative for the SFR site, the SFR repository concept, etc than other available data. In general, excluding such data from subsequent use in the safety assessment does not require justification. The exception is if the data constitutes a well-known part of the basis of previous safety assessments (or equivalent tasks), and/or have a significant impact on the perception of the appropriate choice of data value. If it could be seen as a significant inconsistency or omission not to use the data, their exclusion should be explicitly justified. Providing an appropriate justification is particularly important if the excluded data disagree with the presently used data.

2.3.5 Conditions for which data are supplied

The data of the different subject areas are likely affected by different conditions. Conditions refer to initial conditions, boundary conditions, barrier states, and other circumstances, which potentially may affect the data to be estimated. In the process of qualifying data for subsequent use in the safety assessment, an important part is to account for the conditions for which data were acquired, and to compare these conditions with those of interest for the safety assessment.

In the section “Experience from previous safety assessments” it is stated for what conditions data were used in the previous safety assessments. These conditions should not limit the conditions for which data are examined, but merely point out conditions that are likely to be of importance for a safety assessment. The supplier may have been given instructions from the assessment team, or may have opinions about important conditions, which lead to modifications of the previous safety assessments conditions.

In this section, the conditions for which the data have been obtained should be discussed and, as appropriate, justified as relevant to the safety assessment. Such a condition is often a single value (e.g. temperature), a range (e.g. salinity range), or a gradient (e.g. hydraulic gradient). Other factors of relevance for repository safety may be included as conditions, at the discretion of the supplier. Conditions that are deemed to be of particular importance for repository safety should be highlighted. Other conditions that do not significantly relate to repository safety, but may be of importance for data qualification, are also important to note. Such information is valuable when, for example, crosschecking data sets with those of other studies or evaluations. The supplier representative may list ranges of applied conditions during data acquisition, excluding conditions that are both general (such as the gravitational constant) and self-evident.

In many cases, it is expected that the conditions for which data are supplied will differ from those that apply in the safety assessment. For example, a set of supplied data may not represent the full temperature range required or may have been obtained at a different pressure than expected in situ. The differences identified by the supplier representative should be outlined in this section. Furthermore, for each deviating condition of importance for the assessment results, the implications should be discussed.

2.3.6 Conceptual modelling uncertainty

This section concerns conceptual modelling uncertainty of the subject area data. Two types of conceptual uncertainty should be discussed. The first concerns how well the data, and the models wherein they are used, represent the physical reality, and the second concerns conceptual uncertainties introduced in the acquisition, interpretation, and refinement of the data. Generally, data are included in models that represent an idealised reality, which to some degree differs from the physical reality. Therefore, one can expect that a degree of conceptual uncertainty is associated with all data compiled in this report.

To the extent possible, the supplier should describe such conceptual uncertainty. This should be done in the context of the models in which the data are used, intended to describe certain postulated processes. Also, it may be appropriate to discuss alternative conceptualisations in which the data may be used in different ways. If comprehensive discussions on the subject have already been documented, for example in process reports, such documents may be referred to and a short summary of the conceptual uncertainty will suffice. Aspects of the conceptual uncertainty that are obviously unrelated to repository safety may be disregarded.

Conceptual uncertainty may also be introduced in the acquisition, interpretation, and refinement of the data. For example, the data may have been obtained by inverse modelling of experimental results, where conceptual uncertainty is introduced by the model. The data may also have been obtained by using some correlation relationship, where there is conceptual uncertainty in the correlation. Many other sources of conceptual uncertainty are conceivable and may be discussed at the discretion of the supplier. In doing this, the supplier representative should carefully differentiate between uncertainties introduced due to conceptual issues and data uncertainty introduced by measurement errors, etc. Data uncertainty should be discussed in the following section.

2.3.7 Data uncertainty – precision, bias, and representativity

In this section data uncertainty should, if possible, be discussed in terms of precision, bias, and representativity, in the context of their application in this safety assessment. Such uncertainty is associated both with the acquisition of data, for example in the site investigations, and subsequent refinement of data, for example in the site-descriptive modelling. Data uncertainty includes neither conceptual uncertainty nor natural variability.

If comprehensive discussions on these matters are documented elsewhere, such documents should be referred to, and a short summary of the discussion will suffice. The supplier should begin with discussing the precision of the supplied data. To the extent possible, data spread due to precision should be separated from data spread due to natural variability. Precision issues are both associated with the method used in acquiring the raw data and subsequent interpretation of data. Concerning acquiring raw data, limitations in precision are not only associated with the equipment and method used when performing the measurements, but also with the sampling procedure, sample preparation, etc. Precision issues associated with interpretation of the data depend to a large degree on the procedure used and should be discussed at the discretion of the supplier. As an example, it may not be straightforward to estimate the precision of data that are a function of other acquired data, with their intrinsic limitations in precision.

Thereafter, the supplier representative should discuss the bias of the supplied data. Similar considerations apply as when discussing precision, both for bias associated with the acquisition of raw data and with their subsequent interpretation. Bias in observed data is often associated with the method used for acquiring data and its calibration, and with effects of sample preparation. Bias is also associated with the sampling procedure, sample size, and differences in conditions for example between those in the laboratory and in situ. Bias issues associated with data interpretation depend to a large degree on how the interpretation is made and should be discussed at the discretion of the supplier representative.

Finally, the supplier representative should discuss the representativity of the supplied data, both in terms of data acquisition, and data interpretation and refinement. Issues associated with the representativity of acquired data often concern the sampling procedure, the sample size relative to natural variability and correlation length, and differences in conditions between, for example, those in the laboratory and in situ.

An important issue is whether the data are generic or site and/or technique specific. In the case of access to generic data only, the supplier should discuss whether, and to what degree, the lack of site and/or technique-specific data influences the data uncertainty. Representativity issues associated with data interpretation and refinement depend much on the specific interpretation and refinement process and should be discussed at the discretion of the supplier representative.

As well known, the precision, bias, and degree of representativity often depend on a mixture of the above-suggested sources of data uncertainty and may not be easily separated. However, the supplier representative is asked to reflect carefully on these issues, as an assessment of data uncertainty is crucial in data qualification. If data uncertainty cannot be discussed in terms of precision, bias, and representativity, for example as the resolution in data does not allow for such separation, it will suffice to provide a general data uncertainty discussion.

Comprehensible illustrations of different data sets are of high value. The objective of the illustrations is not necessarily to provide a detailed basis and description of the numerical values of the individual data. Sometimes the objective may be to give the reader an understanding of how much, and in what ways, the data vary and the data sets differ from each other. An example of presenting different data sets is given in Figure 2-2, where the reader can get an immediate perception about differences between the data sets. Examples of other illustrations of data sets are given in Figure 2-3 in Section 2.3.10.

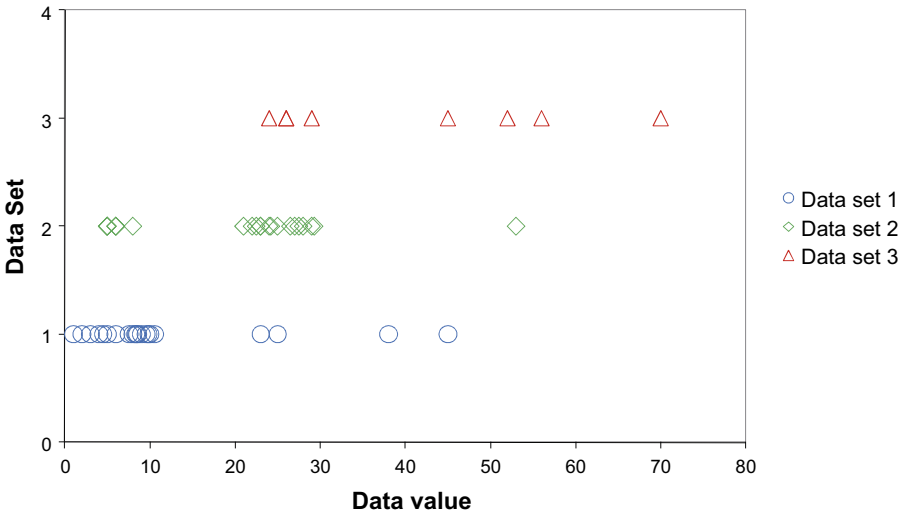

Figure 2-2. *Example of presenting differences in data sets.*

2.3.8 Data uncertainty – spatial and temporal variability

In this section the supplier should discuss the spatial and temporal variability of the subject area parameters. The natural variability should as far as possible be separated from data uncertainty, discussed in the above section.

The supplier should describe what is known about the spatial variation, sometimes referred to as heterogeneity, of the subject area data. This may result in different data sets for different volumes or elements of the repository system, or for different time periods. If comprehensive discussions on the natural variability are documented elsewhere, such documents should be referred to and a short summary of the natural variability will suffice.

In the process of describing the spatial variability, it may be helpful to reflect on the following line of questions.

- Is there spatial variability of the data, and if so, is it of consequence for the safety assessment?
- Is the spatial variability scale dependent? If so, can an appropriate approach of upscaling to safety assessment scale be recommended?
- What is known about correlation lengths from, for example, variograms?
- Can the spatial variability be represented statistically as a mean of data qualification and, if so, how is this done?
- Is there any information about the uncertainty in the spatial variability?

In the process of describing the temporal variability, it may be helpful to reflect on the following line of questions.

- Is there temporal variability of the data, and if so is it of consequence for the safety assessment?
- What processes affect the temporal variability of the data and how is the temporal variability correlated with these processes?
- Does the temporal variability follow any pattern, for example a cyclic pattern?
- Could the temporal variability be represented statistically as a mean of data qualification and if so, how is this done?
- Is there any information about the uncertainty in the temporal variability?

In addition, other relevant issues concerning the natural variability may be addresses at the discretion of the supplier. Comprehensible illustrations of different data sets from different volumes, elements, or time periods are of high value.

2.3.9 Data uncertainty – correlations

An appropriate treatment of probabilistic input data requires that any correlations and functional dependencies between those data are identified and quantified. In the extensive work with the FEP database and the process reports, many correlations and functional dependencies between parameters have been identified. Where appropriate, these correlations and functional dependencies should also be implemented in the safety assessment models. It should be an aim to aid those performing probabilistic modelling, by giving well defined and usable information on how to handle correlations between input data.

Correlations and functional dependencies may also have been used when acquiring, interpreting, and refining data. For example, concerning sorption coefficients, data have not been acquired for all relevant radionuclides. For chemical species for which there is a lack in observations, the supplied sorption coefficient will have been estimated from data obtained for one or more analogue species. This has implications for how to correlate input data in stochastic safety assessment modelling.

In this section the supplier representative is requested to reflect on the following questions:

- For the subject area data, are there correlations or functional dependencies between parameters of the same or of different subject areas? If so, account for these and if possible assess their consequences for the safety assessment.
- If correlations have been used in acquiring, interpreting, and refining data, how was this done? Furthermore, is the outcome based solely upon correlations, or on both measurements and correlations?
- If the data vary in space and time – is anything known about its autocorrelation structure?
- Is there any other reason (apart from already cited correlations and functional dependencies) to suspect correlations between parameters considered as input to the safety assessment modelling?

2.3.10 Results of supplier's data qualification

In this section the supplier is requested to present data that are considered to be appropriate as a basis for suggesting input data for use in the safety assessment. Comprehensive information relating to each parameter requested in the bullet list under the heading "Defining the data requested from the supplier" (cf Section 2.3.1) should be given. Only one set of data should be delivered for each specified condition, volume, element, time period, etc.

The general process of reducing and interpreting data, valuing different data sets, and finally selecting the recommended data for delivery to the assessment team should be fully accounted for, if not already accounted for in the previous sections or in supporting documents. In the latter case, it is sufficient to briefly summarise the process of selecting the delivered data.

If the data presented in supporting documents need reinterpretation and further refinement, in the light of this instruction and/or other information, this should be fully documented. If the supporting documents give more than one data set for a specified condition, volume, element, time period, etc further data reduction is required. Such data reduction may include the merging of data sets, and there may be a need to give different weight to different data sets. Much weight should be given to peer-reviewed data judged as representative for the SFR site and repository system. Generally, more weight should be given to qualified data than to supporting data. The degree to which the data are representative in the context of their application in the safety assessment should also be a factor in the weighting. Exactly how much weight should be given to individual data sets must be decided upon by the supplier. The process of further reinterpretation, refinement, and data reduction should be fully documented. If it increases the readability of the text to also utilise other sections for such documentation, this is allowed. Also, if this requires much space, some information may be appended.

The data sets that the supplier recommends to the assessment team should be in the form of single point values, probability distributions, mean or median values with standard deviations, percentiles, ranges, or as otherwise appropriate. If the data have significant variability and/or uncertainty, the spread in data could be described as a range. However, the meaning of the range has to be provided, e.g. does it represent all possible values, all "realistically possible" values or just the more likely values? The supplier may provide more than one range, representing different probabilities, as exemplified below:

- The range wherein the likelihood of finding the data is high.
- The range for which the likelihood of finding the data outside this range is very low.

All data should be recommended in the context of input data to safety assessment modelling, wherefore the final uncertainty estimate should encompass conceptual modelling uncertainty and data uncertainty (cf Section 2.3.6 to Section 2.3.9). If the supplier representative has used a mathematical expression to account for the uncertainty and natural variability, this expression should be provided and justified.

If the data are suggested to be described by a well-defined probability distribution, it should be justified on statistical grounds that the data indeed are (sufficiently well) distributed accordingly. The usage of standard deviation is often perceived to imply that the data are normally distributed; even through the definition of standard deviation is unrelated to a specific probability distribution. Therefore, when giving the standard deviation, it should be remarked upon whether or not the normal distribution appropriately describes the data. If there are obvious differences between how the data set is actually distributed, and the probability distribution (or range) finally recommended, the reasons for, and implications of, this should be discussed. Outliers should not be dismissed without justification.

It should be noted that in many cases, at some stage probability distributions must be assigned to numerical data being the input to probabilistic safety assessment modelling. If the supplier feels inadequate to deliver a defined distribution, but for example delivers a best estimate, an upper, and a lower limit for data, it may fall on the assessment team to transform such information into probability distributions. This is justified as the assessment team may have a better understanding of how the shape of the assigned distributions (especially in their tails) affects the assessment results. The assessment team may also, in some cases, have a better understanding of the underlying statistics of the suggested distribution.

The above instructions are not applicable to all data, as all data are not necessarily in the form of numerical values. Examples are exit locations for groundwater flowpaths, given as co-ordinates, or information on solubility limiting phases, given as chemical species and reactions.

For a spatially varying function well described by a given stochastic process, e.g. through a variogram or as realised in a Discrete Fracture Network, a potential statement may be that all realisations of this spatially varying function are equally probable.

Finally, it may be impossible to express the uncertainty by other means than a selection of alternative data sets. There are several uncertainties that cannot be managed quantitatively in any other rigorous manner, from the point of view of demonstrating compliance, than by pessimistic assumptions. This is allowed, as long as the supplier clearly documents this together with the justification for adopting this approach.

Comprehensible illustrations and tables of the suggested data sets are of high value. In Figure 2-3 three examples (a, b and c) of representations of recommended data are given.

For data which are impractical to tabulate in the report (for example the co-ordinates of thousands of exit locations for groundwater flowpaths), it is sufficient to precisely refer to a SKB database or equivalent.

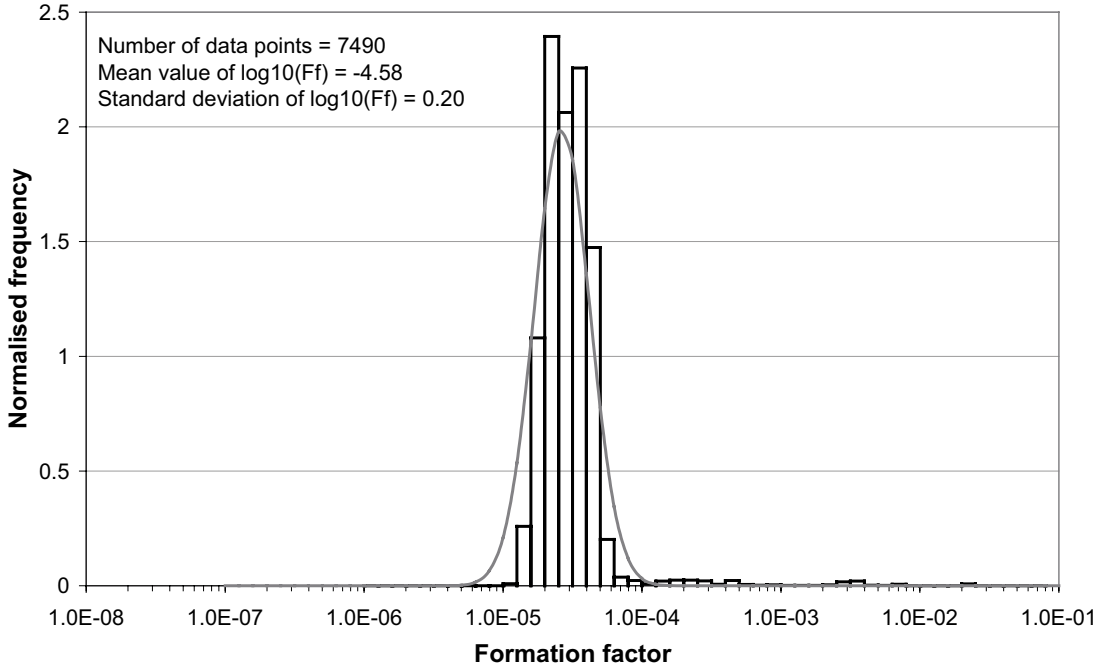

a

b

Nuclide/redox state		Non-saline K_d (m^3/kg)
Ni(II)[1]	best estimate	1.2×10^{-1}
	$K_{d,25\%} - K_{d,75\%}$	$5.5\times10^{-2} - 3.0\times10^{-1}$
	$K_{d,low} - K_{d,high}$	$1.8\times10^{-2} - 5.4\times10^{-1}$
Sr(II)[1]	best estimate	1.3×10^{-2}
	$K_{d,25\%} - K_{d,75\%}$	$6.5\times10^{-3} - 4.1\times10^{-2}$
	$K_{d,low} - K_{d,high}$	$1.0\times10^{-3} - 6.1\times10^{-1}$

c

	Limiting specie	Reaction
Ag(0)	Ag(s)	$Ag(s)+H^{+}+0.25O_2 = Ag^{+}+0.5H_2O$
Ag(I)	AgCl(cr)	$AgCl(cr) = Ag^{+}+Cl^{-}$
Am(III)	$Am(OH)_3(am)$	$Am(OH)_3(am)+3H^{+} = Am^{+3}+3H_2O$

Figure 2-3. *Examples of representations of recommended data, taken from the SR-Can Data report (SKB TR-06-25).*

2.3.11 Judgements by the assessment team

In this section, the customer representative, on behalf of the assessment team, should document the examination of the delivery provided by the supplier, and make judgment on the data qualification. This text should be produced in close cooperation with persons of the assessment team with special knowledge and responsibility. In the case of unresolved issues, the final phrasing should be decided upon by the assessment team. Comments should be made on all the sections listed below:

Sources of information and documentation of data qualification.

- Conditions for which data are supplied.
- Conceptual modelling uncertainty.
- Data uncertainty – precision, bias, and representativity.
- Data uncertainty – spatial and temporal variability.
- Data uncertainty – correlations.
- Results of supplier's data qualification.

Concerning the section "Sources of information and documentation of data qualification" the customer should judge if appropriate documents are referenced, and if the categorisation of data sets into qualified or supporting data is adequately performed and justified.

Concerning the section "Conditions for which data are supplied" the customer should focus upon whether the conditions given by the supplier are relevant for the modelling. If not, it should be stated how this is handled in the safety assessment (for example by extrapolating data, using generic data, or assuming pessimistic values) and what degree of uncertainty such a procedure induces.

Concerning the section "Conceptual modelling uncertainty" the customer should judge whether the discussion provided by the supplier is reasonable and sufficiently exhaustive. If the customer sees the need to include additional sources of conceptual uncertainty, such should be described and if possible quantified. Finally, where necessary the impact of the conceptual uncertainty on the assessment should be discussed, as well as how conceptual uncertainty is handled in the safety assessment modelling (for example by applying pessimistic adjustment factors to the data).

Concerning the section "Data uncertainty – precision, bias, and representativity", the customer should make a judgment on the account provided by the supplier. Also, if the customer sees the need to include additional sources of data uncertainty, these should be described and if possible quantified. If necessary, the impact of the data uncertainty on the assessment should be discussed, as well as how data uncertainty is handled in the safety assessment modelling (for example by applying data uncertainty distributions or using adjustment factors for the data).

Concerning the section "Data uncertainty – spatial and temporal variability" the customer should focus upon whether the spatial and temporal variability are adequately characterised and whether they are of relevance for the safety assessment modelling. Also, if the customer sees the need to include additional sources of spatial and temporal variability, such should be described and if possible quantified. If necessary, the impact of the spatial and temporal variability on the assessment should be discussed, as well as how this is handled in the safety assessment modelling (for example by applying data distributions or different data for different model times and volumes).

Concerning the section "Data uncertainty – correlations" the customer should scrutinise the correlations and functional relationships suggested by the supplier. Also, if correlations other than those suggested by the supplier are identified in the safety assessment programme (for example in Process reports) these should be briefly described where necessary. If appropriate, a summary should be provided concerning which correlations are of actual importance for safety assessment modelling and results.

Concerning the section "Result of data qualification" the customer should make judgement on the choice of data by the supplier, based on scientific adequacy, usefulness for the safety assessment, and the data qualification process. Comments should be made on the delivered estimates of data uncertainty and natural variability, as well as on the data reinterpretation/refinement/reduction process. Furthermore, the delivered distributions, data ranges, etc should be scrutinised from a statistical point

of view. It should be judged whether the suggested way of representing data, for example by a log-normal distribution, is adequate for the safety assessment modelling. If the assessment team chooses to promote other data than those suggested by the supplier, the choice should be fully documented.

For all the sections listed above, supplier statements or supplied data believed to be extra uncertain, dubious, or even erroneous should be highlighted by the customer. These matters should be raised with the supplier and, if possible, resolved and accounted for in this section.

2.3.12 Data recommended for use in the assessment

The main delivery of the **Data report** to the safety assessment modelling is recommendations of data that generally are numerically well defined. Such recommended data should be given in this section.

Based on all the available information, but also on the needs from the safety assessment modelling, the customer representative and assessment team should make a final choice of data in form of single point values or well-defined probability distributions, encompassing natural variability, data uncertainty and other uncertainty. These data should be clearly tabulated (or otherwise presented) in this section. Alternatively, precise referencing to tables or equivalent in the previous section can be made. For data which are impractical to tabulate in the report it is sufficient to precisely refer to a database or equivalent.

Also, short guidelines for how to use the data in subsequent modelling should be given, as required. Justifications and guidelines should be kept short so that this section mainly contains tabulated data that are easily extractable for the safety assessment modelling.

3 Radionuclide decay

The radionuclide inventory of the SFR repository relates to a large number of radionuclides. However, most of them do not have any significant consequences for a safety assessment, as they do not have a long enough half-life, large enough radiotoxicity, and/or produce decay products with the above attributes.

As the result of nuclear decay, the inventory of radionuclides SFR will change over time. The nuclear decay will also influence which radionuclides that will result in any significant dose once released from the repository. The half-lives of the radionuclides are therefore needed in all the parts of the safety assessment.

3.1 Modelling in this safety assessment

This section describes what data are expected from the supplier, and in what modelling activities the data are to be used.

Defining the data requested from the supplier

- The half-lives, $t_{1/2}$ (y).

In the SR-PSU Data report (SKB TR-14-10) it was concluded that the half-life uncertainties were too small to be significant in the safety assessment context. Hence, half-life uncertainties are not requested from the supplier except for some radionuclides that are reported to have larger uncertainties. These radionuclides are Ni-59, Se-79, Mo-93, Ag-108m and Sn-126.

Modelling activities in which data will be used

Half-lives are used in the radionuclide transport (near-field, geosphere and biosphere) and dose modelling, as the inventory will constantly evolve due to the nuclear decay.

Half-lives were also used for predicting the radionuclide inventory of the repository at closure (SKB R-18-07). The half-lives used for predicting the initial radionuclide inventory were those recommended in the SR-PSU Data report (SKB TR-14-10), i.e. taken from Firestone et al. (1998) except for Ag-108m from Schrader (2004) and Se-79 from Jörg et al. (2010).

3.2 Experience from previous safety assessments

This section briefly summarises experience from previous safety assessments, especially the SR-PSU and SAR-08 safety assessments, which may be of direct consequence for the data qualification in this report.

Modelling in previous safety assessments

In previous safety assessments the radionuclide half-lives were required in the same modelling activities as in the present assessment.

In SR-PSU, half-lives were used to calculate the inventory at repository closure (SKB R-15-15) and in the radionuclide transport and dose calculations in the near-field, geosphere and biosphere (SKB TR-14-09).

In SAR-08, half-lives were used in both inventory calculations (Almkvist and Gordon 2007), predicting the inventory of the selected radionuclides in the repository at the time of closure, in the radionuclide transport calculations in the near-field and geosphere (Thomson et al. 2008), and in the biosphere radionuclide transport and dose calculations (Bergström et al. 2008).

Conditions for which data were used in previous safety assessments

No special conditions for half-life data were used in previous assessments.

Sensitivity of assessment results in previous safety assessments

No sensitivity analyses with regard to the half-lives were performed in previous safety assessments.

Alternative modelling in previous safety assessments

No alternative modelling with regard to the half-lives was performed in previous safety assessments.

Correlations used in previous safety assessment modelling

Many of the radionuclides are correlated through decay chains. No other correlation with regard to the half-lives is present.

Identified limitations of the data used in previous safety assessment modelling

The data recommended for use in the SR-PSU (SKB TR-14-10) were from more than one reference and the main reference Firestone et al. (1998) is outdated. From the quality assurance perspective, it is preferable to use data from one consistent source. More recent data are available for two radionuclides of importance for the post-closure safety, Ni-59 and Mo-93, and hence need to be scrutinised.

Between SAR-08 and SR-PSU, results of new measurements of the half-lives of the radionuclides Ag-108m and Se-79 were published. These articles reported decay times differing from the ones reported in Firestone et al. (1998) by one order of magnitude with regards to Se-79, and by around twenty years with regard to Ag-108m. Hence, the half-lives of Ag-108m and Se-79 were changed in SR-PSU compared with SAR-08. The half-lives of these two radionuclides and that of Sn-126 are still being focused on by the scientific community and are hence further scrutinised in this report.

3.3 Supplier input on use of data in this and previous safety assessments

The supplier agrees with the general approach of the previous safety assessments when considering conditions and uncertainties. However, the supplier recommends that the assessment team use harmonised half-life data in all modelling activities. Therefore, the recommended data below should be used in as many modelling activities as possible.

3.4 Sources of information and documentation of data qualification

Sources of information

The data in ICRP Publication 107 (ICRP 2008) is used in calculations of published dose coefficients for the intake of or exposure to radionuclides in the workplace and the environment. Hence, using decay data from ICRP (2008) implies consistency with the dose coefficients used. In ICRP Publication 107 (ICRP 2008), the Commission provides an electronic database of the physical data needed in calculations of radionuclide-specific protection and operational quantities. This database supersedes the data of ICRP Publication 38 (ICRP 1983).

In the section describing data uncertainty, Section 3.7, half-lives for Ni-59, Se-79, Mo-93, Ag-108m and Sn-126 are scrutinised.

The sources of information are given in Table 3-1.

Categorising data sets as qualified or supporting data

Table 3-2 shows qualified and supporting data sets used in the qualification for this section.

Excluded data previously considered as important

As explained above, it is preferable to have one consistent source for the half-life values. The half-lives in the previous used source, Firestone et al. (1998), are however the same as in the new source for many radionuclides (exactly the same for more than half of the radionuclides defined in the inventory). The half-lives used in SR-PSU for Ag-108m from Schrader (2004) and Se-79 from Jörg et al. (2010) are scrutinised together with more recent studies, see Section 3.7.

Table 3-1. Main sources of information used in data qualification.

Sources of information
ICRP, 2008. Nuclear decay data for dosimetric calculations. Oxford: Pergamon. (ICRP Publication 107; Annals of the ICRP 38(3)).
A few peer reviewed scientific publications from the open literature, as referred to in the present text.

Table 3-2. Qualified and supporting data sets.

Qualified data sets	Supporting data sets
ICRP, 2008. Nuclear decay data for dosimetric calculations. Oxford: Pergamon. (ICRP Publication 107; Annals of the ICRP 38(3)).	Several data taken from scientific publications as referred to in Tables 3-3 to 3-7

3.5 Conditions for which data are supplied

The half-lives of radionuclides are not affected by external conditions such as temperature, pressure, chemical conditions and magnetic or electrical fields and therefore are valid under all conditions of the assessment.

3.6 Conceptual modelling uncertainty

Radioactive decay has been thoroughly studied experimentally over a long period of time. The theoretical understanding of the process is good and sufficient for the needs of the safety assessment. No conceptual uncertainties are therefore reported.

3.7 Data uncertainty – precision, bias, and representativity

Even though the half-lives of many radionuclides are known with good accuracy, some are still not precisely known. This knowledge gap concerns especially isotopes close to the line of stability, but it also includes isotopes with medium or long half-lives that are readily produced within nuclear facilities. Five radionuclides, for which the half-lives are still being studied and updated, are briefly discussed below.

Ni-59

The only direct measurement for the half-life of Ni-59 was performed by Nishiizumi et al. (1981) and was reported to be $7.6 \pm 0.5 \times 10^4$ years. This was the value used in SR-PSU (SKB TR-14-10). Some other indirect measurements have been performed, see Table 3-3, for example relative measurements using the thermal Fe-54 neutron capture cross section resulted in a reported value

of $1.08 \pm 0.13 \times 10^5$ years (Rühm et al. 1994). Using more recent available data for cross sections and Kα yield, the value by Rühm et al. (1994) was recalculated to be to $9.7 \pm 0.9 \times 10^4$ years by Wallner et al. (2008). The value recommended for use in the PSAR is 1.01×10^5 years (ICRP 2008).

Table 3-3. Ni-59 half-life from scientific publications.

Half-life (years)	Source
$7.6 \pm 0.5 \times 10^4$	Nishiizumi et al. 1981
$1.08 \pm 0.13 \times 10^5$	Rühm et al. 1994
$9.7 \pm 0.9 \times 10^4$	Wallner et al. 2008

Mo-93

The half-life of Mo-93 in ICRP (2008) recommended for use in the PSAR is 4 000 years and is the same as recommended in SR-PSU (SKB TR-14-10). However, the currently accepted half-life of 4 000 ± 800 years is regarded as tentative and carrying a significant uncertainty since it is not directly measured but determined from yields of nuclear reactions (Dmitriev et al. 1967). Recently the first direct determination of the Mo-93 half-life was published (Kajan et al. 2021). The result of this study was a half-life of 4 839 ± 63 years, see Table 3-4.

Table 3-4. Mo-93 half-life from scientific publications.

Half-life (years)	Source
4 000 ± 800	Dmitriev et al. 1967
4 839 ± 63	Kajan et al. 2021

Se-79

The half-life of the relatively stable isotope Se-79 is, even though several studies in radioactive waste context have been performed, still being debated in the scientific community. Later studies have been able to narrow the half-life to a range between about 1×10^5 and 11×10^5 years, see Table 3-5. There is also the value on which the Decay data evaluation project (DDEP) working group base their recommendation (consult e.g. Helmer et al. (2002) for participants of DDEP). The recommended DDEP value for the Se-79 half-life ($3.56 \pm 0.40 \times 10^5$ years) is not a measured value but a weighted average of the two latest reported values available, at the time, in the open literature.

The values in Table 3-5 shows that the half-life is stabilising at a value around 2.80×10^5 to 3.80×10^5 years. In the SR-PSU (SKB TR-14-10) the value recommended for use was 327 000 years reported by Jörg et al. (2010). The half-life recommended for used in the PSAR from (ICRP 2008) is 295 000 years.

Table 3-5. Se-79 half-life from scientific publications.

Half-life (years)	Source
$4.8 \pm 0.4 \times 10^5$	Yu et al. 1995
$1.1 \pm 0.2 \times 10^6$	Jiang et al. 1997
$1.24 \pm 0.19 \times 10^5$	He et al. 2000
$2.95 \pm 0.38 \times 10^5$	Jiang et al. 2001
$2.80 \pm 0.36 \times 10^5$	He et al. 2002
$3.77 \pm 0.19 \times 10^5$	Bienvenu et al. 2007
$3.27 \pm 0.08 \times 10^5$	Jörg et al. 2010
$2.78 \pm 0.18 \times 10^5$	Liang et al. 2014

Ag-108m

The large differences between the measured half-lives of Ag-108m as well as the large uncertainties reported, see Table 3-6, indicate the difficulty in determine this half-life. The half-life of Ag-108m is still being studied in the scientific community and new data are successively being published. The half-life recommended to be used in the PSAR, 418 years, from ICRP Publication 107 (ICRP 2008) is, as can be seen in Table 3-6, based on the measurements by Schötzig et al. (1992).

Table 3-6. Ag-108m half-life from scientific publications.

Half-life (years)	Source
310 ± 132	Vonach et al. 1969
127 ± 21	Harbottle 1970
418 ± 15	Schötzig 1992
437.7 ± 8.8	Schrader 2004
448 ± 27	Shugart et al. 2018

Sn-126

The old established approximate value of 100 000 years was used for the half-life of Sn-126 in SR-PSU. The half-life recommended to be used in the PSAR, 230 000 years, from ICRP (2008) is based on more recent data, see Table 3-7.

Table 3-7. Sn-126 half-life from scientific publications.

Half-life (years)	Source
$2.07 \pm 0.21 \times 10^5$	Haas et al. 1996
$2.5 \pm 0.2 \times 10^5$	Zang et al. 1996
$2.33 \pm 0.10 \times 10^5$	Catlow et al. 2005

3.8 Data uncertainty – spatial and temporal variability

Spatial variability of data

Not relevant.

Temporal variability of data

Not relevant.

3.9 Data uncertainty – correlations

Radionuclides as decay parents and daughters are correlated through decay chains. No other relevant correlations have been reported.

3.10 Result of supplier's data qualification

The half-lives, taken from ICRP Publication 107 (ICRP 2008), for radionuclides present in the Inventory report (SKB R-18-07) and their decay products are reported in Table 3-8.

Table 3-8. Half-lives recommended for use in the PSAR. Data taken from ICRP Publication 107 (ICRP 2008) are given in y = years, m = months, d = days, h= hours or s = seconds. The half-lives have also been recalculated to the unit years.

Radionuclide	Half-life	Unit	Half-life (y)	Radionuclide	Half-life	Unit	Half-life (y)
Ac-225	10	d	2.74×10^{-2}	Pb-210	22.2	y	2.22×10^{1}
Ac-227	21.772	y	2.18×10^{1}	Pb-211	36.1	m	6.86×10^{-5}
Ac-228	6.15	h	7.02×10^{-4}	Pb-212	10.64	h	1.21×10^{-3}
Ag-108	2.37	m	4.51×10^{-6}	Pb-214	26.8	m	5.10×10^{-5}
Ag-108m	418	y	4.18×10^{2}	Pd-107	6 500 000	y	6.50×10^{6}
Am-241	432.2	y	4.32×10^{2}	Pm-147	2.6234	y	2.62×10^{0}
Am-242	16.02	h	1.83×10^{-3}	Po-210	138.376	d	3.79×10^{-1}
Am-242m	141	y	1.41×10^{2}	Po-211	0.516	s	1.64×10^{-8}
Am-243	7 370	y	7.37×10^{3}	Po-212	0.000000299	s	9.47×10^{-15}
At-217	0.0323	s	1.02×10^{-9}	Po-213	0.0000042	s	1.33×10^{-13}
At-218	1.5	s	4.75×10^{-8}	Po-214	0.0001643	s	5.21×10^{-12}
At-219	56	s	1.77×10^{-6}	Po-215	0.001781	s	5.64×10^{-11}
Ba-133	10.52	y	1.05×10^{1}	Po-216	0.145	s	4.59×10^{-9}
Ba-137m	2.552	m	4.85×10^{-6}	Po-218	3.1	m	5.89×10^{-6}
Be-10	1 510 000	y	1.51×10^{6}	Pu-238	87.7	y	8.77×10^{1}
Bi-210	5.013	d	1.37×10^{-2}	Pu-239	24 110	y	2.41×10^{4}
Bi-211	2.14	m	4.07×10^{-6}	Pu-240	6 564	y	6.56×10^{3}
Bi-212	60.55	m	1.15×10^{-4}	Pu-241	14.35	y	1.44×10^{1}
Bi-213	45.59	m	8.67×10^{-5}	Pu-242	375 000	y	3.75×10^{5}
Bi-214	19.9	m	3.78×10^{-5}	Ra-223	11.43	d	3.13×10^{-2}
Bi-215	7.6	m	1.44×10^{-5}	Ra-224	3.66	d	1.00×10^{-2}
C-14	5 700	y	5.70×10^{3}	Ra-225	14.9	d	4.08×10^{-2}
Ca-41	102 000	y	1.02×10^{5}	Ra-226	1 600	y	1.60×10^{3}
Cd-113	7.7×10^{15}	y	7.70×10^{15}	Ra-228	5.75	y	5.75×10^{0}
Cd-113m	14.1	y	1.41×10^{1}	Rn-218	0.035	s	1.11×10^{-9}
Cl-36	301 000	y	3.01×10^{5}	Rn-219	3.96	s	1.25×10^{-7}
Cm-242	162.8	d	4.46×10^{-1}	Rn-220	55.6	s	1.76×10^{-6}
Cm-243	29.1	y	2.91×10^{1}	Rn-222	3.8235	d	1.05×10^{-2}
Cm-244	18.1	y	1.81×10^{1}	Sb-125	2.75856	y	2.76×10^{0}
Cm-245	8 500	y	8.50×10^{3}	Sb-126	12.35	d	3.38×10^{-2}
Cm-246	4 760	y	4.76×10^{3}	Sb-126m	19.15	m	3.64×10^{-5}
Co-60	5.2713	y	5.27×10^{0}	Se-79	295 000	y	2.95×10^{5}
Cs-134	2.0648	y	2.06×10^{0}	Sm-147	1.06×10^{11}	y	1.06×10^{11}
Cs-135	2 300 000	y	2.30×10^{6}	Sm-148	7×10^{15}	y	7.00×10^{15}
Cs-137	30.1671	y	3.02×10^{1}	Sm-151	90	y	9.00×10^{1}
Eu-152	13.537	y	1.35×10^{1}	Sn-126	230 000	y	2.30×10^{5}
Eu-154	8.593	y	8.59×10^{0}	Sr-90	28.79	y	2.88×10^{1}
Eu-155	4.7611	y	4.76×10^{0}	Tc-99	211 100	y	2.11×10^{5}
Fe-55	2.737	y	2.74×10^{0}	Te-125m	57.4	d	1.57×10^{-1}
Fr-221	4.9	m	9.32×10^{-6}	Th-227	18.68	d	5.11×10^{-2}
Fr-223	22	m	4.18×10^{-5}	Th-228	1.9116	y	1.91×10^{0}
Gd-152	1.08×10^{14}	y	1.08×10^{14}	Th-229	7 340	y	7.34×10^{3}
H-3	12.32	y	1.23×10^{1}	Th-230	75 380	y	7.54×10^{4}
Hg-206	8.15	m	1.55×10^{-5}	Th-231	25.52	h	2.91×10^{-3}
Ho-166m	1 200	y	1.20×10^{3}	Th-232	14 050 000 000	y	1.41×10^{10}
I-129	15 700 000	y	1.57×10^{7}	Th-234	24.1	d	6.60×10^{-2}
In-115	4.41×10^{14}	y	4.41×10^{14}	Tl-206	4.2	m	7.99×10^{-6}
Mo-93	4 000	y	4.00×10^{3}	Tl-207	4.77	m	9.07×10^{-6}
Nb-93m	16.13	y	1.61×10^{1}	Tl-208	3.053	m	5.80×10^{-6}
Nb-94	20 300	y	2.03×10^{4}	Tl-209	2.161	m	4.11×10^{-6}
Nd-144	2.29×10^{15}	y	2.29×10^{15}	Tl-210	1.3	m	2.47×10^{-6}
Ni-59	101 000	y	1.01×10^{5}	U-232	68.9	y	6.89×10^{1}
Ni-63	100.1	y	1.00×10^{2}	U-233	159 200	y	1.59×10^{5}

Table 3-8. Continued.

Radionuclide	Half-life	Unit	Half-life (y)	Radionuclide	Half-life	Unit	Half-life (y)
Np-237	2 144 000	y	2.14×10^{6}	U-234	245 500	y	2.46×10^{5}
Np-238	2.117	d	5.80×10^{-3}	U-235	704 000 000	y	7.04×10^{8}
Np-239	2.3565	d	6.45×10^{-3}	U-235m	26	m	4.94×10^{-5}
Pa-231	32 760	y	3.28×10^{4}	U-236	23 420 000	y	2.34×10^{7}
Pa-233	26.967	d	7.38×10^{-2}	U-237	6.75	d	1.85×10^{-2}
Pa-234	6.7	h	7.64×10^{-4}	U-238	4 468 000 000	y	4.47×10^{9}
Pa-234m	1.17	m	2.22×10^{-6}	Y-90	64.1	h	7.31×10^{-3}
Pb-209	3.253	h	3.71×10^{-4}	Zr-93	1 530 000	y	1.53×10^{6}

3.11 Judgements by the assessment team

Sources of information

The assessment team considers the sources of information used by the supplier as sufficient.

Conditions for which data is supplied

The assessment team agrees with the supplier regarding the lack of special conditions for half-lives given in Section 3.5.

Conceptual modelling uncertainty

No conceptual uncertainties have been reported by the supplier. The assessment team agrees with this.

Data uncertainty – precision, bias, and representativity

The assessment team agrees with the uncertainties described.

Data uncertainty – spatial and temporal variability

No spatial or temporal variabilities have been reported by the supplier. The assessment team agrees with this.

Data uncertainty – correlations

The supplier has identified correlations in data through the decay chains only. The assessment team agrees.

Results of supplier's data qualification

The supplier has given data on half-lives in Table 3-8. The assessment team accepts the data for all radionuclides.

3.12 Data recommended for use in the assessment

The data presented in Table 3-8 are recommended for use in the safety assessment.

4 Uncertainties in the radionuclide inventory

4.1 Modelling in this safety assessment

Several methods for estimating the radionuclide inventory in SFR have been applied depending on the type and origin of waste, which is described in the Inventory report (SKB R-18-07). Each method is associated with uncertainties. The uncertainties in the radionuclide inventory are handled differently in this safety assessment as compared with the previous assessment and can be divided into two parts. Firstly, a base case radionuclide inventory where methodology uncertainties are handled in a probabilistic manner is estimated. This inventory is further described in Section 4.4. Secondly, three alternative radionuclide inventories representing a selection of changes in operational conditions at the Swedish nuclear power plants are evaluated. These inventories are further described in Section 4.5.

Defining the data requested from the supplier

- A base case radionuclide inventory where methodology uncertainties are handled in a probabilistic manner.
- Three alternative radionuclide inventories representing a selection of changes in operational conditions at the Swedish nuclear power plants to make it possible to further evaluate the robustness of the repository.

Modelling activities in which data will be used

The data will be used in the radionuclide transport calculations in the main scenario and in a residual scenario, respectively.

4.2 Experience from previous assessments

For the main scenario in the SR-PSU, a best estimate radionuclide inventory was calculated where no uncertainties were considered. This inventory was used in the main scenario. Uncertainties were handled by the high inventory scenario, which contributed to the total risk as a less probable scenario with an estimated probability. The radionuclide inventory for this high inventory scenario was estimated by applying the maximum uncertainty factor to each method for activity estimation used and each radionuclide respectively. This estimate thus represented a total maximum radionuclide inventory.

Correlations used in previous safety assessment modelling

No correlations were used in the previous assessment.

Identified limitations of the data used in previous safety assessment modelling

In the SR-PSU, no probability density functions were constructed to describe the uncertainty in the methods used to estimate the radionuclide inventory. The uncertainties could therefore not be estimated in a probabilistic manner. Other operational events that could result in additional changes in the radionuclide inventory were furthermore not considered.

4.3 Supplier input on use of data in this and previous safety assessments

The supplier finds the methodology for handling of uncertainties in the previous assessment insufficient and requires an alternative method for the handling of uncertainties in this assessment. The methodology developed is thus described in the following sections.

4.4 Base case radionuclide inventory

The radionuclide inventory is compiled from measured activities for each radionuclide and waste package for disposed packages, activities estimated from various models of activity build-up in the different waste types and scaling factors. Probability density functions (PDFs) have been constructed for each method used to estimate the radionuclide inventory. These PDFs are based on information about the uncertainty in the different measurements, amounts of ion-exchange resins in the waste and the applied models as well as the distribution of activity reported for already disposed packages (the latter PDFs are used to estimate the activity in operational waste forecasts). The probabilistic assessment of the uncertainty in the radionuclide inventory is achieved through sampling of these PDFs in Monte Carlo simulations.

For each realisation, the sampling is performed as follows:

- Measured activity is sampled for each measured radionuclide (disposed packages).
- The amount of ion-exchange resins is sampled for each package where present.
- Total activities data that is associated with waste streams rather than specific waste packages (so called non-package-bound data) is sampled for each producer, radionuclide, and waste stream.
- Correlation factor is sampled for each radionuclide and waste package.
- Forecast activity is sampled for each radionuclide and forecasted waste package.

This results in 10 000 samples (or realisations), a thousand of which are propagated into the radionuclide transport calculation. The methodology is described in the Inventory report (SKB R-18-07), where the 5th and 95th percentiles of the 10 000 realisations also are given.

4.5 Alternative radionuclide inventories

In addition to the probabilistic handling of the uncertainties as described in the previous section, three hypothetical alternative inventories representing changes in operational conditions have been created to make it possible to further evaluate the robustness of the repository. The three changes in operational conditions comprise extended operation of the remaining reactors from 60 years to 80 years, increased fuel-damage frequency during the remaining operation and extended use of molybdenum alloy fuel spacers.

Each alternative inventory is briefly described below and the resulting factors that the base case radionuclide inventory are to be multiplied with are given. Also, the waste types that are identified to be affected by the three different changes in operational conditions are listed.

4.5.1 Extended operation of reactors

Extended operation of the remaining reactors from 60 years to 80 years affects only the radionuclide inventory for future waste and sites that are still in operation (including Clab). All radionuclides in both forecast operational waste types as well as decommissioning waste types are assumed to be affected since it can be anticipated that all operational events are expected to occur in the same manner as previously during the prolonged operation time (e.g. activation, fuel damage, contamination etc). The affected waste types are listed in Table 4-1.

Since the activation is a time-linear process and the extended operation time is about one third, an increase of activity of 35 % is chosen for this alternative inventory. The increase in activity should not be applied to waste that has already been disposed in SFR, which is why the activity proportion of disposed waste/forecast waste is considered. This proportion is calculated for each radionuclide and waste vault (Ahlford 2021) based on the radionuclide inventories presented in the Inventory report (SKB R-18-07). Furthermore, the increase in waste volume that a prolonged operation could give rise to is also not considered for simplification. Therefore, it is only the change in radioactivity that is evaluated in this alternative inventory.

The resulting factors that the base case radionuclide inventory is to be multiplied with are presented for each radionuclide and waste vault respectively, see Table 4-2. Since 2BTF is full, no forecasted waste is planned to be disposed in this waste vault and the inventory is hence the same as in the base case.

Table 4-1. Waste types that are affected in the alternative inventory "extended operation of reactors". 2BTF is already full, hence not influenced.

Silo	1BMA	2BMA	1BRT	1BTF	1BLA	2–5BLA
C.02	C.23	C.23	F.23R:D	O.07	F.12	C.12:D
C.16:D	F.17	C.23:D	O.23R:D	O.07:09	O.12	C.12C:D
C.24	F.17:01	F.17	R.23R:D	R.10	O.12:01	C.12M:D
F.18	F.17:02	F.23		R.23	R.12	F.12
F.18:D	F.23	F.23:D			R.12:01	F.12:D
O.02	O.23	F.23C:D				F.12C:D
O.02:09	O.23:09	O.23				F.12M:D
O.16:D	R.10	O.23:D				F.12S:D
R.16	R.15	O.23C:D				O.12
R.16:D	R.23	O.23S:D				O.12:D
R.24	R.29	R.10				O.12C:D
		R.15				O.12M:D
		R.23				O.12S:D
		R.23:D				R.12
		R.23C:D				R.12:D
		R.29				R.12C:D
						R.12M:D
						R.12S:D

Table 4-2. Factors to be multiplied with the base case radionuclide inventory for the alternative inventory "extended operation of reactors". 2BTF is already full, hence not influenced.

Radionuclide	Silo	1BMA	2BMA	1BRT	1BTF	1BLA	2–5BLA
H-3	1.29	1.06	1.35	1.35	1.33	1.05	1.35
Be-10	1.18	1.02	1.34	1.00	1.28	1.03	1.29
C-14(inorg)	1.13	1.04	1.35	1.00	1.25	1.00	1.35
C-14(org)	1.13	1.01	1.35	1.00	1.09	1.00	1.35
C-14(ind)	1.00	1.00	1.35	1.35	1.00	1.00	1.35
Cl-36	1.14	1.00	1.35	1.34	1.03	1.00	1.35
Ca-41	1.00	1.00	1.35	1.00	1.00	1.00	1.35
Fe-55	1.35	1.22	1.35	1.35	1.35	1.08	1.35
Co-60	1.35	1.15	1.35	1.35	1.35	1.06	1.35
Ni-59	1.22	1.01	1.35	1.34	1.17	1.01	1.33
Ni-63	1.24	1.01	1.35	1.34	1.18	1.00	1.34
Se-79	1.15	1.02	1.24	1.00	1.26	1.01	1.34
Sr-90	1.24	1.03	1.32	1.35	1.31	1.04	1.34
Zr-93	1.27	1.02	1.35	1.35	1.28	1.03	1.34
Nb-93m	1.35	1.05	1.35	1.35	1.32	1.04	1.35
Nb-94	1.32	1.01	1.35	1.35	1.28	1.02	1.32
Mo-93	1.27	1.02	1.34	1.35	1.27	1.05	1.14
Tc-99	1.20	1.01	1.16	1.34	1.21	1.01	1.09
Pd-107	1.16	1.02	1.35	1.00	1.26	1.01	1.35
Ag-108m	1.27	1.02	1.35	1.35	1.28	1.01	1.35
Cd-113m	1.27	1.06	1.30	1.00	1.31	1.02	1.34
In-115	1.00	1.00	1.35	1.00	1.00	1.00	1.00
Sn-126	1.21	1.02	1.32	1.35	1.26	1.01	1.35
Sb-125	1.35	1.21	1.35	1.35	1.35	1.02	1.35
I-129	1.15	1.02	1.07	1.00	1.23	1.01	1.24

Table 4-2. Continued.

Radionuclide	Silo	1BMA	2BMA	1BRT	1BTF	1BLA	2–5BLA
Cs-134	1.35	1.24	1.35	1.00	1.35	1.02	1.35
Cs-135	1.14	1.01	1.04	1.00	1.12	1.00	1.33
Cs-137	1.21	1.03	1.27	1.00	1.28	1.02	1.35
Ba-133	1.30	1.08	1.35	1.00	1.33	1.05	1.35
Pm-147	1.35	1.22	1.35	1.35	1.35	1.05	1.35
Sm-151	1.17	1.02	1.30	1.35	1.27	1.01	1.35
Eu-152	1.27	1.06	1.34	1.35	1.23	1.00	1.35
Eu-154	1.31	1.10	1.34	1.35	1.33	1.02	1.35
Eu-155	1.35	1.17	1.35	1.35	1.34	1.04	1.35
Ho-166m	1.18	1.02	1.35	1.00	1.28	1.03	1.34
U-232	1.19	1.01	1.05	1.35	1.18	1.04	1.29
U-234	1.21	1.01	1.15	1.35	1.15	1.03	1.35
U-235	1.15	1.02	1.04	1.35	1.00	1.00	1.19
U-236	1.17	1.01	1.11	1.35	1.19	1.03	1.30
U-238	1.16	1.01	1.17	1.35	1.23	1.00	1.20
Np-237	1.16	1.02	1.11	1.35	1.19	1.02	1.27
Pu-238	1.24	1.01	1.15	1.35	1.09	1.05	1.25
Pu-239	1.18	1.01	1.05	1.35	1.16	1.03	1.24
Pu-240	1.19	1.01	1.33	1.35	1.13	1.04	1.24
Pu-241	1.27	1.04	1.12	1.35	1.28	1.07	1.28
Pu-242	1.19	1.01	1.10	1.35	1.12	1.04	1.24
Am-241	1.16	1.01	1.06	1.34	1.08	1.03	1.23
Am-242m	1.21	1.01	1.13	1.35	1.15	1.03	1.25
Am-243	1.20	1.01	1.12	1.33	1.17	1.01	1.25
Cm-243	1.24	1.02	1.11	1.35	1.20	1.05	1.26
Cm-244	1.29	1.03	1.18	1.35	1.23	1.05	1.28
Cm-245	1.22	1.01	1.16	1.35	1.14	1.02	1.26
Cm-246	1.23	1.01	1.18	1.35	1.16	1.03	1.27
H-3-act_steel				1.35			
C-14(ind)-act_steel				1.35			
Cl-36-act_steel				1.34			
Fe-55-act_steel				1.35			
Co-60-act_steel				1.35			
Ni-59-act_steel				1.34			
Ni-63-act_steel				1.34			
Nb-93m-act_steel				1.35			
Nb-94-act_steel				1.35			
Mo-93-act_steel				1.35			
Tc-99-act_steel				1.34			
Sb-125-act_steel				1.35			

4.5.2 Increased fuel-damage frequency

Increased fuel-damage frequency during the remaining operation affects only the radionuclide inventory for future waste and sites that are still in operation (including Clab). Radionuclides present in fuel (fission products and transuranic radionuclides) in both forecast operational waste types as well as decommissioning waste types are assumed to be affected. The affected waste types are listed in Table 4-3 and the radionuclides that are considered are listed in Table 4-4.

For this alternative inventory, the activity is chosen to be increased by a factor of 10. This factor is cautiously selected corresponding to a substantial change in how the reactors are operated today. The increase in activity is not applied to waste that has already been disposed in SFR, which is why the activity proportion of disposed waste/forecast waste is considered. This proportion is calculated for each radionuclide and waste vault (Ahlford 2021) based on the radionuclide inventories presented in the Inventory report (SKB R-18-07).

The resulting factors that the base case radionuclide inventory is multiplied with are presented for each radionuclide and waste vault respectively, see Table 4-4. Since 2BTF is full, no forecast waste is planned to be disposed in this waste vault and the inventory is hence the same as in the base case.

Table 4-3. Waste types that are affected in the alternative inventory "increased fuel-damage frequency". 2BTF is already full, hence not influenced.

Silo	1BMA	2BMA	1BRT	1BTF	1BLA	2–5BLA
C.02	C.23	C.23	F.23R:D	O.07	F.12	C.12:D
C.16:D	F.17	C.23:D	O.23R:D	O.07:09	O.12	C.12C:D
C.24	F.17:01	F.17	R.23R:D	R.10	O.12:01	C.12M:D
F.18	F.17:02	F.23		R.23	R.12	F.12
F.18:D	F.23	F.23:D			R.12:01	F.12:D
O.02	O.23	F.23C:D				F.12C:D
O.02:09	O.23:09	O.23				F.12M:D
O.16:D	R.10	O.23:D				F.12S:D
R.16	R.15	O.23C:D				O.12
R.16:D	R.23	O.23S:D				O.12:D
R.24	R.29	R.10				O.12C:D
		R.15				O.12M:D
		R.23				O.12S:D
		R.23:D				R.12
		R.23C:D				R.12:D
		R.29				R.12C:D
						R.12M:D
						R.12S:D

Table 4-4. Factors to be multiplied with the base case radionuclide inventory for the alternative inventory "increased fuel-damage frequency". 2BTF is already full, hence not influenced.

Radionuclide	Silo	1BMA	2BMA	1BRT	1BTF	1BLA	2–5BLA
Be-10	5.51	1.40	9.79	1.00	8.10	1.70	8.39
Se-79	4.86	1.40	7.20	1.00	7.61	1.29	9.86
Sr-90	7.17	1.68	9.31	9.92	8.87	1.92	9.76
Zr-93	8.03	1.40	9.99	9.92	8.10	1.70	9.82
Nb-94	9.10	1.32	10.00	10.00	8.11	1.44	9.35
Tc-99	6.16	1.25	5.16	9.87	6.29	1.25	3.26
Pd-107	5.02	1.40	9.98	1.00	7.61	1.29	9.90
Ag-108m	7.99	1.42	9.99	9.95	8.15	1.21	10.00
Cd-113m	7.88	2.53	8.72	1.00	8.89	1.53	9.77
Sn-126	6.29	1.40	9.21	10.00	7.61	1.29	9.99
Sb-125	10.00	6.53	10.00	10.00	9.99	1.52	10.00
I-129	4.79	1.41	2.77	1.00	6.95	1.19	7.20
Cs-134	10.00	7.28	10.00	1.00	9.98	1.58	10.00
Cs-135	4.54	1.30	2.10	1.00	4.02	1.04	9.57
Cs-137	6.48	1.80	7.99	1.00	8.32	1.40	9.88
Ba-133	8.82	2.93	9.98	1.00	9.54	2.24	9.90
Pm-147	10.00	6.58	10.00	10.00	9.99	2.21	9.99
Sm-151	5.41	1.51	8.77	10.00	7.88	1.32	9.93
Eu-152	7.93	2.60	9.70	10.00	7.03	1.02	9.99
Eu-154	8.99	3.67	9.67	10.00	9.36	1.64	9.99
Eu-155	9.88	5.43	9.98	10.00	9.83	1.91	9.92
U-232	5.87	1.34	2.21	9.91	5.64	2.04	8.57
U-234	6.31	1.25	4.84	9.95	4.86	1.87	9.94
U-235	4.77	1.41	2.08	9.95	1.00	1.12	5.86
U-236	5.33	1.17	3.92	9.95	5.86	1.89	8.70

Table 4-4. Continued.

Radionuclide	Silo	1BMA	2BMA	1BRT	1BTF	1BLA	2–5BLA
U-238	5.21	1.31	5.32	9.96	6.96	1.01	6.16
Np-237	5.17	1.47	3.85	9.93	5.98	1.54	7.85
Pu-238	7.23	1.31	4.81	9.97	3.36	2.25	7.41
Pu-239	5.62	1.25	2.26	9.89	5.04	1.81	7.18
Pu-240	5.87	1.25	9.50	9.95	4.38	1.94	7.28
Pu-241	7.94	2.06	4.12	9.96	8.11	2.76	8.32
Pu-242	5.84	1.25	3.53	9.95	3.97	1.98	7.22
Am-241	5.23	1.25	2.62	9.80	3.17	1.74	6.82
Am-242m	6.41	1.29	4.34	9.96	4.86	1.89	7.50
Am-243	6.11	1.28	4.15	9.57	5.29	1.24	7.48
Cm-243	7.10	1.54	3.91	9.95	6.02	2.24	7.80
Cm-244	8.42	1.76	5.52	9.96	6.87	2.35	8.30
Cm-245	6.67	1.25	5.05	9.94	4.48	1.60	7.71
Cm-246	6.99	1.26	5.58	9.96	5.07	1.75	7.94

4.5.3 Extended use of molybdenum alloy fuel spacers

Extended use of molybdenum alloy fuel spacers affects only the radionuclide inventory for future waste from sites with BWRs still in operation as well as Clab. The radionuclide Mo-93 in forecast operational waste types as well as decommissioning waste types is assumed to be affected as listed in Table 4-5.

For this alternative inventory, the activity is chosen to be increased by a factor of 10. This factor is cautiously selected based on that the highest amount of molybdenum alloy fuel spacers used in one cycle of a Swedish reactor so far has been around 20 %. The increase in activity is not applied on waste that has already been disposed in SFR, which is why the activity proportion of disposed waste/forecast waste is considered. This proportion is calculated for Mo-93 in each waste vault (Ahlford 2021) based on the radionuclide inventories presented in the Inventory report (SKB R-18-07). The resulting factors that the base case Mo-93 inventory is to be multiplied with are given for each waste vault in Table 4-6. Since 2BTF is full, no forecast waste is planned to be disposed in this waste vault and the inventory is hence the same as in the base case.

Table 4-5. Waste types that are affected in the alternative inventory "extended use of molybdenum alloy fuel spacers". 2BTF is already full, hence not influenced.

Silo	1BMA	2BMA	1BRT	1BTF	1BLA	2–5BLA
C.02	C.23	C.23	F.23R:D	O.07	F.12	C.12:D
C.16:D	F.17	C.23:D	O.23R:D	O.07:09	O.12	C.12C:D
C.24	F.17:01	F.17			O.12:01	C.12M:D
F.18	F.17:02	F.23				F.12
F.18:D	F.23	F.23:D				F.12:D
O.02	O.23	F.23C:D				F.12C:D
O.02:09	O.23:09	O.23				F.12S:D
O.16:D		O.23:D				F.12M:D
		O.23C:D				O.12
		O.23S:D				O.12:D
						O.12C:D
						O.12S:D

Table 4-6. Factors to be multiplied with base case radionuclide inventory for the alternative inventory "extended use of molybdenum alloy fuel spacers". 2BTF is already full, hence not influenced.

Radionuclide	Silo	1BMA	2BMA	1BRT	1BTF	1BLA	2–5BLA
Mo-93	7.96	1.43	9.65	9.97	8.06	2.28	4.50

4.6 Judgement by the assessment team

The assessment team finds the methodology presented in this chapter to be sufficient for its use in the safety assessment.

4.7 Data recommended for use in the modelling

The base case radionuclide inventory including uncertainties in the form of probability density functions, as given in the Inventory report (SKB R-18-07), are recommended for its use in the main and less probable scenarios.

The three alternative inventories are recommended for their use in calculation cases in a residual scenario to evaluate the robustness of the repository. For the three alternative inventories the factors given in Tables 4-2, 4-4 and 4-6 are recommended to be applied on the base case inventory.

5 Metal corrosion

This chapter describes the corrosion rates of carbon steel and steel alloys in SFR. Corrosion of metals is a fundamental process that leads to property changes in both the metal packaging, reinforcement bars, and metal waste (either non-conditioned or stabilised in concrete). In the modelling, corrosion is mainly important because it governs the incoherent release of induced radioactivity from the segmented reactor pressure vessels that will be disposed in 1BRT. Second, anoxic oxidation of steel sets a low redox potential in the repository until it is fully corroded. Third, anoxic corrosion with water as the oxidant will produce hydrogen gas, which could affect the transport of radionuclides if the gas pressure becomes sufficiently large.

A general description of the corrosion processes is found in the metal-corrosion chapters in the **Waste process report** and the **Barrier process report**.

5.1 Modelling in this safety assessment

Defining the data requested from the supplier

Several parameters affect the corrosion rate, especially environmental factors and the bulk and surface properties of the corroding metal. Corrosion-rate data are applied in all assessment scenarios, but the environmental conditions vary between some of them. The resulting data requested is outlined in Table 5-1, followed by a brief description under respective sub-headings of the most relevant parameters and how their values are expected to evolve over time in SFR.

Table 5-1. Summary of requested corrosion-rate data.

	Carbon steel		**Stainless steel**	
	Oxic (high E_h)	**Anoxic (low E_h)**	**Oxic (high E_h)**	**Anoxic (low E_h)**
Non-passivating (intermediate pH)	Requested	Requested	Requested	-
Passivating (high pH)	Requested	Requested	-	Requested

Type of steel

Steel is generally divided into stainless and carbon steel. For both types, formation of corrosion products on the steel creates a physical barrier on the surface, called passivation (see for example “passivation in electrochemical corrosion” in McNaught and Wilkinson 1997). The corrosion rate is thus limited by the transport of corrosive species through the barrier layer resulting in a decreasing corrosion rate with time, eventually reaching a steady state when the rates of formation and dissolution/removal of corrosion products are balanced. Carbon-steel corrosion products are fairly soluble as long as they are continuously removed and not allowed to saturate the solution. Therefore, steady-state rates for carbon steel are generally higher than those for stainless steel, an inherently passive material in which the corrosion products are insoluble and form a uniformly covering, protective oxide layer on the surface.

Most steel waste in SFR is carbon steel. The reactor pressure vessels destined for 1BRT also consist predominantly of carbon steel, but the stainless-steel fraction is nevertheless significant. Thus, data for both carbon and stainless steel are requested.

pH

Since the anoxic-corrosion chemical reactions involve protons H^+ and/or hydroxide ions OH^- depending on pH, the rates depend strongly on the pH value. Within SFR, all waste vaults contain significant amounts of cementitious materials, mainly concrete, setting a high pH. Thus, corrosion-rate data from experiments conducted in cementitious environments are most relevant. Nevertheless, temporal and spatial variabilities affect the pH (Section 5.8). The pH development in SFR is assessed through modelling (Cronstrand 2014, Höglund 2014, 2018, 2019).

The region of passivating conditions, i.e. formation of protective oxide films, starts at about pH 9 (Figure 5-1). Thus, corrosion-rate data for both pH ≤ 9 and pH ~9–13 are requested from the supplier, respectively.

Redox potential as determined by the presence of oxygen

As evident from Figure 5-1, the most stable corrosion product is determined not only by pH but also by the redox potential E_{SHE} or E_h. Upon repository closure, oxygen from the ventilated operational period remains in significant quantities, setting oxidising conditions (high redox potential E_h). However, these oxygen quantities are quickly depleted through microbially mediated degradation of organic matter and initial corrosion of accessible metals in the repository. Hence, the period of initially oxic conditions is estimated to be on the order of days to months, depending on organic-material availability (Duro et al. 2012), which is so short that it is neglected in the PSAR modelling. Reducing conditions are thus assumed to generally prevail for the full assessment period, with anoxic mechanisms dominating the corrosion of steel materials (Hedström 2019).

Consequently, data for anoxic corrosion of carbon steel are the most relevant for most time periods in most radionuclide-transport calculation cases, including the base case (**Radionuclide transport report**). However, oxic conditions can result from glaciation and/or after eventual degradation of all reactive reductants in the repository, of which steel is the most important (Hedström 2019). Hence, also data for oxic conditions are requested.

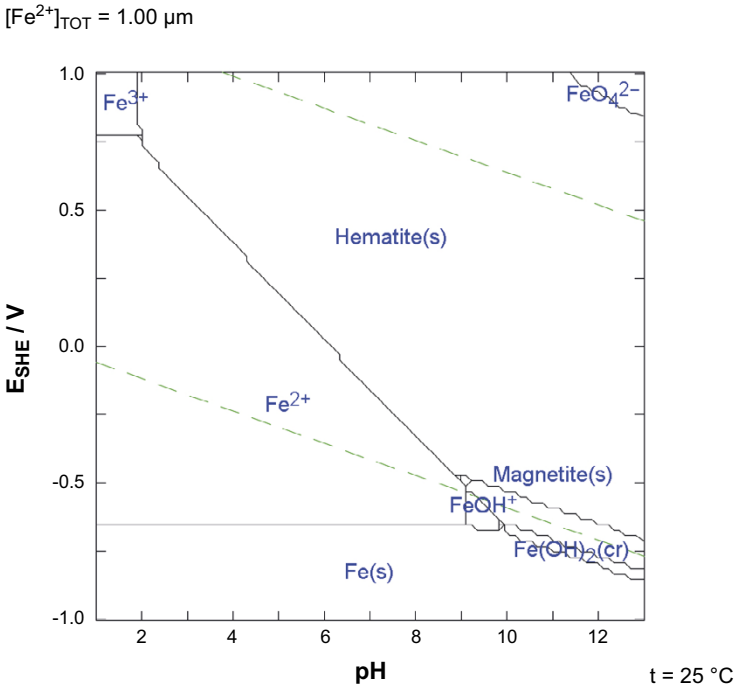

Figure 5-1. *Pourbaix diagram at 25 °C, showing the most thermodynamically stable Fe species as a function of pH and redox potential E_{SHE}, calculated from data from the ThermoChemie database (Giffaut et al. 2014). The diagram is valid for the system of iron $[Fe^{2+}]_{tot}$ = 1.0 µm and pure water.*

Water composition

The supplied data are requested to reflect the groundwater compositions relevant for SFR, see Table 5-2.

Table 5-2. Groundwater composition, for penetrating brackish groundwater during the first 1 000 years of the temperate climate domain (Gimeno et al. 2011, Nilsson et al. 2011, Auqué et al. 2013), and for shallow groundwater in the SFR area valid for both temperate and periglacial terrestrial periods (modified from Auqué et al. 2013).

Groundwater parameter	Penetrating brackish		Shallow		
	Reference	Range	Reference	Range ≲ 40 000 AD	Range ≳ 40 000 AD
pH	7.3	6.6 – 8.0	7.4	6.6 – 8.3	6.6 – 8.3
E_h (mV)	−225	−100 – −350	−210	−135 – −300	−135 – −300
Cl^- (mg/L)	3 500	2 590 – 5 380	190	16 – 503	5 – 357
SO_4^{2-} (mg/L)	350	74 – 557.2	50	25 – 163	17 – 110
HCO_3^- (mg/L)	90	40 – 157	300	300 – 500	120 – 324
Na^+ (mg/L)	1 500	850 – 1 920	180	65 – 400	38 – 250
K^+ (mg/L)	20	3.8 – 60	5	5 – 15	2 – 5.3
Ca^{2+} (mg/L)	600	87 – 1 220	50	24 – 105	7 – 48
Mg^{2+} (mg/L)	150	79 – 290	12	7 – 24	2 – 13
SiO_2 (mg/L)	11	2.6 – 17.2	12	2 – 21	12 – 31

Earth currents

Earth currents have been shown to give only a minor contribution to the general corrosion rate of carbon steel and steel alloys under post-closure conditions at SFR1 (SKB 2014). Later modelling studies confirm this conclusion with the exception of long metal structures (Löfgren and Sidborn 2018). Hence, earth-current contributions to corrosion of reactor pressure vessels are smaller when these are segmented, as is currently planned. Due to the small influence of earth currents on corrosion, it is assumed that this effect is negligible compared with other uncertainties with regard to corrosion rates.

Modelling activities in which data will be used

The requested steel corrosion rates will be used in the assessment of:

- Radionuclide release from the boiling-water reactor pressure vessels in the 1BRT waste vault, as probabilistically calculated from statistical distributions (probability density functions, PDF) of the corrosion rates. It is assumed that the fraction of the radionuclides that originates from neutron activation is gradually released as the steel slowly corrodes. In principle, corrosion-controlled release could be credited also to other metallic waste in other vaults with known surface area and composition, but this is pessimistically omitted in this safety analysis.
- Redox-level development in the vaults, since steel is the main reducing material which determines the redox potential as long as sufficient amounts remain uncorroded (Hedström 2019).

The corrosion-rate data adopted in PSAR is not planned to, but could in principle, be used for an updated assessment of:

- Gas generation rates
- Concrete fracturing due to expansive corrosion products

The data are not judged applicable for assessment of:

- Local corrosion, e.g. for assessment of breach of containment of steel waste packaging (steel moulds, drums, ISO-containers).

5.2 Experience from previous safety assessments

This section briefly summarises experience from previous safety assessments, especially the SAFE, SAR-08 and SR-PSU safety assessments, which may be of direct consequence for the data selection in this report.

Modelling in previous safety assessments

In the SAFE and SAR-08 safety assessments which treated only SFR1, the corrosion rates were only used for calculations of gas formation and possible resulting pressure-driven radionuclide transport. For SAFE, the calculations were performed by Moreno et al. (2001).

For SR-PSU, the gas calculations were updated with new input data in Moreno and Neretnieks (2013). Within SR-PSU the corrosion rates of carbon steel were also used to determine the radionuclide release rate from the reactor pressure vessels within the 1BRT waste vault, as well as assessing the global redox evolution of the repository (Duro et al. 2012). In all safety assessments previous to the current assessment, corrosion rates were selected and applied as deterministic values.

Conditions for which data were used in previous safety assessments

As gas generation was the focus regarding corrosion in SAR-08, the corrosion rates used in Moreno et al. (2001) reflect a pessimistic case for generating corrosion gases (hydrogen) in order to evaluate the effects of such a case. The corrosion rate used in those calculations does not necessarily reflect the corrosion rates appropriate for calculations of radionuclide release from the reactor pressure vessels. Hence, the data found in Moreno et al. (2001) had to be updated with more realistic corrosion rates for the SR-PSU safety assessment (Moreno and Neretnieks 2013). In SR-PSU, a literature review of rates under SFR-relevant conditions resulted in the suggested values in Table 5-3.

Table 5-3. Anoxic corrosion rates for carbon steel used in the SR-PSU safety assessment.

Conditions within the repository	Rate (μm a^{-1})	Reference
Alkaline, anoxic	0.05	Smart et al. (2004)
Non-alkaline, near-neutral pH, anoxic	2.8	Simpson and Weber (1988), Schenk (1988) and Simpson et al. (1985)

Sensitivity to assessment results in previous safety assessments

The corrosion rate sets the radionuclide release rate of the steel reactor pressure vessels. For SR-PSU, the intact vessels were planned to be grouted and deposited directly in 1BRT without packaging. Later SKB decided that they should be segmented and deposited in moulds in the vault (Hellman 2017). The cement in the grout and the surrounding concrete provides a pH high enough to ensure a slow corrosion rate for a long period of time (see further Section 5.8), but not long enough to ensure passivating conditions throughout the entire analysis period. In the assessment of the redox evolution (Duro et al. 2012), its sensitivity to corrosion rates was investigated by varying the corrosion rate by four orders of magnitude.

Within the SAFE and SAR-08 safety assessments no sensitivity analysis was performed.

Alternative modelling in previous safety assessments

No alternative modelling was reported in SAFE, SAR-08 and SR-PSU.

Correlations used in previous safety assessment modelling

In the previous safety assessments, no correlations were applicable to the corrosion rates. The rates were applied as deterministic values.

Identified limitations of the data used in previous safety assessment modelling

In the metal-corrosion chapters in the **Waste process report**, the uncertainty associated with using corrosion rates from literature is discussed as these rates can span over more than four orders of magnitude, depending on the type of material studied and the conditions imposed. One reason for this variance is the different methods used for measuring metal-corrosion rates; in some cases, the rates are obtained by measuring hydrogen generation, other cases by measuring metal mass loss, and sometimes by measuring the corrosion current. A discussion on the adequacy of the different techniques for corrosion rate measurements is included in Kursten et al. (2004).

Many of the data on alkaline anoxic corrosion rates of steels found in the literature were obtained in alkaline water solutions where corrosion products have a large volume of water to dissolve in. Such conditions may not completely resemble the situation in 1BRT with steels embedded in cement or concrete where corrosion-product concentration build-up may be quicker, leading to earlier decrease of corrosion rates.

For obvious reasons no experiments have been carried out over the time frames most relevant for SFR (millennia). The results from shorter experimental investigations must thus be extrapolated to long time spans. Adopting the experimental results from short-term corrosion experiments may overestimate the corrosion rate for longer times because corrosion is initially fast but decelerates as the oxide film forms and thickens, limiting access between oxidant and reductant: water and Fe (Section 5.1).

Spatial difference in pH across the repository might lead to different corrosion rates of the waste (Section 5.8). This might limit the validity of broadly applying the obtained rates from different measurements.

5.3 Supplier input on use of data in this and previous safety assessments

The corrosion rates suggested below by the data supplier for use in this safety assessment are to be used primarily in estimations of release rates of radionuclides from corroding reactor pressure vessels. The process of metal corrosion is very complex, particularly in its sensitivity to various environmental variables. The corrosion mechanism is quite different under oxic and anoxic conditions as one example (see e.g. the **Waste process report**), giving rise to different rates of corrosion. The rate of overall corrosion is also affected by secondary effects such as the build-up of various reaction products on the metal surfaces that increases the electrical resistivity at the surface and limits the accessibility of corrosive agents in the surrounding groundwater, and thus lowers the corrosion rate. The stability of the protective layer of products determines whether the steel is in an active or passive state of corrosion, which may depend on the chemical properties of the environment. For a cement-based repository such as SFR, several safety functions are dependent on prevailing alkaline conditions, which are expected to extend over very long times (see e.g. Cronstrand 2014, Höglund 2014, 2018, 2019). Under these conditions, steel corrosion products are typically relatively stable which causes low corrosion rates.

Due to the reasons briefly described above, a general corrosion rate that spans over the entire lifetime of the repository cannot be given. Instead, ranges of corrosion rates for specific environmental conditions expected at different stages of the analysis period are suggested by the supplier for use in the safety assessment. The rates suggested are based on experimental data, the relevance of which have been thoroughly reviewed by Swanton et al. (2015) and Diomidis (2014).

5.4 Sources of information and documentation of data qualification

Steel corrosion rates for conditions relevant to radioactive-waste repositories have been compiled and thoroughly reviewed in Swanton et al. (2015) as part of the Carbon-14 Source Term (CAST) project within the EURATOM programme. Diomidis (2014) has reviewed and compiled experimental corrosion data specifically in relation to the cement-based repository in the Swiss radioactive-waste programme. Both reviews, as listed in Table 5-4, contain rates for a range of conditions relevant for different stages in the expected temporal evolution of the SFR (Tables 5-5 to 5-10). The rates suggested by the supplier in the following are based on the experiments and expert judgements provided in these reports.

Sources of information

Table 5-4. Main sources of information used in data qualification.

Sources of information
Swanton S W, Baston G M N, Smart N R, 2015. D 2.1 State of the art review of steel corrosion and C14 release. EURATOM Program FP7/2207-2013.
Diomidis N, 2014. Scientific basis for the production of gas due to corrosion in a deep geological repository. Arbeitsbericht NAB 14-21, Nagra, Switzerland.

Categorising data sets as qualified or supporting data

Table 5-5. Data sets for carbon steel corrosion under oxic near-neutral conditions.

Qualified data sets	Supporting data sets
Swanton et al. (2015, Table 7) The data provided in the table spans over a wide range of conditions. Data for very saline seawaters and temperatures exceeding 50 °C were disregarded.	

Table 5-6. Data sets for carbon steel corrosion under oxic alkaline conditions.

Qualified data sets	Supporting data sets
Swanton et al. (2015, Table 11) Data obtained from samples exposed to very high chloride and temperatures exceeding 50 °C were disregarded.	

Table 5-7. Data sets for carbon steel corrosion under anoxic alkaline conditions.

Qualified data sets	Supporting data sets
Swanton et al. (2015, Table 13) Swanton et al. (2015, Table 10) Diomidis (2014, Table 3.4)	Swanton et al. (2015, Table 13) Swanton et al. (2015, Table 10)
Data in Swanton et al. (2015, Tables 10 and 13): Data for temperatures exceeding 50 °C were disregarded. Data for acidic and near-neutral test solutions were disregarded. Data for degreased and pre-rusted samples were disregarded.	Data given in Swanton et al. (2015, Tables 10 and 13) clearly indicate an initial transient attributed to the build-up of a passivating layer. This transient is not relevant for use in the safety assessment modelling for reasons given in Section 5.10. Thus, data obtained for times < 700 d are excluded from the qualified data sets, although included as data sets supporting the conceptual understanding of passivation and quantifying the transient approach towards steady-state corrosion rates.

Table 5-8. Data sets for carbon steel corrosion under anoxic near-neutral conditions.

Qualified data sets	Supporting data sets
Swanton et al. (2015, Table 8) Data obtained by instantaneous electrochemical measurements are discarded as data from long-term exposure tests are judged more reliable when assessing long-term corrosion rates.	

Table 5-9. Data sets for stainless steel corrosion under oxic near-neutral conditions.

Qualified data sets	Supporting data sets
Swanton et al. (2015, Table 14) Most literature has focussed on localised corrosion since the general corrosion of stainless steel is typically very low. Data obtained from weight-loss experiments have been considered. Corrosion data obtained in highly saline solutions are discarded.	

Table 5-10. Data sets for stainless steel corrosion under anoxic alkaline conditions.

Qualified data sets	Supporting data sets
Swanton et al. (2015, Table 17) Diomidis (2014, Table 4.1)	

Excluded data previously considered as important

In SR-PSU, the assessment of corrosion rates was based on the review by Smart and Hoch (2010), which comprises studies that to a large extent overlap with the ones in Swanton et al. (2015), including all those listed in Table 5-3. While the newer reviews by Swanton et al. (2015) and Diomidis (2014) have replaced the older one by Smart and Hoch (2010), no specific data have intentionally been excluded in the PSAR.

5.5 Conditions for which data are supplied

The data supplied are deemed to be valid over a pH range 7–12.5. Separate rates are suggested for the four possible combinations of oxic/anoxic and near-neutral/alkaline conditions. It is important to note that the suggested corrosion rates for anoxic alkaline conditions may not be valid at very high pH (see further Section 5.6).

5.6 Conceptual modelling uncertainty

One conceptual uncertainty is related to the evolution of corrosion rates with time. A passive state of carbon steel is obtained as corrosion products are formed on the metal surfaces, providing a barrier that limits the accessibility for further corrosion. This implies a growing film thickness and decreasing corrosion rate with time. At some point the rate is slow enough to be balanced by a certain rate of dissolution/removal of corrosion products which results in a steady-state film thickness and corrosion rate. In experimental corrosion rates obtained as a function of time, the transient with initial acute corrosion declining exponentially due to passivation is often obvious. It is however difficult to judge from the experimental results to what extent a steady-state, chronic corrosion rate has been reached.

There is a conceptual uncertainty regarding steel corrosion rates under anoxic conditions at very high pH, i.e. pH > 13. Thermodynamically, the typical passivation of the steel surfaces by precipitation of insoluble iron oxide (i.e. magnetite) as the main corrosion product under alkaline conditions may be replaced by the formation of non-passivating soluble iron hydroxides at pH > 13.

5.7 Data uncertainty – precision, bias, and representativity

A large amount of experimental data listed in the review by Swanton et al. (2015) were disregarded in the qualification of relevant corrosion rates.

Corrosion rates are often sensitive to the temperature, e.g. following an Arrhenius-type dependence with higher rates at higher temperatures. With respect to corrosion rates, the temperature in SFR can be regarded as stable. Corrosion rates sensitive to temperature that were obtained at elevated temperatures (higher than 50 °C) are therefore generally disregarded in the qualification of relevant corrosion rates.

Corrosion, in particular under non-passivating conditions, is often sensitive to variations in salinity, with higher rates at high salinity. Data obtained for solutions with high salinity are therefore generally discarded in the qualification of data for use in the assessment.

Experimental data obtained as a function of time often show an initial peak of acute corrosion that eventually declines to lower rates with time. For steel corrosion in alkaline anoxic environments in particular, this transient was shown in Swanton et al. (2015) to extend for around 700 days and is explained by the build-up of a passivating film of corrosion products on the fresh metal surfaces. In the repository evolution, corrosion under anoxic alkaline conditions is preceded by a short period of oxic conditions, and the anoxic corrosion rate is therefore assumed to initiate at the low, long-term level. For that reason, the initial transient is regarded as irrelevant and rates obtained from experimental times of less than 700 days were disregarded in the qualification of relevant corrosion rates.

5.8 Data uncertainty – spatial and temporal variability

Spatial variability of data

Variations in chemical conditions over different parts of the SFR repository are expected. With respect to corrosion, important parameters are e.g. oxygen access, temperature, chloride concentrations, and pH. It should be emphasised that the corrosion rates in Section 5.10 are suggested by the supplier with the main purpose of parametrising the calculations of corrosion-controlled radionuclide release, i.e. from waste forms comprising metals with induced activity. Spatial variations of most parameters between waste forms in different parts of the repository are deemed to be relatively low. One possible exception is the amount of cement which may be different in different waste vaults. Upon degradation of the cement, pH decreases in a stepwise manner, corresponding to different degradation regimes with different chemical reactions buffering the pH. Parts of the repository containing lower amounts of cement, e.g. the BLA vaults, are therefore expected to reach a change in pH prior to parts with large amounts of cement (Cronstrand 2014).

Temporal variability of data

Due to the large amounts of cement in SFR, the water in the waste forms comprising steel with induced radioactivity are expected to be alkaline. Modelling of the degradation of cement (Cronstrand 2014, Höglund 2014, 2018, 2019), indicates that pH > 11 can be expected to prevail for at least 100 000 years after closure (except in the BLA vaults that contain less cement). Corrosion rates suggested by the supplier for use in this safety assessment for near-neutral conditions are included for completeness, although the relevance of these data under repository conditions may be limited.

At the time of closure, oxic alkaline conditions in the repository are expected, resulting in a relatively high corrosion rate that decreases as oxygen is consumed. The period of oxic conditions is estimated to be short (Section 5.1). As oxygen is depleted in the repository, water becomes the dominating oxidant in the corrosion mechanism. Under anoxic alkaline conditions, the corrosion rate is expected to stabilise at a very low level due to build-up of a passivating layer of corrosion products on the metal surface.

Upon shoreline regression, the groundwater chloride content is expected to decline with time. Under anoxic alkaline conditions, however, the effect of chloride on corrosion rates is shown to be small (Swanton et al. 2015).

Passivation, described in Section 5.1, arises over time, entailing gradually decreasing corrosion rates that eventually reach a steady state. In the recommendation of representative corrosion rates under passivating conditions the aim has been to avoid data that are far from steady state.

5.9 Data uncertainty – correlations

The qualified data has not been acquired, interpreted or refined by using correlations.

5.10 Result of supplier's data qualification

The corrosion rate is dependent on several variables such as the oxygen availability, electrical conductivity of the solution, temperature, pH, etc (Section 5.1).

The reactor pressure vessels in 1BRT, as well as other metal wastes with appreciable induced radioactivity, will be deposited in SFR embedded in ordinary Portland cement (CEM I) concrete waste forms. Alkaline conditions are therefore expected at the metal surfaces immediately upon water saturation of 1BRT. Near-neutral conditions are not expected until after advanced degradation of the cement (Höglund 2014, 2018, 2019).

The initial period during which corrosion under oxic alkaline conditions may occur is negligibly short (Section 5.1). Hence, anoxic conditions are generally assumed to apply after closure. An exception is glacial periods, which may occur after severe cement degradation and entail inflow of oxygen-rich meltwater.

Carbon steel – oxic, near-neutral conditions

Based on the data provided in Swanton et al. (2015) typical oxic, near-neutral corrosion rates for carbon steel are roughly estimated to be 10–400 µm/a (Table 5-11).

Table 5-11. Corrosion rate of carbon steel under oxic near-neutral conditions.

Corrosion rate suggested by data supplier	Comment
10–400 µm/a	Estimated from a wide range of experimental conditions based on the qualified data set described in Table 5-5.

Carbon steel – oxic, alkaline conditions

Ordinary Portland cement confers alkaline conditions. An initial acute oxic corrosion rate for steel in different cement mixtures on the order of 200 µm/a was measured by Arya and Xu (1995) as reported in Swanton et al. (2015). The rate decreased exponentially with time during curing, presumably reflecting the passivation of the steel surface, build-up of corrosion-product concentration, and possibly reduction in the availability of water. Passivation was typically reached within 20 days for cement mixtures containing 1 wt% and after 80 days for mixtures containing 3 wt% chloride. Chronic (long term) corrosion rates in grout without chloride and carbonation affects were estimated in Swanton et al. (2015) to be less than 1 µm/a. For rebars in concrete structures where carbonation may be important, higher values reported in the range 10–50 µm/a were noted. The rates are summarised in Table 5-12.

Table 5-12. Corrosion rate of carbon steel under oxic alkaline conditions.

Corrosion rate suggested by data supplier	Comment
< 1–100 µm/a	Estimated range of chronic corrosion rate based on the qualified data set described in Table 5-6. Passivation is reduced in the presence of chloride and carbonation effects which gives rise to the higher rates in the suggested range.
~200 µm/a	Initial (acute) corrosion rate

Carbon steel – anoxic, alkaline conditions

As oxygen is depleted, corrosion under anoxic alkaline conditions, with water as the oxidant, becomes increasingly important. Anoxic alkaline conditions are presumed to characterise the SFR environment throughout most of the repository lifetime and the corrosion rate during this period is therefore the most important with respect to the long-term radionuclide release. In common with the oxic alkaline conditions, passivation of the metal surfaces controls the corrosion rate. This passivation is indicated in experimental results on fresh surfaces where an initial acute rate declines exponentially to very low rates after ~700 days. In the safety assessment however, the corrosion rate under anoxic alkaline conditions is assumed to initiate at a low level due to the pre-corroded and passivated surfaces from previous corrosion events under oxic conditions. The most relevant data are therefore those that are obtained over very long time periods by hydrogen evolution experiments.

The corrosion rates obtained in long-term experiments are typically very low, and it is difficult to judge whether a steady state has been achieved. Corrosion rates as low as 0.0002 µm/a have been measured for carbon steel embedded in cement (see Table 3.5 in Diomidis 2014). The experimental data for long-term corrosion reported in Swanton et al. (2015) and Diomidis (2014) however generally falls in the range 0.001–0.1 µm/a.

The qualified corrosion rate data are shown in Figure 5-2 together with cumulative distribution functions (log-normal and truncated log-normal). Parameters for the distributions are given in Table 5-13. The truncated log-normal distribution is truncated for values outside the range 0.001–0.1 µm/a, corresponding to a ~98 % confidence interval. It is emphasised that fitting a distribution function to the experimental data is done mainly to illustrate the distribution and spread of the reported data. No mechanistic motivation for a specific statistical distribution is made at this point. It is also not clear, as mentioned previously, if true steady-state conditions are reached in the underlying experiments.

It may be noted that only minor effects of irradiation, chloride and sulfur species was seen on the anoxic corrosion rate under alkaline conditions (Swanton et al. 2015). It was also concluded that temperature had little effect on the long-term rates due to the formation of the protective magnetite film on the steel surfaces.

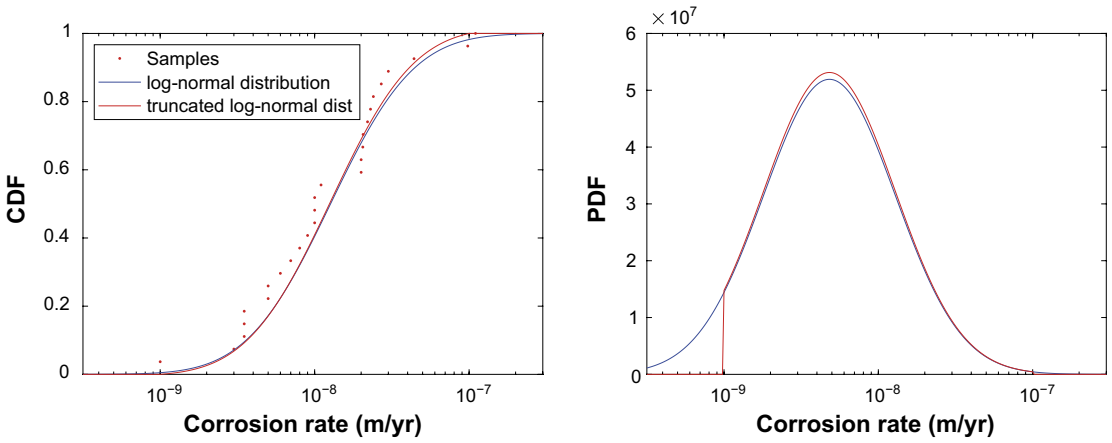

Figure 5-2. *Cumulative distribution (left panel) of qualified data (red dots) for carbon steel corrosion under anoxic alkaline conditions deemed relevant for use in the assessment. A log-normal distribution (red line, with mean = 2.5×10^{-8} m/a and std = 2.62×10^{-8} m/a), truncated for corrosion rates outside the range 0.001–0.1 µm/a (i.e. ~98 % confidence interval) is shown together with the corresponding log-normal distribution without truncation (blue line). The right panel shows the corresponding log-normal and truncated log-normal PDFs.*

Table 5-13. Corrosion rate of carbon steel under anoxic alkaline conditions.

Corrosion rate suggested by data supplier	Comment
0.001–0.1 µm/a	Estimated range of chronic corrosion rate based on the qualified data sets described in Table 5-7.
(mean, std) = (2.5×10^{-8}, 2.62×10^{-8}) (a, b) = (10^{-9}, 10^{-7})	Mean and standard deviation (m/a) for the fitted truncated log-normal distribution function suggested for use in stochastic radionuclide release modelling. Suggested lower and upper truncation limits a and b (m/a), respectively.

Carbon steel – anoxic, near-neutral conditions

As the cement becomes severely degraded, its ability to maintain alkaline conditions in the repository declines and eventually the passivating film of corrosion products formed on the steel surfaces under alkaline conditions may become thermodynamically unstable and its protective properties become deteriorated. This, along with anticipated increased diffusion rates of corrosive agents in severely degraded concrete, leads to an expected increase in corrosion rates.

There are many experiments on the steel corrosion rate under anoxic near-neutral conditions. The rates reported in Swanton et al. (2015) typically fall in the range of 1–100 µm/a (Table 5-14). The rates are found to be relatively insensitive to temperature variations.

The qualified corrosion rate data is shown in Figure 5-3 together with a log-triangular distribution function. The log-triangular distribution is shown for a distribution mode c = 10^{-5} m/a, and lower and upper limits a = 10^{-6} m/a and b = 10^{-4} m/a respectively. A better fit to experimental data can be obtained by modifying the distribution parameters. However, the parameters suggested tends to bias the distribution towards higher rates. This is deemed to be a cautious assumption in stochastic radionuclide release calculations, given the uncertainties in underlying experimental data, since the rate controls the release of induced activity remaining after previous corrosion events under alkaline conditions.

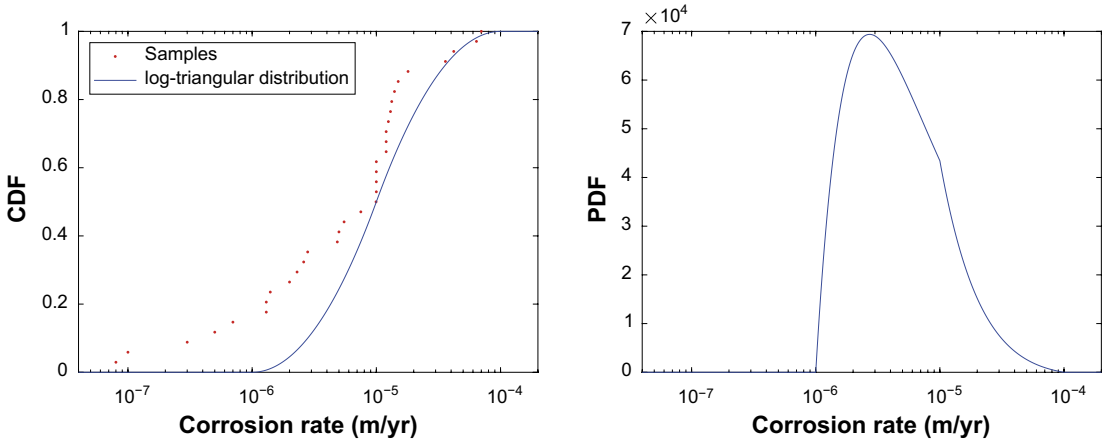

Figure 5-3. *Cumulative distribution (left) of qualified data (red dots) for carbon steel corrosion under anoxic near-neutral conditions deemed relevant for use in the assessment. A log-triangular distribution (blue line, with mode 10^{-5} m/a, and lower and upper limits 10^{-6} m/a and 10^{-4} m/a) are included for reference. The right panel shows the corresponding log-triangular PDF.*

Table 5-14. Corrosion rate of carbon steel under anoxic near-neutral conditions.

Corrosion rate suggested by data supplier	Comment
1–100 μm/a	Estimated range of corrosion rates based on the qualified data sets described in Table 5-8.
(a, b, c) = (10^{-6}, 10^{-4}, 10^{-5})	Parameters (m/a) for the log-triangular distribution function suggested for use in stochastic radionuclide-release modelling. Suggested lower and upper truncation limits are denoted a and b, respectively and the mode of the distribution function is denoted c.

Stainless steel – oxic, near-neutral conditions

Most studies of corrosion of stainless steel in aerobic near-neutral solutions are focussed on localised corrosion, and the effect of different salt concentrations. A range of 0.1 to 0.5 μm/a in corrosion rates at temperatures below 30 °C is given in Swanton et al. (2015) for rates obtained based on weight-loss experiments. This range is suggested by the supplier for use in the assessment (Table 5-15). Despite the effect of localised corrosion, observed corrosion rates of stainless steel under oxic and near-neutral conditions are generally significantly lower than for carbon steel (cf Table 5-11). This difference may be explained by the ability of the passive alloy surface layer on the stainless-steel surface to reconstitute in the presence of oxygen, upon damage due to localised corrosion. Carbon steel surfaces passivated by corrosion products does not share this ability.

Table 5-15. Corrosion rate of stainless steel under oxic near-neutral conditions.

Corrosion rate suggested by data supplier	Comment
0.1–0.5 μm/a	Estimated range of corrosion rates based on the qualified data set described in Table 5-9.

Stainless steel – anoxic, alkaline conditions

The anoxic reaction mechanism of the corrosion of stainless steels is similar to that of carbon steel but with the additional reactions of the main alloying elements. The chemical composition, structure and composition of the passivating layer is therefore different, depending on the specific alloy. The corrosion rate under anoxic alkaline conditions is very low, typically below 0.01 μm/a in Swanton et al. (2015). Mean values as low as 0.0008 μm/a are found in recent long-term (2 years exposure) studies reviewed in Swanton et al. (2015). This range, 0.001–0.01 μm/a, is suggested by the supplier (Table 5-16) and is also consistent with the data provided in the review by Diomidis (2014).

Table 5-16. Corrosion rate of stainless steel under anoxic alkaline conditions.

Corrosion rate suggested by data supplier	
0.001–0.01 μm/a	Suggested range of corrosion rates based on the evaluation in Swanton et al. (2015) and the qualified data sets described in Table 5-10.

5.11 Judgement by the assessment team

According to the instruction given in Section 2.3, the assessment team should make comments on all the sections of the supplier.

Sources of information

Only two sources are given in Section 5.4, but they are both review reports that each contain references to data from a multitude of primary experiments. The sources are furthermore considered up-to-date, given that steel corrosion is a mature field with negligible development expected over the ~7 years since the sources were published. The sources are thus judged sufficient and suitable for safety-assessment use.

Conditions for which data is supplied

The assessment team find that the conditions regarding pH and oxygen access (Section 5.5), as well as salinity, temperature, and passivation (Section 5.7) reflect the conditions assumed in the repository during the analysis period (Section 5.1).

Conceptual modelling uncertainty

The assessment team considers the given uncertainties in Section 5.6 sufficient to describe the conceptual uncertainties related to evolution with time and the passivation processes. The uncertainties regarding possible higher corrosion rates at pH > 13 could be relevant to investigate and clarify since such pH values are conceivable during very early times, due to dissolution of alkali hydroxides in cement in chemical degradation state I.

Data uncertainty – precision, bias, and representativity

The uncertainties given in Section 5.7 are judged accurately presented by the assessment team. The uncertainty stemming from use of different measurement techniques (mass loss, hydrogen gas generation, electrical current) is briefly mentioned in Section 5.2 in the context of the previous safety assessment. For the current assessment, in some cases it is noted that data are taken preferentially from mass-loss and not electrochemical measurements (Tables 5-8 and 5-9), but in other cases the technique used is not specified, and there is no general discussion of the uncertainty relating to measurement methods.

Data uncertainty – spatial and temporal variability

The assessment team accepts the variabilities considered in Section 5.8, as these well represent the expected variabilities of relevant parameters in SFR.

Data uncertainty – correlations

No correlations were used for this data (Section 5.9), which the assessment team finds acceptable.

Results of supplier's data qualification

The assessment team considers the suppliers data qualification to be sufficient and the data will therefore be used in the radionuclide transport calculations.

5.12 Data recommended for use in the assessment

The data presented in Tables 5-11 to 5-16, which underly the PDFs plotted in Figures 5-2 and 5-3, are recommended for use for use in the safety assessment's probabilistic modelling of radionuclide release via corrosion.

6 Bitumen swelling pressure

The silo and BMA vaults of the SFR1 contain hygroscopic waste (ion exchange resins and evaporator salts) solidified in bitumen. Hygroscopic waste can cause swelling of the waste packages. The resulting pressure build-up can in turn affect the structural integrity of repository barriers. Providing expansion volume (void) around bituminised waste is an approach to reduce the swelling pressure around certain waste packages. Knowledge of the swelling pressure as a function of waste composition and expansion volume is important for a detailed structural mechanics analysis of the barriers in different waste storage configurations.

6.1 Modelling in this safety assessment

This section describes what data are expected from the supplier, and in what modelling activities the data are to be used.

Defining the data requested from the supplier

- The data required from the supplier are the swelling pressures as function of expansion volume for the waste types B.05, B.06, F.05, F.17, and F.18. For each waste type, data are to be supplied for a reference waste package composition, according to Almkvist and Gordon (2007), as well as a waste package representing a worst-case composition with respect to swelling pressure. The worst-case composition for each waste type is to be reported and motivated.

Modelling activities in which data will be used

No additional modelling is performed in the PSAR, since the recommended input data are unchanged since SR-PSU (see Section 6.12). However, additional calculations (Olsson 2016, 2017) have been performed to assess the impact of internal pressure and swelling on surrounding structures and the results are consistent or show less impact than previously reported (von Schenck and Bultmark 2014).

6.2 Experience from previous safety assessments

This section briefly summarises experience from previous safety assessments, especially the SAFE, SAR-08 and SR-PSU safety assessments, which may be of direct consequence for the data qualification in this data report.

Modelling in previous safety assessments

In both SAFE and SAR-08, the assessment of the risks associated with the swelling of bituminised waste was based on calculations of the maximum theoretical swelling volume, based on the swelling factor of the embedded waste (i.e. the ratio of resin volume after and before swelling). If the maximum swelling volume exceeded the available void the barriers could be affected.

The calculations (Pettersson and Elert 2001) were based on a maximum volume increase of a factor of 2 for ion-exchange resins (Nilsson et al. 1988) and a factor of 3.5 for evaporator concentrates containing $NaNO_3$. The latter value is the volume increase when dry $NaNO_3$ is dissolved at 25 °C and a saturated solution of sodium nitrate is formed (Pettersson and Elert 2001).

The volume of the various waste constituents was estimated using the densities of the materials given in Table 6-1.

In the SR-PSU the swelling pressures were used in modelling activities to assess the possible impact of the bitumen swelling on the surrounding structures and barriers in the silo and the 1BMA vaults. The modelling activity was performed in COMSOL Multiphysics and is described in the bitumen swelling report (von Schenck and Bultmark 2014).

Table 6-1. Material properties of bitumen used in Pettersson and Elert (2001).

Material	Density (kg/m^3)	Range (kg/m^3)	Reference
Bitumen	1 030	-	Riggare and Johansson 2001
Ion-exchange resin (dry)	1 400	1 140–1 520	Nilsson et al. 1988
		1 230–1 500	Berntsson 1992
Evaporator concentrates	2 680	-	Weast 1985

Conditions for which data were used in previous safety assessments

The available void space was assumed to consist of the void volume in the waste packages, between 10 % and 20 % of the total package volume. For the steel drums stored in the silo there is an additional void volume in the form of a metal box inserted in the middle of a plate with four drums.

Sensitivity to assessment results in previous safety assessments

The swelling factor was estimated from experimental results that show a large degree of variation. The uncertainty in swelling factor was discussed, but no full sensitivity analysis was performed for all variables (e.g. waste content and composition, type of bitumen).

The effect of variations in waste content between different waste packages from the Barsebäck plant was studied. It was concluded that variation in waste mixing ratio had a large effect on maximum volume increase, particularly for the waste from Barsebäck produced before 1993.

The previous data only concerned the maximum theoretical swelling of the waste from water uptake without consideration of the effects of the bitumen matrix, the package, the metal box and surrounding barriers. No estimates were made of the pressures that could be developed as a result of the swelling. Furthermore, no assessment was made of the effects of radiolysis, microbial degradation and ageing upon water uptake.

Alternative modelling in previous safety assessments

No alternative modelling was reported in SAFE, SAR-08 and SR-PSU.

Correlations used in previous safety assessment modelling

No reported correlations were used in SAFE, SAR-08 or SR-PSU.

Identified limitations of the data used in previous safety assessment modelling

In its audit of SAFE (Dverstorp and Sundström 2003) the regulatory authorities pointed out that SKB's position on grouting around bitumen waste was not clearly stated. The authorities noted that grouting may have an important effect on the consequences of swelling of bitumen waste. The authorities concluded that the analysis of swelling was based on theoretical values and not results from tests from representative samples. Furthermore, they requested a better description of the coupling between various processes leading to degradation of waste and barriers, including the swelling of bitumen.

In its audit of SR-PSU (SSM 2019) the regulatory authority SSM concluded that uncertainties related to swelling of bituminised waste still need to be addressed. Actions have been taken to rectify this, but some uncertainties remain.

6.3 Supplier input on use of data in this and previous safety assessments

Given the information in the section above and the need to assess the possible impact of swelling of bituminised waste it is recognised that there is a need for more experimental data on the potential swelling pressure for its use in the structural mechanics analysis. As all the processes that govern the bitumen swelling are not known or fully understood, experimental data from swelling tests performed under conditions similar to those of a closed SFR facility are preferred.

Given these uncertainties regarding the bitumen swelling, the supplier also recommends SKB to continue the investigations and work connected to reduce these uncertainties.

6.4 Sources of information and documentation of data qualification

Bitumen has been used for solidification of ion-exchange resins only in a few countries, mainly in Sweden and Finland. The data sources for water uptake and swelling of bituminised ion-exchange resins originate mainly from research performed in the 1980s and 1990s in Sweden, Finland, Norway and Denmark.

The experiments generating data can be divided into the following categories:

- Swelling of unconfined ion-exchange resins.
- Swelling of confined ion-exchange resins.
- Swelling and water uptake of bituminised ion-exchange resins in an unconfined space.
- Swelling and water uptake of bituminised ion-exchange resins in a confined space.

Furthermore, some relevant data from studies with bituminised evaporator concentrates have been included.

Swelling of unconfined and confined ion-exchange resins

The ion-exchange resins consist of polymer chains that are made stable by side chains (cross-linking) usually formed by adding divinylbenzene during the polymerisation. Different functional groups are added to the polymer structure in order to obtain the specific ion exchange properties of the resins. The cross-linking of the polymer chains reduces the swelling pressure of the resin but will also reduce the exchange capacity.

Tests have been performed on swelling of samples of ion-exchange resins extracted from bituminised waste from Barsebäck (Asea-Atom 1985). The initial water content of the resins was between 3 and 12 %, The observed swelling factor for the resin after addition of water was between 1.8 and 2.4. The type of resin is not given.

Density measurements of cationic bead resin IR120 gave a swelling factor (i.e. the ratio of resin volume after and before swelling) for the resin of 2.43 (Brodersen et al. 1983). Experiments showed a faster and larger swelling in the case the resin was crushed. Tests on powdered resin showed a larger swelling than bead resin.

Aittola et al. (1982) studied the swelling properties of different ion-exchange materials. Swelling experiments were performed studying the effect of various types of heat treatment and treatment with Na_2SO_4. The experiments were performed on unused granular anionic and cationic resins, spent powdered resin and spent mixed bed resin (premade mixtures of cationic and anionic resins). The granular anionic resin was degraded by heat treatment at temperatures higher than 140 °C for a day resulting in a considerably reduced swelling. The swelling capacity of the cationic resin remained unchanged even after a long treatment at 140 °C (swelling factor 2.5–2.6). The experiments with the mixed bed resins indicated that the swelling behaviour of the cationic component was unaffected even after longer drying periods at 180 °C. The powdered resin showed a higher swelling than the granular, explained as being caused by absorption of additional water between the resin grains. The powdered

resins showed a somewhat reduced swelling capacity after long-term treatment at 180 °C. Treatment with Na_2SO_4 caused some reduction of the swelling effect on the powdered resins, while the swelling of the granular resins was unaffected.

Valkiainen and Vuorinen (1985) studied the effect of heat treatment on the swelling properties of cationic and anionic resins. They came to the conclusions that thermal treatment did not affect the swelling properties of cationic resins. For anionic resins treatment at a temperature of at least 105 °C reduced the swelling after a treatment lasting for 10 hours. At a temperature of at least 140 °C the swelling tendency was strongly reduced after 3 hours. In this case the remaining swelling was 18 %. For the cationic resins a swelling of 155 % was measured. The swelling for a mixture of heat treated anionic and cationic resins in volume ratio 2:1 was estimated to be 71 %. The effect of irradiation on the swelling was studied by irradiating samples with a dose of 1.76 MGy and heat-treating samples of resins. For cationic resins the swelling capacity increased by 8 % after irradiation, whereas no effect was found for the anionic resins. Test performed on spent active resins (volume ratio anionic-cationic 2.3:1) showed a swelling capacity of 29 % after heat treatment, which was lower than the estimated swelling capacity for the fresh resin.

Valkiainen and Vuorinen (1985) also studied the swelling pressure of ion-exchange resins mixed with glass powder as well as that of bituminised resins. The measurements were performed in an oedometer for controlling volume and pressure. The ion-exchange resins were mixed with glass powder in a weight ratio 1:1.12 for the purpose of filling the void spaces of the resin particles and thus preventing the deformation of the resin grains. The ion-exchange resins (ARC351 cationic and ARA360 anionic resin in a volume ratio 1:2) were heat treated for 16 hours at 140 °C before mixing with the glass powder. Experiments were also performed with spent, inactive granular mixed bed resins from Forsmark. When the samples were placed in the oedometer a preload pressure between 0.2 and 3 MPa was applied. After adding water to the resins the pressure increased over a couple of tens of minutes. After an equilibration period of a few days, during which a slow increase or decrease in pressure was observed, the available volume for swelling was increased in steps. The results of the tests are shown in Table 6-2.

The results of work on bitumen in a Nordic Study were compiled in Snellman and Valkiainen (1985) and Snellman et al. (1986). The report (Snellman and Valkiainen 1985) refers to Finnish and Swedish measurements of swelling pressures. The constrained swelling was simulated by mixing the ion-exchange resins with quartz powder, glass powder or glass beads. This approach does not completely eliminate the possibility of some volume increase. The results reported in Snellman and Valkiainen (1985) and Snellman et al. (1986) are summarised in Table 6-3. The first experiment was performed in Sweden (Jacobsson 1983, cited in Snellman and Valkiainen 1985), the second in Finland by Valkiainen and Vuorinen (1985).

Table 6-2. Measured swelling pressure of ion-exchange resins at different volume expansions (Valkiainen and Vuorinen 1985).

Sample	Test	Preload MPa	Swelling pressure (MPa)				Water content
			ΔV = 0 %	ΔV = 10 %	ΔV = 20 %	ΔV = 30 %	
Fresh resin	A1	0.5	5.8	0.60	0.15	-	59.3
	A2	1	5.9	0.65	0.15	-	49.2
	A3	1 + 0.2*	7.1	0.70	0.30	-	49.4
	A4	3	11.5	2.40	0.75	0.22	62.0
Spent resin	B1	0.5	3.3	0.22	0.12	-	52.7
	B2	1	4.0	0.26	0.16	-	47.6
	B3	1 + 0.2*	4.2	0.33	0.17	-	51.8
	B4	3	4.5	0.60	0.15	-	67.0
Cationic resin	C1**	3	26.8	15.4	10	8.5***	118

* Preloaded in compactation to 1 MPa, at the beginning of the test 0.2 MPa.

** Test C1 performed without glass beads as a mixing agent.

*** ΔV = 25 %

Table 6-3. Measured swelling pressure of ion-exchange resins at different volume expansions from Snellman and Valkiainen (1985) and Snellman et al. (1986).

Sample	Drying	Swelling pressure (MPa)		
		ΔV = 0 %	ΔV = 10 %	ΔV = 20 %
Anionic and cationic resin ARA 366 40 % + ARC 351 60 %, quartz powder 1:4	24 h, 105 °C	31	2.5	0.3
Anionic and cationic resin ARA 366 67 % + ARC 351 33 %, quartz powder 1:09	16 h, 140 °C	7.1	0.7	0.3

The Swedish Cement and Concrete Research Institute (CBI) has performed investigations of the swelling properties of radioactive ion-exchange resins from Forsmark (Ericsson and Klingstedt 1987). The swelling volume and pressure were measured in an apparatus consisting of a brass cylinder with a movable piston. Water was injected in the bottom of the cylinder. The pressure of the piston was kept at a constant value and the movement of the piston recorded. Tests were performed on powdered resin from the waste treatment plant before and after solidification in bitumen. The solidified samples were washed in xylene to remove the bitumen, rinsed with dichloromethane to remove the xylene and finally dried at 60 °C. No specification is given on the type of resin or how the resin was treated before solidification. The samples extracted from the bituminised product had a water content of around 7 %. The swelling of these samples resulted in a pressure of 15–17 MPa if no volume expansion was allowed. In the tests with a constant pressure of 2.5 MPa, the swelling of the resin was between 11 and 15 % and at a constant pressure of 0.2 MPa, the swelling was 33–34 %. If the volume expansion of the resin is converted to an equivalent swelling of the bituminised product, it would for a waste loading of 50 % correspond to a volume expansion of 5–7 % at a pressure of 2.5 MPa and a volume expansion of 15 % at a pressure of 0.2 MPa. Except for the pressures observed at confined swelling this is within the range of the data reported by Valkiainen and Vuorinen (1985).

In Nilsson et al. (1988) the swelling behaviour of anionic and cationic ion-exchange resins was studied, and a model was set up for the water uptake and the swelling pressures that the swelling causes. Experiments were performed with seven different resins in different chemical forms. For two of the resins the effect of heat treatment was also studied. For each resin the water uptake, density and volume were measured at different water activities. The internal swelling pressure was calculated for the resins. The swelling was measured at a temperature of 25 °C, but estimates were also made for 0 °C. The data provided in Nilsson et al. (1988) can be used to make estimates of the external swelling pressure exerted on waste packages and barriers at different degrees of volume expansion. However, it does not consider water that is present in pores and cracks of the bitumen matrix.

In a study by Matsuda et al. (1992) the swelling pressure developed in confined swelling of ion-exchange resins was measured. The study was focussed on solidification in cement, but as the experiments were performed on ion-exchange resin they are also applicable to bituminised waste. They obtained the confined conditions by pelletising the resin under high pressure. Thereafter, the pressure was relieved and water was injected through a small opening in the experimental apparatus. The study included various types of cationic resins with different functional groups, degrees of cross-linkage and different exchange capacities (a reduction in exchange capacity was obtained by thermal treatment). For a dry resin in H^+-form with 8 % cross-linkage and an exchange capacity of 4.8 meqv/g, the pressure for confined swelling was measured as 51 MPa. For resin with Na^+-form the confined swelling pressure was around 30 MPa. A reduction of the exchange capacity had a more than proportional effect on the confined swelling pressure. An increased initial water content of the resin had a strong reducing effect on the swelling pressure, since the elastic forces from the cross-linkage of the resins become more important for a resin that has taken up water and swelled. The experiment showed that for a resin with 8 % cross-linkage, the swelling pressure was reduced by half at an initial water content of 30 % by weight. A model based on osmosis was also developed that could simulate the experimental results based on ion-exchange capacity, functional group, ionic form, cross-linkage and initial water content.

Clay Technology AB has performed investigations of the swelling properties for two types of ion exchange products, Finex CA875H and Aqua Chem NUC-3WF3, with respect to different initial conditions and water chemistry (Andersson et al. 2014, Jensen et al. 2017). Both products consist of a combination of both cation- and anion-exchange resins. Unconfined swelling resulted in a volume

increase of 100 % for a mixture of the two ion exchangers, which is consistent with other investigations. However, contained swelling experiments resulted in lower swelling pressures than previously reported, which can be explained by the lower density used in the experiments.

Swelling and water uptake of bituminised ion-exchange resins in an unconfined space

In a Nordic study performed during 1978–1982 various types of mixtures of bitumen and ion-exchange resins were immersed in water for a period up to 1 500 days (Aittola and Kleveland 1982). A selection of samples was externally irradiated with Co-60 (0.1 to 1 MGy). The swelling was compared with the theoretical swelling calculated assuming that the ion-exchange resin had a swelling factor of 2.5. This was based on other investigations that had shown a swelling factor for the resin between 2.4 and 3.1 depending on the temperature and duration of the drying. The measured swelling of the samples ranged from about 10 % to 100 % of the theoretical maximum. The samples with irradiated resins had a faster water uptake and reached a swelling of 200 % of the approximated theoretical maximum. However, the swelling factor of the irradiated resins was not measured. The reason for the increased water uptake in the irradiated samples was not discussed in the study. The water uptake and hence the swelling was generally found to be proportional to the square root of time, indicating that the water uptake is a diffusion-controlled process. The results presented by Aittola and Kleveland (1982) correspond to a swelling rate from tenths of millimetres per year to a few mm per year.

The effect of temperature and waste-bitumen ratio on water uptake and swelling of ion-exchange resins solidified in bitumen (Mexphalt 40/50) immersed in water for up to 1 month was studied by Brodén and Wingefors (1992). For a matrix with 40 % resin by weight almost no water uptake or swelling was observed at temperatures between 3 °C and 30 °C. At higher resin fractions (50 %, 60 % and 70 %), the water uptake increased with increasing resin content, but no significant difference between a temperature of 20 °C and 30 °C was noticed. However, at 3 °C the water uptake was considerably higher, with a weight increase of 24 % after 20 days with a 50 % waste loading, a weight increase of 127 % after 28 days with a 60 % waste loading and 149 % weight increase after 27 days with a waste loading of 70 %. At waste loadings of 60 % or higher, the water uptake was so fast that a diffusion-controlled mechanism could be excluded. The weight increase was higher than could be explained from measurements of water uptake by ion-exchange resins (Nilsson et al. 1988), indicating the formation of water-filled cracks and pores in the bitumen matrix.

Long-term water uptake experiments performed on small samples of bituminised mixed anionic and cationic resins have shown a weight increase after 5 000 days (nearly 14 years) of between 50 % and 60 % due to water uptake (Aalto and Valkiainen 1997). The weight increase did not show any signs of diminishing.

The behaviour of bituminised ion-exchange resins under repository conditions has been evaluated (Aalto and Valkiainen 2004). In this study water uptake and leaching were measured in samples placed in artificial concrete water at a temperature between 5 and 8 °C. The low temperature was chosen since earlier studies had found that the rate of water uptake and swelling at lower temperatures was higher than at room temperature (Brodén and Wingefors 1992). The samples consisted of a 50:50 mixture of bitumen and dried ion-exchange resins cast at a temperature of 140 °C. The samples had absorbed between 8 % and 18 % water after 1 250 days. The samples with the higher water uptake had been stored for 6 months before the experiment and it was estimated that they absorbed 5 % water from the air during the storage. Microscopic examination of the wetting front showed that the penetration of the front was proportional to the square root of time for about 500 days, after which a decline in the rate of front advance was observed. The penetration of the front was around 11 mm in about 1 000 days.

Swelling and water uptake of bituminised ion-exchange resins in a confined space

Very few studies have been found on the swelling of bituminised ion-exchange resins in a confined space. Valkiainen and Vuorinen (1985, 1989) report experiments with bituminised resins performed on samples from a test drum with inactive resin from Olkiluoto Power Plant. Four samples were taken at different vertical positions in the drum and the swelling due to water uptake at constant pressure was measured. Initially a constant preload of 1 MPa was applied and the volume changes were monitored. During the course of the experiments the preloading was changed. The results corrected for escape of bitumen in the oedometer are published in Valkiainen and Vuorinen (1989). The samples taken from

the middle and the top of the drum showed only a small volume increase (initially less than 5 % and decreasing with time). After 200 days the preload was reduced to 0.5 MPa, which resulted in a small volume increase (less than 2 %). The behaviour was quite different for the sample from the bottom of the drum. In this case the volume increase with the initial preload of 1 MPa resulted in a swelling of 30 % after 400 days. At that time the swelling was still increasing, but after the loading increased to 2 MPa, the swelling reduced to 26 %. The examination of the resins in the samples showed that due to separation, the bottom sample only contained grains of cationic resin, while the upper two samples mainly contained grains of anionic resin. Also, the resin content was higher in the bottom part of the drum (58 %) compared with that in the middle and top of the drum (43–45 %).

Swelling of evaporator concentrates

Bitumen is commonly used for stabilisation of evaporator concentrates. The swelling behaviour of bituminised evaporator concentrates has been extensively studied in Denmark, France, United Kingdom, Belgium and Germany. Although the processes for water uptake are similar to those of ion-exchange resins, there is a major difference in that the salts giving rise to osmotic pressure can leach out of the waste.

The osmosis-induced swelling, water uptake, pressure increase and $NaNO_3$ leaching of small cylindrical samples of Eurobitum[5] (diameter 38 mm, height 10 mm) have been studied under constant total stress conditions and nearly constant volume conditions (Valcke et al. 2010, Mariën et al. 2013). The studied waste had a matrix of hard (blown and oxidised) bitumen (Mexphalte R85/40) with a waste loading of 40 % out of which about 30 % is $NaNO_3$. The theoretical osmotic pressure of a saturated $NaNO_3$-solution is 42.8 MPa. After four years of testing of water uptake under nearly confined conditions, pressures up to 20 MPa have been measured. Only the outer 1–2 mm of the sample was found to be hydrated and only about 10–20 % of the initial content of $NaNO_3$ was released. The measurements under a constant total stress of 2.2 MPa resulted in a swelling after 900 days of around 8 %. Higher total stress did not result in significantly smaller swelling. A counter pressure of 3.3 MPa gave around 10 % swelling after 900 days and a pressure of 4.4 MPa gave 7 % swelling after 900 days and 16 % swelling after 1 500 days. Examination of the samples with scanning electron microscopy after the tests showed that the high pressure recompresses the leached layer and that a low-permeable layer of recompressed bitumen was formed at the surface of the sample.

A coupled chemical-hydromechanical model has been set up (Mokni et al. 2011). A model prediction of the evolution of the osmosis-induced pressure in the nearly confined tests showed that the pressure would reach a maximal value of about 20 MPa after about 5.5 years, after which the pressure would start to decrease. After about 27 years, the pressure would have decreased to a value of ~2 MPa.

A corresponding numerical model has been developed to reproduce the behaviour of French simplified bituminised waste products with sodium nitrate as the only salt (Melot et al. 2020), taking into account the impact of dissolution, permeation, diffusion, osmosis and the evolution of porosity. The model was mainly used to reproduce the behaviour of water absorption and salt leaching for unconfined bituminised waste exposed to water for up to 1 000 days. The model makes use of both experimentally obtained principal parameters and parameters obtained through calibration of the model. The raw and processed data required to reproduce the results in the study were not available at the time of publication, since the data was part of an ongoing study.

The effect of salt content on leaching properties of synthetic bituminised wastes has also been investigated by Japan Atomic Energy Agency. Both leaching during unconfined conditions (Irisawa et al. 2014), as well as swelling pressure during confined conditions (Irisawa and Meguro 2017), have been investigated. The swelling pressure was monitored over durations of up to 600 days and increased with both time and salt content. The experimental maximum pressure was approximately 15 MPa.

Unconfined leaching and swelling experiments have recently been performed by SKB, with both ion-exchange resin, Dowex 50, and anhydrous sodium sulfate salt, Na_2SO_4, present in the bituminised synthetic waste (Johansson 2017). According to the experimental results both the rate of water uptake

[5] Bituminised radioactive waste produced according to the Eurobitum process at Eurochemic/Belgoprocess reprocessing facility (Mol-Dessel, Belgium).

and leaching increases with decreasing bitumen content, which is consistent with other investigations. A destilled and slightly softer bitumen, Nybit 55, was used during the leaching experiments, resulting in changes of the geometric shape for most of the samples with time.

Data available

Limited data have been found for swelling pressures induced by bituminised ion-exchange resins. Several studies have been performed on the confined swelling of samples containing ion-exchange resins only. These studies indicate very high swelling pressures, in the order of 30–60 MPa, for a completely confined ion-exchange resin. Thermal treatment of the anionic resins results in a reduced swelling, due to a reduction in ion-exchange capacity. Both experimental and theoretical studies indicate that the swelling pressure is drastically reduced if the ion-exchange resins are allowed to swell to a certain degree before being confined.

Presented below is a summary of experimental data on swelling pressure for waste with mixed anionic and cationic resins. Furthermore, theoretical calculations have been performed of the swelling based on the model and data for ion-exchange resins from Matsuda et al. (1992) and Nilsson et al. (1988).

Summary of experimental results

In Figure 6-1 a summary is presented of the available experimental results for mixed resins. It contains both experiments performed in Sweden and Finland with ion-exchange resins mixed with glass powder as well as the Finnish experiments with samples from bituminised mixed anionic and cationic resins.

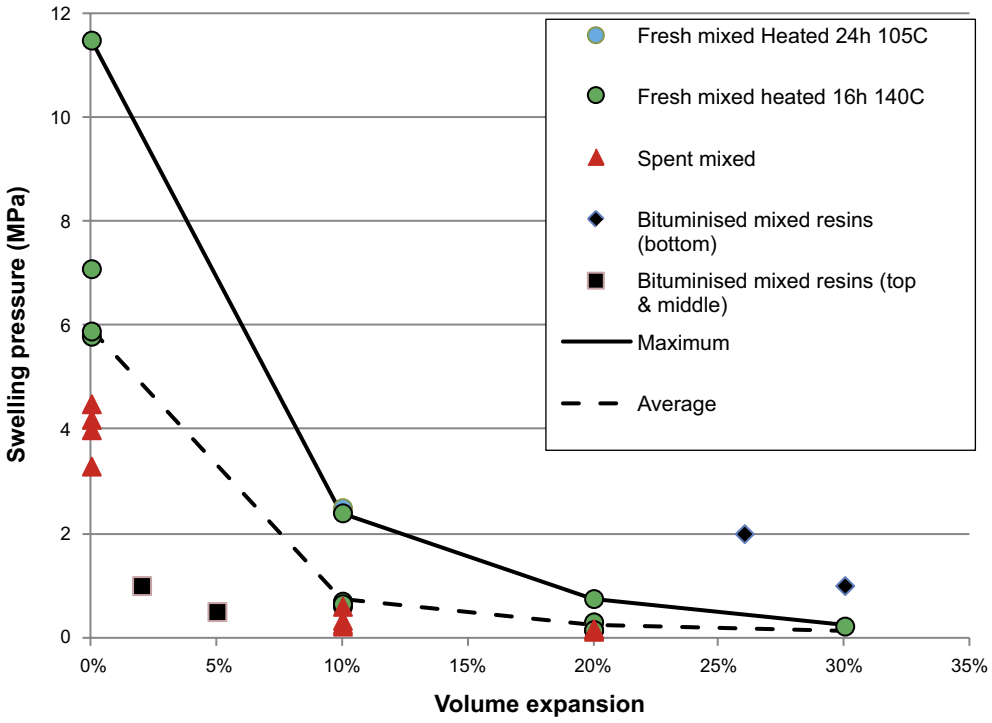

Figure 6-1. *Swelling pressure as function of relative increase in volume of waste for mixed cationic and anionic resins including lines for maximum and average values. Data from Valkiainen and Vuorinen (1985, 1989).*

The measurements on bituminised waste indicate lower swelling from samples from the top and the middle of the waste drum (black squares) as compared with the swelling of resins with glass. The samples from the bottom of the drum (black diamonds) had a high swelling also at high pressure, which was explained as a result of the settling of the cationic resin at the bottom of the drum.

Theoretical approach based on experiments with ion-exchange resins

Using the model and data from Nilsson et al. (1988) and the model and data from Matsuda et al. (1992), the swelling pressure at different degrees of volume expansion has been calculated for various ion-exchange resins and waste loadings. Finally, calculations have been performed for conditions judged to be representative for the various bitumen waste types in SFR.

Figure 6-2 shows the swelling pressure as a function of the relative volume increase of the resin calculated using the model and data from Matsuda et al. (1992). Curves are given for cationic resins with different exchange capacities. The decrease in capacity was obtained by heating the resins at temperatures between 200 and 300 °C. The figure shows that a rather drastic reduction of the exchange capacity is needed in order to reduce the swelling pressure.

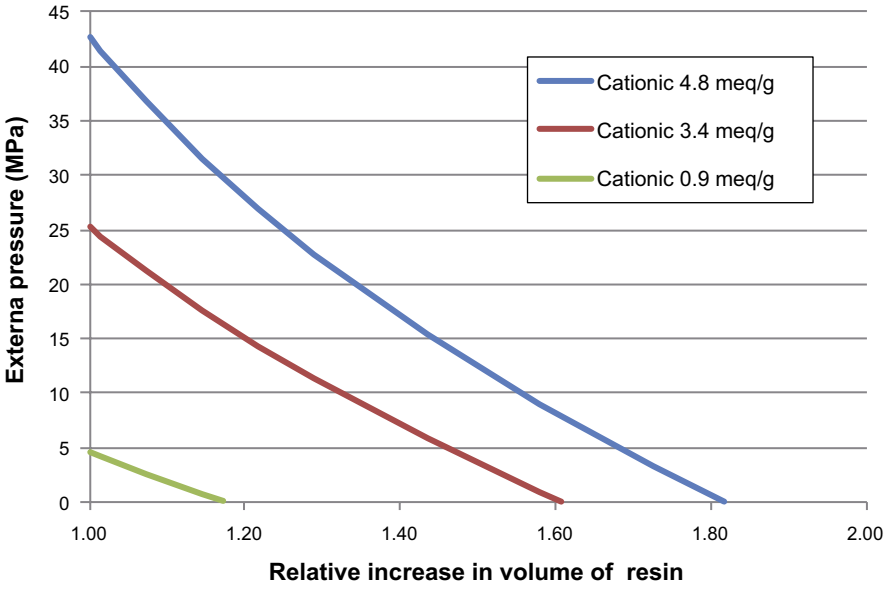

Figure 6-2. *Swelling pressure as function of relative increase in volume of resin for cationic resins with different exchange capacity. Model and data from Matsuda et al. (1992).*

In Figure 6-3 swelling pressures calculated according to the results of Matsuda et al. (1992) for different degrees of cross-linkage are presented together with results for the resins studied by Nilsson et al. (1988). Included are also results for the cationic resin ARC 351 heat treated for 1 hour at 150 °C. The external pressure is very similar to that of the untreated resins, possibly due to the relative short treatment time. Figure 6-4 shows that water uptake in anionic resins results in a lower external pressure compared with that of the cationic resins, but also in this case, the effect of the heat treatment is small. However, there is an uncertainty in the calculation of the external pressure for the heat-treated resins as the resin density is also changed.

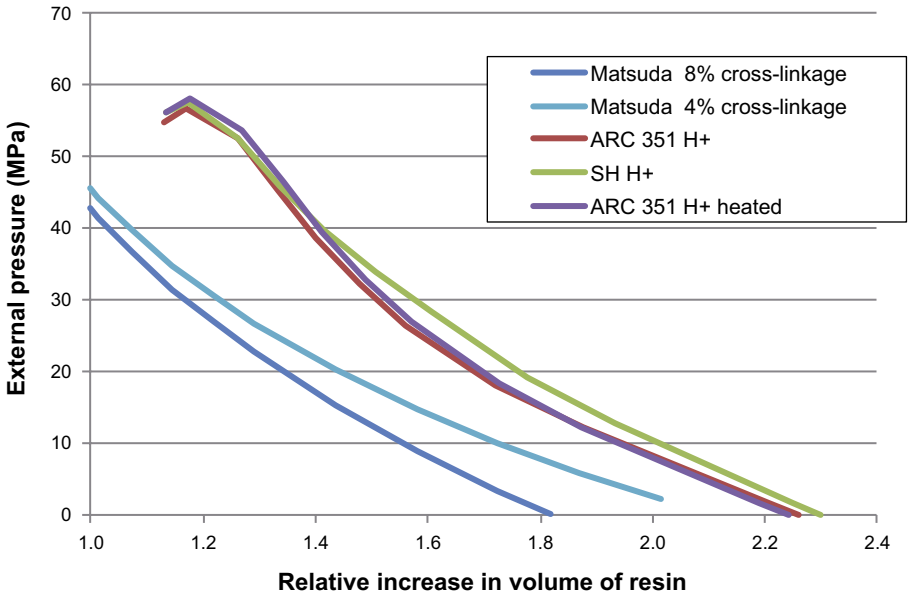

Figure 6-3. *Swelling pressure as function of relative increase in volume of resin for cationic resins. Model and data from Matsuda et al. (1992) and calculated values based on model and data from Nilsson et al. (1988) for cationic resins (granulate ARC and powdered SH).*

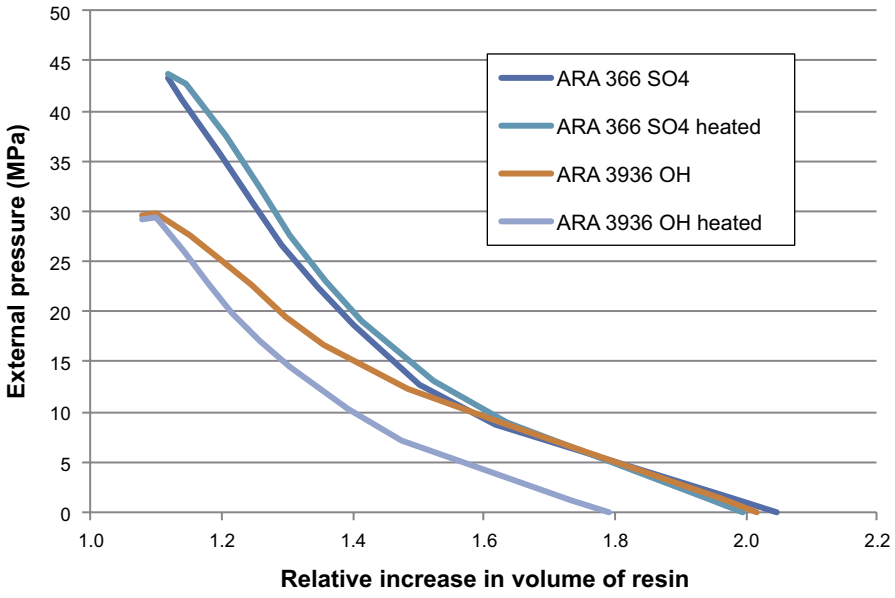

Figure 6-4. *Swelling pressure as function of relative increase in volume of resin for anionic resins. Calculated values based on the model and data from Nilsson et al. (1988) for anionic resins (granulate ARC 366 and ARA 3936).*

The results from the tests with ion-exchange resins have been extrapolated to waste packages taking into consideration the loading of resin in the bitumen matrix, see Table 6-4. No other effects such as elastic properties of the bitumen matrix have been taken into account. The properties of normal packages have been used. It is assumed that 35 % of the resins are in cationic form (ARC 351 H+) and 65 % in anionic form (ARA 9396 OH− heat treated). When estimating the pressure of the mix of resins it is assumed that the water activity of the two types of resins is equal. The results of calculations are presented in Figure 6-5.

Table 6-4. Waste types placed in BMA and silo.

Waste type	Waste loading	Type of waste	Comment
B.05, B.06	25 %	Powdered and ground bead resin. Anionic and cationic	Treated with Na_2SO_4
F.18	38 %	Powdered resin (65 % anionic 35 % cationic) Bead resin (50 % anionic 50 % cationic). Filter aid.	Heat treated 150 °C 15 hours.
F.17	48 %	Powdered resin (65–80 % anionic and 20–35 % cationic) Bead resin (50 % anionic 50 % cationic).	Heat treated 150 °C 15 hours. May include up to 40 % evaporator concentrates
F.05	58 %	Powdered resin (65–80 % anionic and 20–35 % cationic) Bead resin (50 % anionic 50 % cationic).	Heat treated 150 °C 15 hours. Category F05:2 for shorter period.

The results of the theoretical calculations indicate much higher pressures than obtained in the experiments reported by Valkiainen and Vuorinen (1985, 1989) and Snellman et al. (1986), see Figure 6-1. This large discrepancy between theoretical results and experimental measurements has been noted previously. One explanation is the deformation caused by the ion-exchange resins (Emrén 1983). The theoretical calculations of the swelling resins presented in Figure 6-5 also neglect the effect the bitumen matrix has on the water uptake and the related swelling pressure. Recent experiments performed in Belgium indicate that the bitumen matrix may reduce the swelling pressure of the solidified waste (Valcke et al. 2010). However, these experiments were performed on another type of waste (evaporator concentrates) and a harder type of bitumen (blown) than the distilled bitumen used in Sweden. Considering the effects neglected in the theoretical calculations, the emphasis in the evaluation is put on the experimental data presented in Figure 6-1.

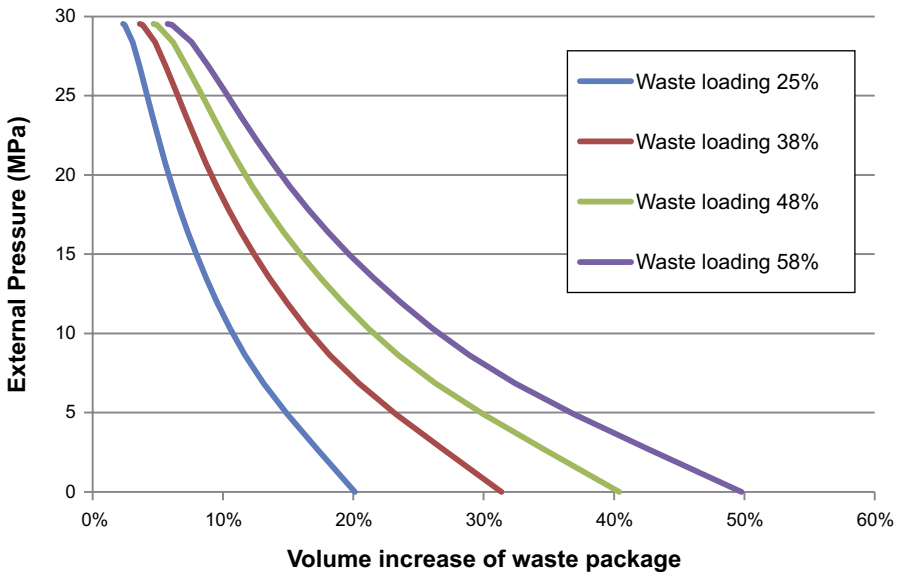

Figure 6-5. *Estimated external pressure as a function of volume increase for different waste loadings corresponding to bituminised waste in silo and BMA.*

Sources of information

The sources of information are given in Table 6-5.

Table 6-5. Main sources of information used in data qualification.

Sources of information
Aalto H, Valkiainen M, 1997. Simulated wetted bituminization product. In Vettyneen bitumointuotteen jatkokarakterisointi. Työraportti VLJ-6/97. VTT Chemical Technology.
Aalto H, Valkiainen M, 2004. Behaviour of bituminized ion-exchangers under repository conditions. In Long term behaviour of low and intermediate level waste packages under repository conditions. Results of a co-ordinated research project 1997–2002. IAEA-TECDOC-1397, International Atomic Energy Agency, 89–100.
Aittola J-P, Kleveland O, 1982. Swelling of bituminized ion exchange resins. NKA AVF (82) 215, Studsvik.
Aittola J-P, Chyssler J, Ringberg H, 1982. Thermal stability of ion-exchange resins. SKBF/KBS TR 81-13, Svensk Kärnbränsleförsörjning AB.
Almkvist L, Gordon A, 2007. Low and intermediate level waste in SFR 1. Reference waste inventory 2007. SKB R-07-17, Svensk Kärnbränslehantering AB.
Andersson L, Karnland O, Hedström M, 2014. Swelling pressure of ion-exchange resins at SFR. Clay Technology AB. SKBdoc 1450664 ver 1.0, Svensk Kärnbränslehantering AB.
Asea-Atom, 1985. B1 – Analys av bitumenprodukter: Svällningstester. Rapport KVC 85-204. (In Swedish.)
Berntsson J, 1992. Typbeskrivning av avfallskollin (B20) – Bitumensolidifierad jonbytarmassa och filterhjälpmedel i plåtfat förpackade i containrar, Beteckning B.20, PBD-9102-05, Sydkraft Barsebäcksverket. (In Swedish.)
Blinder R, Champenois J-B, Leclerc A, Poulesquen A, Guillermo A, Lautru J, Podor R, Bardet M, 2019. NMR 1D-Imaging of water infiltration into porous bitumen-salt matrices: the effect of salt solubility. The Journal of Physical Chemistry C 123, 27105–27115.
Brodén K, Wingefors W, 1992. The effect of temperature on water uptake, swelling and void formation in a bitumen matrix with ion exchange resins. Waste Management 12, 23–27.
Brodersen K, Mose Pedersen B and Vinther A, 1983. Comparative study of test methods for bituminized and other low- and medium-level solidified waste materials. Final report (1981–1982) for contract WAS 235 DK(G). RISØ-M-2415, Risø National Laboratory, Roskilde, Denmark.
Dverstorp B, Sundström B, 2003. SSI:s och SKI:s granskning av SKB:s uppdaterade slutlig säkerhetsrapport för SFR 1. Granskningsrapport. SSI Rapport 2003:21, Swedish Radiation Protection Authority, SKI Rapport 2003:37, Swedish Nuclear Power Inspectorate. (In Swedish.)
Emrén A T, 1983. Theoretical calculation of swelling properties of ion-exchange resins. KEFYDA Konsult AB.
Ericsson K, Klingstedt G, 1987. Svällningsegenskaper hos radioaktiva jonbytarmassor från Forsmarksverket. Rapport 87041, The Swedish Cement and Concrete Research Institute (CBI). (In Swedish.)
Irisawa K, Meguro Y, 2017. Swelling pressure and leaching behaviors of synthetic bituminized waste products with various salt contents under a constant-volume condition. Journal of Nuclear Science and Technology 54, 365–372.
Irisawa K, Ohsone O, Meguro Y, 2014. Effects of salt content on leaching properties of synthetic bituminized wastes. Journal of Nuclear Science and Technology 51, 323–331.
Jensen V, Karnland O, Hedström M, 2017. Swelling capacity and swelling pressure of ion-exchange resins at SFR. Clay Technology AB. SKBdoc 1667888 ver 1.0, Svensk Kärnbränslehantering AB.
Johansson E, 2017. Kemirapport AP TD PSU15-16-025 Volymexpansion och lakningsexperiment åt PSU-1504. SKBdoc 1603429 ver 1.0, Svensk Kärnbränslehantering AB. (In Swedish.)
Le Feunteun S, Diat O, Guillermo A, Poulesquen A, Podor R, 2011. NMR 1D-imaging of water infiltration into mesoporous matrices. Magnetic Resonance Imaging 29, 443–455.
Mariën A, Mokni N, Valcke E, Olivella S, Smets S, Li X, 2013. Osmosis-induced water uptake by Eurobitum bituminized radioactive waste and pressure development in constant volume conditions. Journal of Nuclear Materials 432, 348–365.
Matsuda M, Nishi T, Chino K, Kikuchi M, 1992. Solidification of spent ion exchange resin using new cementitous material, (I). Swelling pressure of ion exchange resin. Journal of Nuclear Science and Technology 29, 883–889.
Melot G, Dangla P, Granet S, M'Jahad S, Champenois J B, Poulesquen A, 2020. Chemo-Hydro-Mechanical analysis of Bituminized waste swelling due to water uptake: Experimental and model comparisons. Journal of Nuclear Materials 536, 152165. doi:10.1016/j.jnucmat.2020.152165
Mokni N, Olivella S, Valcke E, Mariën A, Smets S, Li X , 2011. Deformation and flow driven by osmotic processes in porous materials: application to bituminised waste materials. Transport in Porous Media 86, 635–662.
Nilsson A-C, Högfeldt E, Muhammed M, Wingefors S, 1988. On the swelling of ion exchange resins used in the Swedish nuclear power plants. SKI TR 1988:1, Swedish Nuclear Power Inspectorate.
Pettersson M, Elert M, 2001. Characterisation of bituminised waste in SFR 1. SKB R-01-26, Svensk Kärnbränslehantering AB.
Riggare P, Johansson C, 2001. Project SAFE. Low and intermediate level waste in SFR-1. Reference Waste Inventory. SKB R-01-03, Svensk Kärnbränslehantering AB.

Table 6-5. Continued.

Sources of information
SKB R-08-130, SKB 2008. Safety analysis SFR 1. Long-term safety. Svensk Kärnbränslehantering AB.
Snellman M, Valkiainen M (eds), 1985. Long-term properties of bitumenised waste products. Nordic Liaison Committee for Atomic Energy (NKA).
Snellman M, Valkiainen M, Airola C, Bonnevie-Svendsen M, Brodersen K, Forsström H, Wingefors S, 1986. Long-term behavior of bituminized waste, Waste Management '86 Proceedings of the Symposium on Waste Management at Tucson, Arizona, March 2-6, 1986. American Nuclear Society. Vol 3, 501–507.
Valcke E, Mariën A, Smets S, Li X, Mokni N, Olivella S, Sillen X, 2010. Osmosis-induced swelling by Eurobitum bituminized radioactive waste in constant total stress conditions. Journal of Nuclear Materials 406, 304–316.
Valkiainen M, Vuorinen U, 1985. Properties of bituminzation product from Olkiluoto power plant. Report YJT-85-24, Nuclear Waste Commission of Finnish Power Companies.
Valkiainen M, Vuorinen U, 1989. Long-term properties of TVO's bituminized resins. Report YJT-89-06, Nuclear Waste Commission of Finnish Power Companies.
Weast R C, 1985. CRC Handbook of chemistry and physics: a ready-reference book of chemical and physical data. 65th ed. Cleveland, OH: CRC Press.

Categorising data sets as qualified or supporting data

No qualified data sets have been identified concerning the swelling pressure data for bituminised waste applicable to the waste forms in SFR. Two supporting data sets have been identified, see Table 6-6. Data have been chosen for experiments with heat treated mixed anionic and cationic resins. Results from pure cationic resins have been excluded.

Table 6-6. Qualified and supporting data sets.

Qualified data sets	Supporting data sets
No peer reviewed sources of data have been found in the open literature. Information from technical reports have been found that contain relevant information applicable to the conditions in SFR.	Valkiainen and Vuorinen 1985, Table 5 Valkiainen and Vuorinen 1989, Figure 2-9

Excluded data previously considered as important

No previously considered data have been excluded.

6.5 Conditions for which data are supplied

The experiments have been conducted on mixed anionic and cationic granular resins with a waste loading corresponding to about 50 % waste. The resins have been heat treated at 140 °C for at least 10 hours. Other waste loadings, types of resins, treatments or additives may produce different results.

6.6 Conceptual modelling uncertainty

A significant conceptual uncertainty relates to the behaviour of the bitumen matrix in the swelling waste. The mechanical properties of the bitumen (affected by temperature, ageing, radiation) are important for the possibility to form cracks or fissures that will generate an open porosity in the waste matrix. Furthermore, swelling will initiate at the surface and progressively affect parts of the interior of the waste package. The water uptake and the degree of swelling of waste particles (ion-exchange resin or salt) will be different in different parts of the waste packages. Salts may diffuse out of the package, and thus the potential for swelling will be lost. As a consequence, the actual swelling may only occur in a limited zone. The pressure exerted on the leached zone may recompress the remaining bitumen matrix creating a bitumen layer with very low permeability as was observed in the Belgian experiments (Valcke et al. 2010, Mariën et al. 2013). However, this behaviour may be limited to very

soluble salts since insoluble salts appears to induce fast water uptake in the depth of the bitumen matrix (Le Feunteun et al. 2011, Blinder et al. 2019). Ion-exchange resins on the other hand will remain in the matrix, possibly forming a compressible zone in the outer parts of waste package. Since the long-term swelling of a bitumen matrix with ion-exchange resin has not been investigated it creates large uncertainties in the interpretation of how the swelling of the waste is propagated to the waste package.

Pressure build-up due to confined swelling is difficult to measure. Firstly, the equipment used must be able to ascertain the degree of confinement. It is somewhat uncertain whether confining conditions were maintained in the previous experiments with quartz powder (Snellman and Valkiainen 1985, Snellman et al. 1986). The oedometer type used by Valkiainen and Vuorinen (1985, 1989) and Valcke et al. (2010) to test the swelling of bituminised resins seems to be a usable experimental set up, although problems with bitumen "leakage" have been reported. However, measurements on bituminised resins have a very slow pressure build-up due to the slow diffusion of water into the waste. Another source of uncertainty is that most tests for practical and safety reasons have been performed on inactive samples. Radiation will influence both the resin and the bitumen. In some cases, the effect of radiation has been simulated by external radiation (0.1–1 MGy). Radiolysis has been judged to have negligible effects for an absorbed energy less than 0.1 MGy (Eschrich 1980). The estimated energy absorbed in the bituminised waste placed in SFR is about 0.01 to 0.1 MGy, but a fraction of packages may obtain a dose exceeding 0.1 MGy (Pettersson and Elert 2001).

6.7 Data uncertainty – precision, bias, and representativity

A limited amount of data is available on the swelling pressures that can develop due to water uptake of bituminised ion-exchange resins. The data selected here represent the part of the available data judged to best represent the bituminised wastes disposed in SFR. However, the experimental data do not cover the full range of resin types, waste loadings or content of evaporator salts that is found in the bituminised SFR waste. Furthermore, the data show a variation that is not fully understood. There are uncertainties in how the experimental results can be explained by theoretical calculations of swelling pressure. This limits the possibility to extrapolate the data to other conditions.

6.8 Data uncertainty – spatial and temporal variability

Spatial variability of data

Swelling tests performed on bituminised samples, for example Aittola and Kleveland (1982) show a large variance between samples. This is probably caused by difficulties in preparing homogenous samples. A variation can also be expected in the waste packages in SFR. The investigations performed in Finland show a large variation between samples taken from different parts of the drum due to the settling of the denser cationic resin. The bituminised resins from Barsebäck are ground in order to decrease the effect of settling and produce a more homogeneous product.

Temporal variability of data

The water uptake process is very slow. The water uptake of small samples has been measured to be on the order of 10 g/m^2 and year as an average over 5 years (Aalto and Valkiainen 1997). The time for water uptake in the drum or a container will be very long. During that time changes in the properties of the bitumen and the ion-exchange resins that affect the pressure build-up may occur.

6.9 Data uncertainty – correlations

The bitumen swelling of a waste package is dependent on the amount of anionic or cationic resin deposited in the package. Therefore, the delivered data have been assessed against the amounts of ion exchange resins present in the waste types B.05, B.06, F.05, F.17, and F.18 asked for in Section 6.1. No other correlations have been identified.

6.10 Result of supplier's data qualification

The supplier has requested the swelling pressure as function of expansion volume for the waste types B.05, B.06, F.05, F.17, and F.18. The data are to be supplied for a reference waste package composition and a waste package representing a worst case composition with respect to swelling pressure.

The waste types B.05, B.06, F.17, and F.18 have similar or lower waste loading compared with that for which the data were developed. The types of resins are similar, but not identical; whereas the data set was developed for granular mixed anionic and cationic resins, the actual waste also contains powdered resins or ground granular resins. The actual waste packages have a varying ratio between the anionic and cationic resins, depending on the mix of powdered and granular resins.

The waste type F.05 has a somewhat higher waste loading compared with that for which the data were developed, a maximum of 60–65 % compared with 50 %.

The waste in F.17 and F.18 is heat treated in a similar way as in the experiments, whereas the waste in B.05 and B.06 is treated with Na_2SO_4 and only heated during the actual bituminisation process. No experimental data for swelling pressures from Na_2SO_4-treated waste has been found.

The waste type F.17 may contain up to 40 % evaporator concentrates that may cause swelling. Based on the investigations on the swelling of bituminised evaporates performed in Belgium (Valcke et al. 2010, Mariën et al. 2013), the swelling pressures of evaporator salts (or concentrates) are in the same order as the maximum values obtained due to swelling of ion-exchange resins.

The background material does not allow for confidently differentiating between the different waste types. Therefore, it is recommended that the following data are used for all waste types with the average value representing the reference waste package and the maximum value as a more pessimistic case. Considering the uncertainties, the latter cannot be confidently referred to as a worst case. See Table 6-7 for the recommended data.

6.11 Judgements by the assessment team

Sources of information

The sources of information summarised in Table 6-5 are used in this judgement.

Conditions for which data is supplied

The assessment team accepts the conditions listed in Section 6.5.

Conceptual modelling uncertainty

The supplier notes significant conceptual uncertainties related to the behaviour of bitumen in the swelling waste. The assessment team agrees that the swelling of bituminised waste is a complex, coupled process and that the current understanding of the swelling process is incomplete.

Data uncertainty – precision, bias, and representativity

The supplier notes that the amount of representative experimental data is limited and that theoretical models for swelling bituminised waste are not comprehensive. The assessment team agrees with the supplier that extrapolation of the data to conditions not represented by experiments should be performed with caution.

Data uncertainty – spatial and temporal variability

The supplier notes that the water uptake process is very slow and that the properties of bitumen and ion exchange resin may change over time. The assessment team considers the stationary pressure exerted by swelling.

Data uncertainty – correlations

The assessment team agrees with the supplier on the correlations listed in Section 6.9.

Results of supplier's data qualification

The supplier concludes that the swelling behaviour of waste types B.05, B.06, F.05, F.17, and F.18 cannot be confidently differentiated. In Table 6-7 the supplier suggests a swelling behaviour generic for all bituminised waste forms in the SFR. The assessment team accepts this conclusion.

6.12 Data recommended for use in the assessment

The data presented in Table 6-7 are recommended for use in the safety assessment modelling.

Table 6-7. Data for swelling pressure at different volume increase of the waste.

	Swelling pressure (MPa) at different volume increase			
	0 %	**10 %**	**20 %**	**30 %**
Average	6	0.7	0.3	0.1
Maximum	12	2.5	0.75	0.22

7 Concrete/cement sorption data and Bentonite sorption and diffusivity data

This section concerns sorption data for different barrier materials present in SFR. The information in this chapter is largely unchanged since the previous safety assessment SR-PSU (i.e. SR-PSU Data report SKB TR-14-10, Chapter 7), with unchanged text in black and new information in blue font.

More specifically, the chapter describes the sorption coefficients for use in the radionuclide transport modelling, described in the **Radionuclide transport report,** and the sorption reduction factors (SRF) applied to account for the concentration of complexing agents in each waste vault of SFR. The materials are the different concrete/cement mixtures present in SFR and the different bentonite materials present in the silo, both described below. This chapter also treats initial porosities for both concrete/cement materials and bentonite as well as diffusivity data for bentonite. Diffusivities for concrete/cement materials are handled in Chapter 9. Sorption properties of crushed rock are given in Chapter 8.

The new information since the previous safety assessment (SR-PSU) concerns primarily concrete/cement sorption data based on for instance Nagra's database (Wieland 2014) and specific experimental studies (Tits et al. 2014, Bruno et al. 2018, Tasi 2018). Additional information on SRF is also given based on Keith-Roach et al. (2021).

Concrete/cement

The cementitious materials that can be found in SFR are mainly: structural concrete in structures, waste packaging and waste, grout used as backfill around waste packages and different cementitious materials used for conditioning of waste within waste packages. The mix proportions of different cementitious materials present in SFR are given in Table 7-1. The type of cement used varies over time, but so far ordinary Portland cement has been used in all cementitious materials.

Structural concrete

The structural concrete in SFR is present in the silo, 1–2BMA, 1BRT and 1–2BTF as slabs and lids. The silo, 1–2BMA and 1BRT also have inner and outer walls made of structural concrete. The 1–5BLA vaults have structural concrete slabs, but no lids. The structural concrete is also present as moulds and/or tanks in the silo, 1–2BMA and 1–2BTF. In addition, a large amount of concrete waste, in the form of structural concrete, will be disposed in SFR3.

Grout and other cementitious backfill

Grout is present as backfill, surrounding the waste packages in the silo and 1–2BTF. The void between the waste packages and the vault walls in 1–2BTF will be filled with a cementitious backfill. The void inside the concrete structure in 1BRT is currently planned to be filled with a self-compacting concrete.

Conditioning of waste

Cementitious materials are also used for solidification of ion-exchange resins and sludge, and for stabilisation of trash and scrap metal within many of the different waste packages present in the repository (**Initial state report**).

Table 7-1. Mix proportions for some of the different types of cementitious materials used or planned for use in SFR. For references: see table.

	Silo concrete	1BMA concrete	2BMA concrete	Silo grout	BTF grout*	Conditioning cement
	Jacobsen and Gjørv 1987	Elfwing et al. 2015	Lagerblad et al. 2017	Björkenstam 1997	Initial state report	Initial state report
Cement (kg/m³)	350	280–320	320	325	523	1 180
Water (kg/m³)	164.5	N/A	156.8	366	424	437
Aggregates (kg/m³)	1 829	N/A	1 752	1 302	1 001	-
Limestone filler	-	-	163.3	-	-	-
Bentonite	-	-		-	25	-
Silica	-	-		-	21	-
w/c ratio	0.47 (0.46–0.49)	0.60–0.65	0.49	1.125	0.81	0.37

* Earlier other mix proportions have been reported divided into bottom and top grout, see SKB (R-01-14, Table 4-8).

Bentonite

The bentonite used has the trade name GEKO/QI and is a calcium montmorillonite-based product transformed to the sodium form. The bentonite is used in the silo vault either in an unmixed form or mixed with 90 % sand as a backfill surrounding the concrete silo.

In SKB (R-08-130) the currently installed bentonite parts are described: The silo rests on a 1.5-metre-thick bed made of 90 % sand and 10 % bentonite. The total amount of bentonite used for the bed is 200 ton. The 0.85-metre-wide gap between the concrete silo and rock wall is filled with pure granulated bentonite which has been poured into the space. The top part, which will be installed when the repository closes, will also consist of a mixture of 90 % sand and 10 % bentonite GEKO/QI.

The design is mainly to prevent a high hydraulic flow through the silo vault, but also to retard the diffusion of radionuclides through sorption onto the bentonite minerals. The bentonite barrier also works as mechanical buffer between the rock and the concrete silo.

7.1 Modelling in this safety assessment

This section describes what data are expected from the supplier, and in what modelling activities the data are to be used.

Defining the data requested from the suppliers

- Sorption coefficients K_d (m^3/kg) for the elements of the selected inventory in concrete/cement. As sorption coefficients are only valid for a particular set of conditions, values are supplied for an appropriate range of porewater compositions. For redox-sensitive elements, all relevant oxidation states are considered for data selection. The supplier should deliver data that reflects the sorption for different mechanical and chemical degradation states of the material, from the current condition of the materials to a condition expected at the end of the assessment period.
- Sorption coefficients K_d (m^3/kg) and diffusion parameters (effective diffusivity, diffusion-available porosity) for the bentonite barrier surrounding the concrete silo.
- Sorption reduction factors, SRF, for the elements of the selected inventory of radionuclides in the concrete/cement and bentonite materials. The supplier should indicate the lowest concentration for each complexing agent at which effects on sorption can be expected. The complexing agents

to include are ISA (in both diastereomeric forms if available) as well as NTA, EDTA, gluconate, citrate and oxalate. The effects of cement additives should also be discussed and judged. If data are not available for all the radionuclides requested, a discussion of general sorption reduction factors must be included and argued for. As a provisional example: if the sorption reduction of Ni^{2+} has been studied in the presence of ISA, and Co^{2+} has not, the sorption reduction factor of both radionuclides is set to the Ni^{2+} value based on arguments of chemical similarities between Ni^{2+} and Co^{2+}.

Modelling activities in which data will be used

Radionuclide migration is modelled as diffusive and advective transport through the porous material (**Radionuclide transport report**), in combination with sorption of the radionuclides. The magnitude of sorption depends on physical properties of the sorbent (concrete/cement and bentonite), on the porewater composition and on the migrating species.

SRF apply to radionuclides considered affected by complexing agents. SRF are used in all calculation cases to adjust the sorption coefficients K_d to account for the presence of complexing agents. In a less probable scenario where high amounts of complexing agents are assumed to be present in the repository, the reduction factors are multiplied tenfold (**Post-closure safety report**, Chapter 8).

7.2 Experience from previous safety assessments

This section briefly summarises experience from previous safety assessments, which may be of direct consequence for the data qualification in this data report.

Modelling in previous safety assessments

The radionuclide transport in the SAFE safety assessment was modelled with the NUCFLOW software for the near-field transport and with the FARF31 software for the geosphere transport (Lindgren et al. 2001). In the SAR-08 safety assessment, both the near-field and geosphere transport was modelled with the AMBER software (Thomson et al. 2008). The modelling performed in SR-PSU modelling (SKB TR-14-09) generally agrees with the latter SAR-08 modelling. No significant difference with bearing on the parameters covered in this section has been identified regarding sorption.

In both SAFE (Lindgren et al. 2001) and SAR-08 (Thomson et al. 2008), the complexing agents were handled in a residual scenario where the sorption reduction factors were used to simulate the reduced sorption. It was handled in a residual scenario because the amounts of complexing agents in SFR needed to affect the sorption were deemed very unlikely to occur according to Fanger et al. (2001). For the main scenario in SAR-08 it was stated that the forecast quantity of complexing agents was sufficiently low so that sorption was not judged to be affected to a greater degree than was addressed within the uncertainties for the selected sorption data.

In SR-PSU updated SRF values, dependent on concentrations of complexing agents, were recommended in the SR-PSU Data report (SKB TR-14-10) and the concentrations as a function of time were calculated and reported in Keith-Roach et al. (2014). These data were used in the main scenario, as well as a less probable scenario that evaluated the uncertainties in the amounts of complexing agents and cellulose in the repository by applying a 10-fold increase in the sorption reduction factors.

Conditions for which data were used in previous safety assessments

In SAR-08, to be able to reflect the concrete/cement degradation in the repository during its lifetime, the sorption coefficients were gradually altered as a function of time, from values reflecting materials at initial state to values reflecting completely degraded. This approach was also used in the SR-PSU safety assessment modelling to reflect the repository evolution.

In SR-PSU, sorption coefficients were chosen based on a low redox potential in the repository throughout the assessment period. The same general approach is followed in the PSAR, although the redox sensitivity of Pu and U are somewhat reassessed (**Post-closure safety report** Section 6.2.8 subsection Radionuclide speciation).

Sensitivity to assessment results in previous safety assessments

Both in the SAFE and SAR-08 safety assessments, the sorption data had a major influence on the times of release and doses from radionuclides present in SFR. This was especially the case for the actinides such as Am isotopes and Np-237, as they have high affinities for sorption onto the materials present in SFR (Cronstrand 2005).

In SAR-08, the "High concentrations of complexing agents" scenario resulted in a slightly lower dose in the coastal period of the repository lifetime and a slightly higher dose, by around a factor 2, at the beginning of the mire/forest period, compared with the main scenarios Weichselian variant (SKB R-08-130). For the whole repository, the highest dose was not changed compared with the main scenarios Weichselian variant. This was because the maximum doses were dominated by organic C-14, which was not affected by the presence of complexing agents.

Comparing the dose from three calculations in SR-PSU: the global warming variant of the main scenario, the less probable scenario High concentrations of complexing agents scenario and the residual scenario Loss of barrier function scenario – no sorption in the repository (SKB TR-14-01, Sections 9.2.1, 9.3.6 and 9.4.1) showed that the maximum total annual doses are 7.7, 10.7 and 41.4 μSv for the three scenarios, respectively. In the residual scenario the radionuclides Ni-59, Pu-239 and Pu-240, which are less mobile in the main scenario, account for 92 % of the maximum dose. In the scenario with high concentrations of complexing agents, the dose-dominating radionuclides in the main scenario (Mo-93, C-14-org, U-238, I-129, Cl-36) are not subject to complexation and thus unaffected by higher complexing-agent concentrations. The higher dose in the high concentrations of complexing agents scenario occurs at a later time than in the main scenario and is totally dominated by Ni-59.

Alternative modelling in previous safety assessments

No alternative modelling was reported in SAFE, SAR-08 and SR-PSU.

Correlations used in previous safety assessment modelling

No correlations were used in SAFE, SAR-08 and SR-PSU. The modelling in SAFE and SAR-08 assessments was not probabilistic but rather based on deterministic parameters.

Identified limitations of the data used in previous safety assessment modelling

Sorption data are normally based on experimental studies and are sometimes scarce or non-existent and then reliance is placed on chemical analogies with other elements. Also, there are often limitations in the experimental conditions in relation to the conditions projected to arise in the repository.

Regarding complexing agents, the sorption reduction factors in SR-PSU were calculated as step-functions of the concentration rather than as a continuous function, which is considered to have given data with an unnecessarily low resolution. Furthermore, no out-flow of complexing agents was considered in the SR-PSU safety assessment.

7.3 Sources of information and documentation of data qualification

Sources of information

The main sources of information on sorption properties of concrete/cement and bentonite are given in Table 7-2. The main information sources are in turn based on an extensive evaluation of literature data. In the case of the reports by Wang et al. (2009) and Ochs et al. (2011) on sorption in cement systems, the following underlying key references are pointed out. Both describe the sorption processes of various radionuclides in cementitious materials in different states of degradation and evaluate corresponding reference data:

- Wieland and Van Loon (2002).
- Andra (2005).

Among the references considered to be of major importance in Ochs and Talerico (2004) on sorption on bentonite, the following may be pointed out:

- A Nagra report on selected K_d values for MX-80 bentonite (Bradbury and Baeyens 2003), and original data sources cited therein.
- SKB reports on K_d, D_e, and ε_{diff} (Yu and Neretnieks 1997) and groundwater composition (Laaksoharju et al. 1998), and original data sources cited therein.

Most of the data recommended in the Data report for SR-Site (SKB TR-10-52) are from Ochs and Talerico (2004).

New experiments have been performed on cement relevant for SFR to improve sorption data for Ni(II) and Pu(IV) (Bruno et al. 2018, Tasi 2018). In addition, data from new experiments on Th(IV) (Tits et al. 2014) are available. Also, the Nagra database (Wieland 2014) for sorption on cementitious materials is included as a source for information as well as recent reports on the evaluation of the influence of complexing agents (Keith-Roach et al. 2021, Keith-Roach and Shahkarami 2021).

Table 7-2. Main sources of information used in data qualification.

Sources of information
Bruno J, González-Siso M R, Duro L, Gaona X, Altmaier M, 2018. Key master variables affecting the mobility of Ni, Pu, Tc and U in the near field of the SFR repository. Main experimental findings and PA implications of the PhD thesis. SKB TR-18-01, Svensk Kärnbränslehantering AB.
Keith-Roach M, Lindgren M, Källström K, 2021. Assessment of complexing agent concentrations for the post-closure safety assessment in PSAR SFR. SKB R-20-04, Svensk Kärnbränslehantering AB.
Keith-Roach M, Shahkarami P, 2021. Organic materials with the potential for complexation in the SFR repository for short-lived radioactive waste: Investigation of new acceptance criteria. SKB R-21-03, Svensk Kärnbränslehantering AB.
Ochs M, Talerico C, 2004. SR-Can. Data and uncertainty assessment. Migration parameters for the bentonite buffer in the KBS-3 concept. SKB TR-04-18, Svensk Kärnbränslehantering AB.
Ochs M, Vielle-Petit L, Wang L, Mallants D, Leterme B, 2011. Additional sorption parameters for the cementitious barriers of a near-surface repository. NIROND-TR 2010–06 E, ONDRAF/NIRAS, Belgium.
SKB TR-10-52, SKB 2010. Data report for the safety assessment SR-Site. SKB TR-10-52, Svensk Kärnbränslehantering AB.
Tasi A, 2018. Solubility, redox and sorption behavior of plutonium in the presence of α-D-isosaccharinic acid and cement under reducing, alkaline conditions. PhD thesis. Karlsruhe Institute of Technology, Germany.
Tits J, Fujita T, Harfouche M, Dähn R, Tsukamoto M, Wieland E, 2014. Radionuclide uptake by calcium silicate hydrates: Case studies with Th(IV) and U(VI): PSI Bericht Nr 14-03, Paul Scherrer Institut, Switzerland.
Wang L, Martens E, Jacques D, de Cannière P, Berry J, Mallants D, 2009. Review of sorption values for the cementitious near field of a near surface radioactive waste disposal facility. NIROND TR 2008-23E, ONDRAF/NIRAS, Belgium.
Wieland E, 2014. Sorption Data Base for the Cementitious Near Field of L/ILW and ILW Repositories for Provisional Safety Analyses for SGT-E2. NAGRA Technical Report 14-08, Nagra, Switzerland.
A very large number of peer reviewed scientific publications and technical reports from the open literature, as referred to in the above publications and in the present text.

Categorising data sets as qualified or supporting data

In the main, the recommended data are taken or directly evaluated from:

- Wang et al. (2009), Ochs et al. (2011) and Wieland (2014) for concrete/cement.
- Ochs and Talerico (2004) and SKB (TR-10-52) for bentonite.

All of these reports are dedicated data reports and the data therein are considered as qualified. As discussed in Section 7.4, Section 7.6 and Section 7.9 in more detail, it was verified that the conditions underlying these source data are sufficiently representative with regard to the conditions relevant for SFR. The conditions underlying the source data are based on various input data, such as groundwater and material composition, that fed into geochemical/thermodynamic models. Recent model calculations are available in Höglund (2014, 2018, 2019). The redox conditions are evaluated by Duro et al. (2012) and Hedström (2019). The conditions relevant for bentonite in SFR are taken from SKB (TR-10-52) (see discussion in Section 7.4) and the results of various model calculations for SFR by Gaucher et al. (2005) and Cronstrand (2007).

Table 7-3. Qualified and supporting data sets.

Qualified data sets	Supporting data sets
1. Wang et al. 2009, overview plots and summary tables for Cl, I, Nb, Ni, Sr, Cs, Th, U, Pu, Np, Am, C and Tc in Chapter 4.	
2. Ochs et al. 2011, overview plots and summary tables for Ag, Mo, Se, Sn and Zr in Chapter 3.	
3. Wieland 2014, Sections 4.1.19 and 4.1.21.	
4. Bruno et al. 2018, Section 3.4.3.	
5. Tasi 2018, Sections 3.2.4.1 and 3.2.4.2.	
6. Tits et al. 2014, Section 3.4.	
7. Ochs and Talerico 2004, tables and text in Section 5.4.	
8. SKB TR-10-52, Table 5-16 and Table 5-18.	
9. SKB TR-10-52, Figures 5-5 to 5-10.	
1 & 2. Overview plots of experimental K_d values on hydrated cement phases as a function of degradation state and corresponding summary tables of K_d values and upper/lower limits.	
3. Recommended K_d values on hydrated cement phases for Th(IV) and tetravalent actinides and small organic compounds.	
4. Measured K_d values on hydrated cement for Ni.	
5. Measured K_d values on hydrated cement for Pu(IV).	
6. Measured K_d values on hydrated cement for Th(IV).	
7 & 8. Recommended K_d values on bentonite and upper/lower limits for reference conditions.	
9. Overview plots of effective diffusivities in bentonite as a function of clay dry density for Cs, tritiated water (HTO), anions.	

Excluded data previously considered as important

The data that were previously considered as important for the qualification are also included in the present evaluation.

7.4 Conditions for which data are supplied

It is pointed out in several places of this report that especially sorption coefficients are significantly dependent on chemical conditions. The conditions under which the data are considered to be valid are discussed below for both concrete/cement as well as bentonite. It needs to be kept in mind in this context that the prevailing conditions are dependent on the evolution of the repository. The evolution of the various barrier systems in SFR have been modelled by Gaucher et al. (2005) and Cronstrand (2007). While the results differ in detailed aspects, the following key aspects emerge from these studies:

- The various cementitious barriers are predicted to degrade to a different extent, depending on their composition and location. In the following, the states of degradation of hydrated cement paste (HCP) as outlined by Berner (1990) are considered for the evaluation of radionuclide retention, see below. For the definition of sorption data, a wide range of degradation is considered, including fresh HCP up to nearly fully degraded material (end of state III, pH 10.5); see Section 7.9 for details. The evolution of the degradation and chemical conditions in each waste vault is described in the **Post-closure safety report** (Section 6.2.8 and 7.4.2).
- The evolution of the bentonite barrier in the silo is largely determined by the adjacent concrete barrier and shotcrete lining of the rock wall. The model calculations indicate that largely unperturbed bentonite can be expected for extended time periods. Within this timeframe, the largest portion of the bentonite barrier is predicted to be dominated by Na-smectite and non-alkaline porewater with a pH of about 8. When long time periods are considered, the bentonite barrier may be perturbed by the alkaline fluids; this is discussed further below.

Concrete/cement degradation states and porewater properties

As a result of the interaction with groundwater addressed above, the concrete/cement barrier and other cementitious components will be degraded with time.

While there are differences regarding the details, the degradation of hydrated Portland cement follows the following scheme (Berner 1990, Taylor 1990). With respect to interaction with radionuclides (and other solution constituents) it is important to note that each state is characterised by a specific pH and mineralogy. Therefore, radionuclide sorption coefficients are recommended for each state.

- State I: This corresponds to fresh hydrated cement paste. High concentrations of alkalis are still present and are being leached. This leads to pH $\geq$ 13 and elevated Na and K concentrations in the pore solution. Portlandite is present and the Ca/Si ratio of the CSH phases is high (C/S $\geq$ 1.5).
- State II: When the alkali elements are largely removed, state I is followed by a relatively long and stable phase, which is characterised by equilibrium with portlandite ($Ca(OH)_2$) and pH $\approx$ 12.5. The C/S is about 1.5.
- State III: When most Ca has been leached from the system, portlandite disappears and the Ca/Si ratio of the CSH minerals starts to decrease continuously from about 1.5 to about 0.9 (when C/S reaches a value of about 0.8, roughly the C/S ratio of the mineral tobermorite, the CSH phases dissolve completely). In state III, the alumina-sulfate minerals, such as ettringite, also dissolve (at the end of state III, the actual cement matrix disappears and only residual minerals are left). Because state III is relatively heterogeneous, conditions for the beginning and end of this state are considered separately as follows:
  - State IIIa: CSH with a C/S ratio not much lower than 1.5, presence of Ca-aluminates, pH 12.
  - State IIIb: CSH with a lower C/S ratio (approaching C/S $\approx$ 1), absence of Ca-aluminates, pH 10.5.

Many of the predicted details in the evolution of the cementitious materials (such as the exact C/S ratio of CSH) depend to some degree on the specific model used, and in particular on the underlying thermodynamic database. As there are very limited data from real systems, the models are typically parameterised on the basis of systematic data from simplified laboratory systems. Therefore, the

predicted evolution and the compositional details are associated with a degree of model uncertainty. On the other hand, independently of the composition of inflowing groundwater, some of the main constituents of porewaters in hydrated cement systems are controlled by the solid phases themselves:

- The pH (i.e. the concentration of OH^- ions) is very high. This is caused initially by the dissolution of alkalis in the cement, followed by the equilibrium with portlandite.
- The presence of portlandite also gives rise to fairly high concentrations of Ca and concurrent (calcite equilibrium) low concentrations of dissolved carbonate.

With regard to the sorption[6] of most radionuclides to hydrated cement, it is widely agreed that the CSH minerals are the most important solid phase, and that generally strong sorption can be expected in their presence (Wieland and Van Loon 2002, Wang et al. 2009). As major parameters of the solution composition (in particular pH) are also directly related to the solid characteristics, it is reasonable to assume that data from literature sources are applicable for comparable C/S ratios. The influence of differences in the specific cement formulation and in minor solution constituents is expected to be negligible within the data uncertainty considered.

Wang et al. (2009) and Ochs et al. (2011) derived their data for hydrated cement, based on a very extensive literature review. They report sorption data specifically for each relevant cement degradation state, covering all phases from fresh hydrated cement (state I above) to the point where CSH disintegrates (end of state III above).

The evolutions of the degradation states in each waste vault are not further described here but are described in detail in the **Post-closure safety report** (Section 6.2.8 and 7.4.2).

The corrosion of steel present in the repository is expected to keep the system under reducing conditions (Duro et al. 2012, Hedström 2019). Details regarding the redox potential are further described in the **Post-closure safety report** (Sections 6.2.8 and 7.4.2).

Bentonite and porewater properties

The potential effect which the uncertainties in the porewater compositions may have will differ for the various migration parameters:

- K_d generally depends strongly on the aqueous composition. For alkaline and alkaline earth elements (Cs, Ra, Sr), sorption depends mainly on the concentrations of other cations, and is therefore strongly influenced by salinity. On the other hand, the sorption of most other radionuclides is mainly governed by pH and the concentrations of complexing ligands (especially carbonate).
- The diffusion parameters effective diffusivity D_e and porosity ε depend significantly less on the pore water composition, although extremely high or low ionic strength can have an influence on anion exclusion and enhance cation diffusion effects.

Unperturbed bentonite

As described in Section 7.9, the sorption values for the bentonite barrier in the silo of SFR are taken from values derived for the SFK repository by Ochs and Talerico (2004). Due to the conditional nature of K_d, the difference in conditions between the SFK repository and SFR would require a re-calculation of K_d values on formal grounds. However, a critical prerequisite for the derivation of K_d values is a careful calculation of porewater compositions. In this respect, the chemical boundary conditions regarding the bentonite barrier and contacting solutions are not sufficiently constrained to warrant such an approach. On the other hand, as further discussed below, the conditions in the unperturbed bentonite barrier are viewed as similar enough to those considered by Ochs and Talerico (2004) (within the respective range of variations) for K_d values to fall within the overall data range considered for the SFK repository. The situation for altered bentonite is discussed separately below.

[6] The term 'sorption' is used in the wider sense of uptake when applied to cementitious systems; it includes surface sorption (adsorption) as well as the formation of solid solutions and other incorporation processes.

The migration data for bentonite in Ochs and Talerico (2004) are supplied for MX-80 bentonite at a dry density of 1 590 kg/m^3. The dry density of the bentonite buffer in the silo is expected to be 950–1 120 kg/m^3. As pointed out in Ochs and Talerico (2004), K_d of a trace sorbate is independent of the solid:water ratio (for any given set of conditions). Therefore, no adjustment is needed for the difference in density.

The bentonite used for the silo in SFR is GEKO/QI, which is a Na-montmorillonite type. The mineralogy and cation exchange capacity (CEC) are not known in detail. On the other hand, Ochs and Talerico (2004) only considered MX-80 bentonite (Na-form) in their data derivation. However, they considered the following variations in bentonite composition:

- bentonite converted completely to the Ca-form,
- bentonite completely depleted of soluble impurities and some accessory minerals (NaCl, KCl, gypsum, calcite).

The porewater composition in the bentonite will be affected by both the bentonite composition and density as well as by the composition of the infiltrating water. Further, it is not possible to measure the porewater composition in a straightforward fashion, and porewater composition has to be calculated with the help of a clay-water interaction model taking into account all aqueous reactions, mineral solubility, ion exchange and acid-base reactions at the clay edge surface. As a result, the calculated porewater composition is also dependent, to some degree, on the underlying porewater model and the related specific parameters used. This needs to be kept in mind when the influence of bentonite and properties of the infiltrating water on radionuclide migration parameters is discussed.

The reference groundwater used in Ochs and Talerico (2004) for pore water modelling was saline Beberg water (BFI01B). The main variations for detailed modelling included a non-saline and a highly saline groundwater; two saline groundwaters having alkaline to highly alkaline pH (up to pH 13.15) were also considered. In addition, two cases regarding exchange of gas (CO_2) with the host rock were further considered (a constant CO_2 partial pressure imposed by the host rock versus a closed buffer system).

A representative range of composition of the groundwater at the SFR site is given in SKB (R-08-130), as well as the composition range of the overlying part of the Bothnian Sea (Öregrundsgrepen), which may be more representative for future groundwater compositions. In terms of pH and concentrations of major constituents, the two waters are very similar. Moreover, the indicated composition range, and in particular the expected salinity, is almost fully covered by the span of compositions represented by the reference groundwater and the two main variations considered by Ochs and Talerico (2004).

In all likelihood, the characteristics of the solution infiltrating the bentonite will be strongly influenced by the cementitious materials situated on both sides of the barrier (silo wall, shotcrete). Ochs and Talerico (2004) give the calculated porewater composition for bentonite in contact with two hypothetical saline groundwaters, where the presence of sufficient alkalis was assumed to give a groundwater pH of 10.5 and 13.2. These solutions approximately represent saline groundwater in equilibrium with degraded and fresh hydrated cement. Due to the buffering effect of the bentonite, the porewater pH remained at pH ≈ 7.5, as long as the exchange of CO_2 with the surrounding host rock/groundwater system was considered.

In view of the above-mentioned additional uncertainties in calculating porewater compositions, it is considered that the composition of the porewater in the unaltered parts of the bentonite barrier of the silo can be represented with the range of porewater compositions given in Ochs and Talerico (2004). In particular, the reference porewater (RPW, corresponding to the saline Beberg groundwater) considered in Ochs and Talerico (2004) is expected to have a relatively similar composition.

Perturbed bentonite

Depending on the specific model used for assessing the evolution of the silo barrier system, an altered mineralogy and/or an elevated porewater pH may have to be expected for very long timeframes. Such conditions are obviously outside the range considered in Ochs and Talerico (2004). Accordingly, their values cannot be used for that period, and the conditions in the perturbed material are not defined

well enough to warrant the derivation of new data. Note that the models of both Gaucher et al. (2005) and Cronstrand (2007) indicate a substantial portion of unperturbed material for all time periods in most scenarios.

At least for some of the relevant radionuclides, the minerals formed in perturbed bentonite (e.g. zeolites) should be as good or better sorbents than the original bentonite minerals. However, the uncertainties in the modelling of the evolution of the mineral and solution composition do not allow a quantitative assessment. On the other hand, it is still reasonable to assume a certain level of sorption. Further information is given in Section 7.9.

Sorption reduction factors

The conditions for the SRFs are described in detail in Keith-Roach et al. (2021). The SRFs are calculated based on experiments conducted under repository-like conditions, i.e. alkaline and in presence of solid cement or cement-equilibrated solutions, i.e. porewater. Some data obtained from thermodynamic modelling were extrapolated to SFR conditions (Keith-Roach et al. 2021, Appendix 3). The underlying experiments were performed on timescales of at most the order of years, so extrapolation to longer timescales was performed to obtain data over timescales relevant for the safety assessment, i.e. many millennia.

7.5 Conceptual modelling uncertainty

Concrete/Cement

As discussed in the **Waste and Barrier process reports**, the main uncertainty regarding the quantification of radionuclide sorption in cementitious systems is related to the lack of clear evidence regarding the details on the underlying sorption processes for example adsorption, surface complexation, coprecipitation, solid solutions and ion-exchange (see further the **Waste process report**, Section 3.5.3). When the underlying processes are not identified, it becomes also more difficult to evaluate the influence of conditions on sorption and to assess the appropriateness of experimental procedures that form the basis of the available source data. Therefore, experimental sorption data for hydrated cement systems are possibly associated with larger uncertainties than comparable data for other solids. This becomes particularly relevant in cases where only limited data are available.

On the other hand, hydrated cement exerts a very strong influence on the porewater chemistry. Due to the properties of this material, solution chemistry is invariably dominated by a few constituents, whose concentration can be fairly well predicted. Therefore, the variability within cement systems is limited, and reliable data from laboratory systems can generally be viewed as representative. In a few cases, there is evidence that specific solid or solution constituents have a critical influence on sorption, these are addressed separately (Section 7.9). This may also include organic complexing agents, in cases where significant amounts are introduced with the waste or in the form of concrete admixtures.

It may be summarised that the scientific understanding of sorption in hydrated cement systems is associated with large uncertainties in many cases. However, the properties of the material lead to a comparatively small variability of conditions that need to be considered in data derivation.

Bentonite

For the definition of K_d, the most significant conceptual uncertainties, in terms of representing reality, are related to the description of pore water composition in compacted clay as a function of conditions (cf Ochs and Talerico 2004). In case of compacted bentonite, there are some fundamental conceptual uncertainties which are mainly related to scientific shortcomings regarding:

- The distribution of porosity and porewater types among one versus different types of pores.
- The interpretation of the effects of the negative permanent electrostatic charge residing on the planar surfaces of clay platelets.

As the porewater composition of compacted bentonite cannot be determined experimentally with any certainty, it is calculated through thermodynamic surface chemical models. Several published models are available for this purpose (NEA 2012). While they are based on the same principles, they differ in a number of details regarding e.g. assumptions of single or multiple types of pores and porewaters as well as the treatment of electrostatic effects and of specific surface chemical equilibria. Because of the limited accessibility of the pore space of compacted bentonite, a direct comparison of porewater model and experimental results is extremely difficult. However, there are several comparisons of experimental and model-derived macroscopic migration parameters in compacted bentonite (NEA 2012); see also Ochs and Talerico (2004) which indicate that the available models are sufficiently robust for describing the effect of bentonite and groundwater properties on radionuclide migration within experimental uncertainties. These issues are discussed to some detail in the SR-Site Buffer, backfill and closure process report (SKB TR-10-47) and in the **Barrier process report** for this assessment.

In case of anions, it appears to be well established that an anion exclusion effect is operative. In case of the radionuclides sorbing exclusively via ion exchange (Cs, Ra, Sr), the situation is less clear. To date, there are several different models available (NEA 2012) that are all able to describe most of the observed effects. The degree to which the D_e and K_d for these ions have to be considered as correlated depends on the respective model concept used. This has implications regarding the selection of K_d values for compacted systems. Ochs and Talerico (2004) assigned D_e and K_d for these ions independently: first, K_d was calculated through sorption models calibrated on the basis of ion exchange observed in batch experiments, and D_e was subsequently estimated directly from experimental diffusion data.

Conceptual and numerical uncertainties are further introduced when transferring experimental data (especially K_d values) obtained at a specific set of conditions through models or estimation procedures to different conditions relevant for safety analyses. These are of two types:

- Because of the strong dependency of sorption on chemical conditions and surface properties, the experimental data need to be somehow converted to the safety analysis-specific conditions. This can be done through the use of thermodynamic sorption models, where available, or by the use of (semi-quantitative) conversion procedures. A particularly critical issue is the quantitative evaluation of the influence of differences in radionuclide speciation. These types of uncertainty are largely included in the uncertainty factors applied by Ochs and Talerico (2004).
- Due to the difficulties in conducting systematic experiments (e.g. for a range of conditions) in compacted clay, most data are obtained in disperse batch systems. There are basic questions regarding the assumption that batch data are applicable to compacted systems. While this issue is not resolved yet on a fundamental scientific level (see the discussion on porespace characteristics above), all the available macroscopic evidence is compatible with this assumption (NEA 2012).

As discussed in Section 7.4, there are significant uncertainties associated with the application conditions themselves. It is therefore critical to take the conditional nature of the relevant migration parameters into account. In particular K_d values need to be derived for each specified set of (expected) conditions. In Ochs and Talerico (2004), the potential variability of geochemical conditions was addressed by deriving K_d values explicitly for several sets of possible geochemical conditions that covered a wide range.

Sorption reduction factors

Implementing the effect of complexation on sorption as a single linear divisor to K_d is a simplification that relies on several conceptual assumptions of uncertain validity. The first is that everything is in thermodynamic equilibrium, i.e. limited reaction rates for association and dissociation are not considered. The second is that the sorption surfaces are far from saturation, which is judged as likely based on the large amounts of sorbent materials relative to the radionuclide concentrations. Third, constant chemical conditions are assumed, including the ionic strength (moderate), the pH (~ 12.5), and the redox potential (reducing).

An additional conceptual uncertainty is due to the supplied SRFs being presented separately for ISA and NTA, respectively. In reality, the effects of NTA and ISA (and all other complexing agents) are additive. This is mentioned by Keith-Roach et al. (2021), where it is judged a reasonable simplifica-

tion to apply a single SRF based on only the dominant complexing agent at any given point in time due to the associated uncertainties and applied conservatisms. Further uncertainties are those stemming from the disregard of chemical and microbial degradation of complexing agents (Keith-Roach et al. 2021, Section 2.3.1), and that all complexing agents are instantly released from the solid waste matrix (except the sorbed fraction of ISA) and dissolved in the water in the pore and void volumes in the waste domain.

The SRFs are assumed to be unaffected by variations in the solid-phase composition. This confers additional uncertainty because in reality, the equilibrium distribution of radionuclides between the dissolved:complexed:sorbed states is dependent on their interaction strength with both complexing agents and sorbent materials, where the latter, represented by K_d, changes over time due to cement degradation.

7.6 Data uncertainty – precision, bias, and representativity

The uncertainty of the selected sorption and diffusion parameters has a contribution from experimental uncertainties in the underlying source data, but stems mainly from uncertainties that are introduced in the process of synthesising and scaling those data to the conditions specified for safety assessment. Where appropriate, data uncertainty is therefore discussed together with descriptions of the derivation of sorption and diffusion parameters, as well as the basic results of data derivation. The numerical results are summarised in Section 7.9.

Concrete/cement sorption coefficients

Unlike in the case for bentonite, no underlying dedicated data report is available. Cronstrand (2005) reviewed sorption values on both bentonite and cementitious materials but did not perform a quantitative data derivation based on original experimental data. Therefore, the sorption values for cementitious materials, are based on the comprehensive reviews of Wang et al. (2009) and Ochs et al. (2011). Both of these reviews are directed at defining recommended K_d values as well as upper and lower limits for a cementitious near-surface repository for Belgian category A radioactive waste. To this end, the degradation of the cementitious material was modelled in detail. Subsequently, a comprehensive review of the available literature was conducted and the available data for each radionuclide were analysed in order to allow those data to be assigned to the appropriate specific degradation states. To the degree possible, trends of sorption values as a function of degradation were tied in with the concurrent known or modelled changes in solid composition and speciation.

The processes of radionuclide sorption on hydrated cement are reviewed in the **Waste process report**. This is carried out for each radionuclide in an element-specific fashion. The values proposed in the following are selected to be consistent with the respective sorption process.

A general overview of cement degradation is given in Section 7.4 as well as in the **Barrier process report**. Section 7.4 also discusses how the data recommended by Wang et al. (2009) and Ochs et al. (2011) can be applied to the situation at SFR by considering the C/S ratio as a master variable. For a few elements with specific sorption behaviour, such as Se, the presence of specific host minerals, such as ettringite, also needs to be taken into account.

It follows that the assignment of K_d values hinges on the modelling of the cementitious system evolution, and in particular the change in C/S ratio and other mineralogical properties of the hydrated cement material. The models by Gaucher et al. (2005) and Cronstrand (2007) predict the presence of CSH phases for all periods, with C/S ratios decreasing from 1.8 to 1.1. As outlined in Section 7.4, a somewhat wider range of conditions is considered for the present purpose:

Wang et al. (2009) and Ochs et al. (2011) also evaluated the influence of elevated chloride concentrations on sorption. They considered typical saline solutions such as seawater but did not consider extreme cases such as concentrated brines. It was concluded in both studies that the lack of systematic sorption data obtained under different salinity conditions does not allow a quantitative evaluation.

Moreover, high salinity can affect the pH (release of OH^- due to addition of Na) as well as the mineralogy (uptake of chloride in hydrated cement minerals) of concrete/cement systems. This is often not taken into account in experimental studies. For SFR, such effects on the cementitious-materials development over time are represented in the corresponding modelling by Gaucher et al. (2005) and Cronstrand (2007). As such, those effects are beyond the scope of the present chapter and the effect of salinity is assessed in the following only with regard to the actual sorption process and competition effects.

Based on the available, sparse evidence from sorption experiments and on thermodynamic considerations (influence of chloride on speciation and especially on solubility limits), Wang et al. (2009) and Ochs et al. (2011) made a qualitative assessment of the effect of salinity on sorption of different groups of radionuclides. With respect to the radionuclide of concern in the present case, the following effects are likely:

- High impact: Cs, Sr and Ba will sorb less due to the competition effect by the increased Na concentration. Some soft metal cations (Ag, Cd, Pd) due to their tendency to form very strong chloride complexes.
- Medium impact: Radioactive iodide and chloride will be affected by competition with the stable chloride. The same is assumed for molybdate, selenate and Tc(VII).
- Low impact: ^{14}C assuming isotope exchange, Se(IV), and Zr, Nb, Sn, Ho, U, Pu, Am, Np, Cm, Eu in their relevant oxidation states. Ni assuming isotope exchange and no impact of salinity on the stability of layered double hydroxide (LDH) phases (in the case of actual sorption, a medium effect would have to be assumed due to the relative stability of Ni-chloride complexes). For Tc(IV), medium impact is assumed by Wang et al. (2009) based on expert opinion. Here it is assumed that hydrolysis will be dominating at high pH (as in the case of actinides) and that the impact will be low.

Bentonite data

Sorption coefficients

As discussed in Section 7.4 and Section 7.5, the K_d values selected in Ochs and Talerico (2004) and SKB (TR-10-52) are considered to be applicable to the present conditions within the discussed uncertainties. Similarly, no new information has emerged in the pertinent literature published after Ochs and Talerico (2004) that would motivate a modification of the applied conversion procedures and uncertainty factors. While new thermodynamic sorption models addressing both ion exchange as well as surface complexation have been developed for several radionuclides, many of these models are parameterised only for simple systems (e.g. pure montmorillonite in contact with an inert electrolyte solution) and are therefore not directly applicable to more complex porewater compositions containing carbonate and other strong ligands (see discussions in NEA 2012). Ideally, the derivation of K_d values for safety analyses would be based on sorption models that are parameterised for similar conditions. However, the available experimental database is not sufficient yet to permit such an approach (NEA 2012).

The K_d values selected in Ochs and Talerico (2004) and SKB (TR-10-52) are valid at 25 °C. While the available data do not allow assessment of the influence of temperature on sorption with sufficient certainty, it is not expected that temperature effects will be significant in comparison to the geochemical uncertainties considered.

With regard to the underlying source data used for the derivation of K_d values, the selections made in Ochs and Talerico (2004) are generally still considered to be valid. For many radionuclides, no new relevant data have become available in the meantime, to our knowledge. The cases where new potentially relevant source data have been determined that were not considered in Ochs and Talerico (2004) and SKB (TR-10-52) are discussed in the following.

- In the case of Ni, Tertre et al. (2005) measured sorption edges on montmorillonite (obtained from MX-80) in 0.025 M and 0.5 M $NaClO_4$ solution. Their data show approximately the same trend as the data on SWy-1 by Baeyens and Bradbury (1997) but indicate slightly lower sorption. Similarly, Ochs and Talerico (2004) also noted that the sorption isotherm by Bradbury and Baeyens (2003) on MX-80 gave a lower K_d for Ni than their SWy-1 data. Since Ochs and Talerico (2004)

conservatively based the recommended K_d for Ni on the MX-80 source data, the additional data by Tertre et al. (2005) do not motivate any re-evaluation. Rather, they support the original, conservative choice of source data. More recently, Akafia et al. (2011) also measured Ni sorption on smectite (SWy-2). Their data fall within the range delineated by the data of Baeyens and Bradbury (1997) and Tertre et al. (2005).

- New experimental data have also become available in the case of selenite, Se(IV). Missana et al. (2009) measured several pH edges of selenite on smectite in 0.001 M to 0.5 M background solutions. Their measured K_d values are higher by about factor 5 or more than the data by Bradbury and Baeyens (2003) considered by Ochs and Talerico (2004). Montavon et al. (2009) measured a sorption edge on MX-80 in 0.05 M background solution. At the relevant pH (7.8), these data agree very well with the sorption isotherm by Bradbury and Baeyens (2003). Ochs and Talerico (2004) also did not consider a number of K_d values measured by Shibutani et al. (1994) and Tachi et al. (1999). These data show very large scatter, but their mean is also close to the source value used by Ochs and Talerico (2004). In summary, the mentioned additional data do not give a reason to revise the proposed sorption values. The other potentially relevant oxidation states Se(–II) and Se(VI) were assigned a K_d of zero. No new data were found that would motivate a revision in either case.
- For Mo, no K_d values are given in Ochs and Talerico (2004). In SKB (TR-10-52), a K_d of zero is assigned, based on an analogy between the molybdate anion (which is the only species of Mo occurring in normal aqueous solutions) and selenate. SKB (TR-10-52) did not consider the studies of Motta and Miranda (1989) and Goldberg et al. (1996). The two studies investigated the sorption of molybdate on montmorillonite, but do not give a clear picture. Motta and Miranda (1989) measured sorption isotherms at pH < 5 and saw low but significant sorption. On the other hand, Goldberg et al. (1996) observed a steep decrease of sorption with increasing pH and measured no appreciable sorption at pH > 7. On this basis, it is concluded that the K_d of zero selected in SKB (TR-10-52) may be conservative, but that a re-evaluation of Mo sorption is not warranted.
- Andra (2005) reported a sorption edge for Nb on smectite extracted from MX-80. These data became available after the publication of Ochs and Talerico (2004) and were not considered in SKB (TR-10-52). At a similar pH value, this sorption edge gives a K_d similar to the value measured by Ikeda and Amaya (1998), which was considered in Ochs and Talerico (2004). However, their argument of using a conservative estimate due to the scarcity of data is still considered valid, and no re-evaluation to arrive at a higher value seems warranted.
- For Ag, Ochs and Talerico (2004) did not consider the study by Khan et al. (1995), who measured the sorption of Ag on bentonite. While their data are not conclusive, they indicate K_d values in the range of about 0.01–0.4 m^3/kg. Considering further the potential effect of chloride on Ag sorption, it is proposed to revise the upper limit of 15 m^3/kg given in Ochs and Talerico (2004) down to 1.0 m^3/kg. As in Ochs and Talerico (2004), a lower limit of zero is proposed. Considering the uncertainties regarding Ag speciation in the porewater and its very high sensitivity with regard to complexation by chloride and sulfide, zero sorption is also proposed as a best estimate.
- For Sn (specifically Sn(IV), Sn(II) is not relevant), Ochs and Talerico (2004) did not consider the study by Oda et al. (1999), who measured a sorption edge on untreated Kunigel-V1 bentonite in 0.01 M NaCl. Within the (relatively large) experimental scatter, their dataset is almost identical to the data by Bradbury and Baeyens (2003), which had been considered as potential source data but were not used in the end. Both studies indicate consistently high K_d values of ≈ 1 000 m^3/kg for about pH 4–7, decreasing to ~ 150 m^3/kg at pH 10. Thus, the decision by Ochs and Talerico (2004) to base the K_d for Sn on an analogy with Th can be viewed as conservative and does not warrant reevaluation.
- In the case of Pb, some new sorption data (Akafia et al. 2011) have become available after the publication of Ochs and Talerico (2004) and SKB (TR-10-52). These data show generally a good agreement with the data by Ulrich and Degueldre (1993), which were selected as source data by Ochs and Talerico (2004). However, a part of the data by Akafia et al. (2011) indicate lower sorption than the data by Ulrich and Degueldre (1993). A comparison of the experimental conditions indicates that this can be attributed to the difference in initial Pb concentrations, which are significantly lower in the case of Ulrich and Degueldre (1993). Assuming that trace concentrations are most representative for the migration of radionuclides in a bentonite barrier, the data by Ulrich and Degueldre (1993) are still regarded as the most representative. However, to acknowledge the data by Akafia et al. (2011), it is proposed to reduce the previously derived lower limit by a factor of five while retaining the best estimate and upper limit values given in Ochs and Talerico (2004).

- For Am, new sorption edge data by Bradbury and Baeyens (2006) on Na- and Ca-SWy-1 have become available. The data on Ca-SWy-1 agree well with the data by Gorgeon (1994), which are the source data for the K_d values recommended in Ochs and Talerico (2004) and SKB (TR-10-52). In comparison, the data for Na-SWy-1 indicate higher sorption of Am. As the speciation of Am in the experiments by Bradbury and Baeyens (2006) is more straightforward than in case of Gorgeon (1994), it could be argued that the data recommendation should be re-evaluated, which could only lead to a higher recommended K_d. However, in view of the difference between the Na- and Ca-forms, it is proposed to retain the more conservative value derived on the basis of the data by Gorgeon (1994).
- Ochs and Talerico (2004) and SKB (TR-10-52) base the recommended K_d of Cm on an analogy with Am. Systematic sorption data of Cm have become available from Rabung et al. (2005) for Ca-SWy-1 in simple Ca-electrolyte solution and from Grambow et al. (2006) for MX-80 in synthetic porewaters. The data by Rabung et al. (2005) follow roughly the data by Bradbury and Baeyens (2006) for the Ca-system. The data by Grambow et al. (2006) show a much less pronounced sorption edge; they are similar to the data for Ca-smectite at pH ≈ 7 but are nearly an order of magnitude lower in the range of pH 8–10. Considering the established chemical similarity between Am and Cm and the good agreement between the data by Rabung et al. (2005) and the corresponding data by Bradbury and Baeyens (2006) for Am, the value proposed by Ochs and Talerico (2004) is still considered valid.
- In addition to the sorption edge of Th on SWy-1 determined in 0.1 M $NaClO_4$ (given originally in Bradbury and Baeyens 2003), Bradbury and Baeyens (2005) give a corresponding sorption edge in 1 M $NaClO_4$. The two datasets are nearly identical and show that Th sorption on montmorillonite is not influenced by ionic strength.
- New sorption data for U(VI) by Bradbury and Baeyens (2005) have become available. In comparison to the data by Pabalan and Turner (1997) these data would indicate higher sorption. Thus, the data derived in Ochs and Talerico (2004) may be somewhat conservative with respect to uranium releases. It is noted that a lower sorption of U increases the effect of ingrowth of its daughter radionuclides.
- For Pa, sorption edge measurements on Na-montmorillonite (SWy-1) by Bradbury and Baeyens (2006) became available after the publication of Ochs and Talerico (2004). These data were also not considered in SKB (TR-10-52). They indicate a constant sorption value of about 90 m^3/kg over a pH range from 4 to 10.5. This K_d value is more than an order of magnitude higher than the K_d values estimated previously by Ochs and Talerico (2004) on the basis of data for Pa presented in Yu and Neretnieks (1997). However, due to the lacking detail regarding the composition of the bentonite and porewater in the SFR silo, and hence the speciation of Pa, no re-evaluation of Pa sorption is made and the values proposed in Ochs and Talerico (2004) are accepted as very conservative estimates.
- For all other radionuclides (C, Cl, Sr, Zr, Tc, I, Cs, Ho, Pd, Pu, Np, Cd, Eu, Sm), no new relevant sorption data have become available to the supplier's knowledge at the time of writing.

In the framework of a review of the safety assessment study SAR-08, Zhou et al. (2009) criticised the fact that the data recommended by Ochs and Talerico (2004) are based on a limited database. There are several reasons for the approach of Ochs and Talerico (2004):

- The main reason is the strong dependency of K_d on chemical conditions. This means that K_d values can be directly applied only in case of very similar conditions. In all other cases, it is required to transfer the literature data to the actual conditions (NEA 2005) by means of conversion procedures (or thermodynamic models, where available). The main uncertainty of recommended K_d stems from this transfer of sorption data to different conditions (NEA 2005). The respective uncertainties are considered explicitly in Ochs and Talerico (2004). The resulting overall uncertainties in K_d are significantly larger than the scatter of experimental data from different (reliable) sources.
- Because of the dependency of K_d on chemical conditions, it would be a misconception to assume that a compilation of experimental data from different sources would allow a better assessment of uncertainties in source data. This is because most of the apparent scatter observed in comparisons of experimental data is typically due to the variability of conditions rather than to actual uncertainty. When like is compared with like (i.e. data obtained under matching conditions), the scatter is often

substantially reduced. Accordingly, Ochs and Talerico (2004) carried out a transparent, quantitative derivation on the basis of selected source data rather than a more qualitative expert estimation on the basis of a large data compilation.

- The only datasets considered to be of highest quality are those that are obtained as a function of an important system variable, such as pH (sorption edges), radionuclide concentration (sorption isotherm), or other important solution constituents. The embedding in a series of related data lends additional confidence to the individual data points in terms of both representativeness and decreased bias. Single point measurements or data obtained under a narrow range of conditions are much less useful and more difficult to transfer to different conditions, because no clear trends can be assigned to such datasets. In the present context it is therefore not helpful to 'dilute' state of the art source data (as outlined above) with additional datasets of lesser quality.

Zhou et al. (2009) also comment on the rather high upper limits as well as the best estimate values given for several radionuclides in their tetravalent oxidation state (Tc, Sn, Np, Pu) in Ochs and Talerico (2004) and SKB (TR-10-52). In particular, it is pointed out that such high values have not been recommended for earlier safety assessments. Regarding the recommended values given in Section 7.9 as well as those in the previous assessments of Ochs and Talerico (2004) and SKB (TR-10-52), the following is pointed out:

- From a fundamental point of view, it needs to be made clear that the very strong sorption of tetravalent elements is experimentally confirmed, which is consistent with their pronounced tendency towards hydrolysis. Indeed, the mentioned best estimates are well within the range of experimentally measured K_d values for e.g. Sn(IV) and Th. Thus, they are not unusual according to the present state of the art.
- The values for the abovementioned radionuclides in their tetravalent oxidation state are based on analogy with Th. In turn, the recommended values for Th were selected by Ochs and Talerico (2004) on the basis of high-quality and well-established experimental sorption data (Bradbury and Baeyens 2003).
- The high upper limits are simply the result of the applied uncertainty factors. As pointed out in Ochs and Talerico (2004), it has to be admitted that it is not clearly established whether errors should be distributed around derived K_d values in a linearly or logarithmically symmetrical way. In choosing the latter option, Ochs and Talerico (2004) followed the approach of Bradbury and Baeyens (2003). In any case, when the recommended parameter space is sampled stochastically, the bounding upper/lower values will feed into safety assessment calculations as part of the entire data range.
- As discussed in Section 7.9, the present use of Th data as analogue for tetravalent elements is handled in a simplified way in comparison to the approach used in Ochs and Talerico (2004) and SKB (TR-10-52). Conservatively, the increased uncertainty is not considered to be log-symmetrical with respect to the selected values but is only applied to the lower limit. Thus, some of the high upper limits are avoided.

Diffusivity data

The data of interest are effective diffusivities (D_e) and diffusion-available porosities (ε_{diff}) for the relevant radionuclides. Effective diffusivities are representative for steady-state conditions, i.e. retention processes and in particular sorption are not important. Accordingly, D_e values show little dependence on conditions, in contrast to K_d.

The conceptual uncertainties associated with diffusion parameters are briefly discussed in Section 7.5. With regard to data acquisition, D_e is measured in through-diffusion experiments which are more difficult to perform than sorption batch experiments due to the required experimental timeframe and the challenges in controlling chemical and other boundary conditions. This also puts limits on the existing database in terms of the radionuclides as well as in terms of the conditions treated. D_e values are largely available only for mobile but not for sorbing elements and are only in a few cases available as a function of (limited) systematic variations of chemical conditions. Further, the extraction of D_e values from raw experimental data is not straightforward and requires the fitting of models that must be chosen as a function of boundary conditions. This is an important issue especially in the case of the diffusion of charged species.

On the other hand, diffusion experiments are very similar to the in situ conditions anticipated for a bentonite barrier in terms of clay density and pore characteristics. In combination with the relative insensitivity with respect to chemical conditions, this means that D_e values do typically not need to be recalculated (to the degree that this is required for K_d) to the chemical conditions expected for PA.

Following the above discussion, the recommended data for SFR were evaluated directly from the extensive compilation of D_e values for SR-Can (Ochs and Talerico 2004) which had been updated and extended for SR-Site (SKB TR-10-52). The data in these reports are presented in plots of reported D_e versus clay dry density. Where available, diffusion data obtained as a function of conditions (e.g. ionic strength) were also plotted. Overall, these experimental data cover a very wide range of different conditions in terms of diffusion-relevant bentonite and solution characteristics (including type and ionic form of bentonite) which in turn influence pore size and characteristics. Since the selected D_e values for SR-Can/SR-Site take the overall spread of these data into account, it is assumed that uncertainties related to the influence of conditions are included in the uncertainties given for D_e in each case.

Following the approach of SR-Can (Ochs and Talerico 2004) and SR-Site (SKB TR-10-52), D_e was evaluated separately for neutral diffusants on the one hand, and anions and cations showing anion exclusion and enhanced diffusion effects, respectively, on the other hand. A review of the various model concepts that can be used to explain anion exclusion and enhanced cation diffusion is given in the **Barrier process report** and is not repeated here.

- The term neutral diffusants includes most elements of interest (hydrolysable cations, cations existing mainly as neutral ion pairs, neutral molecules). Many of these elements are moderately or strongly sorbing, and any element-specific D_e data, if available, typically represent isolated measurements. Therefore, it is preferred to base D_e data for this group on data for tritiated water (HTO), whose diffusion behaviour can be evaluated on the basis of a number of studies.
- Anions encompass only true, largely uncomplexed anions such as chloride or oxo-anions. On the other hand, negatively charged, labile complexes of hydrolysable metal ions are not included.
- Cs is the only element for which enhanced cation diffusion is considered. Other cations sorbing exclusively via ion exchange (Ra, Sr, Ba) could also be assigned to this group, but here the argumentation given in Ochs and Talerico (2004) is followed; i.e. it is cautiously assumed that these elements may exist in the form of ion-pairs (or possibly weak complexes) which are not positively charged. Also, the few available experimentally determined effective diffusion data (mainly for Sr^{2+}, see e.g. Muurinen et al. 1987, Choi and Oscarson 1996, Eriksen and Jansson 1996, Suzuki et al. 2004) show significant scatter and do not exhibit a clear trend as a function of dry density.

The recommended data given in Section 7.9 are directly evaluated from the plots of D_e versus dry density given in SKB (TR-10-52). Considering the lack of detailed information regarding the properties of the bentonite barrier in the silo, it is not considered as meaningful to use a mathematical approach (e.g. a regression analysis as in SKB TR-10-52), because the apparent numerical accuracy would not be reflected in the data situation.

Assuming a clay dry density of 950 kg/m^3 to 1 120 kg/m^3 (top to bottom of silo barrier, SKB R-08-130, Section 4.2.1), the following value can be estimated from the plot given for neutral diffusants in SKB (TR-10-52, Figures 5-5 and 5-6). Using the conservative assumption that the bentonites with a relatively low clay content (mainly Kunigel-V1 with about 48 % clay) are most representative for the silo barrier, an average D_e of 4×10^{-10} m^2/s can be estimated for HTO, considering the density range indicated. Similarly, a lower and upper limit of 2×10^{-10} m^2/s and 9×10^{-10} m^2/s can be extracted. To our knowledge, no new data have become available, especially for the clay density of concern. Therefore, the source data used are considered to represent the present state of the art.

For anions, recommended values are also taken directly from the corresponding plot given in SKB (TR-10-52, Figures 5-7 and 5-8). For the range of dry clay density considered, a best estimate value of 4×10^{-11} m^2/s is proposed, with lower and upper limits of 2×10^{-11} m^2/s and 2×10^{-10} m^2/s, respectively. These are to be used in combination with a reduced ε_{diff} value, see below. Again, the underlying source data are considered to represent the state of the art. The only additional datasets that are not given in SKB (TR-10-52) are the D_e values for chloride measured by Glaus et al. (2010) in montmorillonite (obtained from Milos bentonite) and two values measured by Goutelard and Charles (2004) in MX-80. However, both datasets were measured at a much higher dry density than considered for

the present case. Moreover, they are almost identical to the range of data already considered in SKB (TR-10-52). Therefore, it can be concluded that these omitted data would have no influence on the present data selection.

In the case of Cs, the recommended diffusion values given in Ochs and Talerico (2004) and SKB (TR-10-52) are based on a single dataset determined by Sato (1998) for Kunigel-V1 over a wide range of dry densities. The only comparable dataset that also extends to fairly low dry densities are the measurements by Molera and Eriksen (2002) in MX-80. However, they interpreted their experiments considering an additional surface diffusion coefficient. It is therefore not clear whether the resulting D_e values (which are always based on a model interpretation of raw diffusion data), are indeed representative. In either case, their data systematically indicate a lower diffusivity (by about factor 2.5 to 5) of Cs than the data by Sato (1998). Thus, the omission of these data would lead to a more conservative selection of recommended values. Due to the scarcity of experimental data at low dry clay density, recommended values are centred around the regression line given in SKB (TR-10-52, Figure 5-10), which is based on the data by Sato (1998). This results in a best estimate D_e of 7.5×10^{-10} m^2/s for the density range of interest. Since upper/lower limits cannot be based on the data directly, they are somewhat arbitrarily set to 2×10^{-9} m^2/s and 2.5×10^{-10} m^2/s, respectively. This gives a slightly larger uncertainty range than considered in SKB (TR-10-52) to acknowledge the additional uncertainty related to the lack of detailed knowledge on bentonite properties.

For the diffusion-available porosity ε_{diff} of neutral diffusants and cations (Cs), the same value as for the physical porosity is assumed. For this, the value of 0.61 given in Höglund (2001) is accepted; this would also result from use of Equation 5-6 in Ochs and Talerico (2004) and a mean dry density of 1 050 kg/m^3. For the ε_{diff} of anions, the same reduction factor of 2.5 in comparison to the physical porosity as in Ochs and Talerico (2004) and SKB (TR-10-52) is applied, which results in ε_{diff}(anions) = 0.24.

The selected diffusion parameters are valid for a temperature of 25 °C. Following SKB (TR-10-52, p 162), approximately a twofold increase or decrease of D_e can be expected for a 25 °C-increase or -decrease of temperature, respectively. No effect on the diffusion-available porosity is expected (not considering processes like freezing, which change the hydrological parameters of the bentonite, see the **Barrier process report**).

Sorption reduction factors

As discussed in detail in SKB (R-08-130) and Fanger et al. (2001), the silo contains cementitious waste and barrier materials which can be expected to contain cellulose as well as some complexing agents. Their influence on radionuclide sorption directly in the various cementitious materials is discussed in Section 7.9 and the **Waste process report**. Based on the available information, it is difficult to evaluate whether the respective organic substances will also be present in the bentonite barrier, and if so, in which concentration range.

The effect of complexing agents on radionuclide sorption on and diffusion through bentonite is not well defined. This reflects that the measurement of bentonite porewater composition in general is challenging, and the lack of relevant experiments. Wold (2003) found that humic substances, which are complex organic colloids, can enhance Eu(III) diffusion though compacted bentonite. Radionuclides can be bound effectively irreversibly by humic substances and so the effect may not be used directly as an analogue for smaller complexing agents, but the results indicate that organic molecules are not excluded from the bentonite pore space. The speciation of the complexes is important since the available diffusion porosity and the effective diffusivities in bentonite are much lower for anions than for cations and neutral species. Complexing agents may sorb to edge sites in the bentonite, using the analogy with Al-oxides (Kummert and Stumm 1980), but this has not been quantified to our knowledge. Therefore, the complexing agent concentrations in bentonite are difficult to calculate. The effect of a complexing agent on radionuclide sorption on bentonite may not be the same as for cement because bentonite buffers the pH of the porewater (e.g. Gaucher et al. 2005, Cronstrand 2016), affecting the aqueous speciation, and the sorption sites in clays are unlike those in cement. However, in the absence of alternative data, the effect on radionuclide sorption on bentonite can be assumed to be the same as cement as a cautious approach.

An additional uncertainty for the sorption reduction data due to precision, bias and representativity relates to the disposal of polyacrylic filter aids, noted as a major uncertainty in Keith-Roach et al. (2021).

7.7 Data uncertainty – spatial and temporal variability

Spatial variability of data

Within SFR, there is of course spatial variability in the sense that each system component contains a different combination of waste, structural and barrier materials. While this is of relevance for the safety analysis modelling, it is not taken into account here because the data are recommended in a generic fashion for the barrier materials and the specified geochemical conditions.

There is no spatial variability of the type typically encountered in geological media. In principle, both the bentonite as well as the concrete/cement barriers can be considered as completely homogeneous within the scale of radionuclide transport distances, at least in the initial repository period. With progressive evolution of the repository (Section 7.9), zones of degraded material will develop in both types of materials. In the case of bentonite, the altered portion is not addressed explicitly in the data derivation (and is not considered to contribute to sorption in the safety calculations). Some pertaining qualitative information is given in Section 7.9. In the case of concrete/cement, the difference between degraded and fresh material is much more gradual. The values selected for the main degradation states (Section 7.9) are deemed valid for the entire barrier within the uncertainty of the modelling of the cement evolution.

Temporal variability of data

The data themselves and the underlying processes are not subject to temporal variability. However, the temporal evolution of the repository gives rise to concurrent changes in geochemical conditions which influence the magnitude of sorption. The evolution of the bentonite and concrete/cement barriers is addressed in Gaucher et al. (2005) and Cronstrand (2007). In the case of concrete/cement, the temporal evolution of the material properties is addressed directly in the data selection. In the case of bentonite, the data are essentially selected for unperturbed bentonite, a significant portion of which is presumed to be present in most scenarios for all periods. See also Section 7.9.

Sorption reduction factors

The NTA SRFs are supplied as a linearly decreasing function of time, assuming continuous outflow of NTA from the vaults at a speed corresponding to a non-sorbing tracer from the transport modelling (Keith-Roach et al. 2021, Chapter 4).

7.8 Data uncertainty – correlations

The supplied migration parameters for several radionuclides are based on analogies with similar elements for which a better data basis is available. This is described for each radionuclide in Section 7.4 and Section 7.9. Similarly, as pointed out in Section 7.4, the magnitude of sorption correlates with chemical parameters (pH, solids composition, etc) which are the results of initial repository conditions and the subsequent evolution.

Based on their chemical characteristics (which fed into analogy considerations used in the data selection), the radionuclides considered can be organised into correlating groups of elements and oxidation states whose migration behaviour will generally show a similar response to variations in chemical conditions. Overall, the following grouping results are:

- Alkaline and alkaline earth elements: Cs, Ba, Sr.
- Trivalent actinides and lanthanides: Am, Cm, Pu(III), Ho, Eu.
- Tetravalent actinides: U(IV), Pu(IV), Np(IV). Data for these are largely based on Th, which is not included as having relevant radioisotopes for SFR. For some data, Zr and Sn(IV) were also evaluated on the basis of data for Th.
- Pentavalent actinide elements: Np(V), Pu(V).
- Hexavalent actinide elements: U(VI), Pu(VI).

- In terms of diffusion data in bentonite, the three groups defined correlate:
  - Anions.
  - Cs.
  - HTO and all non-anionic radionuclides.

7.9 Result of supplier's data qualification

Concrete/cement sorption data

Sorption coefficients for hydrated cement

The recommended K_d values are given in Tables 7-4 to 7-7. As described in Section 7.6, the principal work was carried out in projects on data derivation in cementitious systems (Wang et al. 2009, Ochs et al. 2011). The present report largely relies on that work, without reproducing the data derivation procedures. This is justified by the expected similarity in conditions, cf Section 7.4. It is noted that in contrast to the present handling of sorption as a function of degradation, the above reports do not divide state III into two parts. Cases where the values of Wang et al. (2009) and Ochs et al. (2011) are not considered clearly valid for the entire state III (i.e. from pH ≈ 10–12.5) are discussed separately below. Similarly, all situations where there may be significant differences in the conditions assumed in these studies in comparison to conditions at SFR are discussed below and alternative values are proposed in some cases.

Following the discussion in Section 7.6, K_d values are provided in Tables 7-4 to 7-7 for the different degradation states of hydrated cement as outlined in Section 7.4 (states I, II, IIIa, IIIb). These can be linked to reference periods in the repository evolution via pH value and mineralogical characteristics (C/S ratio, presence or absence of portlandite and Ca-aluminates).

These tables give values corresponding to non-saline conditions. For those radionuclides where the effect of salinity is deemed significant, an additional discussion is provided further below. The effect of organic complexing agents on sorption is evaluated in the **Waste process report**, the corresponding no-effect levels of organics or reductions factors, where appropriate, are also given in a separate table further below.

Where values given in Tables 7-4 to 7-7 are not taken directly from Wang et al. (2009) or Ochs et al. (2011), additional comments are provided below. This applies especially to values recommended for state III, because these authors do not explicitly distinguish between the different parts of state III.

Note also that the values given in Tables 7-4 to 7-7 correspond to sorption on pure hydrated cement paste (HCP). For calculation of values for the various cementitious materials in SFR listed in Table 7-1, it is assumed that only HCP will be involved in the uptake of radionuclides, which may be conservative in the case of some elements (e.g., Cs could sorb more strongly on some aggregate materials than on HCP). K_d values for the cementitious materials are calculated using the HCP given in Table 7-8.

Actinium: No data are given in Wang et al. (2009) and Ochs et al. (2011), and no other sorption data were found. As pointed out above in the section on bentonite, lanthanide elements are considered as a reasonable chemical analogue for Ac. This analogy had also been used by Wieland and Van Loon (2002). For the present purpose, the values selected for lanthanides and trivalent actinides are applied directly. Considering the consistently high sorption observed for these elements, no additional conservatism is introduced for Ac.

Silver: No sorption data on cement/concrete are available to our knowledge. Ochs et al. (2011) give a best estimate on the basis of an experimental sorption value for Ag on calcite; they give no upper limit and propose zero sorption as a lower limit. However, they were specifically considering a concrete with calcareous aggregate. For the present purpose, the value for calcite is accepted as an upper limit for states I & II. As a lower limit, zero sorption is assumed, and no best estimate is given. Depending on the type of simulation (see Gaucher et al. 2005, Cronstrand 2007), calcite may have disappeared in state III. Thus, no sorption of Ag is assumed for either part of state III (pH 12 and 10.5).

Americium: The values from Wang et al. (2009) are directly accepted. Based on the available experimental data, no distinction between the different parts of state III is warranted.

Barium: No values are given in Wang et al. (2009) or Ochs et al. (2011). The behaviour of Ba can be expected to be intermediate between Sr and Ra. Conservatively, the lower values given for Sr are recommended.

Carbon (^{14}C): Sorption of carbon depends strongly on the form in which it is present (inorganic carbonate species or organic forms). Further, different types of uptake processes need to be considered in case of carbonate.

The uptake of inorganic forms of carbon (carbonate species) by hydrated cement can occur through various sorption reactions or by isotopic exchange. Isotopic exchange is mainly important in the presence of solid carbonates (mainly calcite), while sorption can take place on hydrated cement paste (CSH-phases) (Wang et al. 2009).

Several critical uncertainties need to be considered for the calculation of K_d based on isotopic exchange with solid carbonate (calcite). While the total carbonate content can be measured in fresh concrete or mortar, it can only be estimated for material degraded under in situ conditions. Ideally, such estimations should be based on a good geochemical model for the development of solid and dissolved carbonate concentrations in the concrete as a function of degradation, taking into account initial composition and groundwater chemistry. Second, an estimate is needed regarding the actual availability of solid carbonates for isotope exchange. Bradbury and Sarott (1995) assumed 10 % of all calcite in the cement system to be available for this process, while Pointeau et al. (2002) used a much smaller value of about 0.5 % for calcite fines, based on more systematic measurements.

For the concrete used in SFR, a solid carbonate concentration of 0.65 moles CO_3/kg concrete can be calculated from the measurements of Ecke and Hansson (2012). Assuming this value also for state II in combination with a dissolved carbonate concentration of 6×10^{-6} M (SKB R-01-14) would result in a K_d of about 11 m^3/kg using the approach of Bradbury and Sarott (1995) (10 % availability of calcite). Using the availability estimate of Pointeau et al. (2002) would give a K_d of about 0.6 m^3/kg.

On the other hand, the extent of sorption can only be assessed on the basis of experimental data from systems where no solid carbonates are present. Such sorption data for the sorption of $^{14}CO_3$ on CSH are available from Noshita et al. (2001) and indicate a K_d of about 2–4 m^3/kg. In terms of chemical conditions, these data correspond to degradation state II.

Wang et al. (2009) further list selected sorption data from HCP systems where the dissolved carbonate concentration was below the solubility limit of calcite. While isotope exchange may play a role in these systems, they are conservative in the sense that $^{14}CO_3$ can only interact with CSH and relatively small amounts of (pre-existing) calcite but cannot co-precipitate with calcite.

Based on the evidence discussed above, K_d values for $^{14}CO_3$ are proposed as follows:

- Largely, the general approach and recommended values of Wang et al. (2009) are accepted. It needs to be pointed out that all underlying experimental data represent sorption on CSH in HCP. K_d values recommended on this basis are considered to be more reliable and more conservative than values calculated on the basis of isotopic exchange, in view of the uncertainties regarding the detailed ratio of dissolved:solid carbonate in phases II–III and especially regarding the accessibility of the calcite present.
- The lower limit is based on the assumption that only sorption of $^{14}CO_3$ on CSH will take place; i.e. that no calcite is available. The recommended K_d value of 2 m^3/kg corresponds directly to the data for CSH by Noshita et al. (2001), which are directly applicable to state II. No experimental data on CSH are available for states I and III; therefore, the recommended values are based on the value for state II and the trend of $^{14}CO_3$ sorption on HCP illustrated in Wang et al. (2009, Figure 70), considering in particular the data by Pointeau et al. (2008) showing a sorption maximum at state II pH 12.5 and lower sorption towards both states I and III.
- The best estimate takes into account the range of values measured for CSH as well as further data on HCP. The data given in Wang et al. (2009) span a range of about 2–10 m^3/kg for state II, the proposed best estimate of 5 m^3/kg corresponds to the centre of that range. Considering that in addition to sorption on CSH, isotope exchange with calcite will take place to some degree, this is a reasonable value.

- The upper limit of 20 m^3/kg for state II is based on taking into account isotope exchange with calcite and considering some uncertainty in the predicted ratio of dissolved:solid carbonate concentration. Wang et al. (2009) give no upper/lower limit for the sorption of carbonate in state III, due to the lack of data especially for the second half of state III. For the first part of state III (pH 12), the bounding values are estimated directly from the data by Pointeau et al. (2008) and Bayliss et al. (1988) (given in Wang et al. 2009). For the second part of state III (pH 10.5), the trend indicated by the data of Pointeau et al. (2008) is again used as reference.
- For simple organic compounds, Wang et al. (2009) conservatively propose a value of zero, although it is acknowledged that sorption is very low but not zero. Wieland (2014) proposed low sorption values for small organic molecules that exhibit a carboxylic acid function. These values are adopted for organic carbon.

Cadmium: Only very few data are available for Cd (see also the **Waste process report**). Wang et al. (2009) and Ochs et al. (2011), as well as earlier reports on the derivation of sorption values for cement systems (Wieland and Van Loon 2002, Andra 2005) give no value for Cd. The studies of Pomiès et al. (2001) and Polettini et al. (2002) indicate appreciable sorption of Cd to CSH and hydrated cement, most likely by exchanging against Ca in the CSH and portlandite structure, but do not allow extraction of actual sorption data due to experimental limitations (**Waste process report**). Based on the aqueous chemistry of Cd, reasonable analogues would be divalent class B-type metal ions, such as Ni or Pb, for which sorption data are available. Due to the particular uptake mechanism of Ni, this element is not useful, however. Therefore, it is proposed to base the data for Cd on the values selected for Pb by Ochs et al. (2011). The available data shown there and in Ochs et al. (2003) indicate a strong increase of Pb sorption with increasing degradation (i.e. with decreasing pH from state I to III). To remain on the conservative side, and to acknowledge the additional uncertainty due to the limitations of use of analogy, the Pb data selected for state I by Ochs et al. (2011) are used conservatively for all degradation states, and an additional reduction factor of 5 is applied.

Calcium: Ca is a main component of various minerals that make up the HCP matrix. HCP pore solutions are saturated with respect to dissolved (stable) Ca. Therefore, it can be expected that the solid:solution partitioning of radioactive Ca will take place by isotopic exchange with stable Ca (Wieland and Van Loon 2002, Ochs et al. 2011). To define a corresponding, nominal K_d value, the concentration of stable Ca in the cement/concrete and the accessibility of this stable Ca pool need to be known, as well as the dissolved Ca concentration in the corresponding equilibrium solutions.

In states I and II of cement degradation, total Ca solubility is controlled by portlandite, whereas in state III it is controlled by CSH, under normal conditions. Accordingly, for both portlandite and CSH, their contribution to the total Ca content of HCP plus the corresponding accessibility factors must be estimated. However, these relations are not well established for the cement/concrete components of SFR. To estimate a nominal K_d value corresponding to isotopic exchange, the following approach was taken:

- The concentration of stable Ca in HCP can be estimated from the amount of relevant solid phases (portlandite, CSH, etc) present during the various degradation states. To a first approximation, this information could be taken from the models of Gaucher et al. (2005) and Cronstrand (2007). However, the two models predict different amounts of relevant mineral phases (with variable Ca-content) for states I to III. Further, both studies consider different scenarios that lead to different conditions in the various compartments of SFR. The large spread of conditions and results makes it extremely difficult to select a set of reference data for deriving a nominal K_d.
- A comparison of the model results in Gaucher et al. (2005) and Cronstrand (2007) shows that the results by Cronstrand (2007) are more conservative in the sense that Ca-containing minerals are being degraded faster. Most relevant are the results for the outer concrete part of 1BMA because there degradation is predicted to proceed into state III. Cronstrand (2007) further shows that the different scenarios considered give very similar results for 1BMA.
- Based on these considerations, scenario A from Cronstrand (2007) for the concrete of 1BMA was selected as reference. Conservatively, only the Ca contained in portlandite and CSH phases was considered, Ca contained in further minerals (including calcite) was neglected. The amount of portlandite and CSH present was estimated from the composition predicted for 0–1 000 years after closure for state I (pH > 13), 10 000 – 50 000 years for state II (pH 12.5), and 100 000 years

for state IIIa (pH ≈ 12). For state IIIb (pH ≈ 10.5), no data are available in Cronstrand (2007) (or Gaucher et al. 2005), as such a pronounced degradation was not considered. The Ca content in state IIIb was estimated by considering the same amount of CSH present as in state IIIa, but with a C/S of 0.83 instead of 1.1. The total concentration of Ca in the solid phase was calculated from the molar volume of the mineral phases and their stoichiometry; results were normalised to pure HCP assuming 22 % HCP in the concrete (see Table 7-8).

- The dissolved concentration of Ca corresponding to each pH value was taken from the model calculations of Wang et al. (2009).
- As experimentally determined accessibility factors are not available, the required values were evaluated as follows: Best estimate and upper limit values were defined in analogy to the accessibility of Ni in LDH, where Wieland et al. (2006) determined values in the range of 2.8 to 4.5 %. For the present case, 2.0 % and 5.0 % were used as best estimate and upper limit, respectively. For the lower limit, the lowest accessibility factor considered by Ochs et al. (2011), 0.08 % for Ca in calcite, was used.

The resulting K_d values appear to be conservative in comparison with the values calculated by Ochs et al. (2011) for the exchange of radioactive Ca with stable Ca in calcite and also in comparison with the values calculated by Wieland and Van Loon (2002) for whole HCP.

Chloride and iodide: Values for all degradation states are taken directly from Wang et al. (2009); their value for state III is considered applicable to both pH 10.5 and pH 12. The selected values refer to total chloride concentrations larger than about 1 mM (but not to saline conditions). For lower chloride concentrations, much higher sorption can be expected (see Wang et al. (2009) and the **Waste process report**), however, such low chloride concentrations are viewed as not representative for the present case. The best estimate value for iodide is close to the lower end of the data range, because Wang et al. (2009) placed more weight on diffusion-derived sorption values than on values from batch experiments. This had been done to account for uncertainties in the effect of the solid:liquid ratio on sorption.

Curium: Wang et al. (2009) and Ochs et al. (2011) give no data for Cm, and no systematic data are available, to our knowledge. Based on the very similar chemistry of Am and Cm, the values selected for Am are also proposed for Cm.

Cobalt: Wang et al. (2009) and Ochs et al. (2011) give no data for Co. Some uptake data are available, but these are likely to include precipitation (e.g. Kaplan et al. 2008). On the other hand, based on some literature as well as in-house data, Wieland and Van Loon (2002) argue that Co is not taken up by a sorption process, but is showing a solubility-limited behaviour similar to Ni. In lack of any better evidence, this is accepted for the present purpose. As a cautious approach, the values estimated for Ni are reduced by a factor of five.

Caesium: For state I, Wang et al. (2009) indicate only a range of values (with a conservative lower limit) but give no best estimate. Based on the best estimate for state II and considering the data shown in Figure 38 of Wang et al. (2009) as well as the increased competition by alkali ions in state I, a best estimate of 1×10^{-3} m^3/kg is proposed here. All other values are taken directly from Wang et al. (2009). As very few data are available for the second part of state III, the values selected for pH 12 are also proposed for pH 10.5. Considering the trend of increasing sorption with decreasing pH shown by Cs, this is viewed as a cautious approach. Note that a few additional studies (e.g. Volchek et al. 2011) have become available since the publication of Wang et al. (2009); these concern states I or II and do not provide new information in the light of the large number of studies evaluated by Wang et al. (2009). Accordingly, the carefully evaluated values from Wang et al. (2009) are still considered to give the best representation of the state of the art.

Europium, samarium and holmium: Wang et al. (2009) and Ochs et al. (2011) give no recommended data for Eu, but Wang et al. (2009) use experimental data of both Am and Eu in their evaluation of Am uptake. The available data indicate a higher sorption for Eu than for Am in state I. No reliable and systematic data are available for Eu sorption in the other states, to our knowledge. For the present purpose, the data for Eu are based on analogy with Am. The same approach is followed for the other lanthanide elements of interest, Sm and Ho.

Molybdenum: The sorption of molybdate is strongly related to the presence of ettringite, see the **Waste process report**. Accordingly, Ochs et al. (2011) give values for state III considering the presence and absence of ettringite. As pointed out above, ettringite is assumed to be present during states I, II and the first part of state III, and the values selected by Ochs et al. (2011) for the presence of ettringite are accepted in these cases. On the other hand, the presence of ettringite is not clearly established for the second part of state III, and it is also not likely that a large amount of calcite will be present. Therefore, zero sorption of molybdate must be assumed in state IIIb. All other values taken from Ochs et al. (2011).

Niobium: Wang et al. (2009) give the same K_d values for all degradation states. Their recommended values are accepted for states I and II and the first part of state III. However, they do not consider explicitly the second part of state III, and the underlying experimental data could indicate a downward trend of sorption in this region. Therefore, it is proposed to reduce the values for the second part of state III by an order of magnitude.

Nickel: Based on a review of the relevant literature, Wang et al. (2009) conclude that the uptake of radioactive Ni by hydrated cement is due to isotopic exchange with stable Ni rather than sorption. Earlier reviews by Andra (2005) and Wieland and Van Loon (2002) arrived also at this conclusion. The solubility of Ni in hydrated cement systems is very low, with a Ni-substituted Al-layered double hydroxide (LDH) controlling the solubility in all likelihood. As a result, the low concentration of stable Ni that is typically present in any cement/concrete is sufficient to reach the corresponding solubility limit in the porewater. The partitioning of introduced radioactive Ni is then controlled by isotope dilution rather than by a chemical process. In order to define an apparent K_d value, the concentration of stable Ni in the cement/concrete as well as the accessibility of this stable Ni pool need to be known. Recent experiments investigating Ni(II) sorption onto SKB's cement in degradation state II at pH 12.5 resulted in a K_d of 1.66 ± 0.56 m^3/kg (Bruno et al. 2018, there called R_d). This is within the range for state II cement of 0.16–4.50 m^3/kg estimated by Wang et al. (2009) as cited in Ochs et al. (2016). The recommended value for state II is therefore based on the SKB-specific value from Bruno et al. (2018). The experimental uncertainty is multiplied by two to give the upper and lower K_d limits.

The solubility of stable Ni changes with pH, which means that the amount of Ni present in the solid phase changes during cement degradation. As a result, the K_d of radioactive Ni isotopes changes during cement degradation when isotopic exchange is the dominant sorption process (Ochs et al. 2016). Ochs et al. (2016) concluded that the solubility of Ni decreases by a factor of 6.2 from pH 13.3 (state I) to pH 12.5 (state II), while it is similar in states II and III. Therefore, the Ni K_d value and upper and lower K_d limits recommended for state III are the same as for state II, and the values for state I are lower by a factor of 6.2.

Neptunium: For the different oxidation states, the following approach is taken:

- For Np(IV), the values recommended by Wieland (2014) are applied directly. Wieland (2014) discussed the similarity of the available experimental data for Np(IV) and Th(IV) sorption and recommended using Th(IV) K_d values for Np(IV). Both experimental sorption data as well as expected speciation of Th indicate constant sorption over all degradation states.
- For Np(V), Wang et al. (2009) give only lower limits, which are taken from Wieland and Van Loon (2002). Due to the lack of experimental data, they conservatively estimated K_d values for Np(V) on the basis of sorption data for divalent metal ions, as these have an effective charge similar to those of pentavalent actinide oxo-cations. Their assessment is accepted for the present case as well. No distinction between degradation states is made.

Protactinium: Recommended values for Pa are given in Wieland (2014) and Wang et al. (2009), but the underlying database is very limited:

- As a best estimate for Pa(IV), both Wieland (2014) and Wang et al. (2009) use the analogy with Th(IV). As the data from Wieland (2014) are applied to Th(IV) sorption here, the K_d values and the upper and lower K_d limits for Pa(IV) recommended in Wieland (2014) are accepted directly for all degradation states.
- For Pa(V), Wang et al. (2009) give recommended values, based on a single literature study and circumstantial evidence for Pa(V) sorption on geological materials. As there is also no good chemical analogue for Pa(V), their values are directly accepted. Based on the fairly constant Pa(V) sorption as a function of pH observed on bentonite (see above), the same values are proposed for both parts of state III.

Lead: The values proposed by Ochs et al. (2011) are directly accepted. Their value given for state III is considered to be valid at pH 12. The underlying data from Andra (2005) and Pointeau (2000) as well as the model analysis by Ochs et al. (2003) indicate that sorption should be greater at pH 10.5 than at pH 12. Conservatively, the respective value of Ochs et al. (2011) is proposed here for both parts of state III.

Palladium: In the absence of relevant data, the approach of Ochs et al. (2011) was followed and Pb was used as analogue. The best estimate and upper limit selected for Pb are directly accepted. For the lower limit, the corresponding values for Pb were reduced by an order of magnitude. Both the trend observed for Pb (see above) as well as the speciation of Pd (formation of negatively charged hydrolytic species above pH ≈ 10, cf Ochs et al. 2011) indicate potentially stronger sorption at pH 10.5 than at pH 12. Therefore, the value selected for state IIIa is also proposed for state IIIb.

Polonium: No values for Po are given in Wang et al. (2009) and Ochs et al. (2011). No other sorption data are available to our knowledge. In the section addressing data for sorption on bentonite above, it is argued that selenite may be an appropriate chemical analogue. Considering that sorption on HCP is more complex in comparison to bentonite, this analogy is adopted conservatively as follows: the values selected for Se(IV) are reduced by an order of magnitude; the lower limit is set to zero.

Plutonium: Recent Pu(IV) sorption experiments using SKB's cement (Tasi 2018) generated a K_d value that exceeded the upper-limit K_d recommended by Wang et al. (2009). Here, the value of Tasi (2018) is therefore used as the upper limit. The best-estimate K_d is also increased in line with the new data for the chemical analogue Th(IV) (see below), as recommended by Wieland (2014). For the other oxidation states, no or no complete sets of data are proposed and the following approach is taken:

- No values are given for Pu(III) or Pu(V), because no reliable experimental data are available for these oxidation states. Therefore, we are proposing the same values as for Am(III) and Np(V), respectively.
- For Pu(VI), only a best estimate is given by Wang et al. (2009), based on analogy with U(VI). For the present purpose, this analogy is extended to the upper/lower limits.

Radium: The values given in Wang et al. (2009) for states I and II are directly accepted. In contrast to Sr, the available experimental data do not extend to pH values below ≈ 11.5. The values recommended by Wang et al. (2009) for state III are therefore considered valid for pH 12. Taking into account the general trend of sorption versus pH shown for both Sr and Ra in Wang et al. (2009), higher sorption should be expected for pH 10.5. Considering the lack of direct confirmation through experimental sorption data, it is proposed to conservatively use the values for pH 12 also for the second part of state III.

Selenium: Sorption behaviour and data situation is dependent on the respective oxidation state. Values for Se(IV) and Se(VI) are directly taken from Ochs et al. (2011). The values for Se(VI) in the first part of state III (IIIa) are based on the presence of ettringite; see Gaucher et al. (2005) and Cronstrand (2007)), those for the second part of state III (IIIb) are based on the absence of ettringite. As discussed for molybdate above, zero sorption has to be assumed in this case. On the other hand, Se(IV) appears to sorb on a variety of HCP minerals, and the available data indicate fairly constant sorption across states II–III. For selenide (Se(–II)), no data are available, to our knowledge. Ochs et al. (2011) conservatively propose a value of zero throughout, although they expect that Se(–II) may be immobilised by hydrated cement. Their recommendation is accepted, considering that zero sorption is also proposed for bentonite (see above). Se(0) is not treated, as it is considered to be practically insoluble (this is likely to hold also for selenide).

Tin: Selected values for states I and II are taken directly from Ochs et al. (2011). For state III, no directly applicable experimental data are available, and Ochs et al. (2011) give a very conservative estimate of 0.003 m^3/kg. This is based on the assumption that HCP minerals (especially CSH and ettringite) have disappeared and that calcite is the only remaining sorbing phase. Moreover, it is stated in Ochs et al. (2011) that sorption values in state III with CSH and ettringite present would be close to values in state II. This is corroborated by the sorption data of Sn(IV) on various CSH phases given in Andra (2005), which show approximately constant sorption within a range of C/S from 1.65 to 0.83. These data were all measured at pH ≈ 12.5, but the hydrolysis behaviour of Sn(IV) suggests that

sorption should increase when pH is lowered from pH 12.5 towards pH 9, as the negatively charged and highly hydrolysed species become less important. Therefore, the following approach is taken for state III:

- The upper limit for the first part of state III is directly taken from state II. Best estimate and lower limit are taken as 0.5 × the value for state II, to acknowledge the slightly greater uncertainty.
- In the second part of state III, ettringite may have disappeared, which may have some influence on sorption. CSH still will be present, however. To acknowledge the greater uncertainty in comparison to state II, best estimate and lower limit are reduced by a factor of 5, while the upper limit is directly accepted. This is viewed as sufficiently conservative, since the sorption of other elements with approximately similar behaviour shows either constant (Th) or increasing (Pb, Zr) sorption with increasing degradation, as long as CSH are present.

Technetium: For Tc(IV), the experimental data given in Wang et al. (2009) indicate constant sorption over all degradation states, and their recommended values are directly accepted. For Tc(VII), Wang et al. (2009) provide a best estimate on the basis of very few available experimental data, but give no bounding values. Considering the data situation, upper and lower limits are arbitrarily set an order of magnitude higher and lower, respectively. For the second part of state III, zero sorption has to be assumed, following the argumentation for other oxo-anions above.

Strontium: The values given in Wang et al. (2009) for states I and II are directly accepted. Taking into account the trend of sorption versus pH shown for both Sr and Ra in Wang et al. (2009), we consider their value given for state III as justified for pH 10.5. On the other hand, it is proposed to cautiously reduce the best estimate and lower limit for pH 12 by one order of magnitude in comparison to the values for pH 10.5.

Thorium: The review and recommendations of Wieland (2014) include the results of relatively recent Th(IV) sorption experiments carried out by Tits et al. (2014). Therefore, the K_d values and upper and lower K_d limits recommended in Wieland (2014) are accepted directly.

Uranium: The review and recommendations of Wieland (2014) include the results of relatively recent U(VI) and Th(IV) sorption experiments carried out by Tits et al. (2014). The data proposed by Wieland (2014) for U(VI) and U(IV), with U(IV) values based on analogy with Th(IV), are therefore applied directly.

Zirconium: Recommended values for states II and III are taken directly form Ochs et al. (2011). The underlying experimental data indicate constant sorption across state III. No experimental data are available that correspond directly to state I, however. Based on the hypothesis that the observed trend in Zr sorption is mainly related to the mineralogy of hydrated cement (rather than the aqueous Zr speciation), Ochs et al. (2011) propose the same upper and lower limit as for state II which are directly adopted here, but give no best estimate. To take into account the additional uncertainty, we propose as best estimate half the corresponding value for state II. It can be seen that the resulting values are conservative in comparison to the values for +IV-valent actinides or Sn, which may be considered as reasonable analogues.

Table 7-4. Sorption coefficients (K_d) for hydrated cement paste, corresponding to degradation state I. The listed values correspond to non-saline conditions and absence of organic complexing agents.

Radionuclide (oxidation state)	K_d (m^3/kg)	Upper K_d limit (m^3/kg)	Lower K_d limit (m^3/kg)
Ac(III)	1.00E+01	5.00E+03	1.00E–01
Ag(I)	0	1.00E–03	0
Am(III)	1.00E+01	5.00E+03	1.00E–01
Ba(II)	1.00E–01	3.00E–01	3.00E–02
^{14}C, carbonate species	2.00E+00	3.00E+00	7.00E–01
^{14}C, CH_4, organic acids	1.00E−05	1.00E−03	0
Ca(II)	3.54E–02	8.86E–02	1.42E–03
Cd(II)	6.00E–02	2.00E–01	2.00E–02
Cl(–I)	1.00E–03	1.00E–02	2.00E–04
Cm(III)	1.00E+01	5.00E+03	1.00E–01
Co(II)	6.00E–03	8.00E–02	4.00E–03
Cs(I)	1.00E–03	1.00E–02	1.00E–04
Eu(III)	1.00E+01	5.00E+03	1.00E–01
Ho(III)	1.00E+01	5.00E+03	1.00E–01
I(–I)	1.00E–03	1.00E–02	0
Mo(VI)	3.00E–03	3.30E–02	3.00E–04
Nb(V)	5.00E+01	1.00E+03	1.00E+00
Ni(II)	2.68E–01	7.87E–01	8.77E–02
Np(IV)	1.00E+02	1.00E+03	1.00E+00
Np(V)	1.00E–01	1.40E–01	7.10E–02
Pa(IV)	1.00E+02	1.00E+03	1.00E+00
Pa(V)	1.00E+01	1.00E+03	5.00E–01
Pb(II)	3.00E–01	1.00E+00	1.00E–01
Pd(II)	3.00E–01	1.00E+00	1.00E–02
Po(IV)	2.00E–02	6.00E–01	0
Pu(III)	1.00E+01	5.00E+03	1.00E–01
Pu(IV)	1.00E+02	3.60E+03	1.00E+00
Pu(V)	1.00E–01	1.40E–01	7.10E–02
Pu(VI)	2.00E+00	1.00E+01	4.00E–01
Ra(II)	3.00E–01	1.00E+00	1.00E–01
Se(–II)	0	0	0
Se(IV)	2.00E–01	6.00E+00	1.00E–02
Se(VI)	3.00E–03	2.00E–02	1.00E–03
Sm(III)	1.00E+01	5.00E+03	1.00E–01
Sn(IV)	2.00E+01	2.00E+02	1.00E+01
Sr(II)	1.00E–01	3.00E–01	3.00E–02
Tc(IV)	3.00E+00	2.00E+01	7.00E–01
Tc(VII)	1.00E–03	1.00E–02	1.00E–04
Th(IV)	1.00E+02	1.00E+03	1.00E+00
U(IV)	1.00E+02	1.00E+03	1.00E+00
U(VI)	2.00E+00	1.00E+01	4.00E–01
Zr(IV)	5.00E+00	1.00E+02	1.00E–01

Table 7-5. Sorption coefficients (K_d) for hydrated cement paste, corresponding to degradation state II. The listed values correspond to non-saline conditions and absence of organic complexing agents.

Radionuclide (oxidation state)	K_d (m^3/kg)	Upper K_d limit (m^3/kg)	Lower K_d limit (m^3/kg)
Ac(III)	1.00E+01	5.00E+03	1.00E+00
Ag(I)	0	1.00E–03	0
Am(III)	1.00E+01	5.00E+03	1.00E+00
Ba(II)	3.00E–02	1.00E–01	5.00E–03
^{14}C, carbonate species	5.00E+00	2.00E+01	2.00E+00
^{14}C, CH_4, organic acids	1.00E−05	1.00E−03	0
Ca(II)	3.09E–03	7.72E–03	1.23E–04
Cd(II)	6.00E–02	2.00E–01	2.00E–02
Cl(–I)	1.00E–03	1.00E–02	2.00E–04
Cm(III)	1.00E+01	5.00E+03	1.00E+00
Co(II)	4.00E–02	4.00E–01	1.60E–02
Cs(I)	2.00E–03	5.00E–02	1.00E–04
Eu(III)	1.00E+01	5.00E+03	1.00E+00
Ho(III)	1.00E+01	5.00E+03	1.00E+00
I(–I)	1.00E–03	1.00E–02	0
Mo(VI)	3.00E–03	3.30E–02	3.00E–04
Nb(V)	5.00E+01	1.00E+03	1.00E+00
Ni(II)	1.66E+00	4.88E+00	5.44E–01
Np(IV)	1.00E+02	1.00E+03	1.00E+00
Np(V)	1.00E–01	1.40E–01	7.10E–02
Pa(IV)	1.00E+02	1.00E+03	1.00E+00
Pa(V)	1.00E+01	1.00E+03	5.00E–01
Pb(II)	3.00E+00	1.00E+01	1.00E+00
Pd(II)	3.00E+00	1.00E+01	1.00E–01
Po(IV)	2.00E–02	6.00E–01	0
Pu(III)	1.00E+01	5.00E+03	1.00E+00
Pu(IV)	1.00E+02	3.60E+03	1.00E+00
Pu(V)	1.00E–01	1.40E–01	7.10E–02
Pu(VI)	3.00E+01	3.00E+02	3.00E+00
Ra(II)	1.00E–01	1.00E+00	1.00E–03
Se(–II)	0	0	0
Se(IV)	2.00E–01	6.00E+00	1.00E–02
Se(VI)	3.00E–03	1.00E–02	1.00E–03
Sm(III)	1.00E+01	5.00E+03	1.00E+00
Sn(IV)	2.00E+01	2.00E+02	1.00E+01
Sr(II)	3.00E–02	1.00E–01	5.00E–03
Tc(IV)	3.00E+00	2.00E+01	7.00E–01
Tc(VII)	1.00E–03	1.00E–02	1.00E–04
Th(IV)	1.00E+02	1.00E+03	1.00E+00
U(IV)	1.00E+02	1.00E+03	1.00E+00
U(VI)	2.00E+01	3.00E+02	3.00E+00
Zr(IV)	1.00E+01	1.00E+02	1.00E–01

Table 7-6. Sorption coefficients (K_d) for hydrated cement paste, corresponding to the first part of degradation state III (state IIIa, pH 12). The listed values correspond to non-saline conditions and absence of organic complexing agents.

Radionuclide (oxidation state)	K_d (m^3/kg)	Upper K_d limit (m^3/kg)	Lower K_d limit (m^3/kg)
Ac(III)	1.00E+01	5.00E+03	3.00E+00
Ag(I)	0	0	0
Am(III)	1.00E+01	5.00E+03	3.00E+00
Ba(II)	1.00E–02	3.00E+00	1.00E–03
^{14}C, carbonate species	2.00E+00	5.00E+00	5.00E–01
^{14}C, CH_4, organic acids	1.00E−05	1.00E−03	0
Ca(II)	3.09E–03	7.73E–03	1.24E–04
Cd(II)	6.00E–02	2.00E–01	2.00E–02
Cl(–I)	1.00E–03	1.00E–02	2.00E–04
Cm(III)	1.00E+01	5.00E+03	3.00E+00
Co(II)	4.00E–02	4.00E–01	1.60E–02
Cs(I)	2.00E–02	3.00E–01	1.00E–03
Eu(III)	1.00E+01	5.00E+03	3.00E+00
Ho(III)	1.00E+01	5.00E+03	3.00E+00
I(–I)	1.00E–03	1.00E–02	0
Mo(VI)	3.00E–03	3.30E–02	3.00E–04
Nb(V)	5.00E+01	1.00E+03	1.00E+00
Ni(II)	1.66E+00	4.88E+00	5.44E–01
Np(IV)	1.00E+02	1.00E+03	1.00E+00
Np(V)	1.00E–01	1.40E–01	7.10E–02
Pa(IV)	1.00E+02	1.00E+03	1.00E+00
Pa(V)	1.00E+01	1.00E+03	5.00E–01
Pb(II)	3.00E+01	1.00E+02	1.00E+00
Pd(II)	3.00E+01	1.00E+02	1.00E–01
Po(IV)	2.00E–02	6.00E–01	0
Pu(III)	1.00E+01	5.00E+03	3.00E+00
Pu(IV)	1.00E+02	3.60E+03	1.00E+00
Pu(V)	1.00E–01	1.40E–01	7.10E–02
Pu(VI)	3.00E+01	3.00E+02	1.00E+01
Ra(II)	8.00E–01	8.00E+00	8.00E–02
Se(–II)	0	0	0
Se(IV)	2.00E–01	6.00E+00	1.00E–02
Se(VI)	3.00E–03	1.00E–02	1.00E–03
Sm(III)	1.00E+01	5.00E+03	3.00E+00
Sn(IV)	1.00E+01	2.00E+02	5.00E+00
Sr(II)	1.00E–02	3.00E+00	1.00E–03
Tc(IV)	3.00E+00	2.00E+01	7.00E–01
Tc(VII)	1.00E–03	1.00E–02	1.00E–04
Th(IV)	1.00E+02	1.00E+03	1.00E+00
U(IV)	1.00E+02	1.00E+03	1.00E+00
U(VI)	2.00E+01	3.00E+02	3.00E+00
Zr(IV)	1.00E+02	5.00E+02	1.00E+00

Table 7-7. Sorption coefficients (K_d) for hydrated cement paste, corresponding to the second part of degradation state III (state IIIb, pH 10.5). The listed values correspond to non-saline conditions and absence of organic complexing agents.

Radionuclide (oxidation state)	K_d (m^3/kg)	Upper K_d limit (m^3/kg)	Lower K_d limit (m^3/kg)
Ac(III)	1.00E+01	5.00E+03	3.00E+00
Ag(I)	0	0	0
Am(III)	1.00E+01	5.00E+03	3.00E+00
Ba(II)	1.00E–01	3.00E+00	1.00E–02
^{14}C, carbonate species	7.00E–01	2.00E+00	1.00E–01
^{14}C, CH_4, organic acids	1.00E−05	1.00E−03	0
Ca(II)	4.67E–02	1.17E–01	1.87E–03
Cd(II)	6.00E–02	2.00E–01	2.00E–02
Cl(–I)	1.00E–03	1.00E–02	2.00E–04
Cm(III)	1.00E+01	5.00E+03	3.00E+00
Co(II)	4.00E–02	4.00E–01	1.60E–02
Cs(I)	2.00E–02	3.00E–01	1.00E–03
Eu(III)	1.00E+01	5.00E+03	3.00E+00
Ho(III)	1.00E+01	5.00E+03	3.00E+00
I(–I)	1.00E–03	1.00E–02	0
Mo(VI)	0	0	0
Nb(V)	5.00E+00	1.00E+02	1.00E–01
Ni(II)	1.66E+00	4.88E+00	5.44E–01
Np(IV)	1.00E+02	1.00E+03	1.00E+00
Np(V)	1.00E–01	1.40E–01	7.10E–02
Pa(IV)	1.00E+02	1.00E+03	1.00E+00
Pa(V)	1.00E+01	1.00E+03	5.00E–01
Pb(II)	3.00E+01	1.00E+02	1.00E+00
Pd(II)	3.00E+01	1.00E+02	1.00E–01
Po(IV)	2.00E–02	6.00E–01	0
Pu(III)	1.00E+01	5.00E+03	3.00E+00
Pu(IV)	1.00E+02	3.60E+03	1.00E+00
Pu(V)	1.00E–01	1.40E–01	7.10E–02
Pu(VI)	3.00E+01	3.00E+02	1.00E+01
Ra(II)	8.00E–01	8.00E+00	8.00E–02
Se(–II)	0	0	0
Se(IV)	2.00E–01	6.00E+00	1.00E–02
Se(VI)	0	0	0
Sm(III)	1.00E+01	5.00E+03	3.00E+00
Sn(IV)	4.00E+00	2.00E+02	2.00E+00
Sr(II)	1.00E–01	3.00E+00	1.00E–02
Tc(IV)	3.00E+00	2.00E+01	7.00E–01
Tc(VII)	0	0	0
Th(IV)	1.00E+02	1.00E+03	1.00E+00
U(IV)	1.00E+02	1.00E+03	1.00E+00
U(VI)	2.00E+01	3.00E+02	3.00E+00
Zr(IV)	1.00E+02	5.00E+02	1.00E+00

The best estimates as well as the upper and lower limits are based directly on the available and reliable experimental data, sometimes with extrapolation to the radionuclide in question via analogy arguments. Based on the experimental data, the resulting best estimates and limiting values for many of the radionuclides of concern are approximately symmetrical in the logarithmic space. Therefore, a continuous triangular probability distribution in the logarithmic space is generally recommended, with the best estimate as mode. For some radionuclides, this distribution will be somewhat skewed.

In some cases, it is not possible to use a log-triangular distribution. Despite their skewedness, the proposed linear triangular distributions are preferred over uniform distributions, which would also be possible but do not have a unique modal value.

- Silver: for states I and II, a skewed triangular distribution in the linear space is recommended, with $K_d = 0$ as minimum as well as modal value and with 1×10^{-3} m^3/kg as maximum value.
- Iodine: Again, a skewed triangular distribution in the linear space is recommended, with the best estimate K_d as mode.

Hydrated cement in cementitious materials

The K_d values recommended in Tables 7-4 to 7-7 are for radionuclide sorption onto pure hydrated cement paste (HCP). The amounts of HCP in the cementitious materials in SFR therefore need to be known in order to adjust the recommended K_d values for sorption onto these materials.

The cementitious materials used in SFR are based on specific recipes that state the mass of dry cement used per cubic metre of material produced. For simplicity and consistency, full hydration has been assumed to occur with a water:cement ratio of 0.47 unless the mix proportions states that a lower amount of water was used. This w/c ratio is for the structural concrete in the silo. In general literature it is stated that a w/c ratio of 0.38 will result in full hydration. Larger amounts of water have also been used to produce a more porous concrete, but the excess water is not chemically incorporated into the final cementitious material.

The recommended data for the HCP mass fraction, w_{HCP}, in SFR cementitious materials are given in Table 7-8.

Table 7-8. Hydrated cement paste content (% by mass) for different parts of SFR.[a]

SFR Concrete/Cement type	Dry cement content (kg/m^3)	Reference	Water:cement ratio for full hydration[b]	Reference	Porosity (%)	Reference	Bulk density (kg/m^3)	Reference	w_{HCP} (% by mass)
Structural concrete (general recipe)	350	Höglund 2014, Table 2-4	0.47	Höglund 2014	11	Höglund 2014, p 105 (selected to account for initial cracks)	2350	Höglund 2014, Table 2-4 (sum of values)	21.9
Structural concrete for the existing 1BMA and 1–2BTF	280	Elfwing et al. 2015	0.47	Assumed	14	This concrete is more porous than the general recipe	2270	Density of general recipe adjusted on the basis of porosity	18.2
Structural concrete for 2BMA and the additional concrete structure in 1BMA	320	Lagerblad et al. 2017, Section 9	0.47	Assumed	11	Höglund 2014, Table 7-5	2390	Lagerblad et al. 2017, Section 9 (hydrated cement plus listed components)	19.7
Silo grout	325	Höglund 2014, Table 2-4	0.47	Assumed	30	Höglund 2014, Table 7-5	1790		26.7
1BRT grout	325	Rosdahl (2022)	0.47	Assumed	30	Rosdahl (2022)	2740	Average density within the waste domain	17.4
1BTF grout bottom[c]	340	SKB R-01-14, Table 4-8	0.47	Assumed	20	SKB R-01-14, p 61	2130	SKB R-01-14, Table 4-8 (hydrated cement + ballast)	23.5
1BTF grout top[c]	265	SKB R-01-14, Table 4-8	0.47	Assumed	20	SKB R-01-14, p 61	2280	SKB R-01-14, Table 4-8 (hydrated cement + ballast)	17.1
Concrete conditioning in waste packages	601	Calculated from Cembygg Euroc (1989)	0.43	Cembygg Euroc (1989), Waste type description B.23[d]	15	Based on hydration model in Höglund (1992)	2260	Calculated from Cembygg Euroc (1989)	38.0

[a] The table contains data from several sources which often provide inconsistent data relative to each other. The values in the table are derived to be internally consistent, but some parameter values are not the best estimates. Nevertheless, the table can be regarded as reference for the derivation of sorption data.
[b] For simplicity and consistency, full hydration has been assumed to occur with a w/c ratio of 0.47 unless the recipe states that a lower amount of water was used. This w/c ratios is for the structural concrete in the silo. In general literature it is stated that a w:c ratio of 0.38 will result in full hydration.
[c] Old type. New mix proportions for 1BTF grout is given in Table 7-1.
[d] SKBdoc 1573181 ver 1.0. (Internal document.)

Influence of saline conditions

The influence of saline water on sorption is difficult to quantify, as there are almost no systematic sorption data available that were measured as a function of salinity. A grouping of radionuclides according to the expected impact based on the reviews of Wang et al. (2009) and Ochs et al. (2011) is given in Section 7.6. Cronstrand (2005) indicates that reduction factors would be in the range of 5–10 for a few radionuclides, but up to 100 for some like Sr. It is also not reported how these factors are derived, nor is any underlying information provided.

An approximate evaluation is given in Wang et al. (2009). They used a model developed by Wieland et al. (2008) and Tits et al. (2004) to calculate the effect of salinity on the K_d of Sr. Note that according to the grouping given in Section 7.6, Sr is one of the elements that should be most affected. For an increase in salinity from dilute solutions (less than 0.1 M) to a salinity of about 0.8 M, the calculated K_d decreases only by factor ≈ 2. Considering the data range already considered by Wang et al. (2009) and Ochs et al. (2011) in defining the recommended values, it is concluded that no additional values need to be developed as long as salinity in the porewater does not exceed ≈ 0.8 M.

Bentonite data

With regard to radionuclide migration parameters for a bentonite buffer, the principal work was done in a dedicated SR-Can report (Ochs and Talerico 2004). The present report largely relies on that work, without reproducing the data derivation procedures. This is motivated by the expected similarity in conditions, cf Section 7.4. Only in a few cases (diffusion data to account for the lower clay density, Ag to take into account literature information previously not considered) have the supplied data been changed from those recommended in SR-Can.

Sorption coefficients

The recommended K_d values for bentonite are given in Table 7-9. As discussed in Section 7.4, the values for saline groundwater are taken from Ochs and Talerico (2004). While Ochs and Talerico (2004) report no K_d values that explicitly correspond to a non-saline groundwater, the bentonite pore water composition was also calculated using a non-saline groundwater as well. The calculated ionic strength in this pore water is almost identical as in case of the saline groundwater, because the pore water in compacted bentonite is to a large degree controlled by the soluble constituents of the bentonite itself. Thus, it can be expected that K_d for a non-saline groundwater will lie well within the range given for the saline groundwater.

Table 7-9. Sorption coefficients (K_d) for unperturbed bentonite and reference pore water, corresponding to saline and non-saline groundwaters, as best-estimate values and upper and lower bounds.

Radionuclide (oxidation state)	K_d (m^3/kg)	Upper K_d limit (m^3/kg)	Lower K_d limit (m^3/kg)
Ac(III)	8	233	0.3
Ag(I)	0	1	0
Am(III)	61	378	10
Ba(II)	0.005	0.031	0.0009
C-14, carbonate species	0.00009	0.00018	0.000018
C-14, CH4, organic acids	0	0	0
Ca(II)	0.005	0.031	0.0009
Cd(II)	0.30	13.3	0.007
Cl(–I)	0	0	0
Cm(III)	61	378	10
Cs(I)	0.11	0.60	0.018
Eu(III)	8	93	0.8
Ho(III)	8	93	0.8
I(–I)	0	0	0
Mo(VI)	0	0	0
Nb(V)	3	45	0.2
Ni(II)	0.30	3.3	0.03
Np(IV)	63	700	4
Np(V)	0.02	0.2	0.004
Pa(IV, V)	3	45	0.2
Pd(II)	5	75	0.3
Pb(II)	74	457	2.4
Po(IV)	0.04	0.4	0.003
Pu(III)	61	378	10
Pu(IV)	63	700	4
Pu(V)	0.02	0.2	0.002
Pu(VI)	3	18	0.3
Ra(II)	0.005	0.031	0.0009
Se(–II)	0	0	0
Se(IV)	0.04	0.4	0.003
Se(VI)	0	0	0
Sm(III)	8	93	0.8
Sn(IV)	63	700	2.3
Sr(II)	0.005	0.031	0.0009
Tc(IV)	63	700	2.3
Tc(VII)	0	0	0
Th(IV)	63	700	6
U(IV)	63	700	3.6
U(VI)	3	18	0.5
Zr(IV)	4	103	0.1

Most values derived in Ochs and Talerico (2004) are directly accepted, but some of the values based on analogy considerations are re-evaluated:

- Ochs and Talerico (2004) made direct use of analogue values (e.g., accepting the values for Am directly for Cm) only in those cases where it was felt that the speciation of the two radioelements is sufficiently similar. Such values are accepted also directly for the present report.
- In all other cases, only the experimental data for an analogue element (e.g. Am) had been used by Ochs and Talerico (2004), and the whole data derivation process had been applied again to these experimental data, taking into account the different speciation of the target element (e.g. Pu(III)). For the present case, the bentonite porewater composition is not deemed to be sufficiently well defined to warrant a distinction of the speciation of similar elements.

- In such cases, the K_d values for the analogue element were accepted directly for the present purpose instead of using the recalculated value for the target element. Accordingly, some of the K_d values for these cases differ between the present report and Ochs and Talerico (2004), as follows:
  - all values (best estimate and upper/lower limit) differ in case of Pu(III) and take on a lower value;
  - the upper limits of Np(IV), Pu(IV), Pu(VI), Sn(IV), Tc(IV) and U(IV) are lower,
  - the lower limits of the above radionuclides with (IV) oxidation state would slightly increase by using the direct analogy approach: to be conservative, the lower values of Ochs and Talerico (2004) have been retained;
  - for Zr, the conservative values by Ochs and Talerico (2004) have been kept instead of using the direct analogy with Th.

The elements barium (Ba), calcium (Ca), polonium (Po), actinium (Ac), and cobalt (Co) were not considered in SR-Can (Ochs and Talerico 2004). In the case of inorganic ^{14}C (carbonate), isotopic exchange is indicated in Ochs and Talerico (2004), but no K_d value is given. In SKB (TR-10-52), zero sorption is assumed in lack of further information. Arguments for the proposed K_d values and uncertainties are summarised in the following:

- Ba and Ca were not considered by Ochs and Talerico (2004) and SKB (TR-10-52). It is proposed to treat both elements analogously to Sr and Ra.
- Some experimental data for Po sorption on montmorillonite are available from Ulrich and Degueldre (1993). However, a complete K_d derivation as in SR-Can (Ochs and Talerico 2004) is not deemed reasonable for the bentonite in SFR, based on the lack of detailed information regarding bentonite and porewater composition (see Section 7.4). Bradbury and Baeyens (2003) proposed to use Se(IV) as an analogue for Po, due to the lack of sorption data for Po. In view of the tendency of dissolved Po to easily oxidise to the +IV state (due to self-irradiation) and the similarity between Se(IV) and Po(IV) (Bradbury and Baeyens 2003, Yui et al. 1999), this analogy is also adopted here. A comparison of the limited number of Po sorption data by Ulrich and Degueldre (1993) with data for selenite (see above) indicate that Po sorption is about an order of magnitude higher than Se(IV) sorption. Therefore, the analogy was considered sufficiently conservative to directly use the data proposed for Se(IV) in SR-Can.
- No values for Ac are recommended in Ochs and Talerico (2004). SKB (TR-10-52) gives a K_d and the corresponding uncertainties. These are based on analogy with the lanthanide elements Eu, Ho and Sm, because Ac exists only in the +III form in normal aqueous solutions. SKB (TR-10-52) considers this analogy as conservative, since Ac bears also some similarity to trivalent actinide elements. To be consistent with the data derivation in Ochs and Talerico (2004), increased uncertainties were assumed. The values recommended in SKB (TR-10-52) are also deemed to be valid for the conditions relevant to SFR.
- No values for cobalt are given in either Ochs and Talerico (2004) or SKB (TR-10-52). Co can be expected to exist only in the +II-valent oxidation state in the bentonite porewaters. The aqueous chemistry of Co(II) is generally very similar to that of Ni(II), see e.g. Baes and Mesmer (1976). Relevant experimental data comprise sorption edges on smectite (Akafia et al. 2011) and a sorption edge on Na-illite (Bradbury and Baeyens 2009). Molera and Eriksen (2002) also measured a Co sorption edge on MX-80. Some of their datapoints are derived from diffusion experiments and agree well with the corresponding batch-type data, as well as with the data by Akafia et al. (2011). Tiller and Hodgson (1960) measured Co sorption on a Ca-montmorillonite in 0.1 M $CaCl_2$ in the pH range 4 to 8. Grütter et al. (1994) measured an isotherm at pH 7.9 in synthetic porewater on Na-montmorillonite (Swy-1) as well as on an illite sample. They observed nearly identical sorption of Ni and Co on illite, but significantly higher sorption of Co on montmorillonite. On the other hand, the sorption edge on illite by Bradbury and Baeyens (2009) agrees with the corresponding data for Ni from the same study only up to pH ≈ 8, whereas at higher pH values, the sorption of Co increases more strongly with pH. The datasets for Ni and Co by Akafia et al. (2011) are consistent with this observation. These results indicate some unresolved inconsistencies in the sorption behaviour of Ni and Co but show that the magnitude of Co sorption is equal to or higher than the sorption of Ni. On this basis, it is proposed to base the data for Co on a direct analogy with Ni.

- For ^{14}C in inorganic form, isotopic exchange of radioactive carbonate species with stable C isotopes in bentonite solids, particularly calcite, can be expected as the most relevant uptake mechanism. To define a corresponding, nominal K_d value, the dissolved total concentration of carbonate species in the bentonite porewater and the amount of calcite accessible to isotopic exchange per unit mass of bentonite need to be known.
  - For GEKO/QI bentonite, Pusch and Cederström (1987) report less than 2 % carbonate. No further details are available, to our knowledge. For the calculation of a nominal K_d value, a solid carbonate content of 0.5 % is assumed as a best estimate, with 1 % and 0.1 % as upper and lower limit, respectively.
  - Regarding the accessibility of solid carbonate with respect to isotopic exchange, Bradbury and Baeyens (1997) estimated a very conservative accessibility of 0.27 % of the total calcite in MX-80. This value is accepted for the present purpose, no further uncertainties are considered.
  - The porewater composition and therefore the dissolved carbonate concentration in the bentonite barrier of SFR is not known. As discussed in Section 7.4, it is assumed that the reference porewater (RPW) considered in Ochs and Talerico (2004) represents a good approximation. The respective total dissolved carbonate concentration of 1.48×10^{-3} M is a fairly typical value for bentonite-groundwater equilibria (it corresponds to an elevated pCO_2 and leads to a more conservative K_d than e.g. atmospheric pCO_2).
- In the case of ^{14}C in organic form, isotopic exchange is conservatively neglected. The forms of organic ^{14}C are expected to include CH_4 and small organic acids that do not sorb appreciably.

With regard to transferring the best estimates and the corresponding uncertainty limits to probabilistic distributions for radionuclide transport calculations, the approach documented in SKB (TR-10-52) is generally followed. As a direct result of the calculation of uncertainties, the best estimates and the upper and lower limits are in most cases symmetric in the $\log_{10}$-space. Therefore, triangular distributions in the log-space are generally recommended. For inorganic ^{14}C (carbonate species), uncertainties of sorption are related to uncertainties in the calcite content. As this does not result in upper and lower limits which are symmetric in the $\log_{10}$-space, a continuous triangular distribution in the linear space is recommended. In the case of Ag, a skewed triangular distribution in the linear space is recommended, with $K_d = 0$ as minimum as well as modal value and with 1.0 m^3/kg as maximum value.

The effect of alkaline solutions on sorption is not quantitatively assessed (**Post-closure safety report**). The change in mineralogy should not result in a dramatic decrease of sorption, as at least some of the new minerals to be expected are very good sorbents (possibly better than bentonite, e.g. zeolites, see Gaucher et al. 2005), see also Section 7.4.

For the unperturbed bentonite, the following qualitative assessment can be given for sorption at elevated pH, based on Ochs and Talerico (2004) and some newer literature (for some elements, no relevant information is available):

- III-valent actinides including Ac and lanthanides: In the absence of carbonate, sorption may increase up to pH 11 or so. In the presence of significant carbonate concentrations, sorption may decrease at pH 8–9 due to increased carbonate complexation. In the presence of atmospheric CO_2 levels, Marques Fernandes et al. (2008) measured a K_d for Eu of about 0.1 m^3/kg at pH ≈ 10.5. No reliable data are available for higher pH values.
- IV-valent actinides: Available data indicate no decrease of Th sorption up to pH ≈ 11.5, which is consistent with Th hydrolysis behaviour. Information on the influence of carbonate on Th sorption is limited. Bradbury and Baeyens (2003) report on measured Th sorption isotherms on MX-80 in synthetic porewater including carbonate and sorption edges in carbonate-free solutions. The good agreement of the K_d values obtained in both cases indicates that sorption of ternary Th-hydroxo-carbonato surface complexes is contributing to the overall Th sorption.
- V-valent actinides: The data by Turner et al. (1998) show that Np(V) sorption increases up to pH ≈ 11 in the absence of carbonate. In the presence of atmospheric CO_2 levels, sorption starts to decrease above pH ≈ 8.5; at pH 9.5 Turner et al. (1998) report a K_d of about 0.05 m^3/kg. No reliable data are available for higher pH values. The data by Bradbury and Baeyens (2006) indicate constant sorption of Pa(V) on montmorillonite between pH 4 and pH 11. Data for higher pH and for the presence of carbonate are not available.

- Cs, Sr, Ra, Ba: The main effect of highly alkaline solutions would be the competition by Na- and K-ions. This influence is expected to be within the limits given in Table 7-9, based on the range of porewater compositions predicted by Gaucher et al. (2005).
- Ni and Co: The data by Bradbury and Baeyens (1999, 2005) on Na- and Ca-montmorillonite show that Ni sorption starts to decrease at pH ≈ 9, but that sorption is still substantial ($K_d \approx 1$ m^3/kg) at pH 12. The Co sorption data by Akafia et al. (2011) and Molera and Eriksen (2002) indicate increasing sorption up to pH ≈ 10, but no data for higher pH are available.
- Pb: The data by Akafia et al. (2011) indicate increasing sorption of Pb on smectite up to pH 10. No systematic data for higher pH values were found for either clay minerals or oxides. A very approximate analogy with cementitious materials suggests that Pb sorption may decrease again at pH values above pH ≈ 10 (Ochs et al. 2011). It appears that both increase and decrease in the magnitude of sorption amounts to about an order of magnitude for each pH-unit, with a sorption maximum near pH ≈ 10. This would be consistent with the hydrolysis of Pb (Baes and Mesmer 1976).
- Se(IV) and Po(IV): Despite the considerable scatter, the trend in the data by Missana et al. (2009), Shibutani et al. (1994) and Tachi et al. (1999) indicates that sorption at pH 12 may be about an order of magnitude lower than at pH 7. However, this probably applies only to a system where calcite is present, which seems to be partly responsible for Se(IV) sorption at high pH (Goldberg and Glaubig 1988). In a calcite-free system, sorption would presumably tend towards zero. No additional information for Po is available.
- Tc(IV): Based on the hydrolysis behaviour of Tc(IV), it can be expected that sorption may decrease above pH 10. However, no corresponding sorption data are available.
- Sn: Sorption coefficients at pH ≈ 11.5 are about 5–10 m^3/kg according to the data by Oda et al. (1999). No reliable data are available for higher pH values.
- UVI): The data by Bradbury and Baeyens (2005) suggest that in the absence of carbonate, sorption at pH 11 may be about two orders of magnitude lower than the maximum sorption of U(VI) occurring around pH 6–7. The data obtained by Pabalan and Turner (1997) in the presence of atmospheric CO_2 levels indicate that sorption in the presence of elevated carbonate concentrations may be close to zero at pH > 10.

Diffusivity data

As pointed out in Section 7.6, the diffusion-available porosity for neutral diffusants and Cs is taken as the physical porosity. As best estimate, the value of 0.61 given in Höglund (2001) for a density of 1 050 kg/m^3 is accepted. Considering the density range of 950 kg/m^3 to 1 120 kg/m^3 analogously gives a porosity range of 0.65 to 0.59. For the diffusion-available porosity of anions, the reduction factors (best estimate 2.5, upper limit 1.8 and lower limit 3.5) given in Ochs and Talerico (2004) are accepted. The derivation of the D_e values summarised below is discussed in Section 7.6.

With regard to the probability distributions that should be applied to the data, the approach taken in SKB (TR-10-52) is generally followed:

- The porosity values, see Table 7-10, are given as best estimates with upper and lower limits. As these are approximately symmetric in the linear space, double triangular distributions (with the best estimate as mode) are recommended.
- Effective diffusivities, see Table 7-11, and associated uncertainties are evaluated directly from various plots of experimental data given in SKB (TR-10-52), see Section 7.6. The evaluation was done on the basis of data in the log-space, and accordingly, a distribution in the log-space is recommended. Following the argumentation in SKB (TR-10-52), a log-double triangular distribution is proposed.

Table 7-10. Diffusion-available porosity ε_{diff} in bentonite.

Element	ε_{diff} (–)		
	Lower limit	Best estimate	Upper limit
Neutral diffusants	0.59	0.61	0.65
Anions	0.17	0.24	0.36
Cs	0.59	0.61	0.65

Table 7-11. Effective diffusivity D_e in bentonite.

Element	D_e (m^2/s)		
	Lower limit	Best estimate	Upper limit
Neutral diffusants	2.0×10^{-10}	4.0×10^{-10}	9.0×10^{-10}
Anions	2.0×10^{-11}	4.0×10^{-11}	2.0×10^{-10}
Cs	2.5×10^{-10}	7.5×10^{-10}	2.0×10^{-9}

Influence of organic complexing agents

As discussed in the **Waste process report**, SFR contains a range of soluble organic substances that may be released into the porewater and reduce radionuclide sorption on cement. Some of these substances are present in the waste, while others are part of the cementitious materials, e.g. organic concrete admixtures. Previous work (Fanger et al. 2001, Keith-Roach et al. 2014, 2021, Keith-Roach and Shahkarami 2021) indicates that relevant organics primarily include the following classes of compounds (see the **Waste process report** for a more detailed discussion and underlying references):

- A number of well-defined complexing agents containing carboxylate and/or functional groups, which stem mainly from decontamination processes at nuclear power plants (EDTA, NTA, as well as citric, gluconic and oxalic acid).
- Degradation products of cellulose (isosaccharinic acid, ISA).
- Concrete admixtures and their degradation products.

However, not all of these substances are of concern in terms of radionuclide sorption reduction in SFR:

- Only 10 kg of EDTA has been disposed in SFR (Fanger et al. 2001), thus the EDTA concentrations in the 1BMA compartments and in all SFR vaults are low.
- The concentrations of gluconate in SFR are very low ($< 10^{-9}$ M in all but one waste type) due to the reasonably limited amounts present in the waste (~600 kg) and the sorption of gluconate to cement (Keith-Roach et al. 2014).
- Calcium oxalate precipitation limits the oxalate concentration to approximately 10^{-5} M in the cementitious vaults of SFR (Keith-Roach et al. 2014).
- Thermodynamic modelling of simple systems containing portlandite suggests that while radionuclide-citrate species can form and affect sorption under experimental conditions (e.g. 1 g portlandite/L), they will only form to a very limited degree when the portlandite concentration is representative of SFR. This is due to the preferential formation of Ca-citrate complexes, limiting the dissolved citrate concentration to about 10^{-3} M (Keith-Roach et al. 2021).
- The literature generally suggests that concrete admixtures such as superplasticisers and their degradation products will have a limited effect on radionuclide sorption under repository conditions. Furthermore, they do not contain functional groups with a higher affinity towards metal ions than e.g. NTA (**Waste process report**). Therefore, it is judged that any potential effects of these substances in SFR are within the ranges of other complexing agents.

The large amounts of cellulose deposited in SFR mean that ISA concentrations are of concern even after its sorption on cement is taken into account. In general, the maximum ISA concentration in cement porewater is limited by precipitation with calcium. Bradbury and Van Loon (1998) measured a solubility limit of ≈ 10 mM (pH 12.5) to ≈ 40 mM (pH 13.3) for ISA in cement porewater. NTA

is not expected to sorb to cement or precipitate with calcium at the concentrations and conditions expected in SFR. Thermodynamic modelling suggests that NTA is able to complex Th(IV) effectively in the presence of high concentrations of portlandite (Keith-Roach et al. 2021). It is therefore judged here that ISA and NTA are the main causes of sorption reduction for radionuclides in SFR.

A category of complexing agent of more recent concern is polyamines in paint hardeners (Hedström 2020, Keith-Roach and Shahkarami 2021). These show a strong affinity to particularly Ni(II), potentially enhancing the release of Ni-59 and Ni-63. The effect is somewhat mitigated by the fact that the paints are most often found on the waste-package exterior, and radionuclides are thus not affected until they have been transported out from the package, at which point a portion of the polyamines are expected to have flowed out of the vaults.

The relevant processes affecting the influence of these organic complexing agents on radionuclide sorption are discussed in the **Waste process report**. The extent of radionuclide sorption reduction depends on the concentration and chemistry of the organic substance, the radionuclide, and the competitive complexation of Ca^{2+}- and OH^- ions. In the PSAR, the effect of a complexing agent (ISA or NTA) is quantified in terms of sorption reduction factors (SRF), by which sorption coefficients K_d are divided. SRF = 1 below the "no-effect" concentration of complexing agent, below which no effects are expected. Above this concentration, SRF are assumed to increase linearly as a function of the complexing-agent concentration, with a gradient defined by interpolation between the "no-effect" concentration and an SRF associated with a higher complexing agent concentration, corresponding to10 mM in most cases (Table 7-12). Different no-effect concentrations and gradients are derived for the different groups of chemically similar radionuclides and for the two considered complexing agents NTA and ISA. Since the complexing agent concentrations vary in the different parts of the repository considered in the radionuclide transport model, the SRF equations give SRF values for each radionuclide in each of the relevant parts of the repository. The SRF in Table 7-12 are mainly given for the maximum complexing agent concentration considered, 10 mM. However, in some cases the experimental evidence suggests a non-linear relationship over the concentration range of interest and, in these cases, two SRF are given for two different concentrations. This allows a two-step interpolation, the first line between the no-effect concentration and the SRF given for the first concentration, and the second line between the two SRF at the given concentrations.

The two variables are based on the experimental data and information discussed in the **Waste process report** and are intended to be applied up to a maximum complexing agent concentration of 10 mM, which exceeds the expected concentrations of complexing agents in 1BMA compartments and SFR vaults. As the available literature does not cover the effect of both complexing agents on all of the radionuclides of concern and is not conclusive for many of those cases where data are available, analogies and approximations are used. These are explained below. Similarly, it is pointed out where interpretations made in pertinent literature are accepted directly. The best-estimate values are in many cases cautious estimates, due to the lack of specific information.

For the indicated no-effect concentrations and SRF, the assessments by Wang et al. (2009), Ochs et al. (2011), Thomson et al. (2008) and Bradbury and Van Loon (1998) were considered in addition to the original literature quoted below and in the **Waste process report**. The reasoning regarding each proposed value is summarised below.

- Ag(I): No quantitative information is available, and no realistic SRF can be derived. As a monovalent cation, interactions of Ag^+ with complexing agents are expected to be limited. Additionally, as the K_d for Ag^+ sorption on cement paste is set to zero in this report, sorption reduction of Ag^+ is of low relevance here.
- ^{14}C: The presence of organic ligands is not expected to influence the isotopic exchange process of $^{14}CO_3$ with calcite.
- Ca(II): Organic ligands are not expected to influence isotopic exchange between radioactive and stable Ca.
- Cd(II): No effect is expected in the relevant complexing agent concentration range (< 10 mM), based on analogy with the effect of ISA on Ni sorption (see below).

- Cl(−I) and I(−I): Chloride and iodide are anions and are therefore not expected to interact with organic complexing agents. Organic acid anions could potentially interfere with sorption/uptake processes of chloride/iodide that are driven by electrostatic interactions, but this is considered insignificant in view of the much higher concentrations of OH^- and stable chloride.
- Cs(I): The weak tendency of Cs^+ to form complexes suggests that its sorption/uptake will not be reduced in the presence of organic complexing agents. Available data for gluconate and ISA on fresh hydrated cement (Bradbury and Van Loon 1998, Holgersson et al. 1998) indicate that the sorption/uptake of Cs is not affected by the presence of organics under realistic conditions.
- Lanthanides, trivalent actinides including Ac: Studies by Van Loon and Glaus (1998) and Dario et al. (2004) found that ISA had no effect on Eu sorption at concentrations < 0.1 mM and that the effect of ISA decreased over time. Here, the SRF associated with 10 mM ISA is based on the long-term experiments of Dario et al. (2004).

  Dario et al. (2004) also found that NTA only influenced Eu(III) sorption at concentrations > 1 mM. The data from Dario et al. (2004) and thermodynamic modelling of these experiments (Keith-Roach et al. 2021) indicate that NTA only affects trivalent actinide sorption when the NTA concentration exceeds the dissolved concentration of Ca, due to the preferential formation of Ca-NTA complexes. When a system containing portlandite at a concentration representative of SFR was modelled (Keith-Roach et al. 2021), the availability of Ca^{2+} strongly restricted the formation of trivalent actinide-NTA species.
- The main evidence available for IV-valent actinides, Tc(IV) and Sn(IV) comes from studies using Th and ISA (see the **Waste process report**). However, Tasi (2018) recently examined the effect of ISA on Pu(IV) sorption on cement. The SRF deduced by Tasi (2018) is used here to define the effect of ISA, and by analogy NTA, on Pu(IV) sorption. For all other tetravalent radionuclides, the Th values are used. As the measured no-effect concentrations for Th(IV) show some scatter (see the **Waste process report**), the lowest value (rather than an average) was chosen. The selected SRF may be conservative for [ISA] ≤ 1 mM, where a reduction factor of 10 may be more appropriate. Little experimental evidence is available for NTA but thermodynamic modelling showed that complexed species, Th(IV)-NTA and Th(IV)-ISA respectively, dominate Th(IV) speciation even in the presence of portlandite at a representative concentration for SFR (Keith-Roach et al. 2021). Therefore, the same data is assumed for NTA as for ISA.

  Since Pu(IV) has a lower solubility than Pu in oxidation states III, V and VI, inadvertent oxidation or reduction of Pu(IV) in experiments would increase its measured solubility. The impact of ISA on the sorption of Pu(IV) (Tasi 2018) is lower than the impact of ISA on Th(IV) sorption. This indicates that the oxidation state of Pu(IV) was successfully controlled in the experiments of Tasi (2018).
- No information is available for the V-valent actinides. The approach taken in the derivation of K_d would suggest an analogy with Sr. As a conservative approach, we propose the same effect for Np(V) and Pu(V) as for trivalent actinides and the same effect for Pa(V) as for tetravalent actinides. This approach is the same as in SR-PSU (SKB TR-14-10).
- Hexavalent U/Pu: the proposed values for ISA are based on the assessment given in Wang et al. (2009) for the effect of ISA on U(VI). NTA is not considered to be able to form stable complexes with hexavalent actinides in SFR, since the interaction is expected to be lower than with trivalent actinides.
- Nb(V): The values for Nb(V) are based on Th(IV), which is considered conservative since Nb may behave more similarly to trivalent actinides or even Sr which is considered unaffected by complexing agents.
- Ni(II), Co(II): Recent experiments have shown that ISA can reduce Ni(II) sorption on cement (Bruno et al. 2018). However, the effect seen with 20 mM ISA was reasonably small (SRF of about 5–7). Therefore, the effect is assumed to be within the uncertainties of the Ni(II) K_d value in the complexing agent concentration range considered here (< 10 mM). As a result, organic complexing agents are not considered to affect Ni(II) and, by analogy, Co(II) sorption. This reflects a system where isotope exchange is the dominant process.

- Pb(II): Ochs et al. (2011) estimated SRF for ISA based on a study by Brownsword et al. (2002) carried out with cellulose degradation products. In lack of any other evidence, their recommendation is directly accepted. The concentration of organics in the underlying experiments was not low enough to observe a no-effect level, however. A constant reduction of sorption was observed at estimated ISA levels (calculated from a cellulose loading according to Wang et al. (2009)) from 0.01 mM to 1 mM.; i.e. higher ISA concentration did not lead to a higher reduction in sorption. A no-effect level of 0.02 mM is proposed here, based on the observation that the lowest no-effect levels directly observed for any element considered is 0.1 mM. In view of the uncertainties in the cellulose-loading to ISA conversion, and considering the effect of organic ligands on other elements, the present assessment may be conservative. The strong interaction between Ca^{2+} and NTA (see trivalent actinides) suggests that Pb(II) will not be complexed by NTA when portlandite is present in excess.
- Pd(II): In lack of any other evidence, the assessment for Pb is also accepted for Pd.
- Po(IV): No information is available. Se(IV) is used as an analogue.
- In case of the oxyanions (selenate, molybdate, pertechnetate), no pertinent data are available, but it is expected that organics will have no influence on the relevant sorption process (solid solution formation with ettringite).
- Se(IV): Depending on the experimental setup, the effect of 2 mM ISA has been seen to range from very weak to strong, see the discussion in the **Waste process report**. Pointeau et al. (2006) proposed that sorption of the organic anions competes with the sorption of the selenite anion, see also the **Waste process report**. Due to this uncertainty, the lowest no-effect concentration observed for any radionuclide listed in Table 7-12 is adopted conservatively. Similarly, an SRF of 100 is proposed for a 10 mM ISA concentration. Since NTA is not expected to sorb, it is not expected to affect Se(IV) via competition for sorption sites.
- Sr(II): No effects are expected in the relevant complexing agent concentration range (< 10 mM), based on information for ISA (**Waste process report**). Due to the simple chemistry of Sr in terms of complexation reactions, this is deemed valid for the other organic ligands as well. No reduction factors have been measured at elevated ligand concentrations, to our knowledge. This is also assumed to be the case for the other alkaline earth metals, Ba and Ra.
- Zr(IV): Based on the experiments by Brownsword et al. (2002) (see Pb above), reduction factors between ≈ 30–125 were estimated (Ochs et al. 2011). However, considering the strong similarity between Zr and tetravalent actinides (Baes and Mesmer 1976), we consider the analogy with Th as more reliable.

Sorption reduction factors

The final SRF values for the various waste vaults and 1BMA compartments are not provided here but can be found in Keith-Roach et al. (2021, Tables 4-2 and 4-3).

Table 7-12. No-effect concentrations and sorption reduction factors at defined concentrations of ISA and NTA. Linear interpolation between these values is used to calculate the SRF at the actual complexing agent concentrations [CA] in different waste vaults. The relationships are only considered up to a maximum complexing-agent concentration of 10 mM.

Radionuclide (oxidation state)	No-effect concentration & comments for ISA	Reduction factor for ISA	No-effect concentration & comments for NTA	Reduction factor for NTA
Ag(I)	no effect expected	1	no effect expected	1
^{14}C, carbonate species	no effect expected	1	no effect expected	1
^{14}C, CH_4, organic acids	not relevant (K_d = 0)	1	not relevant (K_d = 0)	1
Ca (radioactive isotopes)	no effect expected	1	no effect expected	1
Cd(II)	no effect expected	1	no effect expected	1
Cs(II)	no effect expected	1	no effect expected	
Ac(III), Eu(III), Am(III), Cm(III), Ho(III), Pu(III), Sm(III)	0.1 mM	100 when [CA] = 10 mM*	no effect expected	1
Mo(VI), Se(VI), Tc(VII)	no effect expected	1	no effect expected	1
Nb(V)	0.1 mM	100 when [CA] = 1 mM; 10 000 when [CA] = 10 mM	0.1 mM	100 when [CA] = 1 mM; 10 000 when [CA] = 10 mM
Ni(II), Co(II)	no effect expected	1	no effect expected	1
Pb(II), Pd(II)	0.02 mM	100, constant	no effect expected	
Th(IV), Np(IV), U(IV), Pa(IV), Tc(IV), Zr(IV), Sn(IV)	0.1 mM	100 when [CA] = 1 mM; 10 000 when [CA] = 10 mM	0.1 mM	100 when [CA] = 1 mM; 10 000 when [CA] = 10 mM
Pu(IV)	0.1 mM	1 000 when [CA] = 10 mM	0.1 mM	1 000 when [CA] = 10 mM
Np(V), Pu(V)	0.1 mM	100 when [CA] = 10 mM	no effect expected	1
Pa(V)	0.1 mM	100 when [CA] = 1 mM; 10 000 when [CA] = 10 mM	0.1 mM	100 when [CA] = 1 mM; 10 000 when [CA] = 10 mM
Se(-II)	Not relevant (K_d = 0)	1	not relevant (K_d = 0)	1
Se(IV), Po(IV)	0.1 mM	100 when [CA] = 10 mM	no effect expected	1
Sr(II), Ba(II), Ra(II)	no effect expected	1	no effect expected	1
U(VI), Pu(VI)	0.5 mM	10 when [CA] = 5 mM; 20 when [ISA] = 10 mM	no effect expected	1

* Based on the long term results in Dario et al. (2004).

7.10 Judgements by the assessment team

Sources of information

The assessment team finds the sources given in Section 7.3 sufficient for safety assessment use.

Conditions for which data is supplied

The assessment team find that the conditions given for cement in Section 7.4 reflect the conditions assumed in the repository during the safety assessment lifetime.

Conceptual modelling uncertainty

The assessment team considers the given uncertainties in Section 7.5 sufficient to describe the uncertainties regarding modelling uncertainty.

Data uncertainty – precision, bias, and representativity

The uncertainties relating to sorption coefficients given in Section 7.6 are considered sufficient according to the assessment team.

Data uncertainty – spatial and temporal variability

The assessment team accepts the variabilities considered in Section 7.7.

Data uncertainty – correlations

The assessment team finds that Section 7.8 describes how K_d data in many cases are based on analogies between radionuclides with assumed similar properties. However, it is not described if or how these should be correlated when sampling from the K_d statistical distributions for the probabilistic radionuclide-transport modelling.

Also, the SRFs rely heavily on analogies between radionuclides, which is not described in Section 7.8, but in Keith-Roach et al. (2021).

Results of supplier's data qualification

The assessment team considers the suppliers data qualification to be sufficient and the data will therefore be used in the radionuclide transport calculations. The final SRF values for the various waste vaults and 1BMA compartments are not provided in Section 7.9 but can be found in Keith-Roach et al. (2021, Tables 4-2 and 4-3).

7.11 Data recommended for use in the assessment

Concrete/cement

The K_d values recommended in Tables 7-4 to 7-7 are for radionuclide sorption onto pure hydrated cement paste (HCP) in the four respective degradation states. The recommended data for the percentage of HCP in cementitious materials are given in Table 7-8. The evolution of the concrete structures is described in the **Post-closure safety report**, Section 6.2.9 and the assumed transition points between degradation states are given in the **Post-closure safety report**, Chapter 7**.**

Bentonite

The recommended K_d data for bentonite are given in Table 7-9. The diffusion available porosities are given in Table 7-10 and the effective diffusivities are given in Table 7-11.

Bentonite/Sand

For the 90 % sand and 10 % bentonite mixture on the bottom and on the top of the silo the K_d values are calculated by weighing using 90 % of the value from the Rock matrix and Crushed rock chapter, Table 8-8 and 10 % from the bentonite Table 7-9.

Sorption reduction factors for sorption on cementitious materials and bentonite

The recommended no-effect concentrations and sorption reduction factors for a particular complexing agent concentration are given in Table 7-12 for defined groups of chemically similar radionuclides. These values are used to define a linear relationship between complexing agent concentration and sorption reduction factor for each complexing agent and group of chemically similar radionuclides. The concentrations of ISA and NTA anticipated in SFR (Keith-Roach et al. 2021, Tables 3-9, 3-10 and 3-13) are used with these linear relationships to define sorption reduction factors, which are not provided in the present report but in Keith-Roach et al. (2021, Tables 4-2 and 4-3). These are recommended for application in the radionuclide transport modelling. The same concentrations and thus SRF values are supplied and recommended for the silo bentonite as for the silo concrete barriers.

8 Rock matrix and Crushed rock sorption data

This section concerns the retardation of radionuclides, by adsorption mechanisms, in both the geosphere rock matrix and the repository backfill, providing suitable sorption coefficients (K_d).

Rock matrix

Since the rock surrounding SFR is similar to that surrounding the planned spent fuel repository the data presented in this chapter are based on the same geologic assumptions made in the SR-Site geosphere K_d report (Crawford 2010) e.g. based on a reference granite to granodiorite, metamorphic medium grained rock type (SKB rock code 101057). This rock type is selected as it is dominant within the domains of both the planned KBS-3 repository and the SFR repository (SKB TR-11-04).

Crushed rock backfill

At final closure of SFR the 1–2BMA, 1BRT and 1–2BTF vaults and repository tunnels will be backfilled with macadam/crushed rock (Mårtensson et al. 2022). The primary function of the backfill is to prevent rock fallout in the vaults and divert the water flow around the concrete barriers, but the backfill may also retard many radionuclides on their way out of the repository due to sorption on the crushed rock.

The crushed rock planned to be used in the waste vaults is macadam in the size range 16–32 mm.

8.1 Modelling in this safety assessment

This section describes what data are expected from the supplier, and in what modelling activities the data are to be used.

Defining the data requested from the supplier

- Rock matrix and crushed rock sorption coefficients, K_d, (m^3/kg) for the selected radionuclides in relevant pH and redox conditions. The conditions deemed relevant in the surrounding groundwater are taken from Auqué et al. (2013) with the treatment and basis for recommendations further described in Crawford (2013).
- Updated information on the sorption of molybdenum, selenium and potential influence of complexing agents based on Crawford (2017, 2018).

Modelling activities in which data will be used

The K_d values are used in the radionuclide transport calculations to model retardation of the radionuclides released from SFR (**Radionuclide transport report).**

8.2 Experience from previous safety assessments

This section briefly summarises experience from previous safety assessments, which may be of direct consequence for the data qualification in this data report.

Modelling in previous safety assessments

In SAR-08, the backfill K_d values were presented and qualified in Cronstrand (2005). The rock matrix K_d values used were taken from the SR-Can safety assessment and are presented and qualified in the SR-Can Data report (SKB TR-06-25).

The SAR-08 radionuclide transport modelling approach (Thomson et al. 2008) does not differ significantly from the modelling performed in SR-PSU (SKB TR-14-09), the only main difference being that the discretisation differs between safety assessments, and the addition of the SFR3 in SR-PSU.

In SR-PSU the K_d data were treated in similar manner as in the preceding assessments with the addition of, and explicitly including, decay products of the most relevant radionuclides.

Conditions for which data were used in previous safety assessments

SAR-08 data conditions for both the crushed rock and the rock matrix K_d were similar to the approach used in SR-PSU. The main difference is the evaluation of K_d for pH > 10, under varying redox-conditions that may prevail in a possible high-pH near-field fracture domain of the geosphere, possibly affecting the rock matrix sorption, in SR-PSU.

Sensitivity to assessment results in previous safety assessments

As the conductivity of the backfill is high relative to the conductivities in the concrete and bentonite, the radionuclides are not retarded for long in the backfill. Therefore, the crushed rock K_d values were not of major importance in retaining the radionuclide output to the geosphere.

As the travel times from the repository to the surface have always been relatively short in SFR safety assessments, the rock matrix K_d values have had a limited impact on the total dose curves. This was highlighted in the SAR-08 Radionuclide transport report (Thomson et al. 2008) where a calculation case (CC13) compared the effect of using geosphere retardation to not considering the geosphere as a barrier at all. Also, in SR-PSU a residual scenario without retention in the geosphere showed limited impact on the total dose curves which are dominated at short to medium times by Mo-93 and C-14. However, the transport behaviour of some radionuclides with relatively high K_d values such as Ni-59, U-238 and U-235 (and the Pa-231/Ac-227 descendants of U-235 decay) are influenced more significantly.

Alternative modelling in previous safety assessments

No alternative modelling was reported for SAR-08 or SR-PSU.

Correlations used in previous safety assessment modelling

No correlations were reported in SAR-08 or SR-PSU.

Identified limitations of the data used in previous safety assessment modelling

No known limitations have been reported in the rock sorption data used in the SAR-08 and SR-PSU. However, additional information on the sorption of molybdenum, selenium and potential influence of complexing agents are requested.

8.3 Supplier input on use of data in this and previous safety assessments

The supplier considers the data used in SAR-08 to be acceptable but out of date since a lot of new research has been performed regarding geosphere sorption since 2008, especially in the SR-Site safety assessment for the KBS-3 repository. In SR-PSU K_d values for alkaline conditions were also supplied, which were not included in preceding assessments. In this safety assessment (PSAR) additional information on the sorption of molybdenum and selenium as well as the potential influence of complexing agents are included.

8.4 Sources of information and documentation of data qualification

Sources of information

The main source of information for this chapter is Crawford (2013, 2017, 2018). In Table 8-1 some of the supporting sources cited in the report are listed also.

Table 8-1. Main sources of information used in data qualification.

Sources of information
Crawford J, 2013. Quantification of rock matrix K_d data and uncertainties for SR-PSU. SKB R-13-38, Svensk Kärnbränslehantering AB.
Crawford J, 2017. Organic complexation in the geosphere for SR PSU. SKBdoc 1577134 ver 1.0, Svensk Kärnbränslehantering AB.
Crawford J, 2018. Technical Note – K_d values for oxyanions in SR-PSU. Updated K_d recommendations for Mo-93 and Se-79. SKBdoc 1689868 ver 1.0, Svensk Kärnbränslehantering AB.
Supporting sources:
Banwart S A, 1999. Reduction of iron(III) minerals by natural organic matter in groundwater. Geochimica et Cosmochimica Acta 63, 2919–2928.
Bernhard G, Geipel G, Reich T, Brendler V, Amayri S, Nitsche H, 2001. Uranyl(VI) carbonate complex formation: validation of the $Ca_2UO_2(CO_3)_3$(aq.) species. Radiochimica Acta 89, 511–518.
Bertetti F, Pabalan R, Almendarez M G, 1998. Studies of neptunium^{V} sorption on quartz, clinoptilolite, montmorillonite, and α-alumina. In Jenne E A (ed). Adsorption of metals by geomedia: variables, mechanisms, and model applications. San Diego, CA: Academic Press, 131–148.
Bradbury M H, Baeyens B, 2005. Experimental measurements and modeling of sorption competition on montmorillonite. Geochimica et Cosmochimica Acta 69, 4187–4197.
Bradbury M H, Baeyens B, 2009. Sorption modelling on illite. Part I: Titration measurements and the sorption of Ni, Co, Eu and Sn. Geochimica et Cosmochimica Acta 73, 990–1003.
Bradbury M H, Baeyens B, 2009. Sorption modelling on illite. Part II: Actinide sorption and linear free energy relationships. Geochimica et Cosmochimica Acta 73, 1004–1013.
Bradbury M H, Baeyens B, 2011. Predictive sorption modelling of Ni(II), Co(II), Eu(IIII), Th(IV) and U(VI) on MX-80 bentonite and Opalinus Clay: a “bottom-up” approach. Applied Clay Science 52, 27–33.
Byegård J, Skarnemark G, Skålberg M, 1995. The use of some ion-exchange sorbing tracer cations in in situ experiments in high saline groundwaters. In Murakami T, Ewing R C (eds). Scientific basis for nuclear waste management XVIII: symposium held in Kyoto, Japan, 23–27 October 1994. Pittsburgh, PA: Materials Research Society. (Materials Research Society Symposium Proceedings 353) 1077–1084.
Byegård J, Johansson H, Skålberg M, Tullborg E-L, 1998. The interaction of sorbing and non-sorbing tracers with different Äspö rock types. Sorption and diffusion experiments in the laboratory scale. SKB TR-98-18, Svensk Kärnbränslehantering AB.
Crawford J, 2010. Bedrock K_d data and uncertainty assessment for application in SR-Site geosphere transport calculations. SKB R-10-48, Svensk Kärnbränslehantering AB.
Goldberg S, Forster H S, Godfrey C L, 1996. Molybdenum adsorption on oxides, clay minerals, and soils. Soil Science Society of America Journal 60, 425–432.
Goldberg S, Johnston C T, Suarez D L, Lesch S M, 2007. Mechanism of molybdenum adsorption on soils and soil minerals evaluated using vibrational spectroscopy and surface complexation modeling. In Barnett M, Kent D (eds). Adsorption of metals by geomedia II: variables, mechanisms, and model applications. Amsterdam: Elsevier. (Developments in Earth & Environmental Sciences 7), 235–266.
Hakanen M, Ervanne H, Puukko E, 2014. Safety case for the disposal of spent nuclear fuel at Olkiluoto. Radionuclide migration parameters for the geosphere. Posiva 2012-41, Posiva Oy, Finland.
Hummel W, Berner U, Curti E, Pearson F J, Thoenen T, 2002. Nagra/PSI chemical thermodynamic data base 01/01. Boca Raton: Universal Publishers.
Marques Fernandes M, Baeyens B, Bradbury M H, 2008. The influence of carbonate complexation on lanthanide/actinide sorption on montmorillonite. Radiochimica Acta 96, 691–697.
Pabalan R, Turner D, Bertetti F, Prikryl J, 1998. Uranium^{VI} sorption onto selected mineral surfaces: key geochemical parameters. In Jenne E A (ed). Adsorption of metals by geomedia: variables, mechanisms, and model applications. San Diego, CA: Academic Press, 99–130.
Panak P J, Kim M A, Klenze R, Kim J-I, Fanghänel T, 2005. Complexation of Cm(III) with aqueous silicic acid. Radiochimica Acta 93, 133–139.
Papelis C, 2001. Cation and anion sorption on granite from the Project Shoal Test Area, near Fallon, Nevada, USA. Advances in Environmental Research 5, 151–166.
Salas J, Gimeno M J, Molinero J, Auqué L F, Gómez J, Juárez I, 2010. SR-Site – Hydrogeochemical evolution of the Forsmark site. SKB TR-10-58, Svensk Kärnbränslehantering AB.
Seiler R L, 2011. ^{210}Po in Nevada groundwater and its relation to gross alpha radioactivity. Ground Water 49, 160–171.
Seiler R L, Stillings L L, Cutler N, Salonen L, Outola I, 2011. Biogeochemical factors affecting the presence of ^{210}Po in groundwater. Applied Geochemistry 26, 526–539.

Categorising data sets as qualified or supporting data

The data set presented in Table 8-2 concerns all the radionuclides presented in Crawford (2013). Updated data regarding molybdenum and selenium are given in Crawford (2018).

Table 8-2. Qualified and supporting data sets.

Qualified data sets
Crawford (2013, Tables 6-1 and 6-2)
Crawford (2018, Table 1)

Excluded data previously considered as important

Not applicable.

8.5 Conditions for which data are supplied

As written in the introduction the rock types assumed are the same as for the SR-Site safety assessment as the sites of SFR and the spent fuel repository is within a rock domain dominated by the same rock type (Crawford 2010, 2013).

Regarding groundwater the following K_d values are based on new speciation calculations performed with the SFR groundwater compositions reported by Auqué et al. (2013). The different compositions are shown in Tables 8-3 to 8-5.

The aforementioned work also includes the possibility of an elevated pH in the repository near-field given its content of, and in a far-future, dissolution of cement and concrete materials. In Crawford (2013) a method is presented to scale the rock matrix K_d values depending on the amount of influence from the repository Ordinary Portland Cement (OPC) water. For the crushed rock data presented below the assumption is made that the influence of cement leachate is sufficiently high that elevated pH conditions can be assumed (e.g. repository water around the backfill at a pH > 10). This is supported by modelling performed in Crawford (2013) showing that mixing even small fractions (< 20 %) of OPC-water with the SFR groundwaters results in large jumps in both pH and Eh, see Figure 8-1.

Table 8-3. Proposed composition and concentration ranges for penetrating brackish saline groundwater when the repository location is submerged under the sea. Data reproduced from Auqué et al. (2013, Table 5-1).

	Composition	Range
pH	7.3	6.6 – 8.0
Eh (mV)	−225	−100 to −350
Cl (mg/L)	3 500	2 590 – 5 380
SO_4^{2-} (mg/L)	350	74 – 557.2
HCO_3^- (mg/L)	90	40 – 157
Na (mg/L)	1 500	850 – 1 920
K (mg/L)	20	3.8 – 60
Ca (mg/L)	600	87 – 1 220
Mg (mg/L)	150	79 – 290
SiO_2 (mg/L)	11	2.6 – 17.2

Table 8-4. Proposed composition of the fresh groundwater around the repository during temperate and periglacial climate domains when the repository is not covered by the sea. Data reproduced from Auqué et al. (2013, Table 5-2).

	Reference composition	Range	Reference composition	Range
	Not extending for more than approximately 40 000 years		Extending for more than 40 000 years	
pH	7.4	6.6–8.3	7.6	6.6 – 8.3
Eh (mV)	−210	−135 to −300	−250	−135 to −300
Cl (mg/L)	190	16–503	90	5 – 357
SO_4^{2-} (mg/L)	50	25–163	40	17–110
HCO_3^- (mg/L)	300	300–500	200	120 – 324
Na (mg/L)	180	65–400	110	38–250
K (mg/L)	5	5–15	3	2–5.3
Ca (mg/L)	50	24–105	30	7 – 48
Mg (mg/L)	12	7–24	6	2–13
SiO_2 (mg/L)	12	2–21	10	12–31

Table 8-5. Proposed composition and concentration ranges for the glacial-derived groundwater expected to reach the repository during a glacial climate domain. Data reproduced from Auqué et al. (2013, Table 5-3).

	Composition	Range
pH	9.3	9.0 – 9.6
Eh (mV)	+400	+900 to −290
Cl (mg/L)	0.5	0.5–178.0
SO_4^{2-} (mg/L)	0.5	0.1–5.8
HCO_3^- (mg/L)	22.7	17.0 – 150.0
Na (mg/L)	0.17	0.17–130.0
K (mg/L)	0.4	0.14–3.6
Ca (mg/L)	6.8	6.6 – 21.0
Mg (mg/L)	0.1	0.05 – 2.0
SiO_2 (mg/L)	12.8	7.9 – 14.5

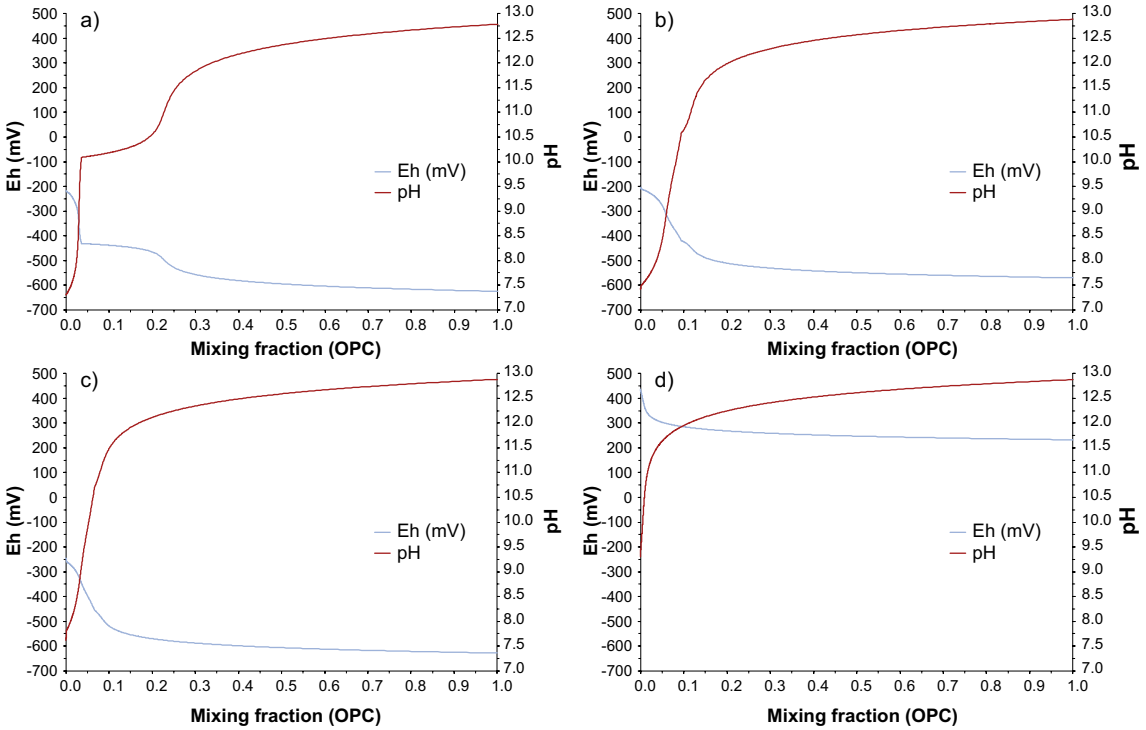

Figure 8-1. *Trends in groundwater composition (Eh and pH) as a function of mixing fraction for mixing of Portlandite equilibrated groundwater with un-affected groundwater. Plots are shown for a) Temperate saline, b) Early Periglacial, c) Late Periglacial, and d) Glacial derived groundwater. Reproduced from Crawford (2013).*

8.6 Conceptual and modelling uncertainty and bias

Methods of estimating K_d values differ between radionuclides. The following text is focused on some of the radionuclides for which sorption estimation methods and underlying data are considered to have large uncertainties and which are shown to be of importance for the post-closure safety of SFR in the previous safety assessment. A more in-depth discussion of all the radionuclides included in the safety assessment is found in Crawford (2013, 2017, 2018), which this chapter is based on.

Carbon-14 (^{14}C)

^{14}C is expected to migrate from the repository both as inorganic and organic compounds. The inorganic forms are expected to be either gaseous CO_2 or dissolved HCO_3^- (Carbonate). Organic forms expected are gaseous or dissolved CH_4 as well as dissolved organic acids. All the organic forms of ^{14}C are deemed as non-sorbing given their either non-polarity (methane) or their negative charge as conjugate bases.

Some earlier estimates of K_d for inorganic ^{14}C, in the form of dissolved carbonate were based on an assumption of isotope exchange with calcite present at low concentrations in the rock matrix as an accessory mineral (e.g., Carbol and Engkvist 1997, Albinsson 1991). In Crawford (2013, Appendix A) an analysis is made of the potential of sorption on calcite in the fracture coatings. Based on thermodynamic calculations of isotope exchange in calcite scaled by the effective fraction of exchangeable carbonate (derived from the measured BET surface area of fracture calcites and an assumed accessible penetration depth for the isotope exchange process) an effective K_d value was estimated to 0.06 m^3/kg for sorption in fracture calcite. Unfortunately, quantitative data for calcite in the rock matrix are lacking in the site-specific investigations of the Forsmark bedrock and an estimate of the impact of this mechanism cannot be made for sorption in the rock matrix. Alternative mechanisms involving surface complexation of free carbonate, or ternary surface complexation reactions with groundwater cations are feasible although these have not been quantified for granitic rock. If quantitative data were available for the abundance of the trace calcite amounts in Forsmark sitespecific rocks (i.e. as secondary precipitates

in the rock matrix), then these could be used in principle to estimate non-zero K_d values for sorption of inorganic ^{14}C in the rock matrix. Since such data are not currently available, the recommendation of non-sorbing status for the rock matrix is deemed cautious for PSAR transport calculations.

Calcium (Ca)

Ca(II) is one of the most abundant major cations present in groundwater and its availability is usually governed by calcite equilibrium although it also participates in cation-exchange reactions. The possible impact of the latter has not been quantified presently**,** although this sorption mechanism is expected to be relatively weak. Isotope fractionation and dilution of ^{41}Ca by reaction with calcite present can occur both within fracture coatings and within the small amounts which are ubiquitous in the rock matrix. The effective K_d for the isotope dilution process involving calcite in fracture coatings can be derived by analogy with that for ^{14}C labelled bicarbonate ion (see Crawford 2013, Appendix A). Unfortunately, quantitative data for calcite in the rock matrix are lacking in the site-specific investigations of the Forsmark rock matrix and an estimate of the impact of this mechanism cannot be made for sorption in the rock matrix. Therefore, for the PSAR, calcium is assumed to be non-sorbing for both the rock matrix and the repository backfill, which can be seen as a cautious estimate.

Molybdenum (Mo) and Selenium (Se)

Molybdenum's only relevant aqueous form in geosphere and repository conditions is the molybdate ion MoO_4^{2-}, although its solubility may be limited by MoS_2 under strongly reducing conditions. A predominance diagram for Mo calculated using PHREEQC with the Thermochimie v10a thermodynamic database (Giffaut et al. 2014) is shown in Figure 8-2. Being negatively charged, MoO_4^{2-} is not expected to sorb significantly on matrix minerals at prevailing groundwater pH levels and even less so under more basic conditions. There have been studies performed which demonstrate sorption on granitic rocks, clay minerals and soils (e.g., Goldberg et al. 1996, 2007, Hakanen et al. 2014). Any sorption of MoO_4^{2-} that does occur is most likely associated with minerals that have point of zero charge around normal groundwater pH levels, such as ferric oxide accessory minerals (including goethite, hematite, or magnetite) in the rock matrix. For SR-PSU, molybdenum was deemed non-sorbing for both the rock matrix and the crushed rock backfill, which can be seen as a conservative assumption.

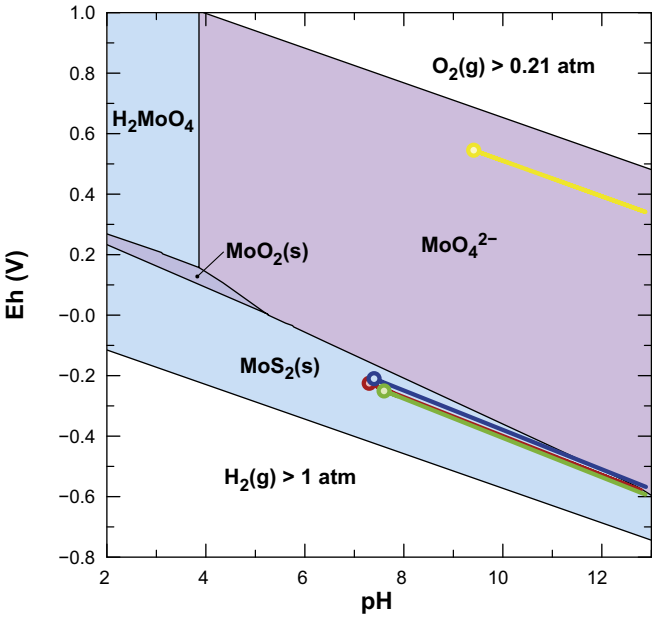

Figure 8-2. *Mo predominance diagram calculated using the ThermoChimie database (version 10a) and with a total Molybdenum concentration of 10^{-9} M assuming a temperature of 15 °C. Trends in groundwater composition (Eh and pH) corresponding to the mixing trajectories in the previous Figure 8-1 are shown for a) Temperate saline (red), b) Early Periglacial (blue), c) Late Periglacial (green), and d) Glacial derived groundwater (yellow) where the marker on the far left indicates unaffected groundwater.*

Since there are presently no data presently available for sorption of Mo on Forsmark site specific rocks, it has been necessary to invoke a geochemical analogy with Se (for which site-specific data are available) to estimate an updated K_d value for the PSAR. An updated evaluation based on the analogy with Selenite, SeO_3^{2-} which also is an oxyanion at normal groundwater pH levels, is based in part on a detailed modelling interpretation of laboratory sorption data (Widestrand et al. 2010a, b) for Se, as well as theoretical treatment of Mo sorption using the diffuse layer model in an attempt to extrapolate a mechanistically reasonable K_d value for Molybdenum. The Se(IV) state has been found in laboratory experiments to sorb relatively well (at intermediate redox-levels) and the K_d value can be directly related to the amount of ferric oxide present in a sample (e.g., Jan et al. 2007, 2008). Under oxidising conditions (≥ + 400 mV) the Se(VI) form is the dominant redox species and poorly sorbing. A predominance diagram for Se calculated using PHREEQC with the Thermochimie v10a thermodynamic database is shown in Figure 8-3.

Using thermodynamic sorption modelling, a scaling factor was used to estimate how the K_d for Mo(VI) should relate to that for Se(IV), assuming that sorption primarily occurs on ferric oxide mineral phases in the rock. The approach to estimate the Mo(VI) sorption given in the work by Crawford (2018 and references therein) is to first evaluate the K_d measured for Se(IV) in site specific rock and then apply the theoretically-calculated scaling factor to obtain a best estimate K_d value for Mo(VI). The theoretical calculations based on the Dzombak and Morel (1990) model assuming inner sphere sorption mechanisms might underestimate sorption of both Se(IV) and Mo(VI) at higher groundwater pH levels where outer sphere surface complexes might play a more prominent role. Recent experimental and modelling work by Li et al. (2020) also suggests that sorption is not restricted to ferric oxides, but can occur directly in association with biotite, although with decreasing intensity at higher pH levels. Furthermore, studies of Se sorption on cement CSH phases by (Missana et al. 2019) suggest a role for ternary reactions involving Ca^{2+} bridging atoms facilitating the sorption of oxyanions at higher pH levels in Ca-rich porewater. The relevance of this for sorption in the geosphere is not clear at present, although it suggests that elevated pH due to influence of cementitious leachate might not have the same effect as that achieved in laboratory experiments by titration with NaOH. Taken together, this information suggests that the low K_d values presently recommended for Se(IV) and Mo(VI) are probably cautiously underestimated. The sorption of both Se(IV) and Mo(VI) is nevertheless expected to be significantly weaker at higher pH levels, although maybe not to the full extent that the simplified modelling appears to indicate.

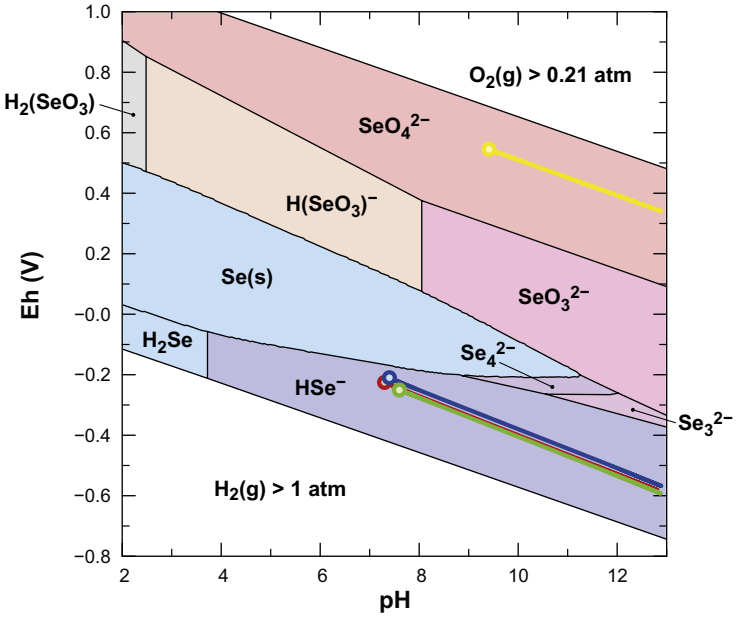

Figure 8-3. *Se predominance diagram calculated using the ThermoChimie database (version 10a) and with a total Selenium concentration of 10^{-9} M assuming a temperature of 15 °C. Trends in groundwater composition (Eh and pH) corresponding to the mixing trajectories in the previous Figure 8-1 are shown for a) Temperate saline (red), b) Early Periglacial (blue), c) Late Periglacial (green), and d) Glacial derived groundwater (yellow) where the marker on the far left indicates unaffected groundwater.*

The theoretical scaling factor relating the apparent K_d of MoO_4^{2-} and SeO_3^{2-} is shown in Figure 8-4 and varies between 1.6×10^{-2} at neutral pH which decreases asymptotically to 1.4×10^{-3} at higher pH levels characteristic of cement leachate affected groundwater.

Based on the interpreted experimental data summarised above and the theoretical scaling factor for Mo(VI) sorptive strength relative to Se(IV), the K_d values for Se and Mo in Table 8-6 are suggested for use in the PSAR. It should be noted that the K_d values estimated for Mo(VI) and Se(VI) sorption are sufficiently low that free aqueous storage in the matrix porosity will dominate the radionuclide retardation. The K_d values therefore may be assumed to be effectively zero in safety assessment.

Table 8-6. Suggested values for Mo(VI), Se(IV), and Se(VI) sorption for use in the PSAR based on modelling interpretation of the LTDE-SD main experiment and independent experiments on Forsmark (3 core samples) and Laxemar (6 core samples) site-specific rock. K_d values for Mo(VI) are extrapolated from the Se(IV) values using a theoretical scaling factor based on thermodynamic modelling of binding reactions on ferrol sites using the model of Dzombak and Morel (1990).

Solute	K_d, best estimate (m^3/kg)	K_d, Geom. Mean	K_d, Geom. Std. Dev.	K_d, Lower trunc.	K_d, Upper trunc.
Mo(VI)	0	5.17×10^{-7}	4.24	1.5×10^{-8}	1.45×10^{-5}
Se(IV)	3.45×10^{-4}	3.45×10^{-4}	4.24	1.0×10^{-5}	9.65×10^{-3}
Se(VI)	0	1.38×10^{-8}	4.24	4.0×10^{-10}	3.86×10^{-7}

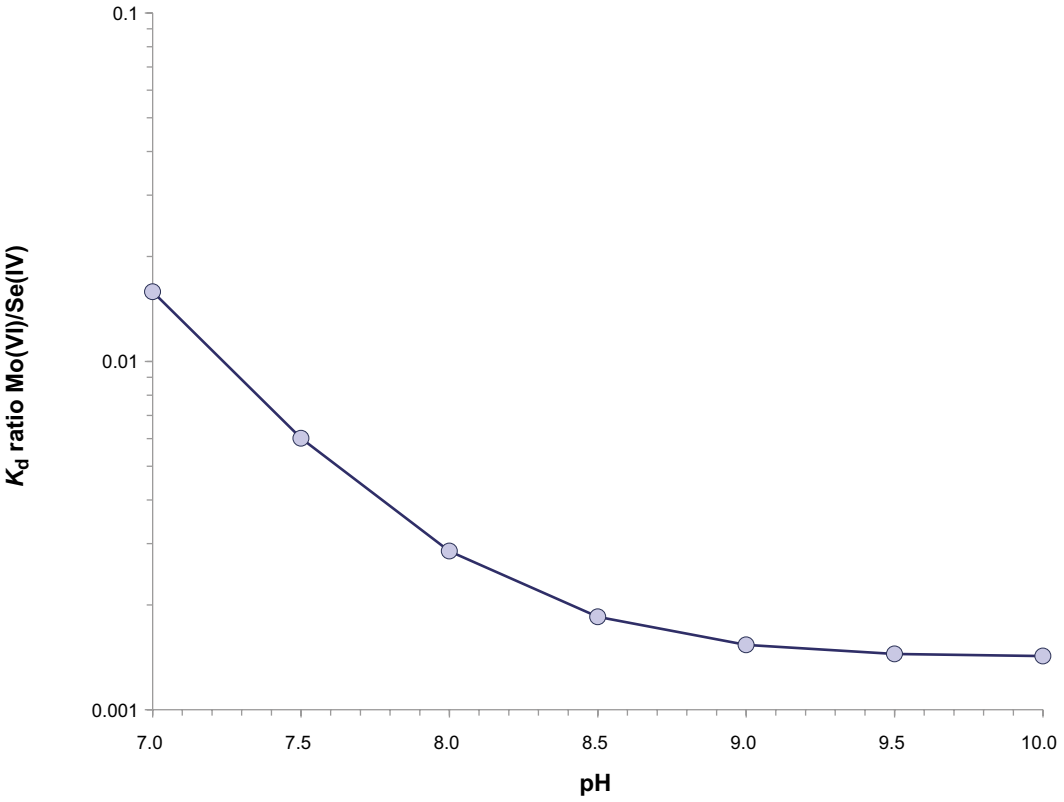

Figure 8-4. *Ratio of K_d values calculated for Mo(VI) and Se(IV) as a function of pH calculated using the diffuse layer model of Dzombak and Morel (1990) for inner sphere surface complexation on hydrous ferric oxide.*

Although the arithmetic mean of the lognormally distributed K_d values obtained in data fitting might be normally considered the best estimate for transport modelling, the uncertainty introduced by the small number of data points (Widestrand et al. 2010a, b) suggest that the median value is more appropriate. The lower truncated K_d limit for Se(IV) is based on the estimated apparent K_d value measured in the experiment under oxidising conditions (Eh = +500 mV but uncertain) or most probably a mixed redox state, while the upper truncated K_d limit for Se(IV) is based on the upper 95 % confidence interval of the t-distribution from the mean and standard deviation of the log-transformed estimated K_d values of the laboratory experimental data (9 core samples). The definitions of the data given in Table 8-6 are further specified in Crawford (2018).

The use of a non-zero K_d value for Se implicitly assumes that Se is predominantly speciated in the Se(IV) form or at least the groundwater is sufficiently reducing that sorption is approximately representative of the Se(IV) redox state. In transitional, or mildly reducing environments (such as that in Widestrand et al. 2010a), and if redox equilibrium amongst Se species can be reasonably assumed, then the K_d value for Se(IV) is deemed the best estimate for transport modelling purposes even if Se(VI) is slightly more dominant in the aqueous phase since Se(IV) will still be the dominant surface sorbed redox state. Under strongly reducing conditions, however, it is more likely that the Se(–II) state is dominant in which case zero K_d might be considered a more cautious assumption. While the central estimates of pH and Eh indicated for the reference waters given in Table 8-3 and Table 8-4 suggest Se(–II) speciation, the specified variability admits the possibility of Se(IV) redox speciation in the aqueous phase. In upper parts of the geosphere, redox conditions are also likely to be less reducing than in the immediate vicinity of the repository and Se(IV) speciation is possible. For this reason, probabilistic calculations of geosphere transport might consider the possibility of Se(IV) sorption even if sorption is conservatively assumed to be negligible due to Se(-II) redox speciation in deterministic calculations.

Table 8-6 should therefore be considered as a generic recommendation for unspecified groundwater compositions likely to be encountered under safety assessment conditions. Under glacial groundwater conditions the redox potential is sufficiently oxidising that the K_d for Se(VI) should probably be assumed in transport calculations.

In the absence of site-specific measurements of Mo(VI) sorption on SFR (ferrous iron binding sites) the uncertainty on the predominant speciation is likely to remain. As a sensitivity case it might be possible to use a K_d value for Mo(VI) that is the same as that specified for Se(IV) in Table 8-6. Although this cannot be considered a conservative assumption, it may give the range of variability if no further efforts to estimate transfer factors based on more detailed mechanistic reasoning is at hand.

Plutonium (Pu)

Plutonium is dominantly present in oxidation state Pu(III) for temperate saline groundwater up until around pH 8.75, after which Pu(IV) becomes more abundant in the aqueous phase. Calculations in Crawford (2013) suggest that Pu sorbs both in the Pu(III) and Pu(IV) form, although with a slight preference for Pu(III) throughout the range of feasible pH arising due to mixing of groundwater with cement leachate. Figure 8-5 shows the predominance of various aqueous phase species of Pu as a function of pH and Eh with Figure 8-5A showing aqueous species only and Figure 8-5B also including surface species. The groundwater compositional trends corresponding to the mixing of each of the reference groundwater types with cement leachate is overlaid in each diagram. As can be seen from Figure 8-5B, neither Pu(V) nor Pu(VI) are predicted to form surface complexes to any great extent for the prevailing groundwater conditions.

Although both Pu(III) and Pu(IV) sorb strongly, the K_d is predicted to decrease at higher pH relative to normal groundwater conditions due to competitive effects of hydrolysis, particularly involving the formation of aqueous $Pu(OH)_4$. As the magnitude of the predicted K_d decrease at high pH is highly uncertain, it was recommended that the K_d value corresponding to Pu(III) sorption should be used although decreased by a factor of 1 000 relative to non-leachate affected groundwater for pH levels above 10. Although this is a greater K_d reduction than what was modelled in Crawford (2013), it was considered cautious given that regions of the migration path not affected by cement leachate would dominate the transport retardation of Pu.

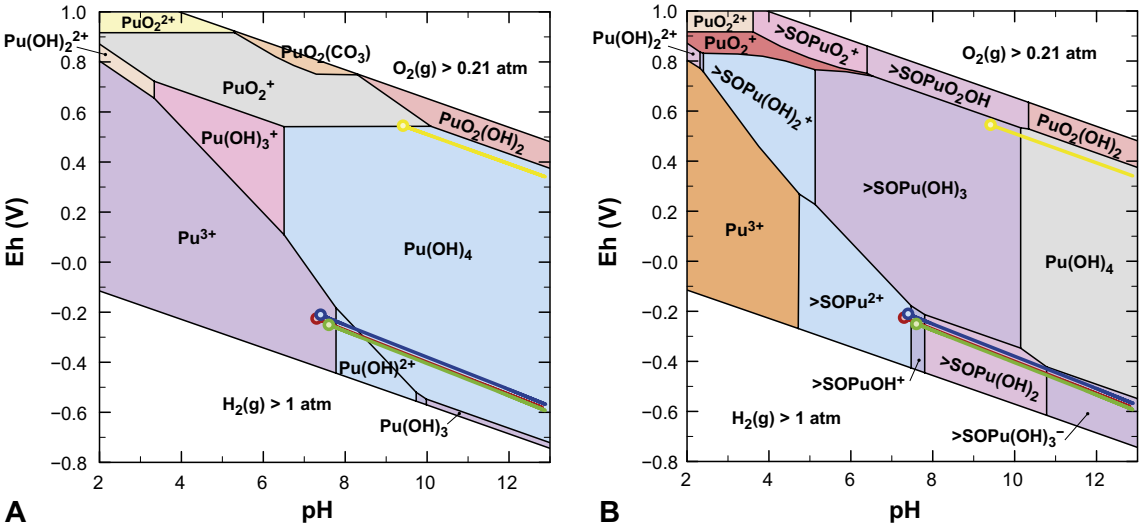

Figure 8-5. *Pu predominance diagram calculated using the ThermoChimie database (version 10a) and with a total Pu concentration of 10^{-10} M assuming a temperature of 15 °C. Panel A shows the aqueous and solid phase (pure mineral precipitates) composition only, while panel B additionally includes feasible surface species calculated using surface complexation modelling (Crawford 2013). Trends in groundwater composition (Eh and pH) corresponding to the mixing trajectories in the previous Figure 8-1 are shown for a) Temperate saline (red), b) Early Periglacial (blue), c) Late Periglacial (green), and d) Glacial derived groundwater (yellow) where the marker on the far left indicates unaffected groundwater.*

Uranium (U)

The uranium radionuclides of interest for SFR are all present in the SR-Site safety assessment for the KBS-3 repository. Therefore, much work has been done regarding the sorption of uranium in rock matrix, for a longer discussion see Crawford (2010, 2013). Owing to the redox sensitivity of U, however, there are still significant uncertainties associated with the recommendation of K_d values. Similarly to the situation described previously for Pu, it is possible for redox speciation of the aqueous and surface sorbed U to differ depending on the prevailing redox and pH conditions and competitive effects among different aqueous and surface sorbed species. Figure 8-6 shows the predominance of various aqueous phase species of U as a function of pH and Eh with Figure 8-6A showing aqueous species only and Figure 8-6B also including surface species. The groundwater compositional trends corresponding to the mixing of each of the reference groundwater types with cement leachate is overlaid in each diagram. For all the non-glacial groundwaters, for example, the redox speciation in the aqueous phase (and solubility determining phases) is predicted to trend from initially U(VI) towards U(IV) at increasing pH. For sorption, however, the redox speciation under normal groundwater conditions is predicted to be initially U(IV) dominated although trending towards U(VI) at high pH levels.

The possible presence of different redox species in aqueous and sorbed phases makes estimating K_d values harder since it might not always be clear which redox state should be assigned to the sorbed phase and whether available measurement data are consistent with the modelled redox status of sorbed species. For more oxidising conditions found in Glacial-derived groundwaters the estimation is more straightforward owing to U(VI) being dominant in both aqueous and sorbed phases.

Similarly to the behaviour shown previously for Pu, the K_d for U is predicted to decrease at higher pH relative to normal groundwater conditions mostly due to competitive effects of hydrolysis, driven by the formation of aqueous $U(OH)_4$. To avoid data inconsistency, the recommended K_d value for temperate saline and periglacial groundwaters not affected by the OPC-water is to use the value previously given for U(IV) in SR-Site. For oxidising conditions (i.e., glacial water) and for other groundwater types with pH above 10, the K_d value for U(VI) from SR-Site is recommended as this is the lowest value quantified in laboratory experiments and is deemed to be a reasonable proxy for the predicted low sorptivity of U at high pH. For the crushed rock backfill the SR-Site K_d value for U(VI) is recommended owing to the likelihood of high pH conditions.

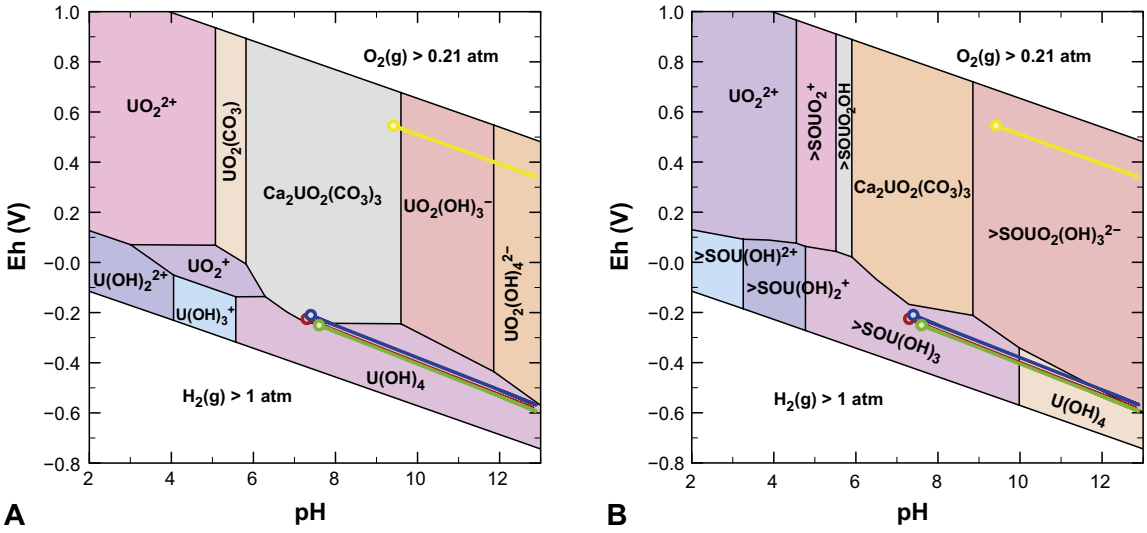

Figure 8-6. *U predominance diagram calculated using the ThermoChimie database (version 10a) and with a total U concentration of 10^{-10} M assuming a temperature of 15 °C. Panel A shows the aqueous and solid phase (pure mineral phases) composition only, while panel B additionally includes feasible surface species calculated using surface complexation modelling (Crawford 2013). Trends in groundwater composition (Eh and pH) corresponding to the mixing trajectories in the previous Figure 8-1 are shown for a) Temperate saline (red), b) Early Periglacial (blue), c) Late Periglacial (green), and d) Glacial derived groundwater (yellow) where the marker on the far left indicates unaffected groundwater.*

Complexing agents – evaluation and uncertainty of the effect on sorption

Organic ligands co-migrating from SFR have the potential to significantly reduce the sorptive retention of certain radionuclides in the geosphere. The approach used to quantify the reduction in sorption caused by radionuclide binding with organic ligands, is broadly the same as that discussed previously (see Chapter 7) and involves the calculation of sorption reduction factors (SRF's) used to modify recommended reference K_d sorption values (when no organic ligands are present). The sorption reduction factor is simply defined as the ratio of total radionuclide concentration and the sum of species that are not organic complexes of the radionuclide; while it is possible to make scoping calculations to identify which radionuclides are most strongly affected and calculate approximate sorption reduction factors, there is significant uncertainty surrounding both the predicted magnitude of K_d modification and the geosphere pH buffering and dilution scenarios used as a basis for such calculations.

The sorption reduction factor was calculated as a function of OPC mixing fraction using equations in Crawford (2017) independently for picomolar concentrations of radionuclide (10^{-12} M) and an excess of organic ligand ($10^{-6} – 10^{-2}$ M). The organic ligands considered were isosaccharinic acid (ISA), nitrilotriacetic acid (NTA), ethylenediaminetetraacetic acid (EDTA), gluconate, citrate, and oxalate. Although not all radioelement-ligand combinations could be assessed owing to a lack of thermodynamic data, enough combinations were studied that more general conclusions can be drawn for the safety assessment. The actual combinations tested are listed in Crawford (2017, Table 1).

8.7 Data uncertainty – spatial and temporal variability

Spatial and temporal variabilities become important when considering the different groundwaters with which the radionuclides come in contact. Groundwater chemical properties such as pH, redox and different naturally occurring ion concentrations are critical when assessing the sorption of the selected radionuclides.

The groundwater compositions, presented in Table 8-3 to Table 8-5, have been produced to account for all possible variations that might occur both in the spatial and in the temporal domain. The K_d values presented in this chapter are differentiated using the same compositions.

8.8 Data uncertainty – correlations

Except for the groundwater compositions from Auqué et al. (2013), presented in Tables 8-3 to 8-5, the presented rock matrix K_d values have not been correlated with any other data set produced within the safety assessment.

In Crawford (2013) a method is presented for the estimation of effective K_d values for crushed rock based on consideration of diffusive disequilibrium on the timescale of radionuclide transport. In the calculations presented in the **Radionuclide transport report** the crushed rock used as backfill is considered to be fully equilibrated owing to the long water residence time and K_d values for rock can therefore be used directly without modification.

In the SR-Site Data report (SKB TR-10-52) correlations, between K_d values for groups of radionuclides with common sorption behaviour, were suggested for the probabilistic selection of K_d values for use in the radionuclide transport calculations for the geosphere. In the SR-Site Radionuclide transport report (SKB TR-10-50, Section 4.5.5) it was concluded that using correlations or not has a negligible influence on the results.

8.9 Result of supplier's data qualification

The rock matrix K_d values for the different groundwater compositions are given in Table 8-7. To be noted is that K_d values less than 10^{-5} (m^3/kg) may be considered to be effectively zero owing to the dominance of dissolved storage in the matrix porosity in such cases. Updated K_d values for Mo and Se are given in Table 8-6.

Very low concentrations of organic ligands are expected in the geosphere, hence radionuclide complexation is not deemed to be significant, which is further shown and elaborated upon in Crawford (2017).

For macadam/crushed rock it is suggested to use K_d values for the rock matrix choosing speciation for high pH.

Table 8-7. Proposed rock matrix K_d values given the groundwater compositions in Tables 8-3 to 8-5. Separate values are given for high pH conditions where deemed feasible to do so. Reproduced from Crawford (2013, Table 6-1 H to Cm and Table 6-2 Ac to Po).

Radionuclide (Redox State)	GW Type	Best estimate K_d (m^3/kg)	μ [a)]	σ [a)]	Lower K_d (m^3/kg)	Upper K_d (m^3/kg)
H(I)	all	0.0	-	-	0.0	0.0
C, HCO_3^-	all	0.0	-	-	0.0	0.0
C, CH_4	all	0.0	-	-	0.0	0.0
C, $–CO_2H$	all	0.0	-	-	0.0	0.0
Cl(–I)	all	0.0	-	-	0.0	0.0
Ca(II)	all	0.0	-	-	0.0	0.0
Co(II)	all	7.4×10^{-4}	−3.13	0.79	2.1×10^{-5}	2.7×10^{-2}
Ni(II)	all	7.4×10^{-4}	−3.13	0.79	2.1×10^{-5}	2.7×10^{-2}
Se(–II)	all	0.0	-	-	0.0	0.0
Se(IV, VI)		See Table 8-6				
Sr(II)	T-Sal	1.5×10^{-5}	−4.83	0.6	9.7×10^{-7}	2.2×10^{-4}
	Per	2.0×10^{-4}	−3.69	0.6	1.3×10^{-5}	3.1×10^{-3}
	L-Per	3.5×10^{-4}	−3.46	0.6	2.3×10^{-5}	5.3×10^{-3}
	Glac	1.6×10^{-3}	−2.79	0.6	1.1×10^{-4}	2.5×10^{-2}
	all, pH > 10	1.5×10^{-5}	−4.83	0.6	9.7×10^{-7}	2.2×10^{-4}
Mo(VI)	all	See Table 8-6				
Nb(V)	all	2.0×10^{-2}	−1.70	0.64	1.1×10^{-3}	3.5×10^{-1}
Zr(IV)	all	2.1×10^{-2}	−1.67	0.35	4.5×10^{-3}	1.0×10^{-1}
Tc(IV)	non-Glac	5.3×10^{-2}	−1.28	0.65	2.8×10^{-3}	9.8×10^{-1}
Tc(VII)	Glac	0.0	-	-	0.0	0.0
Ag(I)	all	0.0	-	-	0.0	0.0
Cd(II)	all	7.4×10^{-4}	−3.13	0.79	2.1×10^{-5}	2.7×10^{-2}
Sn(IV)	all, pH < 10	1.6×10^{-1}	−0.80	0.28	4.5×10^{-2}	5.6×10^{-1}
	all, pH > 10	1.6×10^{-4}	−3.80	0.28	4.5×10^{-5}	5.6×10^{-4}
I(–I)	All	0.0	-	-	0.0	0.0
Ba(II)	T-Sal	1.0×10^{-3}	−3.00	0.46	1.3×10^{-4}	8.0×10^{-3}
	Per	1.4×10^{-2}	−1.86	0.46	1.7×10^{-3}	1.1×10^{-1}
	L-Per	2.4×10^{-2}	−1.62	0.46	3.0×10^{-3}	1.9×10^{-1}
	Glac	1.1×10^{-1}	−0.96	0.46	1.4×10^{-2}	8.9×10^{-1}
	all, pH > 10	1.0×10^{-3}	−3.00	0.46	1.3×10^{-4}	8.0×10^{-3}
Cs(I)	T-Sal	8.8×10^{-4}	−3.05	0.58	6.6×10^{-5}	1.2×10^{-2}
	Per	3.0×10^{-3}	−2.52	0.58	2.2×10^{-4}	4.0×10^{-2}
	L-Per	3.8×10^{-3}	−2.42	0.58	2.8×10^{-4}	5.1×10^{-2}
	Glac	7.7×10^{-3}	−2.12	0.58	5.7×10^{-4}	1.0×10^{-1}
	all, pH > 10	8.8×10^{-4}	−3.05	0.58	6.6×10^{-5}	1.2×10^{-2}
Sm(III)	all	1.5×10^{-2}	−1.83	0.72	5.7×10^{-4}	3.8×10^{-1}
Eu(III)	all	1.5×10^{-2}	−1.83	0.72	5.7×10^{-4}	3.8×10^{-1}
Ho(III)	all	1.5×10^{-2}	−1.83	0.72	5.7×10^{-4}	3.8×10^{-1}
U(IV)	non-Glac, pH < 10	5.3×10^{-2}	−1.28	0.65	2.8×10^{-3}	9.8×10^{-1}
	non-Glac, pH > 10	1.1×10^{-4}	−3.97	0.66	5.5×10^{-6}	2.1×10^{-3}
U(VI)	Glac	1.1×10^{-4}	−3.97	0.66	5.5×10^{-6}	2.1×10^{-3}
Np(IV)	non-Glac, pH < 10	5.3×10^{-2}	−1.28	0.65	2.8×10^{-3}	9.8×10^{-1}
	non-Glac, pH > 10	4.1×10^{-4}	−3.38	0.74	1.5×10^{-5}	1.2×10^{-2}
Np(V)	Glac	4.1×10^{-4}	−3.38	0.74	1.5×10^{-5}	1.2×10^{-2}
Pu(III/IV)	all, pH < 10	1.5×10^{-2}	−1.83	0.72	5.7×10^{-4}	3.8×10^{-1}

Table 8-7. Continued.

Radionuclide (Redox State)	GW Type	Best estimate K_d (m^3/kg)	μ [a)]	σ [a)]	Lower K_d (m^3/kg)	Upper K_d (m^3/kg)
	all, pH > 10	1.5×10^{-5}	−4.83	0.72	5.7×10^{-7}	3.8×10^{-4}
Am(III)	all	1.5×10^{-2}	−1.83	0.72	5.7×10^{-4}	3.8×10^{-1}
Cm(III)	all	1.5×10^{-2}	−1.83	0.72	5.7×10^{-4}	3.8×10^{-1}
Ac(III)	all	1.5×10^{-2}	−1.83	0.72	5.7×10^{-4}	3.8×10^{-1}
Pa(V)	all	5.9×10^{-2}	−1.23	0.48	6.8×10^{-3}	5.1×10^{-1}
Th(IV)	all	5.3×10^{-2}	−1.28	0.65	2.8×10^{-3}	9.8×10^{-1}
Ra(II)	T-Sal	1.0×10^{-3}	−3.00	0.46	1.3×10^{-4}	8.0×10^{-3}
	Per	1.4×10^{-2}	−1.86	0.46	1.7×10^{-3}	1.1×10^{-1}
	L-Per	2.4×10^{-2}	−1.62	0.46	3.0×10^{-3}	1.9×10^{-1}
	Glac	1.1×10^{-1}	−0.96	0.46	1.4×10^{-2}	8.9×10^{-1}
	all, pH > 10	1.0×10^{-3}	−3.00	0.46	1.3×10^{-4}	8.0×10^{-3}
Pb(II)	all	2.5×10^{-2}	−1.60	0.56	2.0×10^{-3}	3.1×10^{-1}
Po(IV)/PoO_3^{2-}	all	~ 1.0×10^{-3}	-	-	3.0×10^{-4}	1.0×10^{-2}
	all, pH > 10	0	-	-	0	0
Po(–II, II, VI)	all	0	-	-	0	0

a) μ and σ represent the mean and standard deviation of the logarithmised ($\log_{10} K_d$) uncertainty distribution.

8.10 Judgements by the assessment team

Sources of information

The assessment team considers the sources of information used by the supplier as sufficient.

Conditions for which data is supplied

The assessment team agrees with the conditions stated by the supplier and find these relevant within the safety assessment.

Conceptual modelling and bias uncertainties

The assessment team considers the information given in Section 8.6 to be sufficient as a background for the data qualification.

Data uncertainty – spatial and temporal variability

The assessment team agrees with the handling of variabilities by the supplier and considers them sufficient with respect to the described groundwater evolution around the repository (Auqué et al. 2013).

The actual dilution and pH buffering along individual migration paths was not studied so it is not possible to say with any high degree of confidence how the flowpath average K_d should vary along flowpaths leading to the biosphere. Given the relatively (hydraulically) transmissive nature of the bedrock surrounding SFR, however, and the presence of crushed rock backfill which functions as a hydraulic cage, we would expect dilution of OPC leachate to occur very close to the repository and the bulk of the geosphere should be relatively unaffected by high pH conditions.

Data uncertainty – correlations

The assessment team agrees with the given correlations. The crushed rock K_d used in the backfill is considered to be fully equilibrated with the surrounding groundwater, owing to the assumed relatively long water residence time, so that equivalent K_d values for rock can therefore be used directly without modification.

Results of supplier's data qualification

The assessment team considers the data supplied in this chapter to be sufficient for usage in the safety assessment. The assessment team agrees with the K_d recommendations given by the supplier for all radionuclides except polonium. The reasoning the supplier has given regarding the polonium is deemed valid for the all the groundwater types presented in Tables 8-3 to 8-5, but as the supplier writes the uncertainties associated with the glacial groundwater polonium K_d value are large. This groundwater type is the one reflecting the uppermost part of the geosphere, i.e. closest to the surface where mixing with other more oxygen-rich waters affects the redox conditions. Due to the half-life of ^{210}Po and its parent radionuclides, the uncertain Po(IV) K_d value might have a concentrating effect on polonium in the upper parts of the geosphere which in turn can lead to dose consequences in well scenarios. Instead, the assessment team chooses to consider polonium in secular equilibrium with its parent ^{210}Pb, given as a suggestion in Section 8.6. The well data given in the SR-PSU Data report (SKB TR-14-10, Figure 8-2) gives support to this approach as a conservative one.

8.11 Data recommended for use in the assessment

Rock matrix

The K_d values that are recommended to be used in the safety assessment is given in Table 8-8 for the rock matrix. For the impact of temporally variable groundwater compositions, K_d values are recommended to be chosen pessimistically to reflect the least favourable conditions for transport retardation (example see Table 8-8, T-Sal representing the most saline condition). The K_d data are given in the form of log-normal distributions characterised by a mean (μ) and standard deviation (σ). For stochastic simulations, it is suggested that the distributions are sampled uniformly between the upper and lower limits defined by the 2.5 % and 97.5 % percentiles. The best estimate K_d value for use in deterministic calculations is given as the geometric mean of the K_d distribution, except for Mo and Se where the K_d values are recommended to be zero.

For the average non-glacial groundwater compositions specified in Table 8-3 and Table 8-4, Se should be predominantly speciated in the non-sorbing Se(-II) form, although based on the possible Eh ranges, it is feasible for reducing conditions to be sufficiently mild in the upper reaches of the geosphere to permit Se(IV) speciation. For this reason, the K_d range corresponding to Se(IV) is considered in stochastic calculations with a lower limit K_d value of 10^{-5} m^3/kg. The lower limit of this range gives a transport residence time distribution and decay attenuation in the geosphere that is, for all practical purposes, indistinguishable from a K_d of zero.

As stated, in Section 8.6, polonium is not calculated separately in the radionuclide transport calculations. Instead, the dose from polonium is recommended to be calculated assuming isotopic equilibrium with ^{210}Pb. Hence, no K_d value for Po is recommended by the assessment team.

As stated, in Section 8.6, the effect of complexing agents is not deemed to be significant and hence no reduction of the K_d values is recommended in the main scenario. One of the residual scenarios, however, represents a worst-case scenario for impact of organic complexation on radionuclide migration as it assumes zero sorption in the geosphere for all safety assessment relevant radionuclides even though this is likely to be highly overpessimistic.

Crushed rock backfill

The K_d values for macadam/crushed rock are recommended to be taken from the rock matrix table (Table 8-8), choosing speciation from the assumption of a high pH for the duration of the safety assessment in the main scenario.

Palladium (Pd) was not included in the requested data set, due to its low total activity in SFR. On cement, Pd(II) is assigned K_d value based on analogy with Pb(II) (Chapter 7). This analogy could in principle be made also for sorption on crushed rock, but for this safety assessment no data is supplied for Pd, and thus a pessimistic $K_d = 0$ m^3/kg is recommended.

Table 8-8. Rock matrix K_d values recommended by the assessment team. K_d values for macadam/ crushed rock are recommended to be the values for high pH.

Radionuclide (Redox State)	GW Type (see Tables 8-3 to 8-5)	Best estimate K_d (m^3/kg)	μ	σ	Lower K_d (m^3/kg)	Upper K_d (m^3/kg)
Ac(III)	all	1.5×10^{-2}	−1.83	0.72	5.7×10^{-4}	3.8×10^{-1}
Ag(I)	all	0.0	-	-	0.0	0.0
Am(III)	all	1.5×10^{-2}	−1.83	0.72	5.7×10^{-4}	3.8×10^{-1}
Ba(II)	T-Sal	1.0×10^{-3}	−3.00	0.46	1.3×10^{-4}	8.0×10^{-3}
	Per	1.4×10^{-2}	−1.86	0.46	1.7×10^{-3}	1.1×10^{-1}
	L-Per	2.4×10^{-2}	−1.62	0.46	3.0×10^{-3}	1.9×10^{-1}
	Glac	1.1×10^{-1}	−0.96	0.46	1.4×10^{-2}	8.9×10^{-1}
	all, pH > 10	1.0×10^{-3}	−3.00	0.46	1.3×10^{-4}	8.0×10^{-3}
C, HCO_3^-	all	0.0	-	-	0.0	0.0
C, CH_4	all	0.0	-	-	0.0	0.0
C, $-CO_2H$	all	0.0	-	-	0.0	0.0
Ca(II)	all	0.0	-	-	0.0	0.0
Cd(II)	all	7.4×10^{-4}	−3.13	0.79	2.1×10^{-5}	2.7×10^{-2}
Cl(−I)	all	0.0	-	-	0.0	0.0
Cm(III)	all	1.5×10^{-2}	−1.83	0.72	5.7×10^{-4}	3.8×10^{-1}
Co(II)	all	7.4×10^{-4}	−3.13	0.79	2.1×10^{-5}	2.7×10^{-2}
Cs(I)	T-Sal	8.8×10^{-4}	−3.05	0.58	6.6×10^{-5}	1.2×10^{-2}
	Per	3.0×10^{-3}	−2.52	0.58	2.2×10^{-4}	4.0×10^{-2}
	L-Per	3.8×10^{-3}	−2.42	0.58	2.8×10^{-4}	5.1×10^{-2}
	Glac	7.7×10^{-3}	−2.12	0.58	5.7×10^{-4}	1.0×10^{-1}
	all, pH > 10	8.8×10^{-4}	−3.05	0.58	6.6×10^{-5}	1.2×10^{-2}
Eu(III)	all	1.5×10^{-2}	−1.83	0.72	5.7×10^{-4}	3.8×10^{-1}
H(I)	all	0.0	-	-	0.0	0.0
Ho(III)	all	1.5×10^{-2}	−1.83	0.72	5.7×10^{-4}	3.8×10^{-1}
I(−I)	all	0.0	-	-	0.0	0.0
Mo(VI)	all	0.0	−6.29	4.24	1.5×10^{-8}	1.45×10^{-5}
Nb(V)	all	2.0×10^{-2}	−1.70	0.64	1.1×10^{-3}	3.5×10^{-1}
Ni(II)	all	7.4×10^{-4}	−3.13	0.79	2.1×10^{-5}	2.7×10^{-2}
Np(IV)	non-Glac, pH < 10	5.3×10^{-2}	−1.28	0.65	2.8×10^{-3}	9.8×10^{-1}
	non-Glac, pH > 10	4.1×10^{-4}	−3.38	0.74	1.5×10^{-5}	1.2×10^{-2}
Np(V)	Glac	4.1×10^{-4}	−3.38	0.74	1.5×10^{-5}	1.2×10^{-2}
Pa(V)	all	5.9×10^{-2}	−1.23	0.48	6.8×10^{-3}	5.1×10^{-1}
Ra(II)	T-Sal	1.0×10^{-3}	−3.00	0.46	1.3×10^{-4}	8.0×10^{-3}
	Per	1.4×10^{-2}	−1.86	0.46	1.7×10^{-3}	1.1×10^{-1}
	L-Per	2.4×10^{-2}	−1.62	0.46	3.0×10^{-3}	1.9×10^{-1}
	Glac	1.1×10^{-1}	−0.96	0.46	1.4×10^{-2}	8.9×10^{-1}
	all, pH > 10	1.0×10^{-3}	−3.00	0.46	1.3×10^{-4}	8.0×10^{-3}
Se(−II)	all, pH > 10	0.0	-	-	0.0	0.0
Se(IV)	non-Glac	3.5×10^{-4}	−3.46	4.24	1.0×10^{-5}	9.65×10^{-3}
Se(VI)	Glac	0.0	−7.86	4.24	4.0×10^{-10}	3.86×10^{-7}
Sm(III)	all	1.5×10^{-2}	−1.83	0.72	5.7×10^{-4}	3.8×10^{-1}
Sn(IV)	all, pH < 10	1.6×10^{-1}	−0.80	0.28	4.5×10^{-2}	5.6×10^{-1}
	all, pH > 10	1.6×10^{-4}	−3.80	0.28	4.5×10^{-5}	5.6×10^{-4}
Sr(II)	T-Sal	1.5×10^{-5}	−4.83	0.6	9.7×10^{-7}	2.2×10^{-4}
	Per	2.0×10^{-4}	−3.69	0.6	1.3×10^{-5}	3.1×10^{-3}
	L-Per	3.5×10^{-4}	−3.46	0.6	2.3×10^{-5}	5.3×10^{-3}
	Glac	1.6×10^{-3}	−2.79	0.6	1.1×10^{-4}	2.5×10^{-2}
	all, pH > 10	1.5×10^{-5}	−4.83	0.6	9.7×10^{-7}	2.2×10^{-4}
Tc(IV)	non-Glac	5.3×10^{-2}	−1.28	0.65	2.8×10^{-3}	9.8×10^{-1}
Tc(VII)	Glac	0.0	-	-	0.0	0.0
Th(IV)	all	5.3×10^{-2}	−1.28	0.65	2.8×10^{-3}	9.8×10^{-1}
U(IV)	non-Glac, pH < 10	5.3×10^{-2}	−1.28	0.65	2.8×10^{-3}	9.8×10^{-1}
	non-Glac, pH > 10	1.1×10^{-4}	−3.97	0.66	5.5×10^{-6}	2.1×10^{-3}
U(VI)	Glac	1.1×10^{-4}	−3.97	0.66	5.5×10^{-6}	2.1×10^{-3}
Pb(II)	all	2.5×10^{-2}	−1.60	0.56	2.0×10^{-3}	3.1×10^{-1}
Pu(III/IV)	all, pH < 10	1.5×10^{-2}	−1.83	0.72	5.7×10^{-4}	3.8×10^{-1}
	all, pH > 10	1.5×10^{-5}	−4.83	0.72	5.7×10^{-7}	3.8×10^{-4}
Zr(IV)	all	2.1×10^{-2}	−1.67	0.35	4.5×10^{-3}	1.0×10^{-1}

9 Cementitious components and Crushed rock hydraulic conductivity data

This chapter concerns the hydraulic conductivity and physical porosity of the cementitious components in SFR as well as the hydraulic conductivity of the crushed rock used as foundation and for backfilling of some of the waste vaults.

Cementitious components

The cementitious components in SFR comprise the concrete structures in the different waste vaults, i.e. the slabs, lids and outer and inner walls of the silo, 1–2BMA and 1BRT, the slabs and lids in 1–2BTF and the slabs in 1–5BLA. They also comprise the shotcrete and grout surrounding the rock bolts in the rock walls in all waste vaults, the grout surrounding the waste packages in the silo and 1–2BTF, and the self-compacting concrete that will fill the void between the concrete tanks and the vault walls in 1–2BTF and between the waste packages in 1BRT. The *hydraulic conductivity in concrete* in the outer concrete structures in 1–2BMA is defined as one of the safety function indicators for the safety function *limit advective transport*.

Concrete moulds are used as waste packaging in the silo, 1–2BMA and 1BTF and concrete tanks are used in 1–2BTF. Cementitious materials are used both for solidification of ion-exchange resins and sludge, and for stabilisation of trash and scrap metal within many of the different waste packages present in the repository (**Initial state report**).

The *hydraulic conductivity in concrete* in the concrete tanks in 1–2BTF is defined as one of the safety function indicators for the safety function *limit advective transport*.

Mix proportions of cementitious materials in SFR

The mix proportions of some of the cementitious materials used or planned for use in SFR is given in Table 7-1. However, the mix proportions for e.g. the cementitious backfill for 1–2BTF or self-compacting concrete for 1BRT remains to be developed which adds some uncertainties to the description of the initial state and temporal evolution of the materials and structures during the post-closure period.

Crushed rock backfill

Crushed rock and/or macadam (crushed rock with no or very little fine material) is used as a foundation for the concrete structures in all waste vaults except for the silo. At repository closure all waste vaults, except the for 1–5BLA and the silo, are planned to be backfilled with macadam. The *hydraulic conductivity in backfill* (including the base of crushed rock) in 1–2BMA and 1–2BTF is defined as one of the safety function indicators for the safety function *limit advective transport*.

9.1 Modelling in this safety assessment

Defining the data requested from the supplier

The supplier should deliver the following data for the specified cementitious components in SFR defined in the second bullet-list below:

- The physical porosity n (–) of the cementitious components in SFR in their initial state, i.e. materials and structures that meet the design requirements of SFR, and in subsequent states as the materials and structures gradually degrade.
- The hydraulic conductivity K (m/s) of the cementitious components in SFR in their initial state, i.e. materials and structures that meet the design requirements of SFR, and in subsequent states as the materials and structures gradually degrade.
- The hydraulic conductivity K (m/s) of crushed rock.

Data should be provided for the following cementitious components:

- **Silo**: Outer and inner walls, slab lid, concrete moulds, grout.
- **1BMA**: Existing outer walls, new outer walls, slab, lid, concrete moulds.
- **2BMA**: External concrete structure, inner walls, concrete moulds, grout in gas evacuation channels.
- **1–2BTF**: Slab, lid, concrete tanks, concrete moulds, grout, cementitious backfill.
- **1BRT**: Outer walls, slab, lid, inner walls, concrete between waste packages.
- **1–5BLA**: Slab.

Modelling activities in which data will be used

The modelling chain and general methodology used to calculate the radionuclide transport is described in the **Radionuclide transport report**. The physical porosity delivered in this section is input data to the radionuclide transport calculations, where the diffusion available porosity is assessed. The radionuclide transport calculations use the diffusion available porosity. Here it is assumed that the whole physical porosity is available for diffusion and hence the diffusion available porosity is equal to the physical porosity. In the radionuclide transport modelling, the porosity is also used to estimate the porewater volume and the cement fraction within the cementitious components.

The hydraulic conductivity of the cementitious materials is used as input to both regional hydrogeological and near-field hydrological calculations.

Since the regional-scale groundwater flow model covers a large volume of the bedrock, the repository is not modelled in detail. However, the concrete structures and surrounding crushed rock are coarsely represented. The regional hydrogeological calculations for the bedrock are performed for some defined times to cover the influence of changes in hydraulic gradient due to changes in the relative sea level. This modelling is further described in Chapter 11 and in Öhman and Odén (2018).

The near-field hydrological calculations are performed for four physical degradation states of the concrete structures. These states comprise intact, moderately degraded, severely degraded and completely degraded concrete. The initial state of the concrete and a completely degraded state are set as limits for these degradation states.

Based on the degradation states it is possible to set up scenarios that prescribe at which time steps the changes between the degradation states occur. Even though the timing of the expected transition between degradation states is not explicitly required from the supplier, the supplied data must be sufficient to define the timepoints of the transition between states. The near-field groundwater flow rates, for each degradation state, are then used as input to the radionuclide transport calculations at the time steps defined by the scenario. This modelling is further described in Abarca et al. (2020) and in the **Radionuclide transport report**. Concrete degradation and groundwater flow are coupled processes and the calculated groundwater flow rates could be feedback as input to the models that estimate the concrete degradation rate. Such coupled modelling has not been performed. However, in Höglund (2014) the groundwater flow through the concrete structures in 1–2BMA has been estimated using a simpler approach and the concrete degradation rate was found to be consistent with the groundwater flow rates.

9.2 Experience from previous safety assessments

This section briefly summarises experiences from the previous safety assessments, SAFE, SAR-08 and SR-PSU, which may be of importance for the data qualification in this data report.

Modelling in previous safety assessments

The regional hydrogeological calculations for SAR-08 were mainly the same as for project SAFE (Holmén and Stigsson 2001a, b). Complementary uncertainty calculations were performed by Holmén (2005, 2007). The finite difference method used and the code, GEOAN, are briefly presented by Holmén (1997).

The regional hydrogeological calculations for the bedrock performed in SR-PSU (Odén et al. 2014) are used as basis for the PSAR (Öhman and Odén 2018), see also Chapter 11.

Detailed near-field hydrological calculations were performed in SR-PSU (Abarca et al. 2013, 2014). These calculations form the basis for the calculations in the PSAR (Abarca et al. 2020).

Conditions for which data were used in previous safety assessments

In SAFE and SAR-08, the degradation of some of the concrete barriers was handled by using a sudden increase in hydraulic conductivity at set points in time during the post-closure period.

In SAFE, a general assumption for the Base Scenario was that the state of barriers at repository closure is in accordance with design criteria (SKB R-01-14). In SAFE and SAR-08, the structural concrete was given an initial conductivity of 8.3×10^{-10} m/s, based on the assumption that the concrete may have initial cracks. It was assumed that intact concrete has a hydraulic conductivity of 1×10^{-11} m/s and that the structures have one fully penetrating crack per metre, each with an aperture of 1×10^{-5} m.

The cementitious grouts in the silo and 1–2BTF, which have a higher porosity due to the higher w/c ratio, were assigned the same initial hydraulic conductivity of 8.3×10^{-9} m/s even though the mix proportions and w/c ratio of these two materials differ somewhat. After degradation, all the concrete barriers were given a conductivity of 1×10^{-8} m/s except for the failed barrier sections in 1–2BMA and 1–2BTF for which a hydraulic conductivity of 1×10^{-5} m/s was assigned.

In SR-PSU four degradation states, intact, moderately degraded, severely degraded and completely degraded concrete were defined to represent the time dependence of hydraulic properties of the concrete structures. Furthermore, a set of timepoints for the transitions of the concrete structures between these degradation states was defined. The conditions for which data were used in SR-PSU are described in detail in the SR-PSU Data report (SKB TR-14-10).

Sensitivity to assessment results in previous safety assessments

In SAFE and SAR-08, the sudden and large increases in the hydraulic conductivities assumed in the modelling activities resulted in sudden increases in the water flow. It was predicted by Holmén and Stigsson (2001a) and by Holmén (2005, 2007) that failed barriers in sections of the vaults would lead to a two to three times higher flow in 1BLA and 1BMA, and a somewhat smaller increase of flow in 1–2BTF caused by a changed flow direction in the vaults.

Also in SR-PSU, the sudden and large increases in the hydraulic conductivities assumed in the modelling activities resulted in sudden increases in the water flow (Abarca et al. 2013, 2014). The release of radionuclides depended on the timing of the transitions between different degradation states. The sensitivity to the timing of the transitions was investigated in the accelerated concrete degradation scenario (SKB TR-14-09).

Alternative modelling in previous safety assessments

No alternative modelling was reported in SAFE, SAR-08 or SR-PSU.

Correlations used in previous safety assessment modelling

Since the porosities and hydraulic conductivities were not treated probabilistically no correlations between hydraulic conductivity, porosity or any other data in the assessment modelling were considered, see also the following heading.

Identified limitations of the data used in previous safety assessment modelling

In the SR-PSU no specific hydraulic data were recommended for the concrete structure in 1BRT. Furthermore, in SR-PSU, the porosities and conductivities of the different cementitious components were not treated probabilistically i.e. no probability density functions were defined.

9.3 Supplier input on use of data in this and previous safety assessments

9.3.1 Overview

Influence of w/c ratio

The hydraulic conductivity of the cementitious components is affected by the porosity of the material as well as by the presence of penetrating cracks, joints or other permeable zones.

In general, the initial porosity of cementitious materials is mainly controlled by the w/c ratio whereas cracks can form during construction, operation as well as during the post-closure period through several different processes as indicated by a few examples in the bullet lists below. A more extensive list of processes that could cause cracking of the cementitious components is found in Höglund (2014, Section 4.2) or the **Barrier process report**.

The porosity for different types of fully hydrated standard concrete is shown in Table 9-1. Note that the values in Table 9-1 represents examples of standard concrete and that the porosity in the cement paste which constitutes only a portion of the concrete is considerably higher. This means that the total porosity of cementitious materials will be dependent on the amount of cement used in the mix proportions and that the total porosity therefore can differ for cementitious materials with the same nominal w/c ratio.

Table 9-1. Porosity for different types of standard concrete at full hydration.

Water:cement ratio	Porosity*	28 days Compressive strength** (MPa)
0.85	0.155	29
0.75	0.154	32
0.65	0.147	39
0.55	0.140	48
0.45	0.127	58
0.35	0.117	70

* The porosity has been obtained from Svensk byggtjänst (2017, Table 10.5:1).

** The compressive strength has been obtained from Svensk byggtjänst (2017, Figure 12.4:1).

The impact of material porosity on the hydraulic conductivity of concrete has been studied by Höglund (2014) and is shown in Figure 9-1 for two different calculation models.

From Figure 9-1, the impact of porosity on conductivity for the range of porosities in Table 9-1 is not considerable although the results from the two models differ. However, for degraded concrete with a porosity of up to 0.25, the modified Kozeny-Carman model indicates a considerable increase of the hydraulic conductivity whereas the impact is smaller for the Kozeny-Carman model. It should be noticed though that the calculated hydraulic conductivities presented in Figure 9-1 are considerably higher than those reported by e.g. Mårtensson and Vogt (2020) which are in the range of 10^{-12} m/s for concrete with a porosity of about 12 %.

The mix proportions of the different types of concrete in SFR (Table 7-1) will give a low porosity with a low degree of pore connectivity. At full hydration of the cement minerals, the major part of the porosity will be gel pores and contraction pores. Neither of these would be expected to contribute significantly to the conduction of water during the early post-closure period. The capillary porosity will be low, and the capillary pores are mainly responsible for the conduction of water in the cement phase. Therefore, it would be reasonable to expect that the hydraulic conductivity of a fresh, fully hydrated concrete, produced according to the mix proportions presented in Table 7-1, could be as low as 1×10^{-12} m/s.

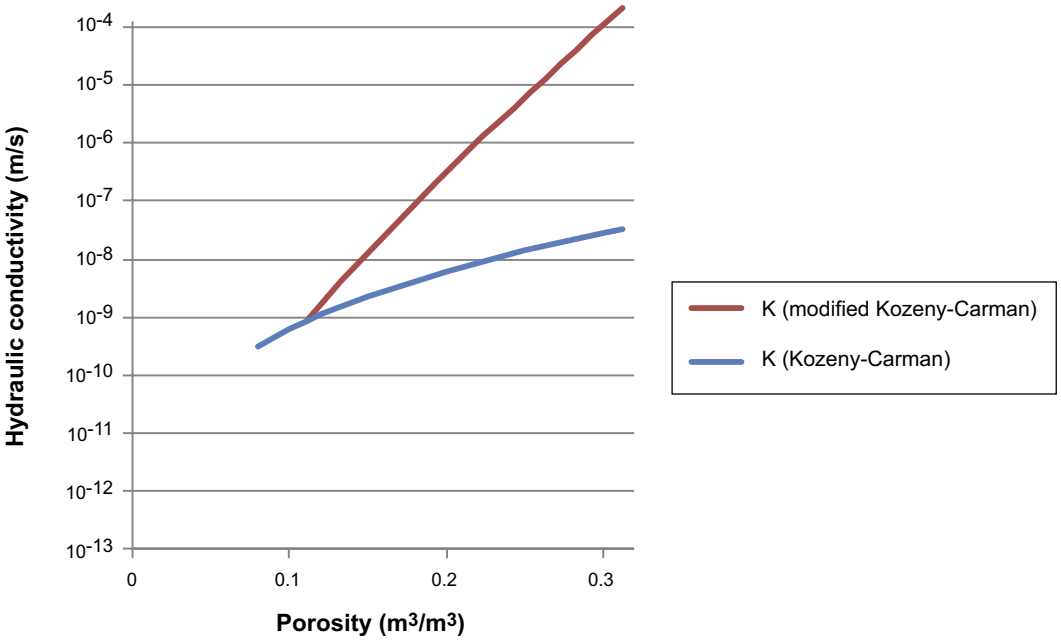

Figure 9-1. *The impact of porosity on the hydraulic conductivity of concrete calculated using two different calculation models (Höglund 2014).*

Influence of cracks

In general cracks can form during construction, operation as well as during the post-closure period through several different processes as indicated by a few examples in the bullet list below. A more extensive list of processes that could cause cracking of the concrete structures is found in Höglund (2014, Section 4.2). The mechanisms leading to the formation of cracks in concrete are also discussed in US DOE (2009) and Cronstrand et al. (2011) as well as in the **Barrier process report**.

- Construction
  - Temperature shrinkage during cooling of the warm concrete
  - Accidents
- Operation
  - Drying shrinkage
  - Accidents
  - Metal corrosion
- Post-closure
  - Gas formation
  - Swelling of waste
  - Metal corrosion
  - Freezing
  - Cooling shrinkage during resaturation
  - Dissolution, precipitation and recrystallisation of the cement minerals
  - Rock fall-out

The presence of fully penetrating cracks enhances advective flow through the concrete barriers and will also mean that the flow will be preferential, hence concentrated to a few locations of the cross-sectional area. Preferential flow also means an increased risk that chemical leaching will be preferential, thus over time further increasing the local damage to the concrete barriers.

Quantitative estimates of the importance of cracks for the barrier integrity have been made and are presented in Höglund (2014). The processes are however complex, and the results and interpretation are subject to uncertainty.

As illustrated in Figure 9-2 the influence of penetrating cracks on the hydraulic conductivity of concrete is significant. Calculations presented by Höglund and Bengtsson (1991), Höglund (2014), Cronstrand et al. (2011) and US DOE (2009) have demonstrated that water flow in cracks will become the dominant hydraulic pathway when one crack of 1–2 µm aperture width occurs every metre in the concrete. It should though be recognised that such narrow cracks are unlikely to be fully penetrating in a thick concrete structure and the statement above should rather be considered as a hypothetical calculation case.

From Figure 9-2, the impact of increasing crack aperture is considerably more severe than that of decreased distance between cracks. For that reason, in concrete structures, steel reinforcement bars are used to minimise the width and penetration of cracks caused by e.g. mechanical loads and dimensional changes caused by temperature and humidity variations.

An important consequence of concrete cracks is an increased flow of groundwater through the barriers (and the waste) after closure and, as a result, a more rapid chemical degradation of the concrete barriers in the vicinity of the cracks. In turn, as the barriers degrade they will allow an increasing amount of groundwater to flow through the barriers and the waste.

Since cracking causes sudden changes of the hydraulic conductivity, the assumption of sudden changes of the hydraulic conductivity of the concrete barriers may be justified for the safety assessment. The impact of the results has been considered in the radionuclide transport calculations (**Radionuclide transport report**).

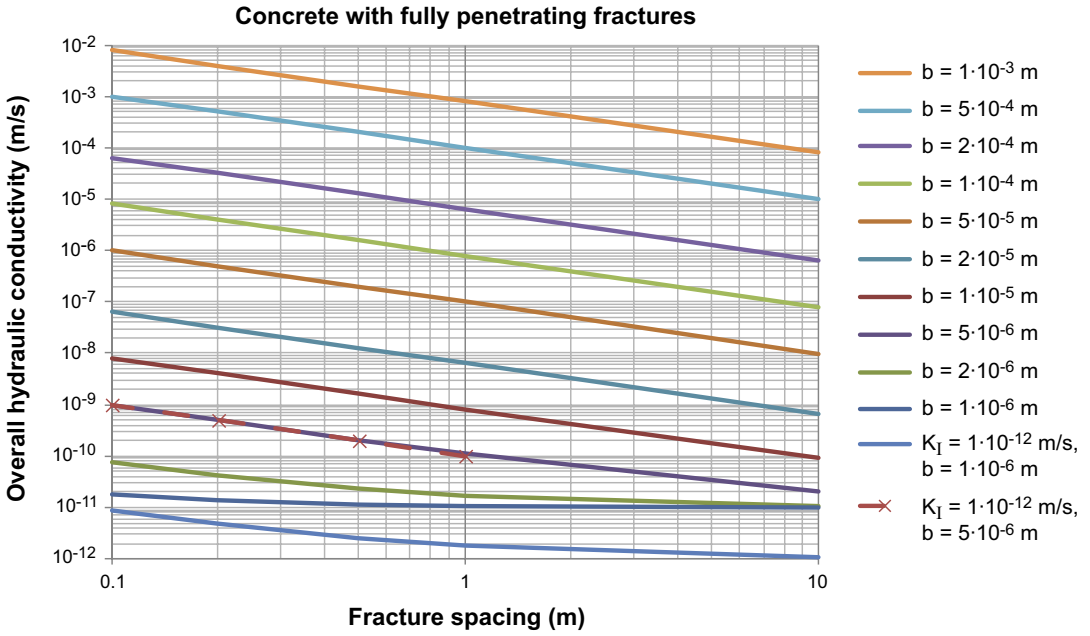

Figure 9-2. *The influence of distance between cracks and crack aperture, b, on the hydraulic conductivity of a concrete structure with an original hydraulic conductivity of* 1×10^{-12} *m/s (Höglund 2014).*

9.3.2 Updates since the previous the previous safety assessment

The updates considered in the PSAR are described separately for each individual waste vaults in the following sections.

Silo

In concrete structures, steel reinforcement bars are used to minimise the width of cracks caused by mechanical loads or by temperature and drying shrinkage. For the silo, the amount of reinforcement has been shown not to meet present day standards for restricting the width of cracks (cf Boverket 2004). The silo bottom and the lower part of the silo wall contain only about 30 and 70 % of the prescribed minimum amount of reinforcement, respectively, to restrict the crack aperture (Cronstrand et al. 2011).

Unfortunately, no inspection protocols from the time of construction of the concrete silo have been identified and therefore no information regarding whether cracks were formed during construction or not is available. Also, as a consequence of the design of the silo, inspections aiming to detect and quantify the number and width of cracks in the concrete structure are not possible during the operational period.

For those reasons, the prediction of the probability for cracks as well as the evolution of material porosity and hydraulic conductivity for the concrete silo must be based on an analysis of the influence of the different processes described in the **Barrier process report**.

1BMA

From the detailed inspection programme carried out for 1BMA and summarised by Elfwing et al. (2015), the current status of the concrete structure in 1BMA is characterised by the presence of a large number of cracks in the walls and the slab as well as by rebar corrosion and partial spalling of the layer of concrete that covers the reinforcement bars.

According to Cronstrand et al. (2011) the amount of reinforcement in the concrete structure in 1BMA does not meet present-day standards for restricting the width of cracks (cf Boverket 2004). As an example, they show that the slab only contains about 50 % of the minimum amount of reinforcement to restrict the crack aperture. This explains why only a few but rather wide cracks have been formed in the concrete structure in 1BMA rather than several smaller ones.

According to present plans, new outer walls will be erected outside the existing ones in order to ensure the post-closure safety of 1BMA (Elfwing et al. 2018). However, at present no suitable method for sealing the cracks in the slab has been identified which means that the initial state of the concrete structure will include a slab with cracks.

For those reasons, the evolution of the hydraulic conductivity of the concrete structure in 1BMA must be updated considering the impact of a cracked slab whereas cracks are not expected in the walls and lid at closure.

2BMA

The concrete components in 2BMA comprise 13 free-standing caissons made of non-reinforced concrete which are erected on a thick slab made of reinforced concrete which rests on a bed of macadam. Prior to construction of the concrete caissons, the reinforced concrete slab will be covered with a plastic foil to eliminate any adhesion between the concrete caissons and the slab.

The slab and walls of the concrete caissons are constructed from a newly developed concrete (Lagerblad et al. 2017) and using construction methods developed by Mårtensson and Vogt (2019, 2020). According to the latest design (Elfwing et al. 2017), the concrete caissons will be provided with concrete inner walls but the detailed mix proportions and construction method for the inner walls have not yet been developed. It can however, be assumed that a similar type of concrete as used in the outer concrete structure will be used. Finally, at closure a concrete lid with a thickness of about 600 mm will be constructed (**Initial state report**).

The concrete caissons will experience temperature and moisture variations during construction that will cause dimensional changes that may result in mechanical stresses. Also, thermal shrinkage of the concrete caissons as a result of groundwater filling the vault after closure must be considered (Höglund 2014). However, from the large-scale production tests carried out by Mårtensson and Vogt (2019, 2020) the levels of strain in a concrete caisson (dimensions $18 \times 9 \times 4.5$ metres) were very low and three years after casting cracking has not yet been observed.

Further, the fact that the concrete caissons are erected as free-standing structures on a concrete slab permits unrestrained shrinkage due to e.g. temperature and humidity variations and the risk for cracking due to intrusion of cooler groundwater during the resaturation period as suggested by Höglund (2014) is therefore limited.

Due to the absence of reinforcement bars or other steel components in the concrete caissons the impact of steel corrosion on the barrier function does not need to be considered for 2BMA.

Based on the findings reported by Lagerblad et al. (2017) and Mårtensson and Vogt (2019, 2020) it is suggested that cracking of the concrete caisson in 2BMA will not occur during construction, operation and resaturation of the repository.

Cracks will instead form if the mechanical loads i.e. from the backfill material exceed the load bearing capacity of the concrete structure. The main process affecting the loadbearing capacity of the concrete structures is general dissolution of the cement minerals and leaching in combination with loss of function of the reinforcement bars.

From the findings by Mårtensson (2017) the load bearing capacity of the lid and outer walls of the concrete structure in 2BMA will be sufficient to withstand the pressure from the intruding groundwater during the resaturation phase as well as the pressure from the backfill materials for the period up to 20 000 years after closure. Mårtensson (2017) therefore concluded that formation of cracks due to extensive mechanical loads in combination with the expected degradation processes are not expected during the first 20 000 years after closure.

Based on the above discussion, it is suggested that the initial state hydraulic conductivity for 2BMA should reflect the properties of a concrete structure without cracks. This is also motivated by the fact that any cracks formed during construction and the operational period could be sealed prior to closure. Finally, the inner walls of 2BMA will be provided with holes to control the hydraulic conductivity and ensure that intruding groundwater can be evenly distributed within the entire waste domain.

1BRT

No hydraulic conductivity data were assigned to the cementitious components in 1BRT in the SR-PSU Data report (SKB TR-14-10). However, as indicated in Section 9.1, the supplier should provide data for the current assessment and the conditions for providing such data also for 1BRT are therefore discussed below.

The concrete structures in 1BRT will comprise a reinforced concrete structure with similar features as that in 1BMA which will be founded on a bed of crushed rock/macadam. However, the concrete structure in 1BRT does not formally constitute a hydraulic barrier and currently strict requirements concerning concrete mix proportions and construction methods are not prescribed.

For that reason, the assignment of hydraulic conductivity data for the concrete structure in 1BRT must consider the likely presence of cracks already at closure of the repository. Further, also the prediction of the evolution of the hydraulic conductivity of the concrete structure must include the effect these cracks.

1–2BTF

The concrete components in 1–2BTF for which data are requested include the slab, lid and concrete tanks.

The concrete tanks are carefully controlled and tested prior to delivery in order to ensure tightness. The outsides of the concrete tanks are also painted with a hydrophobic paint in order to prevent corrosion of the reinforcement bars during the operational period. In addition to this, the interior of the concrete tanks is provided with a rubber lining in which the dewatered ion-exchange resins are placed in order to prevent interactions with the concrete and the reinforcement bars. The selected initial state hydraulic conductivity should therefore be representative of concrete tanks without cracks.

The slabs, on which the concrete tanks are placed, are also used for transport of waste containers by means of a fork-lift truck that causes dynamic loads. Finally, they are also exposed to chlorine containing groundwater during the operational period. With the assumption that the same type of concrete and construction methods as used in 1BMA were also used for the slabs in 1–2BTF cracks must also be expected in the slabs in 1–2BTF. The selected initial state hydraulic conductivity for the slabs should therefore be representative of concrete with a few cracks.

The lid will be constructed at repository closure using carefully selected material and construction methods in order to ensure that the lid will not contain any cracks.

For those reasons, the assignment of the initial state hydraulic conductivity for the concrete components in 1–2BTF should reflect the differences in terms of original design and degradation during the operational period.

Further, the prediction of the evolution of the hydraulic conductivity for different time periods during the post-closure period must reflect these initial differences as well as the impact of the processes that could affect these components during the post-closure period discussed in the **Barrier process report**.

1–5BLA

No hydraulic conductivity data were assigned to the cementitious components in 1–5BLA in the SR-PSU assessment.

The supplier been asked to provide hydraulic conductivity data for the slab in 1–5BLA. With the assumption that the same type of concrete and construction methods as used in 1BMA were also used for the slabs in 1BLA cracks must also be expected in the slabs in 1BLA. The selected initial state hydraulic conductivity for the slabs should therefore be representative of concrete with a few cracks. As the slabs in 2–5BLA do not formally constitute a hydraulic barrier, and currently strict requirements concerning concrete mix proportions and construction methods are not prescribed, the same hydraulic conductivity as for the slab in 1BLA is representative.

9.4 Sources of information and documentation of data qualification

Sources of information

In general, specific data for the cementitious components in SFR are not available, in particular and for unfortunate reasons, no data exist for these components in aged and degraded stages. The safety assessments have therefore been based on judgements of reasonable data sets from typical structural concretes and different modelling approaches and measurements to estimate the hydraulic conductivity and porosity.

In Table 9-2, hydraulic conductivity data from the sources presented in Table 9-3 are compiled.

Table 9-2. Some data on hydraulic conductivities of concrete from safety assessments, literature and model estimates. Included are also measurements of the permeability increase factor when comparing cracked and uncracked concrete.

Material	Hydraulic conductivity (m/s)	Permeability increase factor cracked/ uncracked	Type of data	Source
Concrete without cracks	1×10^{-11}	1	Safety assessment	SKB R-01-14
2BMA concrete	$< 1 \times 10^{-11}$		Measurement	Mårtensson and Vogt 2019
2BMA concrete	$10^{-12} – 10^{-11}$		Measurement	Mårtensson and Vogt 2020
2BMA concrete	$10^{-13} – 10^{-10}$		Measurement	Villar et al. 2019
1BMA concrete*	$(1–2) \times 10^{-11}$		Measurement	Villar et al. 2019
Silo grout	$> 5 \times 10^{-8}$		Measurement	Björkenstam 1997
Silo grout**	$(0.5–100) \times 10^{-8}$		Measurement	Production control
Concrete with 10 µm crack aperture width every metre	8.3×10^{-10}	83	Safety assessment	SKB R-01-14
Cementitious backfill	8.3×10^{-9}	830	Safety assessment	SKB R-01-14
Concrete	$10^{-14} – 10^{-10}$	-	Literature review	Luna et al. 2006
Concrete with 1 µm crack aperture width every metre	1.1×10^{-11}	1.1	Model estimates	Höglund and Bengtsson 1991
Concrete with 1 µm crack aperture width every 0.1 metre	1.6×10^{-11}	1.6	Model estimates	Höglund and Bengtsson 1991
Concrete with 10 µm crack aperture width every 0.1 metre	6.3×10^{-9}	630	Model estimates	Höglund and Bengtsson 1991
Concrete with 100 µm crack aperture width every metre	6.3×10^{-7}	6.3×10^{4}	Model estimates	Höglund and Bengtsson 1991
Concrete with 100 µm crack aperture width every 0.1 metre	6.3×10^{-6}	6.3×10^{5}	Model estimates	Höglund and Bengtsson 1991
Concrete with 10 µm crack aperture width every metre penetrating 60 % of thickness	2.5×10^{-11}	2.5	Model estimates	Höglund 2014
Uncracked concrete but chemically degraded to 60 % of thickness	$2 \times 10^{-11} – 4 \times 10^{-11}$	2–4	Model estimates	Höglund 2014
Evaluation of the overall conductivity of the concrete structures considering the observed cracks in the 1BMA vault	$9.7 \times 10^{-5} – 4.9 \times 10^{-4}$	$9.7 \times 10^{6} – 4.9 \times 10^{7}$	Model evaluation of observed cracks	Höglund 2014 based on inspection by Hejll et al. (2012)
30 MPa concrete, compressive stress 70 % of ultimate load	-	$10^{2} – 10^{4}$	Measurement	US DOE 2009
Ordinary concrete, 100 °C	-	10^{2}	Measurement	US DOE 2009
Ordinary concrete, bending stress 0.1 mm	-	2.25	Measurement	US DOE 2009
Cement paste, tensile stress 110 µm	-	14	Measurement	US DOE 2009
Cement mortar, tensile stress 130 µm	-	10	Measurement	US DOE 2009
Ordinary concrete, tensile stress 130 µm	-	2×10^{3}	Measurement	US DOE 2009
High performance concrete, tensile stress 110 µm	-	10^{2}	Measurement	US DOE 2009
45 MPa concrete, tensile stress 350 µm	-	10^{7}	Measurement	US DOE 2009
45 MPa concrete, tensile stress 550 µm under load	-	10^{7}	Measurement	US DOE 2009
Ordinary concrete, tensile stress 350 µm under load	-	2.5×10^{3}	Measurement	US DOE 2009
High performance concrete, tensile stress 300 µm under load	-	35	Measurement	US DOE 2009
Cement mortar, compressive stress 90 % of ultimate load	-	16	Measurement	US DOE 2009

* Note that the 1BMA specimens used by Villar et al. (2019) were newly prepared using an estimated concrete mix proportions and not obtained from the concrete structure of 1BMA.

** Note that production control uses separately prepared specimens and not cores extracted from the grouted waste in the silo. Variations due to sample preparation can therefore occur.

Table 9-3. Sources of data on hydraulic conductivities of concrete from safety assessments, model estimates and literature.

Sources of information
Björkenstam E, 1997. Utveckling av SFR-bruket. UC 97:4Ö, Vattenfall utveckling AB, (SKBdoc 1439832 ver 1.0, Svensk kärnbränslehantering AB.
Boverket, 2004. Boverkets handbok om betongkonstruktioner: BBK 04. 3rd ed. Karlskrona: Boverket. (In Swedish.)
Hejll A, Hassanzadeh M, Hed G, 2012. Sprickor i BMA:s betongbarriär – Inspektion och orsak. Rapport AE-NCC 12-004, Vattenfall AB. SKBdoc 1430853 ver 1.0, Svensk Kärnbränslehantering AB. (In Swedish.)
Höglund L O, 2014. The impact of concrete degradation on the BMA barrier functions. SKB R-13-40, Svensk Kärnbränslehantering AB.
Höglund L O, Bengtsson A, 1991. Some chemical and physical processes related to the long-term performance of the SFR repository. SKB SFR 91-06, Svensk Kärnbränslehantering AB.
Luna M, Arcos D, Duro L, 2006. Effects of grouting, shotcreting and concrete leachates on backfill geochemistry. SKB R-06-107, Svensk Kärnbränslehantering AB.
Mårtensson P, Vogt C, 2019. Concrete caissons for 2BMA: Large scale text of design and material. SKB TR-18-12, Svensk Kärnbränslehantering AB.
Mårtensson P, Vogt C, 2020. Concrete caissons for 2BMA: Large scale text of design, material and production method. SKB TR-20-09, Svensk Kärnbränslehantering AB.
SKB R-01-14. SKB 2001. Project SAFE. Compilation of data for radionuclide transport analysis. Svensk Kärnbränslehantering AB.
US DOE, 2009. Review of mechanistic understanding and modelling and uncertainty analysis methods for predicting cementitious barrier performance. Cementitious Barriers Partnership. CBP-TR-2009-002, Rev.0, U.S. Department of Energy.
Villar M V, Gutiérrez M G, Barrios B C, Álvarez C G, Martínez R I, Martín P L, Missana T, Mingarro M, Morejón J, Olmeda J, Idiart A, 2019. Experimental study of the transport properties of different concrete mixes. SKB P-19-10, Svensk Kärnbränslehantering AB.

Categorising data sets as qualified or supporting data

Qualified data are presented in Höglund (2014) and the other references given in Table 9-3. Supporting data are provided in the various references used in the derivation of the data in Höglund (2014) (see reference list of this report).

Excluded data previously considered as important

No data used in the SR-PSU assessment have been excluded in the PSAR. However, some data have been revised as a consequence of the increased level of understanding of the current status of some of the cementitious components in SFR, and more detailed descriptions of repair and construction methods for the concrete structures in SFR1 and SFR3.

It is also worth noting the references given as (SKBdoc 123456) are now presented using the name of the authors. As an example (SKBdoc 1430853) in the SR-PSU Data report (SKB TR-14-10) is given as (Hejll et al. 2012) in this report.

9.5 Conditions for which data are supplied

In the following sections, the conditions for which hydraulic conductivity data are supplied is discussed individually for each waste vault.

Silo

Based on the discussion in Section 9.3, it is suggested that the initial state hydraulic conductivity selected for the silo structure should reflect the properties of a concrete with a few minor cracks. This is motivated by the fact that the concrete structure will be under a state of compressive stress caused by the pressure from the surrounding bentonite.

The evolution of the hydraulic conductivity should also reflect the fact that the concrete silo after closure will constitute a concrete monolith which will be protected from interactions with the intruding groundwater by the thick bentonite layer.

The low amount of groundwater in contact with the concrete also ensures that leaching and thus the increase of porosity will be slow. In fact, Cronstrand (2007) has shown that the porosity of the outer concrete silo may slowly be reduced due to precipitation of secondary minerals and eventually the pore system will be entirely clogged.

1BMA

From the information provided in Section 9.3, the hydraulic conductivity data for the cementitious components in 1BMA should be selected based on the new outer walls and lid being free from cracks at closure but that cracks are present in the slab already at closure.

Further, from the findings by Mårtensson (2017), cracking of the new outer walls and lid of the concrete structure in 1BMA is not expected during the first 20 000 years after closure. However, from this time, selected hydraulic conductivity data must consider cracking caused by the combined effect of chemical degradation of the concrete, rebar corrosion and external load from the backfill material in the waste vault.

2BMA

Based on the discussion in Section 9.3, it is suggested that the initial state hydraulic conductivity data selected for 2BMA should reflect the properties of a concrete structure without cracks. This is also motivated by the fact that any cracks formed during construction and the operational period could be sealed prior to closure. However, for the inner walls, selected data must reflect the fact that these will be provided with holes to evenly distribute any intruding groundwater within the waste domain.

For 2BMA, the evolution of the hydraulic conductivity data should also reflect that the concrete caissons are free-standing and designed to handle the pressure from the intruding water during the resaturation period and the loads from the backfill material during up to 20 000 years after closure as shown by Mårtensson (2017). However, for the period beyond 20 000 years after closure, the risk of cracking must be reflected in the choice of hydraulic conductivity data.

Finally, the absence of steel tie rods and reinforcement bars prevents corrosion induced cracking.

1BRT

From Section 9.3, the selection of hydraulic conductivity data for the cementitious components in 1BRT must consider the presence of cracks already at closure. However, the fact that the waste compartment inside the concrete barrier will constitute a concrete monolith including grout-filled waste packaging and self-compacting concrete implies that extensive cracking due to external loads should not be anticipated during the post-closure period.

The assignment of the hydraulic conductivity data should therefore consider early cracking but only limited further cracking due to external loads during the post-closure period.

Instead, cracking due to internal loads caused by corrosion of waste and waste packaging, reinforcement bars and steel tie rods (unless tie rods made from glass-fibre are used) must be considered to be the main cause of cracking of the concrete barriers in 1BRT. For more information concerning the influence of the process; see the **Barrier process report** or Höglund (2014).

1–2BTF

From Section 9.3, the selection of hydraulic conductivity data for the different cementitious components in 1–2BTF must consider the rather large structural differences between these but also the fact that they will be exposed to very dissimilar conditions prior to closure. Further, also the temporal evolution of the different cementitious components is likely to show considerable dissimilarities as a consequence of the differences discussed above.

1–5BLA

From Section 9.3, the selection of hydraulic conductivity data for the slabs in 1–5BLA must consider the presence of cracks already at closure.

9.6 Conceptual modelling uncertainty

In general, the conceptual uncertainties related to the hydraulic conductivity of concrete are small. Hydraulic processes are well known and intact concrete is known to have a low hydraulic conductivity and a high durability. Uncertainty associated with crack distribution can be handled using different approaches. In estimates of hydraulic conductivities based on the aperture of cracks, the cracks are often represented by two parallel plates with no or very little surface roughness. This is a simplified representation that disregards the varying widths and rough surfaces of cracks in concrete. Concrete with cracks can also be represented as a porous medium with cracks. In the assessment model there are some uncertainties regarding which part of the pore system or cracks should be represented by a porous medium and which should be represented as cracks.

There is also a conceptual uncertainty relating to the effect of chemical degradation on the hydraulic conductivity of the concrete barriers, and vice versa. This is furthermore accentuated by the conceptual uncertainties associated with the assessment of how locally enhanced chemical degradation in the vicinity of the cracks and the influence of the progression of physical degradation processes will affect hydraulic conductivity over time as discussed in US DOE (2009).

9.7 Data uncertainty – precision, bias, and representativity

This section focuses on the uncertainties associated with the initial state and events of critical importance for the post-closure safety. Since the detailed level of understanding of material properties and construction/restoration methods has improved since SR-PSU, the hydraulic conductivity and porosity data uncertainties in the PSAR have been significantly reduced for some of the waste vaults.

From the findings presented in Figure 9-2, the impact of increasing crack aperture on the hydraulic conductivity is significant. In combination with lack of detailed information concerning the presence of cracks in many of the concrete structures at closure as well as the difficulties associated with performing accurate predictions on the crack propagation, suggested data on hydraulic conductivities will still be associated with significant uncertainties.

For those reasons, the recommended hydraulic conductivities shown in Figures 9-4 and 9-5 are significantly higher than the estimated values indicated by the red lines in these figures.

Below, data uncertainty – precision, bias and representativity are discussed for each individual waste vault. The vault specific sections start by discussing the validity of the initial state used in SR-PSU and continues with a re-evaluation of uncertainties associated with the initial state and the evolution of the cementitious components.

Silo

Initial state hydraulic conductivity for the cementitious components of the silo used in SR-PSU assumed basically uncracked concrete in the slab, inner and outer walls as well as in the lid. Even though information concerning the presence of cracks in these structural components is scarce, see Section 9.3, the uncertainty of the initial state hydraulic conductivity data is considered low.

The assigned post-closure hydraulic conductivity data assume an increased level of cracking of all structural components in the silo. However, constituting a concrete monolith and being surrounded by a thick bentonite layer, extensive cracking of the different structural components of the concrete silo during the post-closure period is not expected. Nevertheless, the assigned hydraulic conductivity data in SR-PSU includes significant cracking giving some margins for uncertainties related to extent of cracking.

1BMA

The initial state hydraulic conductivity of the cementitious components in 1BMA used in SR-PSU assumed basically uncracked concrete in the slab, outer walls and lid. For PSAR, this will be valid for the new outer walls and lid which will be constructed at closure. However, since no repair measures are planned for the slab, cracks will be present in the slab already at closure.

The presence of cracks introduces uncertainties for the long-term evolution of the assigned data. The fact that the slab is rather thin and already cracked implies that further cracking will occur in the future due to the combined effect of concrete degradation, rebar corrosion and load from the waste packages. Data need to reflect that the slab will not be included in the repair measures of the concrete structure in 1BMA and that additional cracking could be expected during the first 10 000 years.

For the remaining components of the concrete structure in 1BMA, the initial state uncertainties will be very low because of strict control measures undertaken during construction as discussed in Section 9.3. This will ensure that cracks will not be present in the walls and lid at closure which significantly reduces uncertainty. The temporal uncertainties in the evolution of the load bearing capacity of the concrete structure which has a significant impact on the risk for cracking must though be considered.

2BMA

Hydraulic conductivity data for the cementitious components in 2BMA used in SR-PSU were assumed to follow those of the walls and lid of the outer concrete structure in 1BMA.

The recent information concerning materials and construction methods for 2BMA, discussed in Section 9.3, indicate that uncertainties concerning the initial state hydraulic conductivity will be limited. The fact that detailed information from construction experiments and long-term follow-up in a representative environment has been carried out, reduces the uncertainties of the hydraulic conductivity data for 2BMA significantly compared with the SR-PSU.

Based on the findings by Mårtensson (2017) the risk of formation of cracks during the first 20 000 years after closure is low as was also reflected in the selected hydraulic conductivity data for SR-PSU. Beyond 20 000 years after closure the risk of cracking increases significantly which is also reflected in the suggestion of a wider span of hydraulic conductivity values. The temporal uncertainties in this prediction must though be considered.

Finally, the fact that reinforcement is not used in the concrete caissons in 2BMA implies that extensive cracking can occur which is not covered even by the highest hydraulic conductivity value suggested for the different periods. As Figure 9-2 only covers cracks with a width up to 1 mm, the impact of wider cracks cannot be obtained from this figure which means that the uncertainties are somewhat larger for the latter stages of the assessment period.

1BRT

Hydraulic conductivity data for the cementitious components of 1BRT were not provided in the SR-PSU Data report (SKB TR-14-10).

The main uncertainties related to the concrete structure in 1BRT are related to the fact that the concrete structure is not regarded as a hydraulic barrier and that strict choice of material and construction methods are not prescribed. In order to handle these uncertainties, selection of hydraulic conductivity data will consider the risk of considerable cracking already at closure.

1–2BTF

Hydraulic conductivity data for the cementitious components in 1–2BTF used in SR-PSU reflected more or less intact concrete without cracks during the first 1 000 years after closure after which the assigned hydraulic conductivity data reflect rather extensive cracking.

From the information presented in Sections 9.3 and 9.5, significant dissimilarities in the initial state hydraulic conductivity data as well as in the temporal evolution of these data can be expected between the different cementitious components in 1–2BTF.

Major uncertainties relate to the load bearing capacity of the concrete tanks and thus the risk of early cracking as well as the properties of the grout surrounding the waste packages which cannot be controlled prior to closure. In order to handle these uncertainties, selection of hydraulic conductivity data should consider the risk of significant cracking already at closure.

1–5BLA

No hydraulic conductivity data were assigned for the concrete barriers of 1–5BLA in SR-PSU. The selection of hydraulic conductivity data for the slabs in 1–5BLA must consider the presence of cracks already at closure.

9.8 Data uncertainty – spatial and temporal variability

Spatial variability of data

Cementitious components

There will be a spatial variability in the hydraulic properties of the cementitious components mainly caused by the presence of cracks and other permeable zones. Examples of model applications to demonstrate the impact of such defects are briefly discussed in Section 9.3 with more details presented in Höglund (2014).

For the safety assessment, the spatial variability can be averaged by means of calculating equivalent flow resistances. However, it is currently not possible to use a statistical approach to qualify the data. There is also currently a limited availability of site-specific data on the hydraulic conductivity, porosity and the presence of cracks in the concrete components in the different waste vaults in SFR. However, data do exist for the concrete structure in 1BMA which has been extensively studied as well as for the silo grout and the 2BMA concrete planned for use for construction of the 2BMA caissons because of extensive testing during the development work and production control. It is though still judged inappropriate to produce any statistical representation based on the available data.

However, through continued inspections of the different concrete components in SFR1 in combination with careful selection of materials and methods of construction for the concrete components in SFR3, the initial state uncertainties can be reduced.

The expected progression of different degradation processes, both chemical and physical, may also cause spatial variability. It is also likely that cracks will not be equally distributed in the different concrete components due to dependence on amount and distribution of reinforcement as well as loads.

Crushed rock backfill

The spatial variability of the hydraulic conductivity of the crushed rock backfill is expected to be limited. However, accumulation of mineral particles in the lower parts of the crushed rock backfill could reduce the hydraulic conductivity in these parts.

Temporal variability of data

Cementitious components

The hydraulic conductivity and porosity of cementitious components in SFR will change over time due to chemical and physical degradation processes. The chemical degradation processes are governed by diffusion, the flow of groundwater and the flow resistance in different parts of the repository. The groundwater flow varies in time due to external factors such as shoreline displacement, glaciation periods etc.

The flow resistance of different components in the repository will in turn be affected by the different degradation processes, hence creating a coupled system. Despite the inherent difficulties in assessing the properties of such systems over time in detail, the evolution of the processes can be quantified with reasonable accuracy using existing model tools for alternative scenarios. Results of such model exercises are presented for 1–2BMA and the silo by Höglund (2014).

The progression of physical degradation processes with time, including different processes leading to cracking of the concrete barriers, is difficult to predict given the uncertainties related to these processes and the very significant impact of increasing crack aperture on the hydraulic conductivity of a concrete structure as indicated in Figure 9-2 and discussed in Section 9.3.

Crushed rock backfill

The temporal variability of the hydraulic conductivity of the crushed rock backfill is expected to be limited. Although some clogging due to bacterial growth or accumulation of mineral particles from the intruding groundwater could occur, major alterations are not expected.

9.9 Data uncertainty – correlations

Due to the coupling of processes, correlations exist between crack formation, overall degradation of the cementitious components, hydraulic conductivities and flow. This means that radionuclide migration from the waste vaults is correlated to the degree of cracking (set by loss of load bearing capacity and external loads) and influenced by the uncertainties associated with the hydraulic conductivity of the cracked material.

The porosity of the concrete correlates with its hydraulic conductivity, as shown in Figure 9-1, and therefore also radionuclide migration. In addition, cracks increase the effective porosity of the concrete.

9.10 Result of supplier's data qualification

9.10.1 Porosity data for the cementitious components

In general, the initial porosity of cementitious materials is controlled by the w/c ratio. From Table 9-1 the porosity of standard concrete varies between 0.11 and 0.16 for the range of w/c ratios used in the different types of structural concrete in SFR whereas the porosity of a porous cementitious grout can be as high as 0.3.

The long-term evolution of the porosity of cementitious materials is mainly controlled by the interaction with groundwater and species dissolved in the groundwater. Typically, the porosity increases over time due to dissolution of the cement minerals as shown by the black line in Figure 9-3 in which a maximum porosity of 0.25 is reached at 100 000 years after closure. As a comparison, the relative volume of inert aggregates in standard concrete is about 65–75 % which basically sets the limit for the maximum porosity in concrete when all cement minerals have been dissolved.

Under certain conditions, though, the porosity can also be reduced over time due to precipitation of secondary minerals in the pore system of the cementitious material. As an example, Cronstrand (2007) showed this to be the case for the outer wall of the concrete silo which is in contact with bentonite.

When selecting porosity data for the different cementitious materials in SFR, it must also be remembered that leaching will be gradual and that a leaching front will develop within the materials. This means that the porosity at the surface in contact with the groundwater can be representative for severely degraded concrete at the same time as the porosity in the inner parts of the concrete structure will correspond to that of intact concrete. An example of the evolution of porosity from intact concrete (0.11) to severely degraded concrete (0.25) is shown in Figure 9-3.

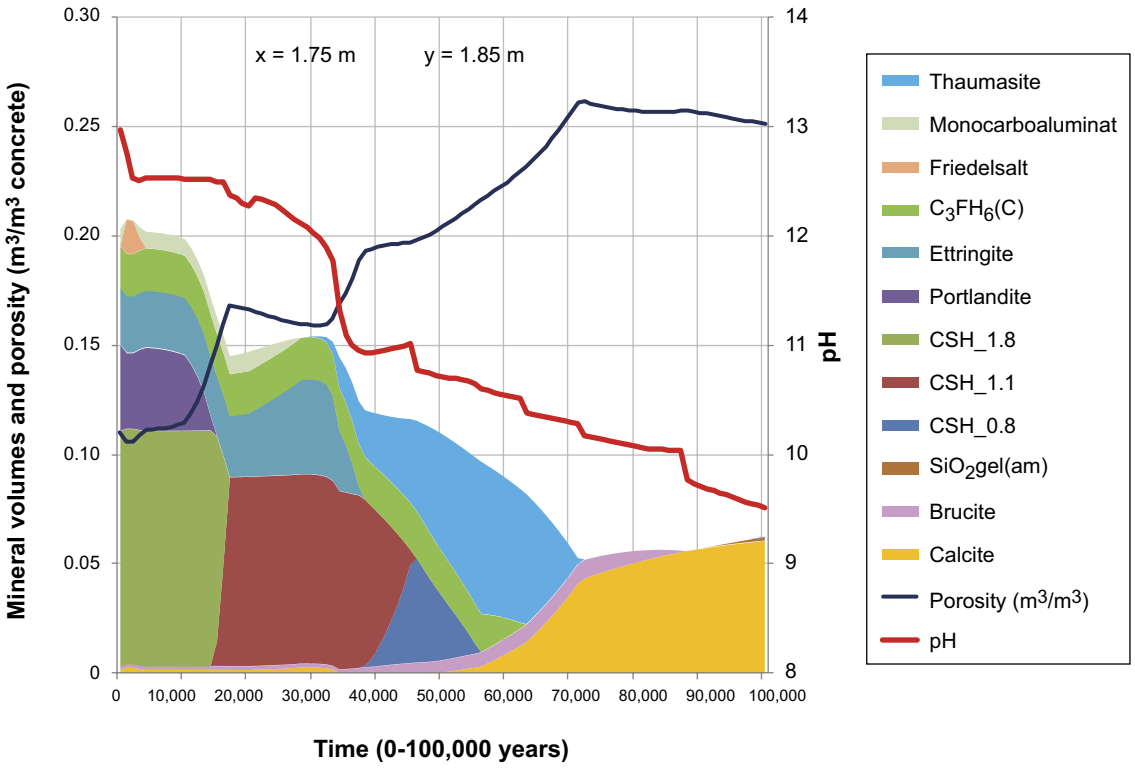

Figure 9-3. *Example of the evolution of the mineral distribution, pH and porosity in a concrete barrier (Höglund 2014).*

Table 9-4 presents porosity data for the different cementitious components in the different waste vaults and time periods recommended by the supplier to be used in the PSAR.

Table 9-4. Data on porosities in cementitious components for different time periods and waste vaults suggested by the supplier to be used in the assessment.

	Porosity (–) for time periods (AD)					
	2000 – 2100	**2100 – 3000**	**3000 – 12 000**	**12 000 – 22 000**	**22 000 – 52 000**	**52 000 – 100 000**
Silo						
Concrete structure	0.11	0.11	0.11–0.14	0.14–0.17	0.17–0.20	0.20–0.25
Grout	0.3	0.3	0.3	0.3	0.3	0.3
Concrete moulds	0.11	0.11	0.11	0.11	0.11	0.11
1BMA						
Existing outer walls, inner walls and slab (1BMA concrete)	0.11	0.11–0.12	0.12–0.14	0.14–0.16	0.16–0.20	0.3
Lid and new outer walls (2BMA concrete)	0.11	0.11–0.12	0.12–0.14	0.14–0.16	0.16–0.20	0.3
Concrete moulds	0.11	0.11–0.12	0.12–0.15	0.15–0.16	0.16–0.20	0.3
2BMA						
Slab, outer walls and lid (2BMA concrete)	0.11	0.11–0.12	0.12–0.14	0.14–0.16	0.16–0.20	0.3
Inner walls	0.11	0.11–0.12	0.12–0.14	0.14–0.16	0.16–0.20	0.3
Grout in gas evacuation channels	0.3	0.3	0.3	0.3	0.3	0.3
Concrete moulds	0.11	0.11–0.12	0.12–0.15	0.15–0.16	0.16–0.20	0.3

Table 9-4. Continued.

	Porosity (–) for time periods (AD)					
	2000 – 2100	2100 – 3000	3000 – 12000	12000 – 22000	22000 – 52000	52000 – 100000
1BRT						
Slab, outer walls, lid and inner walls	0.11	0.11–0.12	0.12–0.14	0.14–0.16	0.16–0.20	0.3
Concrete between waste packages	0.11	0.11–0.12	0.12–0.14	0.14–0.16	0.16–0.20	0.3
1–2BTF Slightly cracked case						
Slab and lid	0.11	0.11–0.12	0.12–0.14	0.14–0.16	0.16–0.20	0.3
Grout	0.2	0.3	0.3	0.3	0.3	0.3
Cementitious backfill	0.11	0.11–0.12	0.12–0.14	0.14–0.16	0.16–0.20	0.3
Concrete tanks and moulds	0.11	0.11	0.2	0.3	0.3	0.3
1–2BTF Cracked case						
Slab and lid	0.11	0.11–0.12	0.2	0.3	0.3	0.3
Grout	0.2	0.3	0.3	0.3	0.3	0.3
Cementitious backfill	0.11	0.11–0.12	0.12–0.14	0.14–0.16	0.16–0.20	0.3
Concrete tanks and moulds	0.11	0.11	0.2	0.3	0.3	0.3

9.10.2 Hydraulic conductivity data for the cementitious components

Overview

As in the previous assessment (SKB TR-14-10) the hydraulic conductivity of intact concrete has been assumed to 1×10^{-11} m/s even though studies indicate the possibility of values as low as 10^{-12} m/s (Mårtensson and Vogt 2019, 2020). In order to handle uncertainties concerning the initial state it has been assumed that all concrete structures initially contain one crack with an aperture of 10 µm per metre, corresponding to an overall hydraulic conductivity of 8.3×10^{-10} m/s. It should be noted though that such narrow cracks cannot be expected to be fully penetrating in the thick concrete structures in SFR. As shown by Mårtensson (2014), cracks with an aperture up to 0.1 mm are not penetrating and will therefore have a limited influence on the hydraulic conductivity of the concrete structure.

Values of the hydraulic conductivity suggested by the supplier to be used in the safety assessment calculations are presented in Table 9-5 for different time periods. As far as possible, the suggested values are based on interpretation of the results from modelling studies and measurements which have been carried out as parts of this and previous safety assessments compiled in Table 9-2 and also illustrated in Figure 9-4 and 9-5 for the silo and 2BMA, respectively.

The time periods considered are indicative and therefore associated with a certain degree of uncertainty. Where intervals are given for the hydraulic conductivities, all values in the range are equally likely, since the results depend on assumptions regarding the crack frequency and aperture. Due to the spatial and temporal variability of crack formation, frequency and size, the hydraulic conductivity values in the range may be representative for different parts of the barriers.

Silo

Outer and inner walls, slab and lid

From Section 9.3, investigations showed that the amount of reinforcement in the concrete silo is not sufficient to restrict the width of the cracks formed in the slab and outer walls. However, due to the fact that the design and construction differs considerably between the silo and the concrete structure in 1BMA, the likelihood for cracking during construction and the operational period is judged to be lower in the silo than in 1BMA. An initial hydraulic conductivity of 8.3×10^{-10} m/s is selected for the concrete structure; outer walls, inner walls, slab and lid of the concrete silo, as discussed in the overview section.

The anticipated progression of different degradation processes in the concrete walls of the silo is described by Höglund (2014, Appendix B). Based on the predicted degradation processes, Höglund (2014) suggests an evolution of the hydraulic conductivity of the concrete structure of the silo as illustrated in Figure 9-4.

The suggested hydraulic conductivities presented in Table 9-4 follow the evolution of proposed values illustrated in Figure 9-4. This will give a considerable margin to the predicted realistic values (curves) shown in the same figure and ensure that overly optimistic values are not used in the radionuclide transport calculations.

Concrete moulds

The evolution of the hydraulic conductivity of the concrete moulds is suggested to follow that of the concrete structure. This is motivated by the consideration that no or only a minor number of concrete moulds contain swelling waste but also because the concrete moulds are protected from extensive degradation by the grout and the concrete structure.

Grout

The hydraulic conductivity of the grout in the silo is controlled every time grouting is carried out. The hydraulic conductivity requirement is 5×10^{-9} m/s to allow for gas transport and from production control documents this has been verified. This value is therefore selected as the initial value for the grout. The evolution of the hydraulic conductivity of the grout is predicted to follow a similar progression to that of the concrete structure as indicated in Table 9-4.

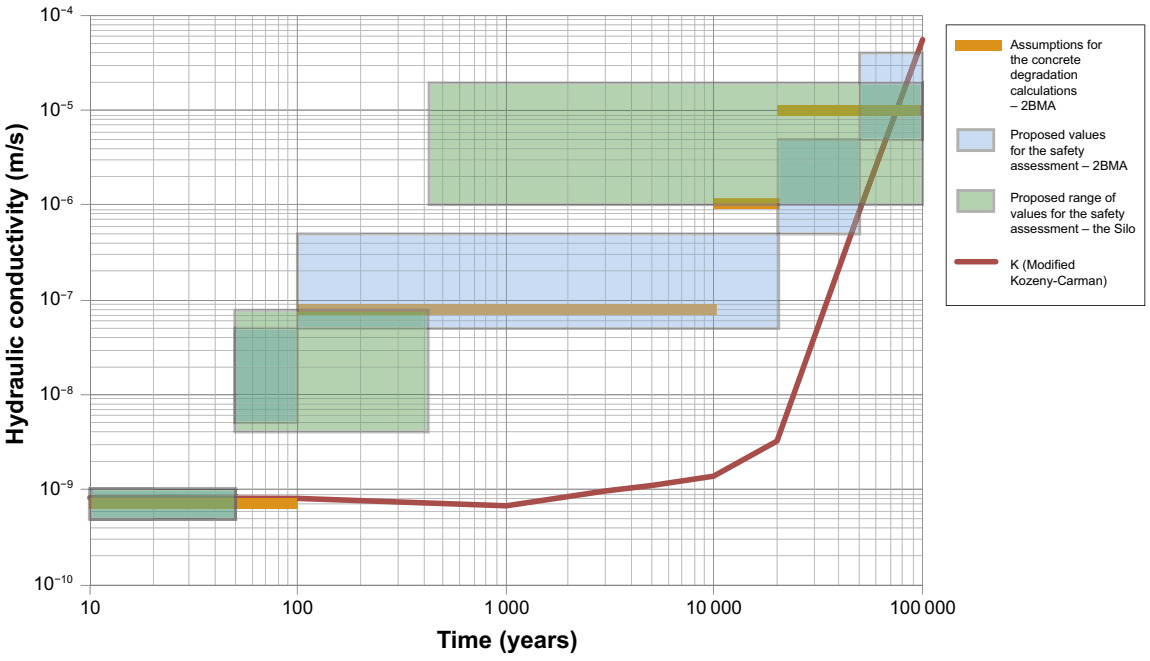

Figure 9-4. *Proposed range of values for the hydraulic conductivity in structural concrete in the silo (blue shading). The hydraulic conductivities proposed for 2BMA (green shading) as well as the initial estimates of the gradual change of the hydraulic conductivity assumed in the PHAST modelling for 2BMA (orange lines) are shown as comparison. The hydraulic conductivities calculated based on the modified Kozeny-carman model using porosity from the PHAST modelling in shown as comparison (red line). From Höglund (2014).*

1BMA

Existing outer walls, inner walls and slab

For the existing outer walls, inner walls and slab, the presence of cracks increases the hydraulic conductivity and from Figure 9-2 a value of 1×10^{-5} m/s is suggested as an initial value. This is somewhat lower than the findings by Höglund (2014) who estimated the hydraulic conductivity of the existing outer walls to be between 2.5×10^{-4} and 5.3×10^{-4} m/s.

From about 20 000 years after closure, additional cracking due to rebar corrosion and loss of load bearing capacity is expected to increase the hydraulic conductivity of the existing walls, inner walls and slab to 10^{-3} m/s, i.e. the same as for the backfill material.

Lid and new outer walls

For the lid and new outer walls in 1BMA, hydraulic conductivity data is recommended based on the assumption that the repair measures described by Wimelius (2021) will ensure that the new outer walls and lid will be free from cracks at closure. As shown by Mårtensson (2017) these structural components will resist the pressure from intruding groundwater during the resaturation period as well as the pressure from the backfill material during the first 20 000 years after closure, thus preventing cracking during this period.

The anticipated progression of different degradation processes in the new outer walls and lid is based on the findings reported by Höglund (2014). Based on the predicted degradation processes, it is suggested that the evolution of the hydraulic conductivity of the lid and new outer walls will follow that suggested by Höglund (2014) for 2BMA illustrated in Figure 9-5.

Concrete moulds

For the concrete moulds in 1BMA, the same hydraulic conductivity data as for the lid and new walls are selected for the entire assessment period.

2BMA

Outer walls, lid and slab

As in SR-PSU the hydraulic conductivity of intact concrete is assumed to be 1×10^{-11} m/s. In order to handle uncertainties concerning the initial state of the external concrete structure an overall hydraulic conductivity of 8.3×10^{-10} m/s is suggested as an initial value for the walls and lid of the concrete barriers in 2BMA as discussed in the overview section.

The anticipated progression of different degradation processes in the concrete structures is based on the findings reported by Höglund (2014), the most important being the formation of cracks. As shown by Mårtensson (2017), the risk for cracking due to loss of load bearing capacity is low during the first 20 000 years after closure. Based on the predicted degradation processes, it is suggested that the evolution of the hydraulic conductivity of the outer walls, lid and slab will follow that suggested by Höglund (2014) illustrated in Figure 9-5.

It should, however, be noticed that for a concrete structure without reinforcement such as the concrete caissons in 2BMA, cracking will lead to the formation of a few larger cracks rather than several smaller ones. This will probably lead to a higher hydraulic conductivity than that indicated in Figure 9-5 and add some uncertainty to the suggested values.

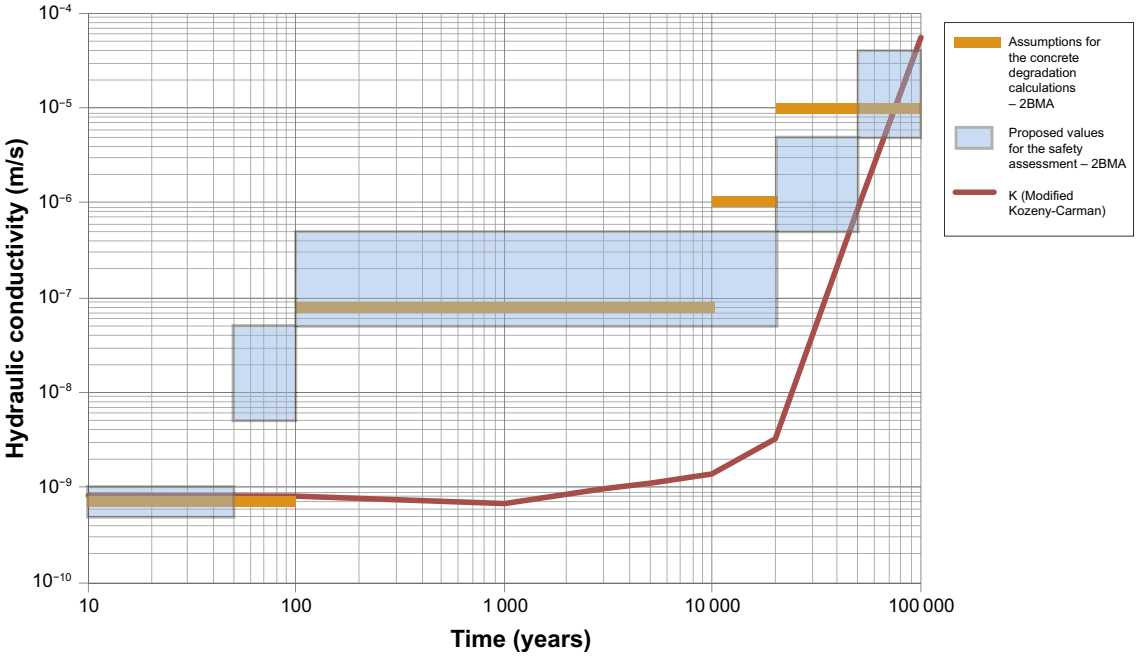

Figure 9-5. *Proposed values for the hydraulic conductivity (blue shading) in the outer walls, lid and slab in 2BMA. The hydraulic conductivities calculated based on the modified Kozeny-carman model using porosity from the PHAST modelling in shown as comparison (red line). The initial estimates of the gradual change of the hydraulic conductivity assumed in the PHAST modelling are also shown in the figure (orange lines). From Höglund (2014).*

Grout in gas evacuation channels

The initial state hydraulic conductivity of the grout in the gas evacuation channels in 2BMA is expected to be the same as that of the grout in the silo. However, the fact that the amount of grout is much smaller in 2BMA than in the silo and also that this grout is more exposed than that in the silo motivates the selection of different hydraulic conductivity data for the grout in the gas evacuation channels in 2BMA than that of the grout in the silo.

Concrete moulds

For the concrete moulds in 2BMA, the evolution of the hydraulic conductivity is predicted to follow that of the outer walls, lid and slab illustrated in Figure 9-4 during the entire assessment period.

1BRT

Outer walls and inner walls, lid and slab

For the outer and inner walls, lid and slab of the concrete structure in 1BRT, hydraulic conductivity data have been selected based on the design and method of construction used for the existing concrete structure in 1BMA and assuming that both steel reinforcement and tie rods (glass fibre or steel) will be used.

From the inspections of the concrete structure in 1BMA (Hejll et al. 2012, Elfwing et al. 2015) it can be expected that cracks may form during construction even though careful considerations during construction can mitigate the extent of cracking. Although tie rod corrosion can be avoided by using glass fibre tie rods, rebar corrosion and the consequences thereof are cautiously expected in the long-term.

The anticipated progression of different degradation processes of the concrete structure in 1BRT will follow that described for the existing outer walls, slab and inner walls in 1BMA. Values of the hydraulic conductivity suggested for the safety assessment calculations are presented in Table 9-5.

Concrete between waste packages

The evolution of the hydraulic conductivity of the concrete between the waste packages in 1BRT is assumed to follow that of the existing outer walls, inner walls and slab in 1BMA during the entire assessment period. This is motivated by the consideration that cracking must be expected since the concrete does not contain any reinforcement. Also, as for the outer walls, inner walls, lid and slab in 1BRT, there is only a requirement on the amount of cement in the concrete between the waste packages and hence the recommended hydraulic conductivities are rather high.

1–2BTF

For 1–2BTF, two different data sets have been suggested: *slightly cracked* and *cracked*. The purpose has been to provide alternative scenarios that can be applied in different cases in the safety assessment. *Slightly cracked* refers to cementitious components which are essentially intact, but with some minor cracks. *Cracked* refers to cementitious components in which significant cracks are present at an early stage that significantly affect the hydraulic properties of the cementitious components.

The selected values in the *cracked case* permit the formation of cracks with a width of up to 1 mm but are not representative for extensively cracked structures as could be anticipated for the concrete tanks once their load bearing capacity against the external pressure from the backfill material is lost or extensive rebar corrosion has occurred. For that reason, a value of 1×10^{-3} m/s is suggested for the concrete tanks beyond 12 000 AD.

Slab

The evolution of the hydraulic conductivity of the slabs in 1–2BTF are expected to follow a similar trend as that of the slab, inner walls and existing outer walls in 1BMA during the entire assessment period for both the *Slightly cracked case* and the *cracked case.* This is motivated by the fact that similar concrete and construction method are expected to have been used for the slabs in 1–2BTF as in 1BMA.

Lid

The evolution of the hydraulic conductivity of the lids in 1–2BTF (*Slightly cracked case*) are expected to resemble that of the new outer walls and lid in 1BMA during the entire assessment period.

For the *cracked case* an initial hydraulic conductivity of 1×10^{-5} m/s is selected and because of anticipated degradation, a value of 1×10^{-3} m/s is selected for the final part of the assessment period.

Cementitious backfill

The evolution of the hydraulic conductivity of the cementitious backfill between the waste packages and the vault walls in 1–2BTF (*Slightly cracked case*) are expected to resemble that of the new outer walls and lid in 1BMA during the entire assessment period.

For the *cracked case* an initial hydraulic conductivity of 1×10^{-5} m/s is selected and because of anticipated degradation, a value of 1×10^{-3} m/s is selected for the final part of the assessment period.

Concrete tanks and moulds

The evolution of the hydraulic conductivity of the concrete tanks in 1–2BTF (*Slightly cracked case*) are expected to resemble that of the new outer walls and lid in 1BMA during the entire assessment period.

For the *cracked case* an initial hydraulic conductivity of 1×10^{-5} m/s is selected and because of anticipated degradation, a value of 1×10^{-3} m/s is selected for the final part of the assessment period.

Grout

The evolution of the hydraulic conductivity (*Slightly cracked case*) of the grout between the waste packages in 1–2BTF is expected to follow that of the grout in the silo during the entire assessment period. For the *cracked case*, the evolution of the hydraulic conductivity of the grout follows that of the concrete tanks and moulds in 1–2BTF.

1–5BLA

The evolution of the hydraulic conductivity of the slabs in 1–5BLA are suggested to follow that of the slab in 1BMA and 1–2BTF.

Table 9-5. Data on hydraulic conductivities for the cementitious components in SFR for different time periods and waste vaults suggested by the supplier to be used in the assessment.

	Hydraulic conductivity (m/s) for time periods (AD)				
Silo	**2000–2050**	**2050–2500**	**2500–22 000**	**22 000–100 000**	
Outer and inner walls, lid and slab	8.3×10^{-10}	4×10^{-9}– 7×10^{-7}	1×10^{-6}– 2×10^{-5}	1×10^{-6}– 2×10^{-5}	
Grout	5×10^{-9}	4×10^{-7}	4×10^{-5}	4×10^{-5}	
Concrete moulds	8.3×10^{-10}	4×10^{-9}– 7×10^{-7}	1×10^{-6}– 2×10^{-5}	1×10^{-6}– 2×10^{-5}	
1BMA	**2000**	**2000–2100**	**2100–22 000**	**22 000–52 000**	**52 000–100 000**
Existing outer walls, inner walls and slab (1BMA concrete)	1×10^{-5}	1×10^{-5}	1×10^{-5}	1×10^{-3}	1×10^{-3}
New outer walls and lid (2BMA concrete)	8.3×10^{-10}	5×10^{-9}– 5×10^{-8}	5×10^{-8}– 5×10^{-7}	5×10^{-7}– 5×10^{-6}	$5 \times 10^{-6} – 5 \times 10^{-5}$
Concrete moulds	8.3×10^{-10}	5×10^{-9}– 5×10^{-8}	5×10^{-8}– 5×10^{-7}	5×10^{-7}– 5×10^{-6}	$5 \times 10^{-6} – 5 \times 10^{-5}$
2BMA	**2000**	**2000–2100**	**2100–22 000**	**22 000–52 000**	**52 000–100 000**
Outer walls, lid and slab (2BMA concrete)	8.3×10^{-10}	5×10^{-9}– 5×10^{-8}	5×10^{-8}– 5×10^{-7}	5×10^{-7}– 5×10^{-6}	5×10^{-6}– 5×10^{-5}
Grout in gas evacuation channels	5×10^{-9}	5×10^{-7}	5×10^{-5}	5×10^{-4}	1×10^{-3}
Concrete moulds	8.3×10^{-10}	5×10^{-9}– 5×10^{-8}	5×10^{-8}– 5×10^{-7}	5×10^{-7}– 5×10^{-6}	5×10^{-6}– 5×10^{-5}
1BRT	**2000**	**2000–2100**	**2100–22 000**	**22 000–100 000**	
Outer walls and inner walls, lid and slab	1×10^{-5}	1×10^{-5}	1×10^{-5}	1×10^{-3}	
Concrete between waste packages	1×10^{-5}	1×10^{-5}	1×10^{-5}	1×10^{-3}	
1–2BTF (Slightly cracked case)	**2000–2100**	**2100–3000**	**3000–12 000**	**12 000–22 000**	**22 000–100 000**
Slab	1×10^{-5}	1×10^{-5}	1×10^{-5}	1×10^{-4}	1×10^{-3}
Lid	5×10^{-9}– 5×10^{-8}	5×10^{-8}– 5×10^{-7}	5×10^{-8}– 5×10^{-7}	5×10^{-8}– 5×10^{-7}	5×10^{-7}– 5×10^{-5}
Grout	5×10^{-9}	4×10^{-7}	4×10^{-5}	4×10^{-5}	4×10^{-5}
Concrete tanks and moulds	8.3×10^{-10}	8.3×10^{-8}	5×10^{-8}– 5×10^{-7}	5×10^{-8}– 5×10^{-7}	5×10^{-7}– 5×10^{-5}
Cementitious backfill	5×10^{-9}– 5×10^{-8}	5×10^{-8}– 5×10^{-7}	5×10^{-8}– 5×10^{-7}	5×10^{-8}– 5×10^{-7}	5×10^{-7}– 5×10^{-5}

Table 9-5. Continued.

	Hydraulic conductivity (m/s) for time periods (AD)				
1–2BTF (Cracked case)	**2000–2100**	**2100–3000**	**3000–12 000**	**12 000–22 000**	**22 000–100 000**
Slab	1×10^{-5}	1×10^{-5}	1×10^{-5}	1×10^{-4}	1×10^{-3}
Lid	1×10^{-5}	1×10^{-5}	1×10^{-4}	1×10^{-4}	1×10^{-3}
Grout	1×10^{-5}	5×10^{-5}	5×10^{-4}	1×10^{-3}	1×10^{-3}
Concrete tanks and moulds	1×10^{-5}	1×10^{-5}	1×10^{-4}	1×10^{-3}	1×10^{-3}
Cementitious backfill	1×10^{-5}	1×10^{-5}	1×10^{-4}	1×10^{-4}	1×10^{-3}
1–5BLA	**2000**	**2000–2100**	**2100–22 000**	**22 000–52 000**	**52 000–100 000**
Slab	1×10^{-5}	1×10^{-5}	1×10^{-5}	1×10^{-3}	1×10^{-3}

9.10.3 Hydraulic conductivity data for the crushed rock backfill

The hydraulic conductivity of the planned backfill material (macadam 16–32 mm) has recently been measured and found to be 0.29 ± 0.08 m/s (Lagerlund 2020) and 0.23 m/s (Lagerlund 2022). The same value as was used in the SR-PSU (10^{-3} m/s) for the whole assessment period is suggested by the supplier to be used also in the PSAR. This choice gives some margin for uncertainties related to clogging of the backfill that potentially could reduce the hydraulic conductivity.

9.11 Judgements by the assessment team

In this section the assessment team presents its judgement on the data qualification made by the supplier to verify that it is sufficient for the safety assessment.

Sources of information

The assessment team agrees with the sources of information used in Section 9.4.

Conditions for which data is supplied

The assessment team finds the conditions given in Section 9.5 valid and reflecting the conditions assumed in the repository.

Conceptual modelling uncertainty

The assessment team agrees with the given uncertainties in Section 9.6.

Data uncertainty – precision, bias, and representativity

The assessment team agrees with the given uncertainties in Section 9.7. The spatial variability of the porosity introduces additional uncertainties in the representability, see the following section.

Data uncertainty – spatial and temporal variability

The assessment team agrees with the given variabilities given in Section 9.8. The spatial variability of the porosity introduces uncertainty when it comes to estimating the cement fraction within the concrete structures. The assessment team agrees with the statements regarding the need for further research, given in Section 9.8.

Data uncertainty – correlations

The correlations mentioned in Section 9.9 are valid in the safety assessment. Since the porosities and hydraulic conductivities are not treated probabilistically no correlations between hydraulic conductivity, porosity or other data in the assessment modelling are considered.

Results of supplier's data qualification

The assessment team considers the data given in Tables 9-4 and 9-5 in combination with the information provided by the supplier in the previous sections sufficient for use in the recommendation of data for the safety assessment. However, minor modifications to adapt the data to the modelling are recommended in Section 9.12.

9.12 Data recommended for use in the assessment

9.12.1 Porosity data

The porosity data recommended by the assessment team for use in the PSAR are given in Table 9-6 and are also discussed separately for each individual waste vault in the following sections.

The recommendations are mainly based on the following sources:

- Values suggested by the supplier in Table 9-5.
- Values suggested in the SR-PSU Data report (SKB TR-14-10, Table 10-4).

Silo

The recommended initial porosity for the concrete structure is 0.11 (same value as suggested in Table 9-4). This value is considered to be valid until 3000 AD. From 3000 AD until 22 000 AD the recommended porosity is 0.14 (within the range of the suggested values). Between 22 000 AD and 52 000 AD the recommended porosity is 0.18 (within the range of the suggested values). After 52 000 AD until the end of the assessment period the recommended porosity is 0.3 (the same as recommended for other structural concrete in SFR, although a lower porosity is suggested by the supplier).

The porosity for the grout in the silo is recommended to be 0.3 for the whole assessment period, as suggested by the supplier in Table 9-4. The porosity for the concrete in the concrete moulds is recommended to be 0.11 for the whole assessment period as suggested by the supplier in Table 9-4.

1BMA existing outer walls, slab and inner walls

A recent summary of the available information of the structural concrete used for 1BMA shows that the cement content in the existing structure is lower than was reported as initial state in SR-PSU (Elfwing et al. 2015). The recommended initial porosity is 0.14 (as in Table 7-8 and also the average of the suggested values (0.11–0.16) for these components for the time period 2100 AD to 22 000 AD in Table 9-4). This value is recommended to be valid until 22 000 AD.

Between 22 000 AD and 52 000 AD the recommended porosity is 0.18 (the average of the suggested values (0.16 – 0.20) for these components during this time period).

After 52 000 AD until the end of the assessment period the recommended porosity is 0.3 (the same as in Table 9-4). All these porosities and time periods are consistent with what was used in the updated analysis of the post-closure safety of 1BMA (Elfwing et al. 2018).

1BMA new outer walls, lid and concrete moulds

The recommended initial porosity for the new outer walls, lid and concrete moulds in 1BMA is 0.11 (same value as suggested in Table 9-4), this value is considered to be valid until 3000 AD.

From 3000 AD to the end of the assessment period the porosity for these components are recommended to be the same as for the existing 1BMA concrete structure.

2BMA

As the same concrete will be used in the concrete structures in 2BMA is in the repair measures in 1BMA the same porosities are recommended. Also, the concrete moulds are recommended the same porosities.

1BRT

For 1BRT the recommended porosities for the structural concrete are the same as for the existing structural concrete in 1BMA.

For the concrete between the waste packages in 1BRT the same values as for the grout in the silo are recommended until 12 000 AD. Thereafter the same values as recommended for grout in 1BMA in Table 10-4 in SKB (TR-14-10) is recommended. These values do exceed the limit for the maximum porosity in concrete when all cement minerals have been dissolved. The motivation for using such high values is that physical degradation processes will affect the uncertainty in the spatial variability of the porosity to such an extent that a pessimistic choice of values is motivated. The suggested values in Table 9-4 reflect that the reference design recently has been specified to a concrete with lower porosity.

1–2BTF

The porosity for the slab and lid in 1–2BTF between 2000 AD and 3000 AD is recommended to be the same as for the existing walls and slab in 1BMA. The recommended porosity for the slab and lid after 3000 AD is that suggested by the supplier for the cracked case Table 9-4.

The porosities for the grout between waste packages and cementitious backfill is recommended to be the same as the values given for the grout in BTF in Table 10-4 in SKB (TR-14-10). These values do exceed the limit for the maximum porosity expected in concrete when all cement minerals have been dissolved. The motivation for using such high values is that physical degradation processes will affect the uncertainty in the spatial variability of the porosity to such an extent that a pessimistic choice of values is motivated. The suggested values in Table 9-4 reflect that the reference design for the cementitious backfill recently has been specified to a concrete with lower porosity.

The recommended porosities for the concrete tanks and moulds are those suggested by the supplier in Table 9-4.

Table 9-6. Data on porosities for the different cementitious components in SFR recommended by the assessment team for use in the PSAR.

	Porosity (–) for time periods (AD)					
	2000–2100	**2100–3000**	**3000–12 000**	**12 000–22 000**	**22 000–52 000**	**52 000–100 000**
Silo						
Concrete structure	0.11	0.11	0.14	0.14	0.18	0.3
Grout	0.3	0.3	0.3	0.3	0.3	0.3
Concrete moulds	0.11	0.11	0.11	0.11	0.11	0.11
1BMA						
Existing outer walls, slab and inner walls	0.14	0.14	0.14	0.14	0.18	0.3
New outer walls and lid	0.11	0.11	0.14	0.14	0.18	0.3
Concrete moulds	0.11	0.11	0.14	0.14	0.18	0.3
2BMA						
Outer walls, lid and slab	0.11	0.11	0.14	0.14	0.18	0.3
Concrete moulds	0.11	0.11	0.14	0.14	0.18	0.3

Table 9-6. Continued.

1BRT						
Slab, outer walls, lid, inner walls	0.14	0.14	0.14	0.14	0.18	0.3
Concrete between waste packages	0.3	0.3	0.3	0.4	0.5	0.5
1–2BTF						
Slab and lid	0.14	0.14	0.2	0.3	0.3	0.3
Grout between waste packages	0.2	0.2	0.4	0.5	0.5	0.5
Cementitious backfill	0.2	0.2	0.4	0.5	0.5	0.5
Concrete tanks and moulds	0.11	0.11	0.2	0.3	0.3	0.3

9.12.2 Hydraulic conductivity data for cementitious components

The hydraulic conductivities for the cementitious components recommended for use in the assessment by the assessment team are summarised in Table 9-7.

The recommendations are mainly based on the following sources:

- Values suggested by the supplier in Table 9-5.
- Calculated values from Höglund (2014) shown as curves in Figure 9-4 and 9-5 (same curve in both figures).
- Value ranges proposed by Höglund (2014) shown in Figure 9-4 and 9-5.

In Table 9-7, hydraulic conductivities are given for four degradation states; intact, moderately degraded, severely degraded and completely degraded as well as the time periods for the states in the main scenario. The transition times in Table 9-7 are important input data to the radionuclide transport calculations as explained in Chapter 7 in the **Post-closure safety report**.

Cementitious materials in general

Over time, as concrete physically degrades, the hydraulic conductivity values of the concrete structures change between values representative of different degradation states. The basis for the degradation states in general are that the concrete barriers are assigned to have an initial hydraulic conductivity of 10^{-9} m/s and for each degradation state the hydraulic conductivities of the structures are increased by two orders of magnitude until the limiting value of 10^{-3} m/s is reached. Stepwise changes are not entirely based on degradation processes, but also made to simplify the modelling of near-field flow and radionuclide transport.

The transition between the physical concrete degradation states is assumed to occur at different times for different vaults since the impact of different degradation processes varies between the vaults. Different concrete structures within a vault can degrade at different rates, for example the concrete in a concrete barrier can be in a different degradation state compared with the concrete waste packages within the same vault.

Hydraulic conductivity data suggested by the supplier in Table 9-5 has been used to define a set of degradation states for the different vaults and their subcomponents. The vault degradation states are named *intact* (base case in Abarca et al. (2020)), *moderately degraded, severely degraded and completely degraded* given by the state of the main flow barrier in the vault. The details in the implementation of the different degradation states are given in Abarca et al. (2020, Appendix A).

The hydraulic conductivities recommended by the assessment team for use in the assessment are presented in Table 9-7.

Silo

Outer and inner walls, slab and lid

The recommended average hydraulic conductivity of the outer and inner walls, slab and lid between 2000 AD and 3000 AD is 1×10^{-7} (m/s) (within the range of the values suggested by the supplier for these structural components between 2050 AD and 2500 AD Table 9-5).

Between 3000 AD and 52 000 AD the recommended conductivity is 1×10^{-5} (m/s) (within the range of the values suggested by the supplier for these structural components in Table 9-5). After 52 000 AD to the end of the assessment period the recommended conductivity is 1×10^{-3} (m/s) (higher than suggested in Table 9-5).

Sand in gas evacuation channels

The silo lid is equipped with gas evacuation channels filled with sand. Although not formally a cementitious component the sand in the gas evacuation channels is a required in the near-field hydrological calculations, the recommended conductivity for the sand is 1×10^{-4} m/s.

Grout and concrete moulds

Details in the implementation of the hydraulic conductivities in the waste domain are given in Abarca et al. (2020, Appendix A).

1BMA

Existing outer walls, slab and inner walls

The values suggested by the supplier for the existing outer walls, slab and inner walls in 1BMA in Table 9-5 are recommended, these values are consistent with what was used in the updated analysis of the post-closure safety for 1BMA (Elfwing et al. 2018).

New outer walls and lid

The initial hydraulic conductivity of new outer walls and lid in 1BMA is recommended to be 8.3×10^{-10} (m/s) (the initial values suggested by the supplier for these structural components in Table 9-5). This value is assumed to be valid until 3000 AD, because no cracks are expected to form during resaturation.

Between 3000 AD and 22 000 AD the recommended conductivity is 1×10^{-7} m/s (within the range of the values suggested by the supplier in Table 9-5). Between 22 000 AD and 52 000 AD the recommended conductivity is 1×10^{-5} m/s (higher than the range of the suggested values in Table 9-5). After 52 000 AD to the end of the assessment period the recommended conductivity is 1×10^{-3} m/s (higher than the range of the suggested values in Table 9-5). The hydraulic conductivities are consistent with the partial repair case in the updated analysis of the post-closure safety for 1BMA (Elfwing et al. 2018).

Concrete moulds

The main assumption made in the SR-PSU and in the PSAR concerning the hydraulic properties of the waste in 1BMA is that the waste does not constitute a flow barrier (Abarca et al. 2013, 2014). In the PSAR the hydraulic conductivity of the waste in 1BMA is assumed to be even higher than in the SR-PSU. The details in the implementation of the hydraulic conductivities in the waste domain are given in Abarca et al. (2020, Appendix A).

2BMA

Outer walls, lid and slab

The recommended initial conductivity of the 2BMA concrete used in slab, lid and outer walls is 1×10^{-9} m/s (close to the suggested values for these structural components in Table 9-5). The initial value is assumed to be valid until 3000 AD because no cracking is considered to occur during resaturation.

For the rest of the assessment period the conductivity of the structural concrete in 2BMA is recommended to be the same as for the concrete in the new outer walls and lid in 1BMA.

Grout in gas evacuation channels

The values suggested by the supplier for grout in the gas evacuation channels between 2000 AD and 3000 AD, see Table 9-5, are recommended. Between 3000 AD and 22 000 AD the conductivity of the gas evacuation channels is recommended to be one order of magnitude higher than for the structural concrete. From 22 000 AD the hydraulic conductivity of the gas evacuation channels is recommended to be the same as that of the structural concrete.

Concrete moulds

The main assumption made in the SR-PSU and in the PSAR concerning the hydraulic properties of the waste in 2BMA is that the waste does not constitute a flow barrier (Abarca et al. 2013, 2014). In the PSAR the hydraulic conductivity of the waste in 2BMA is assumed to be even higher than in the SR-PSU. The details in the implementation of the hydraulic conductivities in the waste domain are given in Abarca et al. (2020, Appendix A).

1BRT

In the near-field hydrological model an average hydraulic conductivity of the concrete structure surrounding the waste and its interior was used for 1BRT (Abarca et al. 2020).

The recommended average hydraulic conductivity of the lid, outer and inner walls and grouted waste between 2000 AD and 52 000 AD is 1×10^{-4} m/s. The recommended conductivity for the slab between 2000 AD and 52 000 AD is 1×10^{-5} m/s (representative for cracked concrete). After 52 000 AD until the end of the assessment period the recommended conductivity for the concrete structure and the slab is 1×10^{-3} (m/s).

1–2BTF

Slab, lid and concrete tanks and moulds

The recommended average hydraulic conductivity of the slabs, lids, concrete tanks and moulds in 1–2BTF between 2000 AD and 3000 AD is 1×10^{-7} (m/s) (in-between the suggested values for the tanks in the *slightly cracked case* and *cracked case* in Table 9-5). Between 3000 AD and 12 000 AD the recommended conductivity is 1×10^{-5} (m/s) (in-between the suggested values for the tanks in the *slightly cracked case* and *cracked case* in Table 9-5). After 12 000 AD until the end of the assessment period the recommended conductivity is 1×10^{-3} (m/s) (the same as the suggested value between 22 000 AD and 100 000 AD for the *cracked case* in Table 9-5).

Grout, cementitious backfill

The recommended average hydraulic conductivity of the grout between the waste packages and the cementitious backfill between the rock wall and waste packages between 2000 AD and 3000 AD is 1×10^{-6} (m/s) (in-between the suggested values for the grout and cementitious backfill in the *slightly cracked case* and *cracked case* in Table 9-5). Between 3000 AD and 12 000 AD the recommended conductivity is 1×10^{-4} (m/s) (the same as the suggested value the cementitious backfill (*cracked case*) in Table 9-5). After 12 000 AD to the end of the assessment period the recommended conductivity is 1×10^{-3} (m/s) (the same as the suggested value for the cementitious backfill between 22 000 AD and 100 000 AD (*cracked case*) in Table 9-5).

Details in the implementation of the hydraulic conductivities in the waste domain are given in Abarca et al. (2020, Appendix A).

1–5BLA

The slabs in 1–5BLA do not constitute a flow barrier, and the hydraulic conductivities recommended are therefore cautiously chosen. For simplicity, a constant hydraulic conductivity for moderately degraded concrete, 1×10^{-7} m/s is recommended for the whole assessment period. The near-field hydrological calculations have been performed for all degradation states and the water flow rates are only 3 % higher for completely degraded concrete. Hence, this simplification is judged to be acceptable.

Table 9-7. Hydraulic conductivity (m/s) of cementitious components is SFR recommended by the assessment team for use in the PSAR.

	Hydraulic conductivity (m/s) for time periods (AD) Degradation state			
	Intact	**Moderate**	**Severe**	**Complete**
Silo		**2000–3000**	**3000–52 000**	**52 000–100 000**
Outer and inner walls, slab and lid	1.0×10^{-9}	1.0×10^{-7}	1.0×10^{-5}	1.0×10^{-3}
Sand in gas evacuation channels	1.0×10^{-4}	1.0×10^{-4}	1.0×10^{-4}	1.0×10^{-4}
1BMA	**2000–3000**	**3000–22 000**	**22 000–52 000**	**52 000–100 000**
Existing outer walls, slab and inner walls (1BMA concrete)	1.0×10^{-5}	1.0×10^{-5}	1.0×10^{-3}	1.0×10^{-3}
New outer walls and lid (2BMA concrete)	8.3×10^{-10}	1.0×10^{-7}	1.0×10^{-5}	1.0×10^{-3}
2BMA	**2000–3000**	**3000–22 000**	**22 000–52 000**	**52 000–100 000**
Outer walls, lid and slab (2BMA concrete)	1.0×10^{-9}	1.0×10^{-7}	1.0×10^{-5}	1.0×10^{-3}
Grout in gas evacuation channels	5.0×10^{-9}	1.0×10^{-6}	1.0×10^{-5}	1.0×10^{-3}
1BRT			**2000–52 000**	**52 000–100 000**
Concrete structure and grouted waste	1.0×10^{-8}	1.0×10^{-6}	1.0×10^{-4}	1.0×10^{-3}
Slab	1.0×10^{-9}	1.0×10^{-7}	1.0×10^{-5}	1.0×10^{-3}
1–2BTF		**2000–3000**	**3000–12 000**	**12 000–100 000**
Slab and lid	1.0×10^{-9}	1.0×10^{-7}	1.0×10^{-5}	1.0×10^{-3}
Grout	1.0×10^{-8}	1.0×10^{-6}	1.0×10^{-4}	1.0×10^{-3}
Cementitious backfill	1.0×10^{-8}	1.0×10^{-6}	1.0×10^{-4}	1.0×10^{-3}
Concrete tanks and moulds	1.0×10^{-9}	1.0×10^{-7}	1.0×10^{-5}	1.0×10^{-3}
1–5BLA	Concrete degradation is not included in the radionuclide transport model of 1–5BLA, only the moderately degraded case is used.			
Concrete slab	1.0×10^{-9}	1.0×10^{-7}	1.0×10^{-5}	1.0×10^{-3}

9.12.3 Hydraulic conductivity of crushed rock backfill

The hydraulic conductivity of the planned backfill material (macadam 16–32 mm) is recommended to be 10^{-3} m/s for the whole assessment period, as suggested by the supplier in Section 9.10.3.

10 Cementitious components diffusivity data

This chapter concerns the effective diffusivity of radionuclides in the cementitious components in SFR such as structural concrete in structures and waste packaging, cementitious materials used around the waste packages in the silo, 1BRT and 1–2BTF vaults as well as conditioning material for the waste (**Initial state report**).

For further details concerning the cementitious components and materials used in SFR, see the introduction to Chapter 9.

10.1 Modelling in this safety assessment

This section describes the data expected from the supplier, and in what modelling activities the data are to be used.

Defining the data requested from the supplier

The supplier should deliver data for the effective diffusivity D_e (m^2/s) for the cementitious materials in SFR defined in the bullet list below. Data should be supplied for different chemical and mechanical degradation states covering the span from fresh to completely degraded.

- **Silo**: Outer and inner walls, slab lid, concrete moulds, grout.
- **1BMA**: Existing outer walls, new outer walls, slab, lid, concrete moulds.
- **2BMA**: External concrete structure, inner walls, concrete moulds, grout in gas evacuation channels.
- **1BRT**: Outer walls, slab, lid, inner walls, concrete between waste containers.
- **1**–**2BTF**: Slab, lid, concrete tanks, concrete moulds, grout, cementitious backfill.
- **1**–**5BLA**: Slab.

Based on the degradation states it is possible to set up scenarios that define at which timepoints the changes between the degradation states occur. Even though the timing of the expected transition between degradation states is not explicitly required from the supplier, the supplied data must be sufficient to define the timepoints of the transitions between states.

Modelling activities in which data will be used

The effective diffusivity of the cementitious components is used as input to the radionuclide transport calculations. The modelling chain and general methodology used to calculate the radionuclide transport are described in the **Radionuclide transport report**.

10.2 Experience from previous safety assessments

This section briefly summarises experience gained from the previous safety assessments, SAFE, SAR-08 and SR-PSU which may be of direct consequence for the data qualification in this data report.

Modelling in previous safety assessments

Calculation of radionuclide release including transport by diffusion has been an important part of all previous safety assessments for SFR.

Conditions for which data were used in previous safety assessments

Previous safety assessments for SFR presented values for effective diffusivity in fresh, aged and degraded SFR concrete; the values were selected using relevant literature data as a guide. The diffusivity data have not been assessed specifically in terms of concrete crack size or density (as opposed to degradation), and the impact of cracks has been assessed with a focus on increased flow.

For reference, concrete degradation states are defined as follows (for more details; see Section 7.4):

State I: Corresponds to fresh hydrated concrete. Alkali metal hydroxides leach out causing the porewater pH to be above 12.5.

State II: The concrete porewater is controlled by the dissolution of portlandite to a pH of 12.5.

State III: Portlandite is exhausted, and the pH is buffered by the incongruent dissolution of CSH phases. The pH of the porewater gradually decreases from 12.5 to about 10.5 as CSH phases lose Ca.

In the SAFE safety assessment, a general assumption for the Base Scenario was that the state of barriers at repository closure was in accordance with their design criteria (SKB R-01-14). Since Höglund (2001) calculated that the concrete barriers would only become completely depleted of CSH phases to a depth of 0.2 m in the 10 000-year period considered in SAFE, the effective diffusivity was considered to be constant over time. The value for the effective diffusivity was representative of State II (SKB R-01-14) of concrete degradation.

Cementitious grout has a higher porosity than structural concrete due to its higher w/c ratio. For that reason, the effective diffusivity in the grouts was considered to be ten times higher than that of the structural concrete. In the SAFE analysis the same diffusivity was assigned for the silo grout (30 % porosity) as for the BTF grout (20 % porosity) although the diffusivity in the BTF grout would be expected to be somewhat lower. The scenario analysis that addressed the possibility of initial defects in the engineered barriers focussed on increased water flow, thus the diffusivity was not altered in the calculations.

In the SAR-08 safety assessment (Thomson et al. 2008), the diffusivity assigned to the structural concrete was lower than that used in SAFE and was a typical value for State I of concrete degradation. However, since radionuclide transport was calculated over a longer time period in this assessment, the diffusivity was increased by a factor of ten for the period from 66 000 years post-closure onwards. Again, since cementitious grout has a higher porosity than structural concrete, an initial diffusivity ten times higher than for concrete after 66 000 years was assigned for the cementitious grouts in SFR. This diffusivity was used throughout the time period considered. The project included assessments of the effects of early barrier failure but, as with SAFE, this did not account for any changes in diffusivity.

In the SR-PSU safety assessment a more detailed temporal evolution of the diffusivity during the post-closure period was assigned to the structural concrete than in SAFE and SAR-08 with different values assigned for different time periods (SKB TR-14-09).

Sensitivity to assessment results in previous safety assessments

The use of a lower initial effective diffusivity for structural concrete in SAR-08 reduced the calculated release of radionuclides relative to SAFE. The sudden increase in the diffusivity of the structural concrete assumed in the SAR-08 safety assessment model is caused by the assumed failure of the barriers, thus it is accompanied by a sudden increase in the water flow. It was calculated by Holmén and Stigsson (2001a) and Holmén (2005, 2007) that failed barriers in sections of the vaults would lead to a two to three times higher flow in the BLA and BMA vaults, and a somewhat smaller flow in the BTF vaults as result of the changed flow direction in the vaults. These changes make it difficult to assess the sensitivity of the analyses to the change in the diffusivity of the concrete barriers alone.

In the SR-PSU safety assessment the sensitivity of the radionuclide release to increased diffusivity of concrete structures caused by concrete degradation was assessed in the accelerated concrete degradation scenario.

Alternative modelling in previous safety assessments

No alternative modelling was reported in SAFE, SAR-08 or SR-PSU.

Correlations used in previous safety assessment modelling

Correlations between the degradation, the effective diffusivities and the radionuclide migration from the waste vaults were used both in SAFE and SAR-08 as well as in SR-PSU. Since other data affected by concrete degradation such as porosities and hydraulic conductivities were not treated probabilistically no correlations between diffusivity and any other data in the assessment modelling was considered.

Identified limitations of the data used in previous safety assessment modelling

The diffusivity used in SAR-08 for the first 66 000 years post closure is representative of fresh concrete, and thus is likely to underestimate diffusion in this period. The tenfold increase in the diffusivity after 66 000 years gives a diffusivity in the range representative of intact concrete in the portlandite leaching stage, whereas the concrete would be expected to be significantly degraded by this point.

The diffusivities used in SR-PSU were more reflective of the expected temporal evolution of the different cementitious materials and degradation states than those used in the SAR-08.

No specific diffusivity data were recommended for the concrete structure in 1BRT and the design of 1BMA has been altered.

10.3 Supplier input on use of data in this and previous safety assessments

10.3.1 Overview

When selecting representative data for the effective diffusivity of the cementitious components for the different time periods covered in the safety assessment, detailed knowledge about the concrete mix proportions is essential as this determines the initial porosity of the material. Further, also detailed understanding of the different degradation mechanisms is required as this determines the evolution of porosity in the material as well as the risk for formation of cracks and thus both the diffusivity and hydraulic conductivity.

The influence of both porosity and presence of cracks on the effective diffusivity has been investigated by Höglund (2014) and is shown in Figures 10-1 and 10-2. From Figure 10-1, the effective diffusivity of standard concrete with a porosity of about 12 % (corresponding to a concrete with a w/c ratio of about 0.5) is about 3×10^{-12} m^2/s.

Figure 10-2 shows that the formation of cracks does not have a dramatic influence on the effective diffusivity of the concrete as long as the distance between the cracks does not fall below one metre. As a comparison, an inspection of cracks in the concrete walls in 1BMA shows that the distances between cracks are considerably larger than one metre (Hejll et al. 2012).

In the SAFE safety assessment, a general assumption for the Base Scenario was that the state of the barriers at repository closure was in accordance with design criteria (SKB R-01-14). The structural concrete is a high-quality concrete with the purpose of providing high mechanical strength, which also means that the effective diffusivity will be very low.

The low w/c ratio of the different types of concrete used in the concrete structures in SFR (Table 7-1) will give a low porosity with a low pore connectivity. At full hydration of the cement minerals, the major part of the porosity will be gel pores and contraction pores, both of which would present a high degree of tortuosity and thus low effective diffusivity, whereas the capillary porosity is low. Capillary pores enable greater diffusive transport through the cement phase.

The diffusivities encountered for concrete in SFR safety assessments only range over three orders of magnitude; species have a fairly low diffusivity in water (2×10^{-9} m^2/s), and it is reasonable to

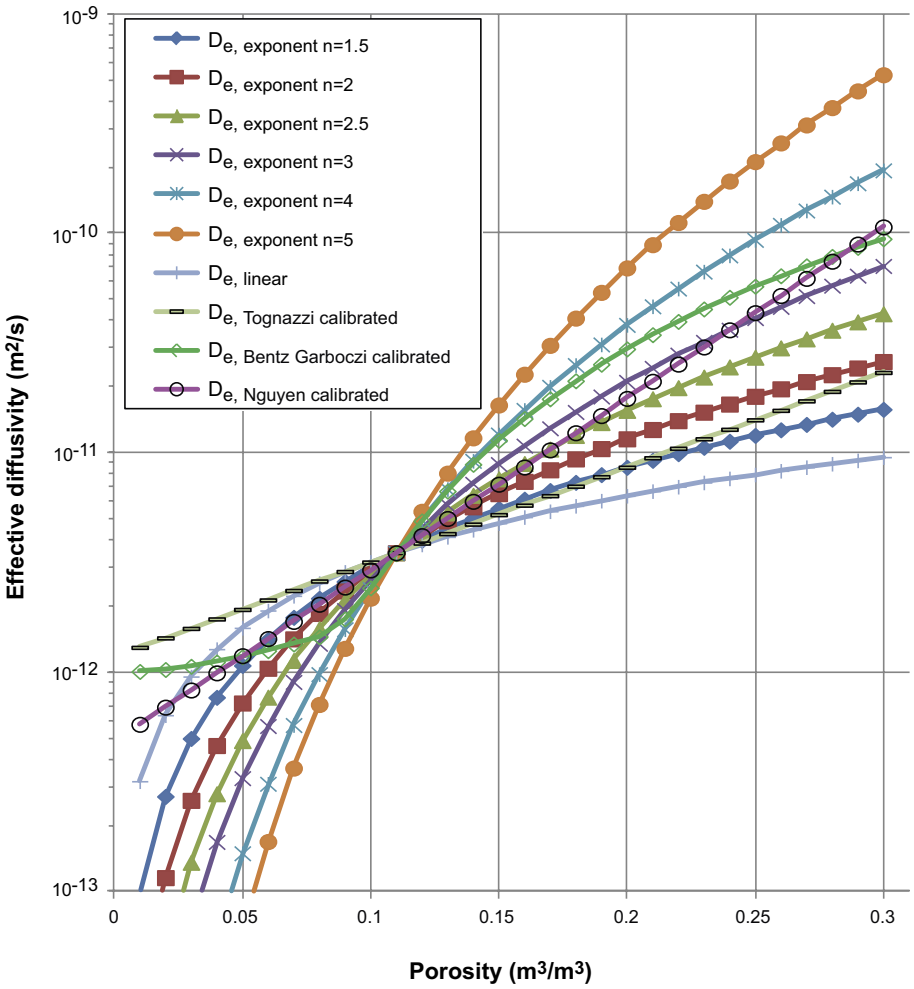

Figure 10-1. *Effective diffusivity as a function of porosity for different suggested relationships (Höglund 2014).*

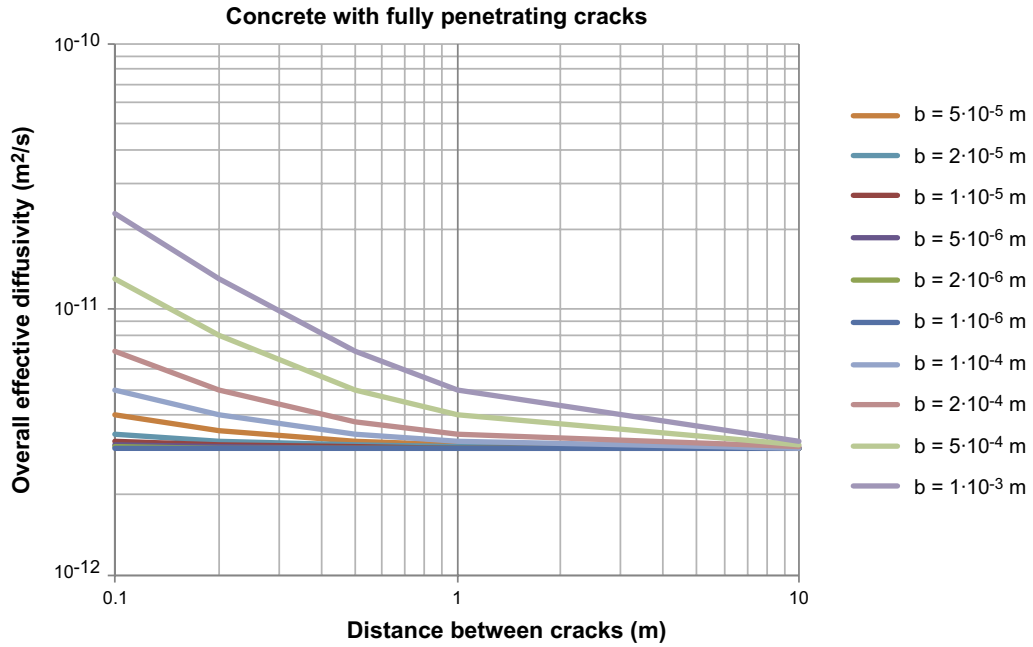

Figure 10-2. *Effective diffusivity of a concrete structure with fully penetrating cracks as a function of distance between cracks and crack aperture, b, and considering an effective diffusivity of 3×10^{-12} m/s in intact concrete. (Höglund 2014).*

expect that the effective diffusivity of a fresh, fully hydrated concrete, produced according to the mix proportions used for structural concretes in SFR, would be on the order of 3×10^{-12} m^2/s as shown in Figure 10-1. However, as shown in Figure 10-2, the presence of cracks in the concrete structures will increase the overall effective diffusivity of the material in question even though not as dramatically as for the hydraulic conductivity as shown in Figure 9-2.

The implications of a more cracked concrete at an early stage are an increased overall porosity of the barriers (and the waste) after closure, and as a result, an increased effective diffusivity and an increased rate of chemical degradation due to faster diffusion exchange of dissolved components. Hence, significant early cracking would change the basis for the assessment of the chemical degradation of the concrete barriers.

As a consequence of the consideration that cracks can form during all periods of the lifetime of the repository, it is judged necessary that the selection of effective diffusivities should reflect the observed and likely occurrence of cracks. This means that the overall effective diffusivities of the corresponding concrete barriers must be assumed to be higher than in intact concrete. For the SR-PSU it was therefore considered necessary to update the data selected in the SAFE and SAR-08 studies describing the effective diffusivity of different concrete structures in SFR.

10.3.2 Updates since the previous safety assessment

The new information motivating the updates of hydraulic conductivity and porosity data for PSAR is presented separately for each waste vault in Section 9.3 also motivates updates of the diffusivity data. The reader is therefore referred to Section 9.3 for more details.

10.4 Sources of information and documentation of data qualification

Sources of information

In general, specific data for the cementitious materials and components in SFR are scarce, in particular and for obvious reasons, no data exist for these materials and components in aged and degraded states. The safety assessments have therefore been based on judgements of reasonable data sets from typical structural concretes and different modelling approaches to estimate the diffusivity. See also Section 10.2.

In Table 10-1 some data from different sources have been compiled.

Table 10-1. Some data on effective diffusivities of concrete from safety assessments, literature and model estimates. Included are also measurements of the diffusivity increase factor when comparing cracked and uncracked concrete.

Material	Effective diffusivity (m^2/s)	Diffusivity increase factor due to ageing or cracking*	Type of data	Source
SFR Structural concrete				
Fresh structural concrete (porosity 15 %)	3×10^{-12}	10 (aged); 300 (degraded)	Data report	SKB R-01-14
Structural concrete in the silo, stage I of concrete degradation	3×10^{-12}	10 (state II); 300 (state III)	Performance assessment	Höglund and Bengtsson 1991
Structural concrete in BMA (equivalent to stage II of concrete degradation)	3×10^{-11}	30 (after 1 000 years)	Performance assessment	Höglund and Bengtsson 1991
Structural concrete (porosity 15 %)	1×10^{-11}	None, this represents State II	Performance assessment	Höglund 2001
Uncracked structural concrete (porosity 15 %)	1×10^{-11}	None, this represents State II	Safety assessment	SKB R-01-14
Structural concrete (silo, BMA and BTF) stage I of concrete degradation	2.5×10^{-12}	10 (state II); 200 (state III)	SKI data report	Savage and Stenhouse 2002
Structural concrete (silo, BMA and BTF)	3×10^{-12}	10 (after 66 000 years)	Safety assessment	Thomson et al. 2008
Structural concrete (silo and BMA)	1×10^{-11}	2−5 every freeze-thaw cycle	Performance assessment	Cronstrand 2007
Structural concrete in the silo	1.5×10^{-11}	Diffusivity of all materials was related to porosity using a pore diffusivity of 1×10^{-10}		Gaucher et al. 2005
2BMA concrete	5×10^{-12}	-	Measurement	Villar et al. 2019
1BMA concrete	8×10^{-12}	-	Measurement	Villar et al. 2019
SFR backfill grout				
Porous concrete (porosity 20 %)	3×10^{-10}	-	Data report	SKB R-01-14
Porous backfill concrete in SFR	3×10^{-10}	-	Performance assessment	Höglund and Bengtsson 1991
Porous concrete (silo and BTF) state I of concrete degradation	6.3×10^{-10}	No change with degradation	SKI data report	Savage and Stenhouse 2002
Concrete backfill (porosity 20−30 %)	1×10^{-10}	-	Safety assessment	SKB R-01-14
Backfill concrete in SFR (porosity 36 %)	1.2×10^{-10}	-	Literature review and adjustment for porosity	Luna et al. 2006
Concrete cement conditioning and waste package concrete in silo, BMA and BTF)	3×10^{-10}	-	Safety assessment	Thomson et al. 2008
Other concretes				
Self-compacting concrete based on Portlandite cement, calcite and river sand and gravel; w/c ratio = 0.46	2.4×10^{-12}	~10 with 3−5 cracks of 390 ± 70 µm width per 100 mm	Experimental data of chloride penetration into artificially cracked concrete	Mu et al. 2013
Concrete prepared with w/c ratio = 0.51, cement: sand: pea gravel = 1: 2: 4.	-	10 (concrete with a 1.3 mm crack in an 8.9 cm diameter sample vs intact concrete)	Laboratory measurements of Rn gas diffusion through artificially cracked concrete	Daoud and Renken 1999
Structural concrete	10^{-12}	10	Sensitivity analysis	Zhang and Lounis 2006
Modified Portlandite cement (Type I and II) prepared with a w/c ratio of 0.4 and using a fine aggregate	2×10^{-13}	-	Determined in Tc and I diffusion experiments using soil-concrete half cells	Mattigod et al. 2009

Table 10-1. Continued.

Material	Effective diffusivity (m^2/s)	Diffusivity increase factor due to ageing or cracking*	Type of data	Source
Structural concrete	~ 10^{-12}	1 000 (to the diffusivity in free water) due to damage	Coupled diffusion-damage modelling	Gerard et al. 1998
Ordinary Portland cement concrete; w/c ratio = 0.5	-	2 (crack of ~ 47 µm width at the concrete surface)		Yoon 2012
High performance concrete; w/c ratio = 0.2	-	8 (crack of ~ 20 µm width at the concrete surface)		Yoon 2012
High performance concrete; w/c ratio = 0.2	-	18 (crack of ~ 47 µm width at the concrete surface)		Yoon 2012
High performance concrete reinforced with steel fibre (to introduce complex cracks); w/c ratio = 0.33	-	4 (crack of ~ 20 µm width at the concrete surface)		Yoon 2012
High performance concrete reinforced with steel fibre (to introduce complex cracks); w/c ratio = 0.33	-	10 (crack of ~ 36 µm width at the concrete surface)		Yoon 2012
High performance concrete reinforced with steel fibre (to introduce complex cracks); w/c ratio = 0.33	-	4−6 (crack of ~ 43−47 µm width at the concrete surface)		Yoon 2012
Bulk mortar; porosity = 18 %	6×10^{-11}	300 (to diffusivity in free water within a crack)	COMSOL Multiphysics simulation validated by µXFR measurement	Lu et al. 2012

* Note that when two factors are given, both are relative to the diffusivity given in the second column.

Categorising data sets as qualified or supporting data

Qualified data is presented in Höglund (2014) and other references stated in Table 10-2. Supporting data constitute various references used in the derivation of the data in Höglund (2014) (see reference list of this report).

Table 10-2. Sources of data on diffusivities of concrete from safety assessments, model estimates and literature and other supporting documents.

Sources of information
Boverket, 2004. Boverkets handbok om betongkonstruktioner: BBK 04. 3rd ed. Karlskrona: Boverket. (In Swedish.)
Cronstrand P, 2007. Modelling the long-time stability of the engineered barriers of SFR with respect to climate changes. SKB R-07-51, Svensk Kärnbränslehantering AB.
Daoud W Z, Renken K J, 1999. Laboratory measurements of the radon gas diffusion coefficient for a fractured concrete sample and radon gas barrier systems. Proceedings of the International Radon Symposium (AARST), 1999, 14.0–14.12.
Gaucher E, Tournassat C, Nowak C, 2005. Modelling the geochemical evolution of the multi-barrier system of the Silo of the SFR repository. Final report. SKB R-05-80, Svensk Kärnbränslehantering AB.
Gerard B, Pijaudier-Cabot G, Laborderie C, 1998. Coupled diffusion-damage modelling and the implications on failure due to strain localisation. International Journal of Solids and Structures 35, 4107–4120.
Hejll A, Hassanzadeh M, Hed G, 2012. Sprickor i BMA:s betongbarriär – Inspektion och orsak. Rapport AE-NCC 12-004, Vattenfall AB. SKBdoc1430853 ver 1.0, Svensk Kärnbränslehantering AB. (In Swedish.)
Höglund L O, 2001. Project SAFE. Modelling of long-term concrete degradation processes in the Swedish SFR repository. SKB R-01-08, Svensk Kärnbränslehantering AB.
Höglund L O, 2014. The impact of concrete degradation on the BMA barrier functions. SKB R-13-40, Svensk Kärnbränslehantering AB.
Höglund L O, Bengtsson A, 1991. Some chemical and physical processes related to the long-term performance of the SFR repository. SKB SFR 91-06, Svensk Kärnbränslehantering AB.
Lagerblad B, Rogers P, Vogt C, Mårtensson P, 2017. Utveckling av konstruktionsbetong till kassunerna i 2BMA. SKB R-17-21, Svensk Kärnbränslehantering AB.

Table 10-2. Continued.

Sources of information
Lu Y, Garboczi E, Bentz D, Davis J, 2012. Modeling chloride transport in cracked concrete: a 3-D image-based microstructure simulation. In Proceedings of COMSOL Conference 2012, Boston, MA, 3–5 October 2012. Available at: http://www.nist.gov/customcf/get_pdf.cfm?pub_id=912153
Luna M, Arcos D, Duro L, 2006. Effects of grouting, shotcreting and concrete leachates on backfill geochemistry. SKB R-06-107, Svensk Kärnbränslehantering AB.
Mattigod S V, Bovaird C, Wellman D M, Skinner D J, Cordova E A, Wood M I, 2009. Effect of concrete waste form properties on radionuclide migration. PNNL-18745, Pacific Northwest National Laboratory, Richland, Washington.
Mu S, De Schutter G, Ma B-G, 2013. Non-steady state chloride diffusion in concrete with different crack densities. Materials and Structures 46, 123–133.
Mårtensson P, Vogt C, 2019. Concrete caissons for 2BMA. Large scale test of design and material. SKB TR-18-12, Svensk Kärnbränslehantering AB.
Mårtensson P, Vogt C, 2020. Concrete caissons for 2BMA. Large scale test of design, material and construction method. SKB TR-20-09, Svensk Kärnbränslehantering AB.
Savage D, Stenhouse, M, 2002. SFR 1 vault database. SKI Report 02:53, Swedish Nuclear Power Inspectorate.
SKB R-01-14, SKB 2001. Project SAFE. Compilation of data for radionuclide transport analysis. Svensk Kärnbränslehantering AB.
Thomson G, Miller A, Smith G, Jackson D, 2008. Radionuclide release calculations for SAR-08. SKB R-08-14, Svensk Kärnbränslehantering AB.
US DOE, 2009. Review of mechanistic understanding and modelling and uncertainty analysis methods for predicting cementitious barrier performance. Cementitious Barriers Partnership. CBP-TR-2009-002, Rev.0, U.S. Department of Energy.
Yoon I-S, 2012. Chloride penetration through cracks in high performance concrete and surface treatment system for crack healing. Advances in Materials Science and Engineering 2012, 294571. doi:10.1155/2012/294571
Zhang J, Lounis Z, 2006. Sensitivity analysis of simplified diffusion-based corrosion initiation model of concrete structures exposed to chlorides. Cement and Concrete Research 36, 1312–1323.
Villar M V, Gutiérrez M G, Barrios B C, Álvarez C G, Martínez R I, Martín P L, Missana T, Mingarro M, Morejón J, Olmeda J, Idiart A, 2019. Experimental study of the transport properties of different concrete mixes, SKB P-19-10, Svensk Kärnbränslehantering AB.

Excluded data previously considered as important

In SR-PSU recent information regarding the status of concrete structures, especially in 1BMA (Hejll et al. 2012), was used as a major information source. These data are not excluded, but judged to be less important since more recent information are now available.

10.5 Conditions for which data are supplied

The conditions for which data are supplied have been discussed separately for each individual waste vault in Section 9.5 and are not repeated here.

10.6 Conceptual modelling uncertainty

In general, the conceptual uncertainties related to the diffusivity of concrete are small. Diffusion processes are well known and intact concrete is known to have low diffusivity and be of high durability.

The general uncertainties relating to the impact of chemical and physical degradation processes on the diffusivity are the same as those discussed for the hydraulic conductivity, see Section 9.6 for more details. However, the uncertainties introduced by considering cracks in concrete structures are smaller for the diffusivity since the sensitivity to crack aperture is smaller.

10.7 Data uncertainty – precision, bias, and representativity

Since the level of understanding of material properties and construction/repair methods has improved since SR-PSU, the diffusivity data uncertainties for the PSAR have been significantly reduced for some of the waste vaults whereas they remain relatively unaffected for others.

Data uncertainty – precision, bias and representativity have been discussed separately for each individual waste vault in Section 9.7 and is not repeated here.

10.8 Data uncertainty – spatial and temporal variability

Spatial variability of data

There will be a spatial variability in the diffusive properties of the concrete structures in SFR. In particular the occurrence of cracks and other heterogeneities in the concrete barriers constitute significant discontinuities in the diffusive properties of the concrete barriers. Examples of model applications to demonstrate the impact of such defects in concrete barriers are presented by Höglund (2014).

For the safety assessment, the spatial variability can be averaged by means of calculating equivalent diffusion resistances. However, it is not currently possible to use a statistical approach to qualify the data. There is also currently a lack of site-specific data on the diffusion properties and the presence of cracks in the concrete structures in the different waste vaults in SFR with the exception of the concrete structure in 1BMA which has been extensively studied.

However, through continued inspections of the different concrete structures in SFR1 in combination with carefully selected materials and methods of construction for the concrete structures in SFR3, the initial state uncertainties can be reduced.

Finally, the expected progression of different degradation processes – both chemical and physical – will cause the spatial variability to evolve over time. It is also likely that cracks will not be evenly distributed in the different concrete structures.

Temporal variability of data

The diffusivity of the cementitious materials in SFR will change over time due to chemical and physical degradation processes. The chemical degradation processes are governed by diffusion or the flow of groundwater in different parts of the repository. The groundwater flow is in turn variable in time due to external factors such as shoreline displacement, glaciation periods etc.

The diffusivity of different components in the repository will in turn be affected by the different degradation processes, hence creating a coupled system. Despite the inherent difficulties in assessing the properties of such systems over time in detail, the evolution of the processes can be quantified with reasonable accuracy using existing model tools for alternative scenarios. Results of such model exercises are presented for 1–2BMA in Höglund (2014). Available data on the long-term chemical degradation of concrete are scarce and do not allow for statistical approaches to study temporal variability.

The progression of physical degradation processes with time, including different processes leading to crack formation in the concrete, is difficult to predict with present day knowledge (US DOE 2009) and is a subject that would require further research.

10.9 Data uncertainty – correlations

Correlations exist between crack formation, overall barrier degradation, diffusivity, hydraulic conductivities, porosity and radionuclide migration from the waste vaults since the processes are coupled. Correlations need to be considered in the evaluations through the use of relevant models.

10.10 Result of supplier's data qualification

Overview

As in SR-PSU an initial effective diffusivity of intact structural concrete of 3×10^{-12} m^2/s is considered. In order to handle uncertainties concerning the initial state it is assumed that all concrete structures initially contain one crack with an aperture of 10 µm per metre, resulting in an overall effective diffusivity of 3.5×10^{-12} m^2/s. It should be noted though that such narrow cracks cannot be expected in the thick concrete structures in SFR. As shown by Mårtensson (2014), cracks with an aperture from 0.1 mm and below are not penetrating and will therefore have a limited influence on the diffusivity of the concrete structure.

Silo

Outer and inner walls, slab and lid

From Section 9.3, investigations showed that the amount of reinforcement in the concrete silo is not sufficient to restrict the width of the cracks formed in the slab and outer walls. This could mean an increased risk for the formation of larger cracks such as those found in the existing concrete structure in 1BMA. However, because the design and method of construction differs considerably between the silo and the concrete structure in 1BMA, the likelihood for such cracking during construction and the operational period is judged to be lower in the silo than in 1BMA. For that reason, an initial effective diffusivity of 3.5×10^{-12} m^2/s is selected for the concrete structures in the silo.

The anticipated progression of different degradation processes in the concrete walls of the silo is described by Höglund (2014, Appendix B). Based on the predicted degradation processes, Höglund (2014) proposes an evolution of the effective diffusivity of the different structural components of the silo as illustrated in Figure 10-3. The scientific background that forms the basis for the proposed values in Figure 10-3 is considered well-based. For that reason, the proposed effective diffusivities illustrated by the green rectangles in Figure 10-3 are suggested by the supplier for use in the assessment, Table 10-3 follow. These values are considerably higher than those indicated by the models and illustrated by red, green and blue lines and ensures that overly optimistic values are not used in the assessment.

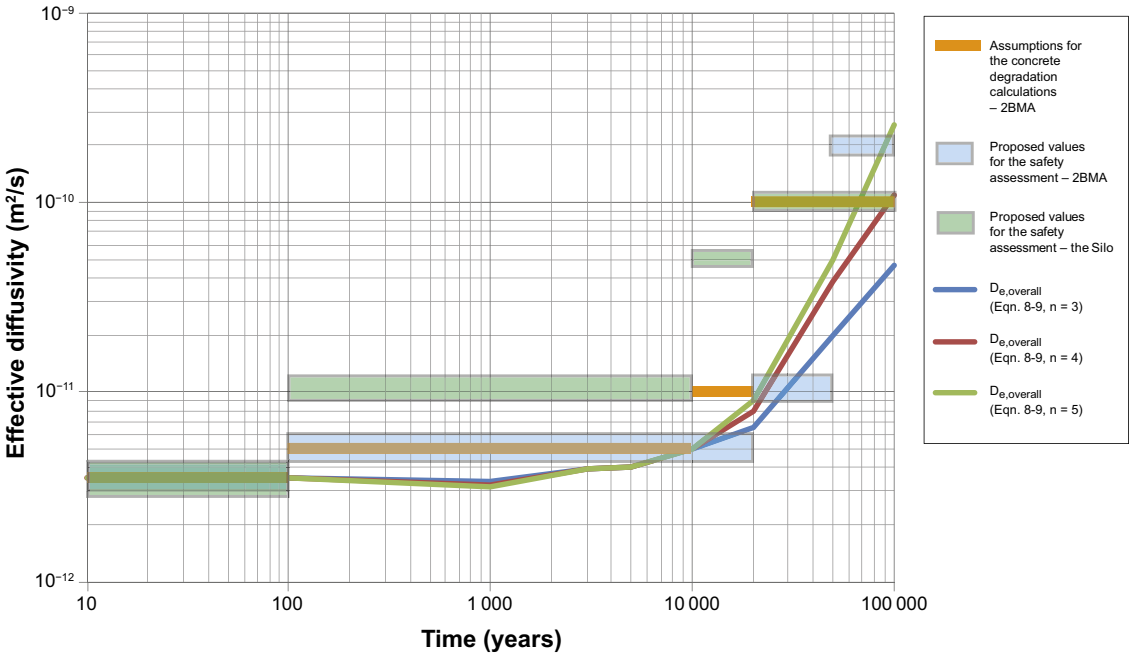

Figure 10-3. *Proposed range of values for the effective diffusivity in structural concrete in the silo (green shading). The effective diffusivities proposed for 2BMA (blue shading) as well as the initial estimates of the gradual change of the effective diffusivity assumed in the PHAST modelling for 2BMA (orange line) are shown as comparison. Predicted effective diffusivities in the upstream side concrete wall in 2BMA for three different models are shown as comparison (blue, red and green lines). From Höglund (2014).*

Concrete moulds

An initial effective diffusivity of 3.5×10^{-12} m^2/s is selected for the concrete moulds in the silo, i.e. the same as was suggested for the concrete structure. Since the wall thicknesses of the concrete moulds are less than the thickness of concrete structure a somewhat faster increase of the moulds is suggested. The suggested evolution of the effective diffusivity of the concrete moulds in the silo is presented in Table 10-3.

Grout

The expected porosity of the grout between the waste packages in the silo is 30 %. From Figure 10-1, the corresponding effective diffusivity is in the region of 10^{-11} to 10^{-10} m^2/s. An initial effective diffusivity of 3.5×10^{-10} m^2/s is selected for the grout in the silo.

Being protected by both the concrete structure and the surrounding bentonite, chemical degradation of the grout is expected to be slow. However, as suggested by von Schenck and Bultmark (2014) some cracking could be caused by swelling waste which will increase the effective diffusivity, in particular, in the nine central shafts of the silo where the bituminised waste is disposed. It is therefore predicted that the effective diffusivity of the grout will increase over time with a final value of 1×10^{-9} m^2/s selected for the period from 50 000 years after closure and throughout the remaining part of the assessment period.

1BMA

Existing outer walls, inner walls and slab

For the existing outer walls, inner walls, and slab the presence of cracks will increase the effective diffusivity and based on Figure 10-2 an initial value of 5×10^{-12} m^2/s is selected.

Based on the predicted degradation processes, it is suggested that the evolution of the effective diffusivity of the existing outer walls, inner walls and slab of 1BMA will follow that suggested by Höglund (2014) for 2BMA illustrated in Figure 10-4. However, a higher effective diffusivity during the initial period is expected as mentioned above as well as during the period 12 000 to 22 000 AD due to expected corrosion of tie rods and reinforcement bars.

New outer walls and lid

For the new outer walls and lid of the concrete structure in 1BMA, data are selected based on the assumption that the repair measures described by Wimelius (2021) and analysed by Elfwing et al. (2017) will ensure that the new outer walls and lid will be free from cracks at closure. For the new outer walls and lid an overall effective diffusivity of 3.5×10^{-12} m^2/s is therefore selected as an initial value as discussed in the overview section.

The anticipated progression of different degradation processes in the new outer walls and lid will be affected by the presence of cracks. As shown by Mårtensson (2017), the risk for cracking due to loss of load bearing capacity is low during the first 20 000 years after closure.

However, from this period and onwards, cracking is expected and the effective diffusivity of the lid and new outer walls will correspond to that of cracked concrete. A value of between 1×10^{-11} m^2/s and 2×10^{-10} m^2/s is therefore selected for the new outer walls and lid from 22 000 AD and throughout the remaining part of the assessment period.

Concrete moulds

The effective diffusivity for the concrete moulds in 1BMA is expected to follow that of the concrete moulds in the silo up to 52 000 AD. For the remaining part of the assessment period, a value of 5×10^{-10} m^2/s is suggested to account for the fact that the concrete moulds in 1BMA are not grouted.

2BMA

Outer walls, slab and lid

For 2BMA, data are selected based on the design of the 2BMA concrete caissons presented by Elfwing et al. (2017) and supported by the findings by Mårtensson and Vogt (2019, 2020).

An overall effective diffusivity of 3.5×10^{-12} m^2/s is suggested as an initial value for the outer walls, slab and lid of the concrete caissons in 2BMA.

The anticipated progression of different degradation processes in the slab, outer walls and lid will be affected by the presence of cracks. As shown by Mårtensson (2017), the risk for cracking due to loss of load bearing capacity is low during the first 20 000 years after closure.

However, from the end of this period and onwards, cracking must be expected and the effective diffusivity of the lid and outer walls will correspond to that of cracked concrete. A value of between 1×10^{-11} m^2/s and 2×10^{-10} m^2/s is therefore selected for the lid and new walls from 22 000 AD and throughout the remaining part of the assessment period.

The suggested values are the same as the values proposed by Höglund (2014) and illustrated in Figure 10-4, except for the timing of the change from 3.5×10^{-12} m^2/s to 5×10^{-12} m^2/s. The later time for this change is motivated by the calculated changes presented as curves in Figure 10-4.

The risk of cracking of the slab due to loss of load bearing capacity is considerably lower than for the lid and outer walls. However, in spite of this, the same progression of the effective diffusivity is selected for the slab as for the outer parts.

Inner walls

The effective diffusivity of the inner walls will be determined by the holes made to ensure that any intruding groundwater will be evenly distributed within the entire waste compartment. A value of 1×10^{-9} m^2/s is therefore suggested for the entire assessment period.

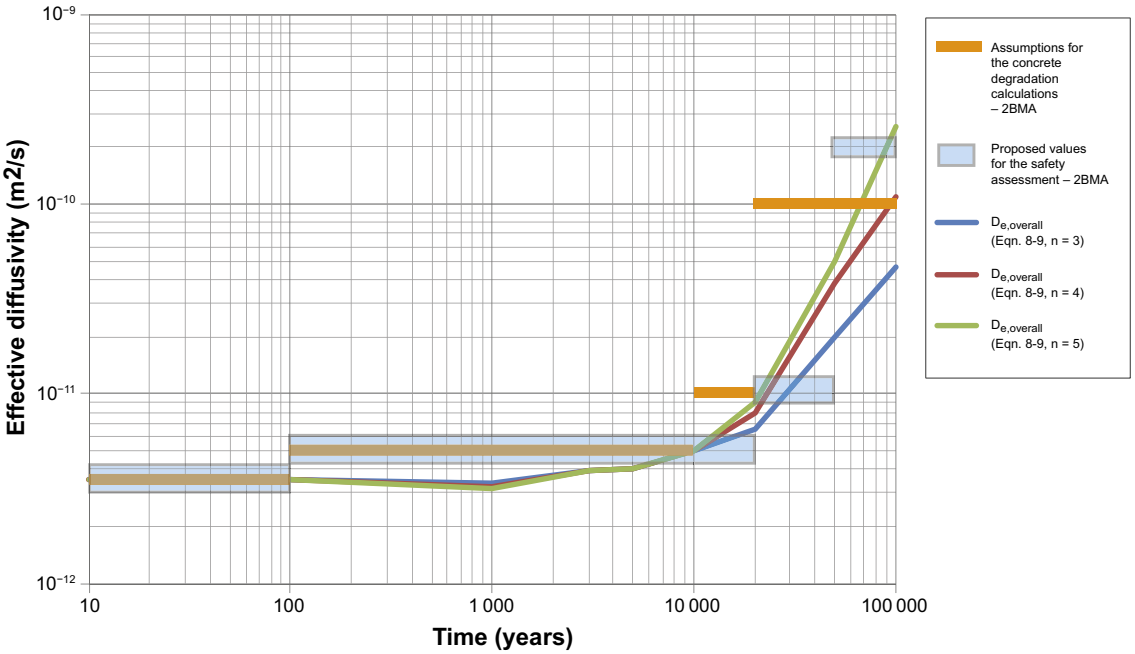

Figure 10-4. *Proposed values for the effective diffusivity (blue shading) in structural concrete in 2BMA. The effective diffusivities calculated based on three different power law models (blue, red, green) using porosity changes extracted from PHAST modelling are shown as comparison. The initial estimates of the graded change of effective diffusivities assumed in the PHAST modelling are also shown in the figure (orange lines). From Höglund (2014).*

Grout in gas evacuation channels

The evolution of the grout in the gas evacuation channels is suggested to follow that of the grout in the silo during the entire assessment period, since the requirement on both of them is to allow gas transport.

Concrete moulds

The suggested effective diffusivity for the concrete moulds in 2BMA follows that of the concrete moulds in 1BMA.

1BRT

Outer and inner walls, slab and lid

For 1BRT, data have been selected based on the design and method of construction used for the existing concrete structure in 1BMA and the use of both steel reinforcement and tie rods (glass fibre or steel) is anticipated.

From the inspections of the concrete structure in 1BMA (Hejll et al. 2012, Elfwing et al. 2015) it can be expected that cracks may form during construction even though careful choice of material and construction method can mitigate the extent of cracking. Even though tie rod corrosion can be avoided by using glass fibre tie rods, rebar corrosion is cautiously expected in the long-term when data are suggested.

The assumptions made for the existing concrete structure in 1BMA are therefore also made for 1BRT and the initial state diffusivity data as well as the evolution of these data are suggested to follow those of 1BMA discussed above.

Values of the effective diffusivity for 1BRT suggested by the supplier for use in the safety assessment calculations are presented in Table 10-3.

Concrete between waste packages

The effective diffusivity in the concrete between the waste packages is expected to be controlled by the presence of cracks already from the start of the assessment period. This is motivated by the fact that no reinforcement is planned to be used in these walls and the probability for cracking during construction is therefore considerable.

For that reason, the same initial effective diffusivity as that of the grout in the silo is suggested, i.e. 3.5×10^{-10} m^2/s.

The evolution of the effective diffusivity in the concrete between the waste packages in 1BRT will be affected by cracking caused by corroding waste and waste packaging. It is therefore suggested that the effective diffusivity will follow that outlined for the grout in the silo during the entire assessment period.

1–2BTF

Slab

For the slabs in 1–2BTF the values of the effective diffusivity are suggested to follow those suggested for the slab and existing walls in 1BMA during the entire assessment period.

Lid

For the lids in 1–2BTF the values of the effective diffusivity are suggested to follow those suggested for the lid and new walls in 1BMA during the entire assessment period.

Grout

The evolution of the effective diffusivity in the grout between the waste packages in 1–2BTF is expected to follow that of the grout in the silo.

Cementitious backfill

For the cementitious backfill in 1–2BTF the values of the effective diffusivity are suggested to follow those suggested for the slab, outer walls and lid in 2BMA during the entire assessment period.

Concrete tanks

For the concrete tanks in 1–2BTF, an initial value of the effective diffusivity of 3.5×10^{-12} m^2/s, corresponding to that of concrete with small cracks is suggested. This is motivated by the fact that careful control of the concrete tanks is undertaken prior to delivery and that cracking during the operational period is not expected.

During the following periods, cracking caused by rebar corrosion and loss of load bearing capacity is expected which is reflected in the suggested values of the effective diffusivity. In order to account for extensive cracking of the concrete tanks during the latter stages of the assessment period, an effective diffusivity of 1×10^{-9} m^2/s is selected for the concrete tanks beyond 22 000 AD.

Concrete moulds

The evolution of the effective diffusivity of the concrete moulds in 1–2BTF is suggested to follow that of the concrete moulds in 1BMA.

1–5BLA

The evolution of the diffusivity of the slabs in 1–5BLA is suggested to follow that of the slab in 1BMA and 1–2BTF.

Table 10-3. Data on effective diffusivities for the cementitious structural components in SFR for different time periods and waste vaults suggested by the supplier to be used in the assessment.

	Effective diffusivity (m^2/s) for the different time periods (AD)				
	2000–2100 AD	**2100–12 000 AD**	**12 000–22 000 AD**	**22 000–52 000 AD**	**52 000–100 000 AD**
Silo					
Concrete structure	3.5×10^{-12}	1×10^{-11}	5×10^{-11}	1×10^{-10}	1×10^{-10}
Grout	3.5×10^{-10}	3.5×10^{-10}	5×10^{-10}	1×10^{-9}	1×10^{-9}
Concrete moulds	3.5×10^{-12}	2×10^{-11}	5×10^{-11}	1×10^{-10}	1×10^{-10}
1BMA					
Existing outer and inner walls and slab	5×10^{-12}	5×10^{-12}	1×10^{-11}	1×10^{-11}	2×10^{-10}
New outer walls and lid	3.5×10^{-12}	3.5×10^{-12}	5×10^{-12}	1×10^{-11}	2×10^{-10}
Concrete moulds	3.5×10^{-12}	2×10^{-11}	5×10^{-11}	1×10^{-10}	5×10^{-10}
2BMA					
Outer walls, slab and lid	3.5×10^{-12}	3.5×10^{-12}	5×10^{-12}	1×10^{-11}	2×10^{-10}
Inner walls	1×10^{-9}	1×10^{-9}	1×10^{-9}	1×10^{-9}	1×10^{-9}
Grout in gas evacuation channels	3.5×10^{-10}	3.5×10^{-10}	5×10^{-10}	1×10^{-9}	1×10^{-9}
Concrete moulds	3.5×10^{-12}	2×10^{-11}	5×10^{-11}	1×10^{-10}	5×10^{-10}
1BRT					
Outer and inner walls, slab and lid	5×10^{-12}	5×10^{-12}	1×10^{-11}	1×10^{-11}	2×10^{-10}
Concrete between waste packages	3.5×10^{-10}	3.5×10^{-10}	5×10^{-10}	1×10^{-9}	1×10^{-9}

Table 10-3. Continued.

	Effective diffusivity (m^2/s) for the different time periods (AD)				
	2000–2100 AD	**2100–12 000 AD**	**12 000–22 000 AD**	**22 000–52 000 AD**	**52 000–100 000 AD**
1–2BTF					
Slab	5×10^{-12}	5×10^{-12}	1×10^{-11}	1×10^{-11}	2×10^{-10}
Lid	3.5×10^{-12}	3.5×10^{-12}	5×10^{-12}	1×10^{-11}	2×10^{-10}
Cementitious backfill	3.5×10^{-12}	3.5×10^{-12}	5×10^{-12}	1×10^{-11}	2×10^{-10}
Grout	3.5×10^{-10}	3.5×10^{-10}	5×10^{-10}	1×10^{-9}	1×10^{-9}
Concrete moulds	3.5×10^{-12}	2×10^{-11}	5×10^{-11}	1×10^{-10}	5×10^{-10}
Concrete tanks	3.5×10^{-12}	5×10^{-11}	2×10^{-10}	1×10^{-9}	1×10^{-9}
1–5BLA					
Slab	5×10^{-12}	5×10^{-12}	1×10^{-11}	1×10^{-11}	2×10^{-10}

10.11 Judgements by the assessment team

In this final section the assessment team presents its judgement on the data qualification made by the supplier to verify that it is sufficient for the safety assessment.

Sources of information

The assessment team agrees with the sources of information used in Section 10.4.

Conditions for which data is supplied

The assessment team finds the conditions given in Section 10.5 valid and reflecting the conditions expected in the repository.

Conceptual modelling uncertainty

The assessment team agrees with the given uncertainties in Section 10.6.

Data uncertainty – precision, bias, and representativity

The assessment team agrees with the given uncertainties in Section 10.7.

Data uncertainty – spatial and temporal variability

The assessment team agrees with the given variabilities given in Section 10.8. The assessment team agrees with the statements regarding the need for further research, given in Section 10.8.

Data uncertainty – correlations

The correlations mentioned in Section 10.9 are valid in the safety assessment. However, systematic and well-defined observations of the physical degradation of the barriers over time are scarce and the given data are not sufficient to allow for a statistical approach to study correlations.

Results of supplier's data qualification

The assessment team considers the data given in Table 10-3 in combination with the information provided by the supplier in the previous sections sufficient for use in the recommendation of data for the safety assessment. Also, the assessment team finds the data presented by the supplier sufficient to define probability density functions allowing for a probabilistic treatment of the diffusivity in the radionuclide transport modelling, see Section 10.12.

10.12 Data recommended for use in the assessment

The data on effective diffusivities recommended by the assessment team for use in the assessment are given in Table 10-4 and discussed separately for each individual waste vault in the following sections.

The recommendations are mainly based on the following sources:

- Values suggested by the supplier in Table 10-3.
- Values suggested and recommended in the SR-PSU Data report (SKB TR-14-10, Table 9-4).
- Calculated values from Höglund (2014) shown as curves in Figure 10-3 and 10-4 (same curves in both figures).
- Values proposed by Höglund (2014) shown in Figure 10-3 and 10-4.
- Values used in the updated analysis of the post-closure safety of 1BMA (Elfwing et al. 2018).

Silo

Outer and inner walls, slab and lid

For the outer and inner walls, slab and lid the initial value is recommended to be 3.5×10^{-12} m^2/s (suggested in Table 10-3). This is consistent with Figure 10-4, which also provides the basis for the recommended changes of the diffusivity with time.

Between 2100 AD and 3000 AD a log-triangular distribution is recommended with a minimum and best estimate following the curves in Figure 10-4, i.e. 3.5×10^{-12} m^2/s and a maximum of 1×10^{-11} m^2/s (the suggested value). Between 2100 AD and 3000 AD a log-triangular distribution is recommended with a minimum and best estimate following the curves in Figure 10-4, i.e. 3.5×10^{-12} m^2/s and a maximum of 1×10^{-11} m^2/s (the suggested value). The higher values proposed in Höglund (2014) was motivated by rebar corrosion caused by chloride concentrations above the threshold where corrosion can be assumed. The time lag for reaching chloride concentrations above the threshold concentration is dependent on the thickness of the concrete cover of the reinforcement bars. The time lag for reaching threshold concentration for the rebars embedded in the silo concrete structure is judged to be longer than previously expected, hence the effects of rebar corrosion is considered to be smaller.

For the period 3000 AD to 12 000 AD a log-triangular distribution is recommended with a minimum of 3.5×10^{-12} m^2/s (lowest value of the curves in Figure 10-4), best estimate of 5×10^{-12} m^2/s (the proposed value for 2BMA in the figure) and maximum of 1×10^{-11} m^2/s (the suggested value).

Between 12 000 AD and 22 000 AD a log-triangular distribution is recommended with a minimum and best estimate of 5×10^{-12} m^2/s (lowest value of the curves in Figure 10-4 during the actual period) and maximum value of 5×10^{-11} m^2/s (the suggested value for the silo). Again, this might be a too pessimistic recommendation, especially the maximum value.

Between 22 000 AD and 52 000 AD a log-triangular distribution is recommended with a minimum of 7×10^{-12} m^2/s (lowest value of the curves during the actual period in Figure 10-4) and a best estimate of 1×10^{-11} m^2/s (the proposed value for 2BMA) and maximum of 1×10^{-10} m^2/s (the suggested value). Again, this might be a too pessimistic recommendation, especially the best estimate and maximum value.

After 52 000 AD to the end of the assessment period a log-triangular distribution is recommended with a best estimate of 1×10^{-10} m^2/s (the suggested value for the silo), a minimum of 2×10^{-11} m^2/s (lowest value of the curves during the actual period in Figure 10-4) and a maximum of 3×10^{-10} m^2/s (highest value of the curves during the actual period).

Grout

The assessment team agrees with the data for the grout suggested by the supplier in Table 10-3.

Concrete moulds

The assessment team agrees with the data suggested by the supplier for the concrete moulds in Table 10-3.

1BMA

Existing outer walls, inner walls and slab

For the 1BMA concrete the recommended initial value of the effective diffusivity, 5×10^{-12} m^2/s, is chosen, corresponding to a concrete structure with cracks and an expected porosity of 0.14. This value is assumed to be valid until 22 000 AD. This is consistent with the updated analysis of the post-closure safety of 1BMA (Elfwing et al. 2018).

After the initial 100 years until 12 000 AD a log-triangular distribution is recommended with a best estimate and minimum of 5×10^{-12} m^2/s (the suggested value) and a maximum of 1×10^{-11} m^2/s (the proposed value for silo).

Between 12 000 AD and 22 000 AD a log-triangular distribution is recommended with a best estimate and minimum of 5×10^{-12} m^2/s (the suggested value) and a maximum of 5×10^{-11} m^2/s (the proposed value for silo).

Between 22 000 AD and 52 000 AD a log-triangular distribution is recommended with a best estimate of 1×10^{-11} m^2/s (the suggested value and used in the updated analysis of the post-closure safety of 1BMA (Elfwing et al. 2018)), a minimum of 7×10^{-12} m^2/s (lowest value of the curves in Figure 10-3 during the actual period) and a maximum of 1×10^{-10} m^2/s (the suggested value for silo since it is higher than the highest value of the curves during the actual period).

After 52 000 AD to the end of the assessment period a log-triangular distribution is recommended with a best estimate of 2×10^{-10} m^2/s (the suggested value and consistent with the updated analysis of the post-closure safety (Elfwing et al. 2018), a minimum of 2×10^{-11} m^2/s (lowest value of the curves in Figure 10-3 during the actual period) and a maximum of 3×10^{-10} m^2/s (highest value of the curves during the actual period).

New outer walls and lid

The recommended effective diffusivities for the new outer walls and lid will be somewhat lower than the corresponding values for the existing outer walls, inner walls and slab during the earlier parts of the assessment period due to the lesser degree of cracking in these components. The new outer walls and lid in 1BMA are recommended to have the same effective diffusivities as the outer walls, slab, and lid in 2BMA.

Concrete moulds

The assessment team agrees with the data suggested by the supplier for the concrete moulds in Table 10-3.

2BMA

Outer walls, slab and lid

The recommended initial diffusivity for the outer walls, slab and lid (2BMA concrete) is chosen to be 3.5×10^{-12} m^2/s corresponding to a porosity of 0.11. This is consistent with the findings by Höglund (2014) illustrated in Figure 10-4, which also provides the basis for the recommended changes of the diffusivity with time.

Between 2100 AD and 3000 AD a log-triangular distribution is recommended with a minimum and best estimate following the curves in Figure 10-4, i.e. 3.5×10^{-12} m^2/s and a maximum of 5×10^{-12} m^2/s (the proposed value for 2BMA concrete).

For the period 3000 AD to 12 000 AD a log-triangular distribution is recommended with a minimum of 3.5×10^{-12} m^2/s (lowest value of curves) and best estimate and maximum of 5×10^{-12} m^2/s (the proposed value for 2BMA in Figure 10-4).

Between 12 000 AD and 22 000 AD a log-triangular distribution is recommended with a minimum and best estimate following the curves in Figure 10-4, i.e. 5×10^{-12} m^2/s (the suggested value) and a maximum of 9×10^{-12} m^2/s (highest value of the curves during the actual period).

Between 22 000 AD and 52 000 AD a log-triangular distribution is recommended with a best estimate of 1×10^{-11} m^2/s (the suggested value), a minimum of 7×10^{-12} m^2/s (lowest value of the curves during the actual period in Figure 10-4) and a maximum of 5×10^{-11} m^2/s (highest value of the curves during the actual period).

After 52 000 AD to the end of the assessment period a log-triangular distribution is recommended with a best estimate of 2×10^{-10} m^2/s (the suggested value), a minimum of 2×10^{-11} m^2/s (lowest value of the curves during the actual period in Figure 10-4) and a maximum of 3×10^{-10} m^2/s (highest value of the curves during the actual period).

Grout in gas evacuation channels

The grout in the gas evacuation channels is recommended to have the same diffusivity as suggested for the grout in the silo and the grout in gas evacuation channels in 2BMA in Table 10-3. Both these grouts are required to let gas pass through.

Concrete moulds

The assessment team agrees with the data suggested by the supplier in Table 10-3.

1BRT

Outer walls and inner walls, slab and lid

For 1BRT the recommended diffusivities for the structural concrete between 2000 AD and 22 000 AD are the same as for the existing outer walls, inner walls and slab in 1BMA (made from 1BMA concrete) except that only the best estimate value is considered. From the long-term perspective, there is only a requirement on the amount of cement in the structural concrete in 1BRT and hence rather high diffusivity values are cautiously chosen. Between 22 000 AD and 52 000 AD the same log-triangular distribution as for 2BMA is recommended.

Concrete between waste packages

As for the structural concrete in 1BRT, there is only requirement on the amount of cement in the grout in 1BRT.

In comparison with the grout in silo, with a requirement on high gas permeability, it is more likely that the concrete between the waste packages in 1BRT will have a lower diffusivity which implies a lower recommended diffusivity after 12 000 AD. For the concrete between the waste packages in 1BRT the same values as for the silo are recommended until 12 000 AD and thereafter the values suggested for the grout previously planned to be used in 1BMA (SKB TR-14-10, Table 9-4) is recommended.

1–2BTF

The recommended diffusivities for 1–2BTF for all types of concrete i.e. the structural concrete (slab and lid), the grout and concrete tanks are as suggested in SKB (TR-14-10, Table 9-4). The data used for 1–2BTF in the previous assessment is in general more pessimistic or the difference is small compared with the data suggested in Table 10-3. The cementitious backfill is pessimistically recommended the same effective diffusivities as the grout.

Table 10-4. Recommended effective diffusivities (m^2/s) for use in the radionuclide transport modelling. Some data are only given as single point values, while others are recommended a log-triangular distribution. In the case of a log-triangular distribution three values are given in the order best estimate, minimum and maximum.

	Effective diffusivity (m^2/s) for time periods (AD)					
	2000–2100 AD	**2100–3000 AD**	**3000–12 000 AD**	**12 000–22 000 AD**	**22 000–52 000 AD**	**52 000–100 000 AD**
Silo						
Concrete Structure	3.5×10^{-12}	3.5×10^{-12}	5×10^{-12}	5×10^{-12}	1×10^{-11}	1×10^{-10}
		3.5×10^{-12}	3.5×10^{-12}	5×10^{-12}	7×10^{-12}	2×10^{-11}
		1×10^{-11}	1×10^{-11}	5×10^{-11}	1×10^{-10}	3×10^{-10}
Grout	3.5×10^{-10}	3.5×10^{-10}	3.5×10^{-10}	5×10^{-10}	1×10^{-9}	1×10^{-9}
Concrete moulds	3.5×10^{-12}	2×10^{-11}	2×10^{-11}	5×10^{-11}	1×10^{-10}	1×10^{-10}
1BMA						
Existing outer walls, inner walls and slab (1BMA concrete)	5×10^{-12}	5×10^{-12}	5×10^{-12}	5×10^{-12}	1×10^{-11}	2×10^{-10}
		5×10^{-12}	5×10^{-12}	5×10^{-12}	7×10^{-12}	2×10^{-11}
		1×10^{-11}	1×10^{-11}	5×10^{-11}	1×10^{-10}	3×10^{-10}
New outer walls and lid (2BMA concrete)	3.5×10^{-12}	3.5×10^{-12}	5×10^{-12}	5×10^{-12}	1×10^{-11}	2×10^{-10}
		3.5×10^{-12}	3.5×10^{-12}	5×10^{-12}	7×10^{-12}	2×10^{-11}
		5×10^{-12}	5×10^{-12}	9×10^{-12}	5×10^{-11}	3×10^{-10}
Concrete moulds	3.5×10^{-12}	2×10^{-11}	2×10^{-11}	5×10^{-11}	1×10^{-10}	5×10^{-10}
2BMA						
Outer walls, slab and lid (2BMA concrete)	3.5×10^{-12}	3.5×10^{-12}	5×10^{-12}	5×10^{-12}	1×10^{-11}	2×10^{-10}
		3.5×10^{-12}	3.5×10^{-12}	5×10^{-12}	7×10^{-12}	2×10^{-11}
		5×10^{-12}	5×10^{-12}	9×10^{-12}	5×10^{-11}	3×10^{-10}
Grout in gas evacuation channels	3.5×10^{-10}	3.5×10^{-10}	3.5×10^{-10}	5×10^{-10}	1×10^{-9}	1×10^{-9}
Concrete moulds	3.5×10^{-12}	2×10^{-11}	2×10^{-11}	5×10^{-11}	1×10^{-10}	5×10^{-10}
1BRT						
Outer and inner walls, slab and lid	5×10^{-12}	5×10^{-12}	5×10^{-12}	5×10^{-12}	1×10^{-11}	2×10^{-10}
					7×10^{-12}	2×10^{-11}
					5×10^{-11}	3×10^{-10}
Concrete between waste packages	3.5×10^{-10}	3.5×10^{-10}	3.5×10^{-10}	4×10^{-10}	5×10^{-10}	1×10^{-9}
1–2BTF						
Slab	3.5×10^{-12}	2×10^{-11}	2×10^{-11}	1×10^{-10}	5×10^{-10}	5×10^{-10}
Lid	3.5×10^{-12}	2×10^{-11}	2×10^{-11}	1×10^{-10}	5×10^{-10}	5×10^{-10}
Cementitious backfill	3.5×10^{-10}	3.5×10^{-10}	3.5×10^{-10}	5×10^{-10}	1×10^{-9}	1×10^{-9}
Grout	3.5×10^{-10}	3.5×10^{-10}	3.5×10^{-10}	5×10^{-10}	1×10^{-9}	1×10^{-9}
Concrete tanks	3.5×10^{-12}	5×10^{-11}	5×10^{-11}	2×10^{-10}	8×10^{-10}	8×10^{-10}

11 Hydraulic pressure field in the SFR local domain

The site of the existing part of the repository, SFR1, was selected partly because of the low regional hydraulic gradient. The direction and magnitude of the gradient will change over time due to shoreline displacement as well as climate changes: Today, when the repository is below the sea floor, the hydraulic gradient is slightly upward directed. After about 1 000–2 000 years the gradient is expected to increase and be more horizontal. In this and later phases the gradient is expected to be more controlled by local topography. This is further described in the PSAR Bedrock hydrology report (Öhman and Odén 2018).

Within the waste vaults (in both SFR1 and SFR3) local gradient variations are to be expected. To be able to resolve these variations better a detailed near-field groundwater flow modelling activity is performed. This chapter deals with the input data needed for this detailed near-field modelling.

11.1 Modelling in this safety assessment

This section describes what data are expected from the supplier, and in which modelling activities the data are to be used.

Defining the data requested from the supplier

Data are requested for three bedrock cases for the temperate climate domain (four defined time steps; 2000 AD, 2500 AD, 3500 AD and 5000 AD, corresponding to the shoreline displacement in the *base variant* of the reference external conditions (Section 12.9)).

The following data are requested as input to the near-field modelling:

- The dynamic pressure (Pa).
- Groundwater velocities (m/s).
- Rock permeability field (m^2).

It should be noted that it is not the actual data that is delivered. The requested data are delivered in the form of input files for the regional-scale groundwater flow model (DarcyTools input format). The customer then executes DarcyTools, using the delivered files as input, in order to extract the requested data.

Modelling activities in which data will be used

The near-field model extracts pressure and flux boundary conditions as well as the rock permeability field from the supplied regional hydrogeological data. A main goal of the near-field model is to provide detailed information regarding the water flow through vaults, barriers, and waste domains of SFR1 and SFR3. Modelling is carried out in COMSOL Multiphysics and is described in a separate report (Abarca et al. 2020).

The results from the near-field model are used in the radionuclide transport calculations. In addition to the results from the near-field modelling performed for the PSAR (Abarca et al. 2020) results from other reports are used as described in the **Radionuclide transport report**. One example is the water-flow through an unrepaired 1BMA that is taken from the near-field modelling for SR-PSU (Abarca et al. 2014) that used boundary conditions as described in the SR-PSU Data report (SKB TR-14-10). Another example is water-flow during glacial conditions that is based on calculations performed by Vidstrand et al. (2013, 2014).

11.2 Experience from previous safety assessments

This section briefly summarises experiences from previous safety assessments, especially the SAFE, SAR-08 and SR-PSU safety assessments, which may be of direct consequence for the data qualification in this data report.

Modelling in previous safety assessments

In the SAFE safety assessment, hydrogeological modelling was carried out with GEOAN which uses the Finite Difference Method for calculating groundwater flows (Holmén and Stigsson 2001a). The most detailed model was the last model in a chain of three nested models i.e., each one having a smaller volume but a higher flow resolution than the previous one in the chain. At the lowest level of detail, the SFR region covered a total area of 210.8 km^2 and a depth of 1 000 m, see Figure 11-1.

At the highest level of detail, the vaults and the access tunnels, except the ramp tunnel, were covered; a total area of 0.21 km^2 and a vertical extension of 108 m, see Figure 11-2. The detailed model results were presented in a separate report (Holmén and Stigsson 2001b).

For SAR-08 two subsequent reports were made, Holmén (2005, 2007), which used an inverse modelling approach to estimate the uncertainties in the SAFE modelling results. Both of the reports generated uncertainty factors which were also used in the SAR-08 safety assessment along with the results from SAFE (Holmén and Stigsson 2001a, b).

In SR-PSU, hydrogeological modelling was carried out with DarcyTools, which uses the finite volume method for calculating groundwater flow. The modelling methodology, setup and results for SR-PSU are summarised in Odén et al. (2014). The resolution of the model varies over the domain but ranges from 1 to 64 m in the horizontal direction inside the regional domain of SFR and ranges from 16 to 128 m outside of the regional domain of SFR (see Figure 11-3). The outer modelling boundary is irregular and is based on the analysis of natural hydraulic boundaries to be expected in the future, at which no flow boundaries are to be expected. The maximum model area extends about 15 km in the east–west direction and about 20 km in the north–south direction. The model extends vertically from elevation −1 100 to 100 m. Inside the SFR regional model the geometry of SFR1, SFR3 and their respective access tunnels are modelled in great detail (see Figure 11-4). The detailed model results for the temperate climate conditions are presented in Öhman et al. (2014). The detailed model results for the periglacial climate conditions were presented in Vidstrand et al. (2014).

Conditions for which data were used in previous safety assessments

In SAFE, the boundary conditions for each model level were supplied by the results from the previous model level in the chain. Therefore, the hydraulic pressure gradients used for the detailed model level originated from the boundary conditions and resulting calculations done on the regional level, with a local level between them in the chain.

The regional model used somewhat different boundary conditions on the six-sided rectangular domain: For the top side of the part which was not covered by the sea an algorithm (further described in Holmén and Stigsson (2001a) was used to calculate a non-linear boundary condition reflecting the discharge and recharge areas above land. A specified head boundary condition was used for the top part covered by the sea, governed by the water depth and the time dependent shoreline displacement.

The bottom part, at 900 metres depth, of the regional model domain had a no flow boundary condition.

As the general topography gradient in the regional model points northeast a no flow boundary condition was set on the southwest and northwest faces of the model domain (see Figure 11-1 for a visual reference). This was also motivated by the fact that the minimum distance between SFR and these two boundaries were about 7 km, and therefore the boundary conditions were expected to have very little, if any, impact on the groundwater flow passing through the repository. The uppermost cells along the southwest face, coincided with actual surface water bodies, which were assumed to be maintained as lakes in the future; consequently, the uppermost cells along the southeast face were assigned a specified head boundary condition. Below the surface cells a no-flow boundary condition was set. A no-flow boundary condition was also set for the northeast face because this face

is approximately located along the lowest topographic levels in the regional basin. Hence, there will be a groundwater flow from the opposite side of the basin, which prevents further transport towards the northeast.

The chain of running the model simulations was described in Holmén and Stigsson (2001a) in the following way:

- Simulation with the regional level model with set boundary conditions described above.
- Simulation with the local level model using specified head boundary conditions from the results from the regional level simulation.
- Simulation with the repository level model using specified head boundary conditions from the results from the local level simulation.

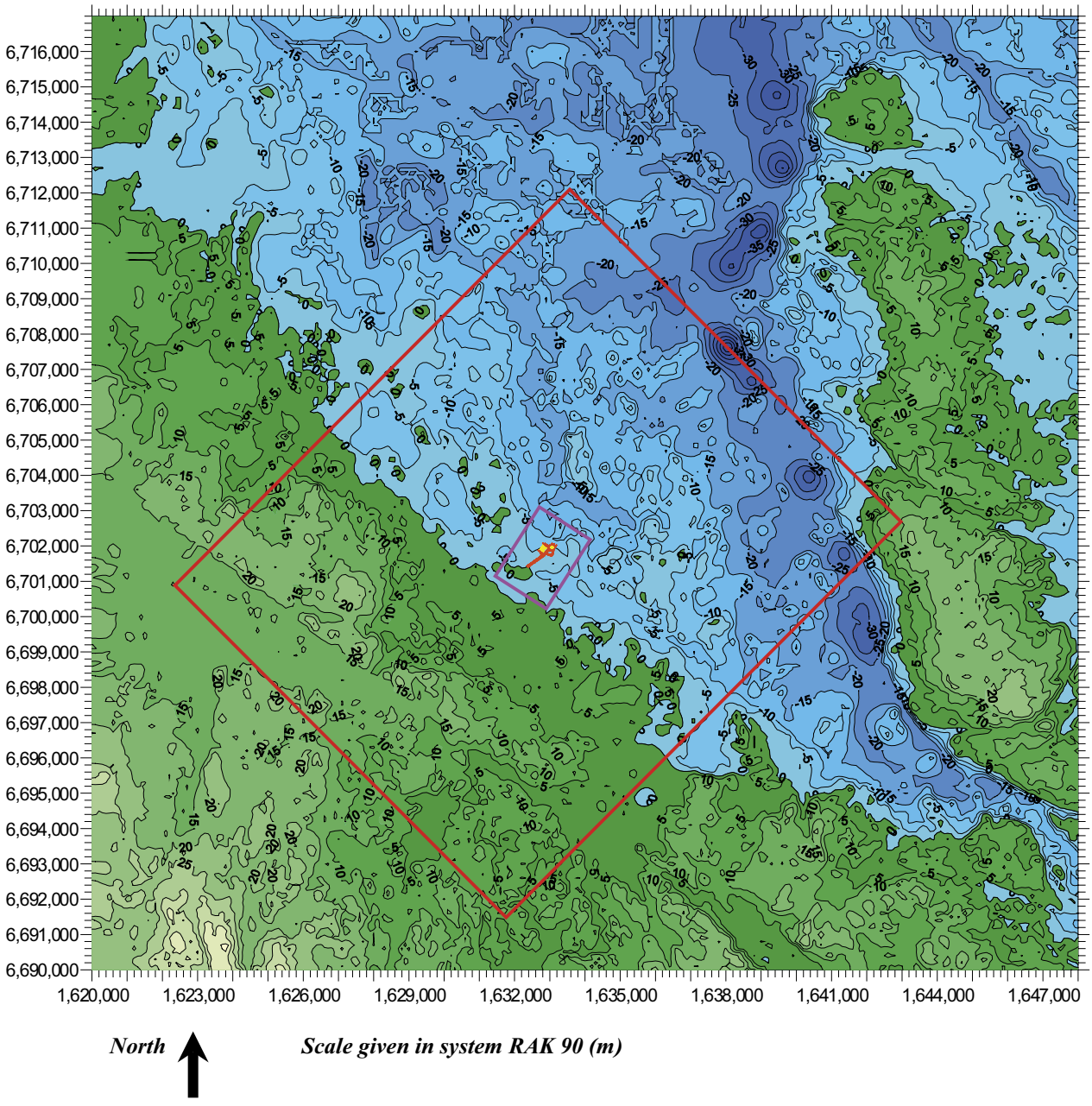

Figure 11-1. *Model boundaries used in SAFE and SAR-08. Regional (lowest level of detail) model boundary in red and local (intermediate level of detail) model boundary in purple. Reproduced from Holmén and Stigsson (2001a).*

In SR-PSU, no-flow boundaries were assigned to the bottom and sides of the model. For the model top boundary, different boundary conditions were applied for different evolutions and times using a hybrid approach. Fixed heads were assigned at surfaces below the sea, rivers or lakes. Fixed fluxes were assigned on land, ranging from 0 to 160 mm/y (full net precipitation), such as to prevent water-levels above ground-level. It should be noted that due to sea-level changes, the location of the shoreline moves over time.

For periglacial conditions, reduced hydraulic conductivities at the upper parts of the model were modelled due to the development of permafrost. A constant heat flux boundary condition was set at the bottom boundary of the model. Three different system scenarios with regards to the degree of exposure to open taliks were investigated.

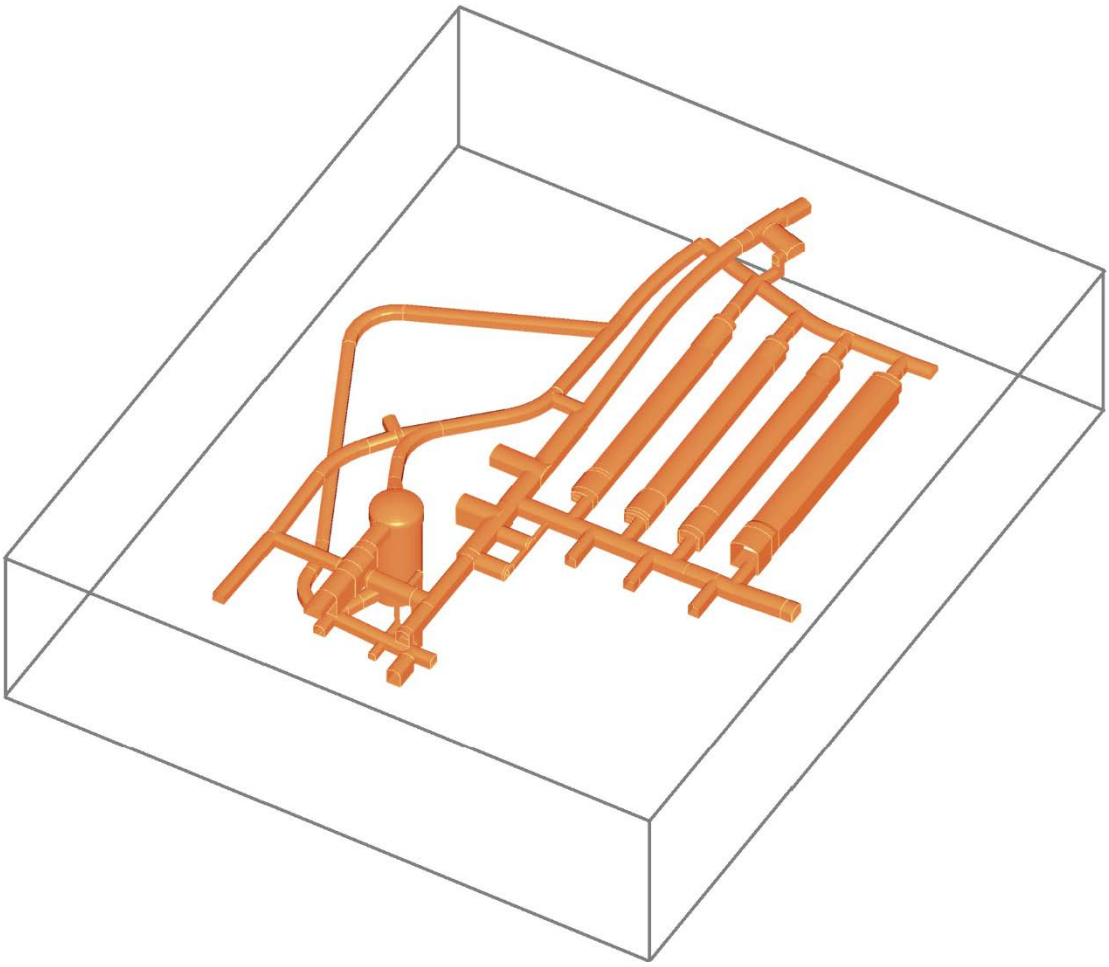

Figure 11-2. *Model boundaries used in SAFE and SAR-08. Boundaries of the most detailed model in grey. Reproduced from Holmén and Stigsson (2001a).*

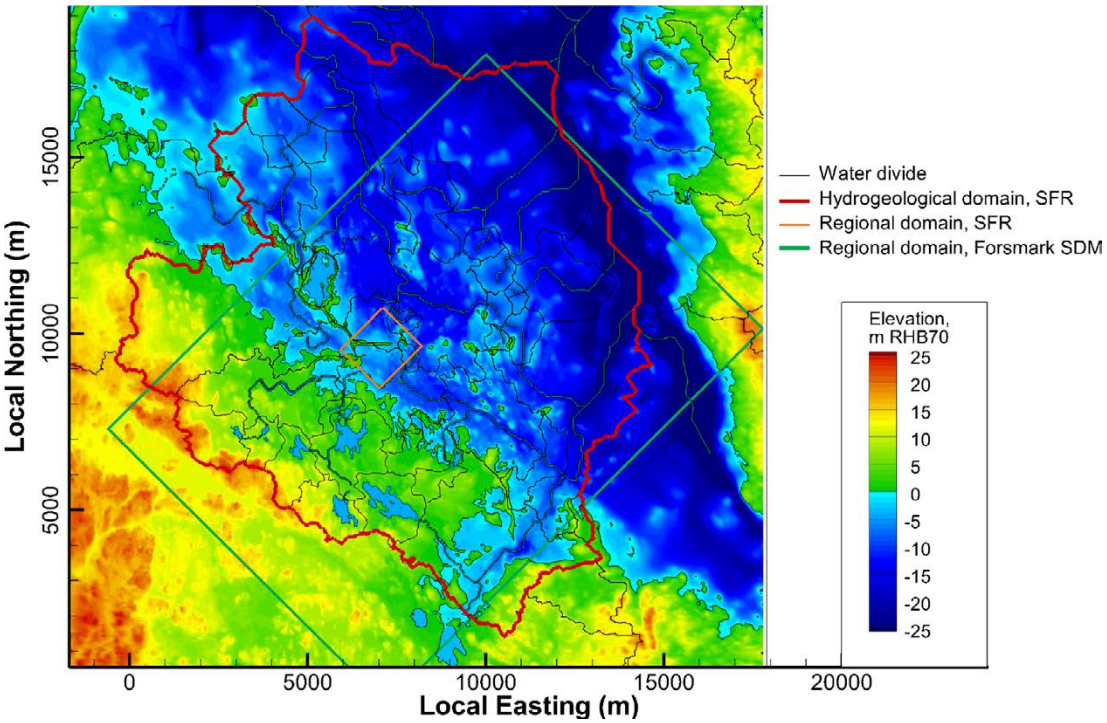

Figure 11-3. *Model domains as used in SR-PSU. The boundary of the flow domain is indicated with a red line. The boundary of the SFR regional domain is indicated with an orange line. Reproduced from Odén et al. (2014).*

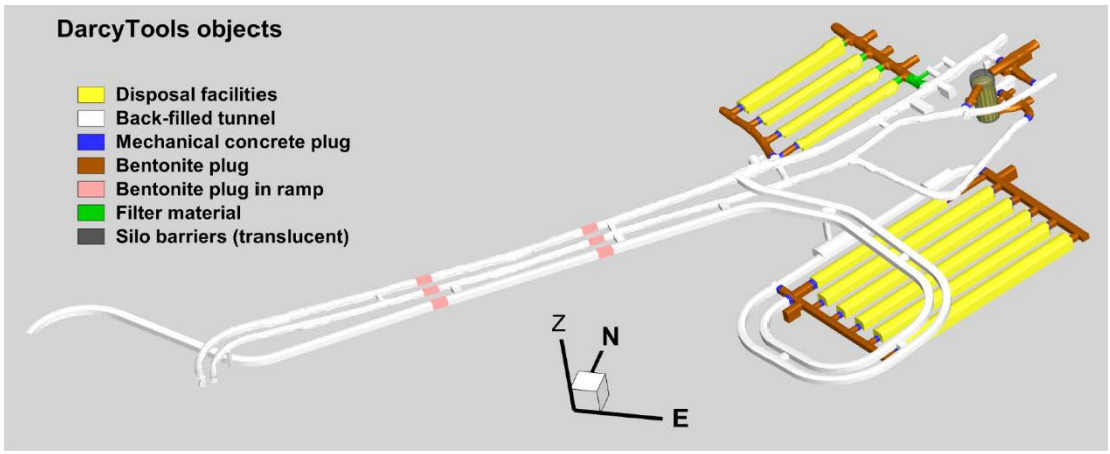

Figure 11-4. *Tunnel geometries of SFR1, SFR3 and their access tunnels as used in SR-PSU. Shown are the model geometries used as input in the DarcyTools calculations. Note that different groups of elements have been distinguished allowing to assign different hydraulic properties. Adapted from Odén et al. (2014).*

Sensitivity to assessment results in previous safety assessments

In the radionuclide transport report for the SAR-08 safety assessment (Thomson et al. 2008) the conclusions state that the SFR facility is sensitive to the regional hydrogeological regime and the assumptions made concerning it. Regarding the input data to the radionuclide transport model used for the SAR-08 the report states that: "The key changes are in rates of groundwater flow within the repository at 1 000, 2 000 and 3 000 years post-closure (and additionally for those in the far future at times when environmental changes are considered, such as development of permafrost, submergence of the site etc). The effects in the near-field are propagated to the geosphere, and so in turn effects in the geosphere will be propagated to the biosphere (Thomson et al. 2008).

In SR-PSU a total of 17 different bedrock variants were explored to investigate the sensitivity to assumptions used in the Hydraulic Conductor Domain (HCD) parametrisation and Hydraulic Rock Domain (HRD) realisation. The sensitivities of the parametrisation of the HCD investigated are: borehole conditioning (yes/no), depth trend (yes/no), in-fault heterogeneity (homogeneous case/two heterogeneous cases), and anisotropy of the southern boundary belt. The sensitivity to the HRD realisations has been investigated using three realisations. It should be mentioned that the two heterogenous HCD realisations and three HRD realisations have been selected from 10 respectively 100 realisations based on earlier investigations and have been selected to represent the spread of calculated flows through the waste vaults. The flow field has been calculated at 0, 500, 1 000, 1 500, 3 000, 7 000 years post-closure for the temperate climate cases, and far in the future for the periglacial climate case. Each time slice considers a different location of the shoreline and different environmental setting (e.g. permafrost, changes from sea to land or lake, etc), which results in significant changes in the hydrogeological flow field that propagates back and forth from near-field, over geosphere to the biosphere.

Alternative modelling in previous safety assessments

For the SAFE safety assessment, analytical approaches were used in conjunction with the GEOAN code, e.g., applied to the regional models, the groundwater saturation at the repository, and the water flows in the vaults and tunnels. This was to make sure that the latter model results were within reasonable order of magnitudes (Holmén and Stigsson 2001a).

For SR-PSU conceptual uncertainties have been explored using the 17 bedrock variants mentioned previously.

Correlations used in previous safety assessment modelling

No correlations have been identified in previous safety assessments.

Identified limitations of the data used in previous safety assessment modelling

In their review of the SAR-08 safety assessment the regulatory authority SSM asked for better motivation and understanding regarding the groundwater flows both within and outside of the repository. SSM especially pointed out that it was difficult reproducing the results from the regional groundwater flow modelling due to lack of data traceability in SKB's work. SSM also found that the handling of the interface between the groundwater flow modelling and the radionuclide transport calculations was lacking traceability.

In their review of SR-PSU the regulatory authority SSM has identified additional uncertainties in the three selected bedrock cases (a base case and two bounding variants) that are not expected to be particularly large. Nevertheless, these uncertainties should be considered in the assessment of the results of the safety analysis.

11.3 Supplier input on use of data in this and previous safety assessments

The method of selecting and using data for the conditions and model chain used in earlier safety assessments was correct in SR-PSU.

In SR-PSU a different approach was used to that adopted in earlier assessments, involving two different numerical codes for the far- and near-field, respectively DarcyTools and COMSOL. The supplied geosphere data from DarcyTools were used to extract requested data for different climate domains (temperate and periglacial) and descriptions of the bedrock to be used in the near-field COMSOL calculation.

In this assessment the same approach as in SR-PSU, of using the geosphere DarcyTools models to set up the near-field COMSOL models, is used.

11.4 Sources of information

The underlying data used to produce the delivered files are described in Öhman and Odén (2018) and its supporting documents, see Table 11-1.

Table 11-1. Main source of information used in data qualification.

Source of information
Öhman J, Odén M, 2018. SR-PSU (PSAR) Bedrock hydrogeology. TD18 – Temperated climate conditions. SKB P-18-02, Svensk Kärnbränslehantering AB

11.5 Conditions for which data are supplied

The supplied model setups are valid for different shoreline positions and descriptions of the rock mass as described in the delivery.

11.6 Conceptual modelling uncertainty

The delivered data represent different descriptions of the rock mass (Bedrock Cases). These cases cover the uncertainty in the description of the bedrock with one base case and two bounding variants.

11.7 Data uncertainty – precision, bias, and representativity

In SR-PSU, based on the outcome of the groundwater flow simulations during temperate climate conditions, three out of seventeen bedrock cases were selected to characterise the observed range of heterogeneity and conceptual uncertainty in bedrock parameterisation. The three bedrock cases were selected based on calculated cross flows through the eleven waste vaults in SFR1 and SFR3.

In Öhman and Odén (2018) the same three hydrogeological host rock property models are compared with a further twenty-seven different hydrogeological host rock property models to further investigate uncertainties arising from heterogeneity and uncertainty in bedrock parametrisation. The evaluation of the performance measures of these models resulted in the conclusion that the same three hydrogeological host rock property models still represent the range of variability. These three models were therefore delivered for use in this safety assessment. As the layout of the SFR3 has changed, and the backfill/tunnel-plug design has been updated in Öhman and Odén (2018), the models are therefore also different. The models delivered comprised the following.

1. One “low-flow” bedrock case: bedrock parameterisation variant with low disposal-facility cross flows; this case is associated with realisation R01 for the identified (deterministic) deformation zone (HCD) and realisation R18 for the less-fractured rock between the deformation zones (HRD).
2. A “base case” bedrock case: a bedrock parameterisation variant with median disposal-facility cross flows; this case is associated with a homogeneous depth trend for the HCD and realisation R85 for the HRD.
3. One “high-flow” bedrock case: a bedrock parameterisation variant with high disposal-facility cross flows; this case is associated with realisation R07 for the HCD and realisation R85 for the HRD.

11.8 Data uncertainty – spatial and temporal variability

Spatial variability of data

The spatial variability is captured with the use of three different bedrock cases.

Temporal variability of data

The temporal variability is captured partly by studying two different climate domains and also different positions of the repository relative the shoreline of the sea for the temperate climate domain:

- Shoreline position 1 (this position corresponds to the situation at 2000 AD): corresponds to a submerged repository.
- Shoreline position 2 (this position would correspond to the situation at 2500 AD): the shoreline is located right over the SFR1 and SFR3. Parts of the repository are situated below a small emerging peninsula.
- Shoreline position 3 (this position would correspond to the situation at 3500 AD): corresponds to an intermediate case in which the shoreline has moved away from the repository.
- Shoreline position 4 (this position would correspond to the situation after 5000 AD): corresponds to a retreating shoreline position, far away from the repository.

11.9 Data uncertainty – correlations

No correlations have been reported.

11.10 Result of supplier’s data qualification

The files delivered are presented in Table 11-2.

Table 11-2. Data files delivered.

Delivered files
BASE_CASE1_DFN_R85_EXT1_RUN_2000AD.zip
BASE_CASE1_DFN_R85_EXT1_RUN_2500AD.zip
BASE_CASE1_DFN_R85_EXT1_RUN_3500AD.zip
BASE_CASE1_DFN_R85_EXT1_RUN_5000AD.zip
ECPM_3_bedrock_cases.zip
SR-PSU_TD18_DTS_Steady_state.f
TD18_DT_to_Amphos_2017-11-21.zip

11.11 Judgements by the assessment team

Sources of information

The assessment team finds the source given in Section 11.4 sufficient for use.

Conditions for which data is supplied

The assessment team finds the conditions given in Section 11.5 are valid for safety assessment use.

Conceptual modelling uncertainty

The assessment team accepts the handling of conceptual modelling uncertainties provided by the supplier in Section 11.6.

Data uncertainty – precision, bias, and representativity

The assessment team accepts the suppliers handling of data uncertainties due to precision, bias and representativity described in Section 11.7.

Data uncertainty – spatial and temporal variability

The suppliers handling of spatial and temporal variabilities in Section 11.8 are accepted by the assessment team.

Data uncertainty – correlations

The assessment team agrees that there are no correlations as reported in Section 11.9.

Results of supplier's data qualification

The assessment team accepts the supplied data sets given in Table 11-2.

11.12 Data recommended for use in the assessment

The assessment team recommends using the data sets the supplier has given in Table 11-2.

12 Shoreline displacement

The area above the repository is currently submerged beneath the Baltic Sea. Due to the ongoing glacial-isostatic uplift, the area will however become terrestrial at some point after closure. This section concerns the future shoreline displacement above SFR. Specifically, this includes the duration of the initial submerged period above the repository as well as the rate of shoreline displacement when the area gradually transitions from submerged to terrestrial conditions.

The initial duration of submerged conditions and the temporal evolution of the shoreline are important for the safety assessment as they control the groundwater flow rates as well as the exposure of new biosphere objects in the landscape where dose consequences are evaluated. Future human actions, including drilling of wells, are also of interest.

12.1 Modelling in this safety assessment

This section describes what data are expected from the supplier, and in which modelling activities the data are to be used.

Defining the data requested from the supplier

The data should include information about the duration after closure of the submerged conditions above the repository, the primary discharge area (biosphere object 157_2, see the **Biosphere synthesis report**) and (iii) the area downstream of the repository where the groundwater is associated with the highest concentrations of radionuclides, i.e. the *well interaction area* (**Biosphere synthesis report**). In addition, the rate of the shoreline displacement that results in the transition to terrestrial conditions is requested.

Modelling activities in which data will be used

Data on duration of submerged conditions and rate of shoreline displacement are used for:

- Groundwater-flow modelling.
- Landscape evolution modelling.
- Radionuclide transport modelling.

12.2 Experience from previous safety assessments

This section briefly summarises experience from previous safety assessments, especially SR-PSU, which may be of direct consequence for the data qualification in this report.

Modelling in previous safety assessments

Data on future relative sea-level change, i.e. the vertical displacement of the shoreline, were included in dedicated SR-PSU studies on landscape and groundwater-flow modelling (Brydsten and Strömgren 2013, Odén et al. 2014). Both studies used the same modelled shoreline displacement, corresponding to an initial vertical displacement rate of 6 mm/a and submerged conditions for the first 1 000 years after closure (described in SKB (TR-13-05) and Brydsten and Strömgren (2013)). This displacement was based on the assumption that the contribution from future sea-level rise is negligible, and it was used in the calculation cases of the main scenario in SR-PSU. In order to account for the effect of future sea-level rise in SR-PSU, a longer initial submerged period of 2 200 years was evaluated in the extended global warming scenario, which was included as a residual scenario.

Conditions for which data were used in previous safety assessments

As described in the previous section, the effect of initial submerged conditions was included in SR-PSU in the main scenario (excluding future sea-level rise) and in a residual scenario (including future sea-level rise). The vertical displacement rate of the shoreline was assumed to be the same in both scenarios.

Sensitivity to assessment results in previous safety assessments

The sensitivity of the assessment results to the initial duration of the submerged period was not specifically investigated in previous safety assessments. In SR-PSU (SKB TR-14-09, Figure 7-22), a lower initial dose was obtained in the residual scenario extended global warming compared with the global warming variant of the main scenario, which included a shorter initial period of submerged conditions. The maximum dose was only somewhat lower and the difference was attributed to reasons other than the longer duration of the submerged period.

Data on the submerged period used in SR-PSU were also important to determine the earliest possible timing for drilling of wells in the wells downstream of the repository scenario and the intrusion wells scenario.

Alternative modelling in previous safety assessments

No alternative modelling was performed in SAR-08 and SR-PSU.

Correlations used in previous safety assessment modelling

No correlations with other data were used in SAR-08 and SR-PSU.

Identified limitations of the data used in previous safety assessment modelling

The uncertainty in the relative sea-level change, and hence the duration of the submerged period, was reported to be large in SAR-08 and SR-PSU (SKB R-08-130, SKB TR-14-01). However, no major limitations in the data have been identified, given the approach taken when using them.

12.3 Supplier input on use of data in this and previous safety assessments

The method of selecting and using data practiced in SAR-08 and SR-PSU was appropriate.

12.4 Sources of information and documentation of data qualification

Sources of information

The sources of information for the data are Brydsten and Strömgren (2013) and the **Climate report** Sections 3.5 and 5.2.2 (Table 12-1). In the **Climate report**, references to relevant lower-level documents can be found.

Table 12-1. Main sources of information used in the data qualification.

Sources of information
Brydsten L, Strömgren M, 2013. Landscape development in the Forsmark area from the past into the future (8500 BC – 40 000 AD). SKB R-13-27, Svensk Kärnbränslehantering AB.
Climate report, 2023. Post-closure safety for SFR, the final repository for short-lived radioactive waste at Forsmark. Climate report, PSAR version. SKB TR-23-05, Svensk Kärnbränslehantering AB.

Categorising data sets as qualified or supporting data

The data on the initial duration of submerged conditions are qualified, see Table 12-2.

Table 12-2. Qualified and supporting data sets.

Qualified data sets	Supporting data sets
Climate report, Figure 5-2, Table 3-18	None
Brydsten and Strömgren (2013, Appendix 1)	

Excluded data previously considered as important

No data previously considered for qualification were excluded.

12.5 Conditions for which data are supplied

The duration of the submerged period above SFR and the shoreline displacement are completely determined by the present sea level and future relative sea-level change at the site. The relative sea level, in turn, comprises the net result of eustatic changes (changes in the sea level elevation, determined by changes in the volume and distribution of sea water in the world's oceans) and isostatic changes (vertical movement of Earth's crust). The present relative sea-level change at Forsmark is dominated by post-glacial isostatic rebound, which results in a slow lowering and off-shore migration of the shoreline at a rate of 4.1 mm/a (**Climate report**, Section 3.5).

The surface above the existing SFR1 and planned SFR3 is, as previously mentioned, presently submerged by the Baltic Sea, with maximum water depths of 7.2 m and 5.3 m, respectively. In the present safety assessment, the transition to terrestrial conditions above the repository is defined to occur when the relative sea level decreases by 5.8 m compared with the present level (**Climate report**, Section 1.4.3). At this reference height, between 75 and 100 % of the surface above the repository has become land. Furthermore, approximately at this height (i) the groundwater flow through the SFR waste vaults begins to converge towards stationary values (Öhman and Odén 2018); (ii) biosphere object 157_2 begins to emerge above sea level (Brydsten and Strömgren 2013); and (iii) the well interaction area emerges 1 m above the sea level, allowing extraction of water from a drilled well without the risk of salt-water intrusion (**Biosphere synthesis report**).

Using this definition, the transition to terrestrial conditions above SFR would take approximately 1 300 years to complete if the current relative sea-level decrease were to continue at the same rate in the future. However, as the global sea-level rise is currently increasing at an accelerating rate and will continue to do so in the near future (**Climate report**, Section 3.5), it is highly likely that the duration of the submerged period will be longer than 1 300 years.

The uncertainty in future global sea-level rise over the next thousands of years is very large, ranging from a few metres to several tens of metres depending on the amount of global warming and how Earth's ice sheets and glaciers respond to that warming (**Climate report**, Section 3.5). At Forsmark, this uncertainty translates into either a marine transgression, resulting in continued submerged conditions and an increased water depth above the repository, or a continued marine regression, resulting in the exposure of more land above the repository within the next thousands of years. Due to the large uncertainty in future sea-level rise, multiple variants of initial submerged conditions above SFR are proposed for this safety assessment.

12.6 Conceptual modelling uncertainty

As described in the **Climate report**, Section 3.5, the processes involved in glacial isostatic adjustment, and their effects upon relative sea-level evolution, are relatively well understood. There are major uncertainties in our understanding for parts of the mechanistic processes that influence relative sea-level change, specifically processes related to the response of ice sheets to global warming. For

other processes also affecting the relative sea-level, such as thermal expansion of warming ocean water, the uncertainties in understanding of the mechanistic processes are small. Another major uncertainty concerns the amount of future anthropogenic greenhouse-gas emissions and consequent warming of the climate, as this strongly influences the thermal expansion of the oceans and how much the ice sheet and glaciers will melt. In summary, taking all uncertainties into account, the total range of the duration of the submerged period is estimated to be between 1 300 and 18 300 years (**Climate report**, Table 3-18).

Uncertainties related to assumptions and discretisation of the glacial-isostatic adjustment model, which is used in Brydsten and Strömgren (2013), are significant (**Climate report**, Section 2.2.4). It should however be noted that the model is able to reconstruct the present rate of isostatic rebound at Forsmark to an acceptable degree (**Climate report**, Section 3.5).

12.7 Data uncertainty – spatial and temporal variability

Spatial variability of data

Relative sea-level changes vary spatially, due to spatial variations in the isostatic and eustatic contributions. The spatial scale of such variations however significantly exceeds the size of the Forsmark region considered in the landscape evolution and groundwater flow modelling performed. Such variations are therefore judged to be irrelevant for the safety assessment.

Temporal variability of data

The relative sea-level varies on shorter (order of hours and days) to long (inter-annual) time scales. Short-term variations, associate with e.g. storm surges, do not influence the long-term sea-level evolution. Such short-term variations are therefore judged not to be important for the safety assessment.

The rate of isostatic rebound will gradually decline with time. Modelling suggests that the present rate of isostatic rebound will be about 50 % lower in 10 000 years and 80 % lower in 20 000 years (**Climate report**, Section 2.2). The rate at which the landscape emerges above the sea is however considered to be of limited importance for the safety assessment compared with total time that the area is submerged and is therefore not considered.

12.8 Data uncertainty – correlations

No correlations are considered relevant and none were used.

12.9 Result of supplier's data qualification

In light of the large uncertainties related to future sea-level rise and resulting duration of the submerged period, several durations of submerged conditions are recommended for the safety assessment. To this end, the variants of reference external conditions, which collectively define the range of climate evolution evaluated in the main scenario (**Post-closure safety report**, Chapter 7), should arguably describe several initial durations of the submerged period. The reference external conditions consist of the *present-day climate variant*, *cold climate variant* and the *warm climate variant* (**Post-closure safety report**, Chapter 6):

- The present-day climate variant represents a simplified future development where present-day climate conditions are assumed to prevail for the complete assessment period of 100 000 years.
- The cold climate variant represents a future development characterised by substantial reductions in anthropogenic greenhouse-gas emissions and/or removal of atmospheric CO_2 by technological measures.

- The warm climate variant represents a future development where similar-to-present levels of anthropogenic greenhouse-gas emissions continue for the next few decades. This is in line with recent "business as usual" projections of future emissions which assume that current policies to mitigate climate change are implemented, but no new policies are adopted in the future (**Climate report**, Section 4.2)[7].

For the *present-day climate variant*, the same shoreline displacement as in SR-PSU is recommended (Brydsten and Strömgren 2013), resulting in submerged conditions for 1 000 years after closure and an initial vertical displacement rate of 6 mm/a. This estimate assumes a negligible contribution from the present and future sea-level rise, and consequently exceeds even the shortest possible duration of submerged conditions as reported in Section 12.6. This simplification is arguably pessimistic as it enables an earlier potential exposure of radionuclides through future land use compared with alternative representations where the present and future sea-level rise is accounted for.

For the *cold climate variant*, the air temperature after closure is not expected to be considerably higher than at present, and hence it is recommended that this variant uses the same initial shoreline displacement as in the *present-day climate variant*.

The relative sea-level evolution for the *warm climate variant* is illustrated in Figure 12-1. These data are further described in the **Climate report** Sections 3.5 and 5.2.2. They are based on glacial isostatic adjustment (GIA) modelling, extrapolations of up-to-present Holocene isostatic uplift rates at the Forsmark site, and peer-review-published data on future sea-level rise under a business-as-usual global warming (**Climate report**, Sections 2.2 and 3.5). The dotted lines show low- and high-end relative sea-level projections at Forsmark for the next 10 000 years. The difference between these estimates hence represents the modelling uncertainty in the multi-millennial sea-level rise under a business-as-usual global warming. Within this range, any relative sea-level development is judged to be equally likely (**Climate report**, Section 3.5). For simplicity, the average relative sea-level evolution within the range (solid line) is therefore recommended for the *warm climate variant*. The resulting initial duration of submerged conditions is 4 500 years, as indicated in Figure 12-1 by the time when the average relative sea-level (red solid line) drops below the reference height for submerged conditions above SFR (black dashed line). The reference height is described in Section 12.5.

As noted in Section 12.8, the rate of shoreline displacement is considered to be of minor importance for the safety assessment compared with the total duration of the submerged period. Therefore, potential effects of global warming on the rate of the delayed shoreline regression are not considered in the present safety assessment. To account for the prolonged submerged period in the PSAR modelling activities, it is instead judged appropriate to assume constant fully-submerged conditions for the first 3 500 years, after which the shoreline displacement of the *present-day climate variant* (Brydsten and Strömgren 2013) is applied[8]. This approach hence assumes that the shoreline regression in the *warm climate variant* is delayed by 3 500 years with respect to the *base variant*.

A consequence of using an average estimate for the *warm climate variant* is that the upper end of the uncertainty range in Figure 12-1 is not considered in the reference external conditions. The upper bound becomes even higher if also considering emissions scenarios that describe even higher cumulative anthropogenic greenhouse-gas emissions than under a business-as-usual scenario. As discussed in Section 12.6, the upper range of the initial submerged period is nearly 20 000 years when taking this uncertainty into account. Such a projection would require most of Earth's ice sheets to disappear. Even if this outcome is not considered to be very likely, it also cannot be excluded given the large uncertainties related to future global warming and the sensitivity of the ice sheets to this warming. In light of this uncertainty, it is recommended that a wider range of possible initial durations of submerged conditions, up to 20 000 years, is also considered in a sensitivity analysis within the safety assessment. The same technique for handling the delayed shoreline regression as for the *warm climate variant* (see above) is recommended for this sensitivity analysis.

[7] These levels of emissions approximately correspond to the Representative Concentration Pathways 4.5 and 6.0 (RCP4.5 and RCP6.0) used in the latest assessment report by the Intergovernmental Panel of Climate Change (IPCC 2013).

[8] Since the initial submerged period of the *present-day climate variant* has a duration of 1 000 years, this approach thus results in 4 500 years of submerged conditions for *warm climate variant*.

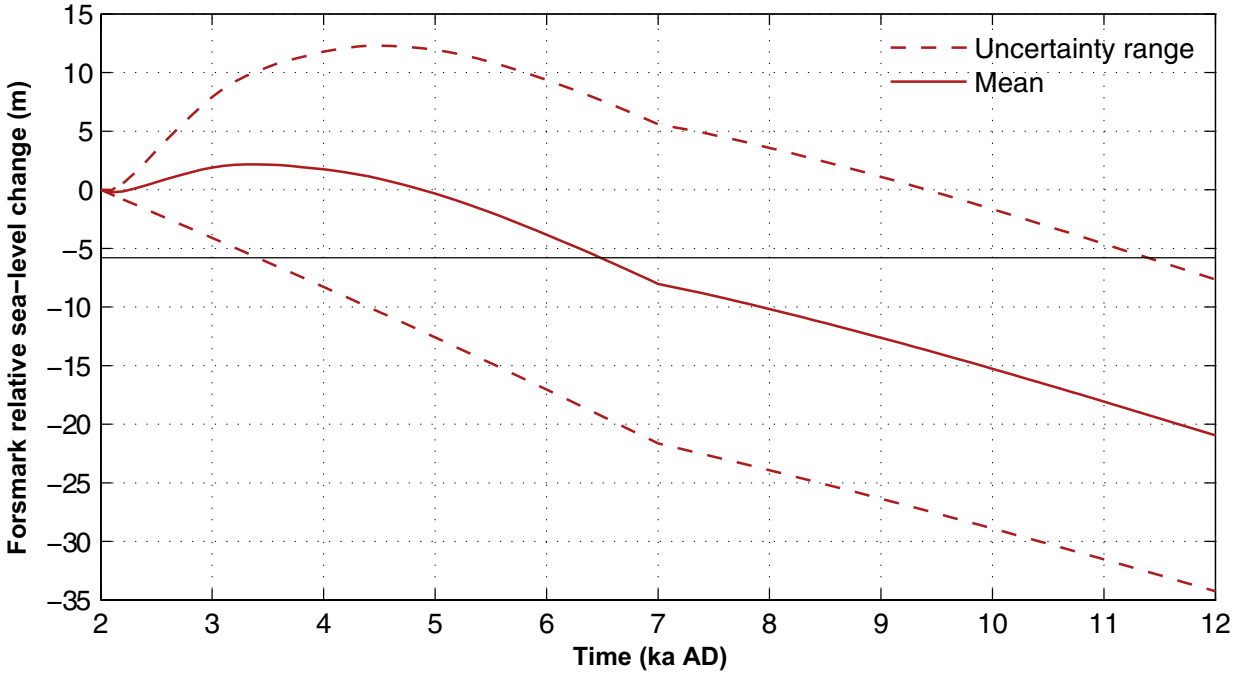

Figure 12-1. *Relative sea-level (RSL) change at Forsmark for the first 10 000 years after closure under a business-as-usual global warming. The red dotted lines represent low- and high-end relative sea-level change based on the lowest and highest global multi-millennial sea level projections, respectively (Climate report, Section 3.5). The red solid line represents the average of the low- and high-end projections. The black solid horizontal line indicates the reference height when the transition from submerged to terrestrial conditions is defined to occur (Section 12.5).*

Alternative climate evolutions that are analysed in less probable and residual scenarios, i.e. the *glaciation scenario* and the *hypothetical early permafrost scenario*, both describe developments towards colder climate conditions and lower sea-level rise, and thus the duration of submerged period in the *present-day climate variant* is recommended for these scenarios. A summary of the recommended data of the duration of the submerged period is given in Table 12-3.

Table 12-3. Summary of data recommended for the duration of submerged period in this safety assessment.

Data item	Initial duration of submerged conditions
Total range taking all scenario and conceptual uncertainties into account	1 000–20 000 years
Present-day climate variant, cold climate variant and all alternative climate evolutions	1 000 years
Warm climate variant	4 500 years

12.10 Judgements by the assessment team

Sources of information

The assessment team considers the source given in Section 12.4 to be sufficient.

Conditions for which data is supplied

The general conditions given in Section 12.5 are deemed sufficient by the assessment team.

Conceptual modelling uncertainty

The assessment team agrees with the supplier's statement that the conceptual modelling uncertainties are well known in Section 12.6.

Data uncertainty – spatial and temporal variability

The handling of spatial and temporal variabilities in Section 12.7 by the supplier is deemed sufficient.

Data uncertainty – correlations

The assessment team cannot find any correlations regarding this data within the safety assessment.

Results of supplier's data qualification

As all these data have been produced within PSAR and data qualification is judged to be adequate.

12.11 Data recommended for use in the assessment

The initial duration of submerged conditions presented in Table 12-3 and the relative sea-level data in Brydsten and Strömgren (2013, Appendix 1) are recommended for use in the assessment.

References

SKB's (Svensk Kärnbränslehantering AB) publications can be found at www.skb.com/publications. SKBdoc documents will be submitted upon request to document@skb.se.

References with abbreviated names

Post-closure safety report, 2023. Post-closure safety for SFR, the final repository for short-lived radioactive waste at Forsmark. Main report, PSAR version. SKB TR-23-01, Svensk Kärnbränslehantering AB.

Barrier process report, 2023. Post-closure safety for SFR, the final repository for short-lived radioactive waste at Forsmark. Engineered barrier process report, PSAR version. SKB TR-23-04, Svensk Kärnbränslehantering AB.

Biosphere synthesis report, 2023. Post-closure safety for SFR, the final repository for short-lived radioactive waste at Forsmark. Biosphere synthesis report, PSAR version. SKB TR-23-06, Svensk Kärnbränslehantering AB.

Climate report, 2023. Post-closure safety for SFR, the final repository for short-lived radioactive waste at Forsmark. Climate and climate-related issues, PSAR version. SKB TR-23-05, Svensk Kärnbränslehantering AB.

FEP report, 2014. FEP report for the safety assessment SR-PSU. SKB TR-14-07, Svensk Kärnbränslehantering AB.

FHA report, 2023. Post-closure safety for SFR, the final repository for short-lived radioactive waste at Forsmark. Handling of future human actions, PSAR version. SKB TR-23-08, Svensk Kärnbränslehantering AB.

Geosphere process report, 2014. Geosphere process report for the safety assessment SR-PSU. SKB TR-14-05, Svensk Kärnbränslehantering AB.

Initial state report, 2023. Post-closure safety for SFR, the final repository for short-lived radioactive waste at Forsmark. Initial state of the repository, PSAR version. SKB TR-23-02, Svensk Kärnbränslehantering AB.

Model tools report, 2023. Post-closure safety for SFR, the final repository for short-lived radioactive waste at Forsmark. Model tools summary report, PSAR version. SKB TR-23-11, Svensk Kärnbränslehantering AB.

Radionuclide transport report, 2023. Post-closure safety for SFR, the final repository for short-lived radioactive waste at Forsmark. Radionuclide transport and dose calculations, PSAR version. SKB TR-23-09, Svensk Kärnbränslehantering AB.

Waste process report, 2023. Post-closure safety for SFR, the final repository for short-lived radioactive waste at Forsmark. Waste form and packaging process report, PSAR version. SKB TR-23-03, Svensk Kärnbränslehantering AB.

Regular references

Aalto H, Valkiainen M, 1997. Simulated wetted bituminization product. In Vettyneen bitumointuotteen jatkokarakterisointi. Työraportti VLJ-6/97, VTT Chemical Technology.

Aalto H, Valkiainen M, 2004. Behaviour of bituminized ion-exchangers under repository conditions. In Long term behaviour of low and intermediate level waste packages under repository conditions. Results of a co-ordinated research project 1997–2002. IAEA-TECDOC-1397, International Atomic Energy Agency, 89–100.

Abarca E, Idiart A, de Vries L M, Silva O, Molinero J, von Schenck H, 2013. Flow modelling on the repository scale for the safety assessment SR-PSU. SKB TR-13-08, Svensk Kärnbränslehantering AB.

Abarca E, Silva O, Idiart A, Nardi A, Font J, Molinero J, 2014. Flow and transport modelling on the vault scale. Supporting calculations for the safety assessment SR-PSU. SKB R-14-14, Svensk Kärnbränslehantering AB.

Abarca E, Sampietro D, Sanglas J, Molinero J, 2020. Modelling of the near-field hydrogeology. Report for the safety assessment SR-PSU (PSAR). SKB R-19-20, Svensk Kärnbränslehantering AB.

Ahlford K, 2021. Alternativa inventarier för osäkerheter i RN. SKBdoc 1929598 ver 1.0, Svensk Kärnbränslehantering AB.

Aittola J-P, Kleveland O, 1982. Swelling of bituminized ion exchange resins. NKA AVF (82) 215, Studsvik.

Aittola J-P, Chyssler J, Ringberg H, 1982. Thermal stability of ion-exchange resins. SKBF/KBS TR 81-13, Svensk Kärnbräsnleförsörjning AB.

Akafia M M, Reich T J, Koretsky C M, 2011. Assessing Cd, Co, Cu, Ni and Pb sorption on montmorillonite using surface complexation models. Applied Geochemistry 26, S154–S157.

Albinsson Y, 1991. Sorption of radionuclides in grantic rock SKB AR 91-07, Svensk Kärnbränslehantering AB.

Almkvist L, Gordon A, 2007. Low and intermediate level waste in SFR 1. Reference waste inventory 2007. SKB R-07-17, Svensk Kärnbränslehantering AB.

Andersson L, Karnland O, Hedström M, 2014. Swelling pressure of ion-exchange resins at SFR. Clay Technology AB. SKBdoc 1450664 ver 1.0, Svensk Kärnbränslehantering AB.

Andra, 2005. Dossier 2005 Argile. Référentiel de comportement des radionucléides et des toxiques chimiques d'un stockage dans le Callovo-Oxfordien jusqu'à l'homme. Site de Meuse/Haute-Marne, Tome 1/2. Rapport C.RP.ASTR.04.0032, Andra, France. (In French.)

Arya C, Xu Y, 1995. Effect of cement type on chloride binding and corrosion of steel in concrete. Cement and Concrete Research 25, 893–902.

Asea-Atom, 1985. B1 – Analys av bitumenprodukter: Svällningstester. Rapport KVC 85-204. (In Swedish.)

Auqué L, Gimeno M, Acero P, Gómez J, 2013. Composition of groundwater for SFR and its extension, during different climatic cases, SR-PSU. SKB R-13-16, Svensk Kärnbränslehantering AB.

Baes C F, Mesmer R E, 1976. The hydrolysis of cations. New York: Wiley-Interscience.

Baeyens B, Bradbury M H, 1997. A mechanistic description of Ni and Zn sorption on Na-montmorillonite. Part I: Titration and sorption measurements. Journal of Contaminant Hydrology 27, 199–222.

Bayliss S, Ewart F T, Howse R M, Smith-Briggs J L, Thomason H P, Willmott H A, 1988. The solubility and sorption of lead-210 and carbon-14 in a near-field environment. In Apted M J, Westerman R E (eds). Scientific basis for nuclear waste management XI: symposium held in Boston, Massachusetts, USA, 30 November – 3 December 1987. Pittsburgh, PA: Materials Research Society. (Materials Research Society Symposium Proceedings 112), 33–42.

Bergström U, Avila R, Ekström P-A, de la Cruz I, 2008. Dose assessment for SFR 1. SKB R-08-15, Svensk Kärnbränslehantering AB.

Berner U, 1990. A thermodynamic description of the evolution of pore water chemistry and uranium speciation during the degradation of cement. PSI Bericht 62, Paul Scherrer Institute, Switzerland.

Berntsson J, 1992. Typbeskrivning av avfallskollin (B20) – Bitumensolidifierad jonbytarmassa och filterhjälpmedel i plåtfat förpackade i containrar, Beteckning B.20, PBD-9102-05, Sydkraft Barsebäcksverket. (In Swedish.)

Bienvenu P, Cassette P, Andreoletti G, Bé M-M, Comte J, Lépy M-C, 2007. A new determination of ^{79}Se half-life. Applied Radiation and Isotopes 65, 355–364.

Björkenstam E, 1997. Utveckling av SFR-bruket. UC 97:4Ö, Vattenfall Utveckling AB. SKBdoc 1439832 ver 1.0, Svensk kärnbränslehantering AB.

Blinder R, Champenois J-B, Leclerc A, Poulesquen A, Guillermo A, Lautru J, Podor R, Bardet M, 2019. NMR 1D-Imaging of water infiltration into porous bitumen-salt matrices: the effect of salt solubility. The Journal of Physical Chemistry C 123, 27105–27115.

Boverket, 2004. Boverkets handbok om betongkonstruktioner: BBK 04. 3rd ed. Karlskrona: Boverket. (In Swedish.)

Bradbury M H, Baeyens B, 1997. Far-field sorption data bases for performance assessment of a L/ILW repository in a disturbed/altered Palfris marl host rock. Nagra NTB 96-06, Nagra, Switzerland.

Bradbury M H, Baeyens B, 1999. Modelling the sorption of Zn and Ni on Ca-montmorillonite. Geochimica et Cosmochimica Acta 63, 325–336.

Bradbury M H, Baeyens B, 2003. Near-field sorption data bases for compacted MX-80 bentonite for performance assessment of high-level radioactive waste repository in Opalinus Clay host rock. Nagra NTB 02-19, Nagra, Switzerland.

Bradbury M H, Baeyens B, 2005. Experimental measurements and modeling of sorption competition on montmorillonite. Geochimica et Cosmochimica Acta 69, 4187–4197.

Bradbury M H, Baeyens B, 2006. Modelling sorption data for the actinides Am(III), Np(V) and Pa(V) on montmorillonite. Radiochimica Acta 94, 619–625.

Bradbury M H, Baeyens B, 2009. Sorption modelling on illite. Part I: Titration measurements and the sorption of Ni, Co, Eu and Sn. Geochimica et Cosmochimica Acta 73, 990–1003.

Bradbury M H, Sarott F-A, 1995. Sorption databases for the cementitious near-field of a L/ILW repository for performance assessment. PSI Bericht 95-06, Paul Scherrer Institute, Switzerland.

Bradbury M H, Van Loon L R, 1998. Cementitious near-field sorption data bases for performance assessment of a L/ILW disposal facility in a Palfris Marl Host Rock, CEM-94: Update I, June 1997. PSI Bericht 98-01, Paul Scherrer Institute, Switzerland.

Brodén K, Wingefors W, 1992. The effect of temperature on water uptake, swelling and void formation in a bitumen matrix with ion exchange resins. Waste Management 12, 23–27.

Brodersen K, Mose Pedersen B, Vinther A, 1983. Comparative study of test methods for bituminized and other low- and medium-level solidified waste materials. Final report (1981–1982) for contract WAS 235 DK(G). RISØ-M-2415, Risø National Laboratory, Roskilde, Denmark.

Brownsword M, Manning M C, Pilkington N J, Williams S J, 2002. The effect of cellulose degradation products on the solubility and sorption of zirconium and the sorption of lead under cementitious repository conditions. Report AEAT/R/ENV/0549, AEA Technology, UK.

Bruno J, González-Siso M R, Duro L, Gaona X, Altmaier M, 2018. Key master variables affecting the mobility of Ni, Pu, Tc and U in the near field of the SFR repository. Main experimental findings and PA implications of the PhD thesis. SKB TR-18-01, Svensk Kärnbränslehantering AB.

Brydsten L, Strömgren M, 2013. Landscape development in the Forsmark areafrom the past into the future (8500 BC – 40 000 AD). SKB R-13-27, Svensk Kärnbränslehantering AB.

Carbol P, Engkvist I, 1997. Compilation of radionuclide sorption coefficients for performance assessment. SKB R-97-13, Svensk Kärnbränslehantering AB.

Catlow S A, Troyer G L, Hansen D R, Jones R A, 2005. Half-life measurement of ^{126}Sn isolated from Hanford nuclear defense waste. Journal of Radioanalytical and Nuclear Chemistry 263, 599–603.

Cembygg Euroc, 1989. Fiberbruk 50 VF Produktblad. SKBdoc 1262740 ver 1.0, Svensk Kärnbränslehantering AB. (In Swedish.)

Choi J-W, Oscarson D W, 1996. Diffusive transport through compacted Na- and Ca-bentonite. Journal of Contaminant Hydrology 22, 189–202.

Crawford J, 2010. Bedrock K_d data and uncertainty assessment for application in SR-Site geosphere transport calculations. SKB R-10-48, Svensk Kärnbränslehantering AB.

Crawford J, 2013. Quantification of rock matrix K_d data and uncertainties for SR-PSU. SKB R-13-38, Svensk Kärnbränslehantering AB.

Crawford J, 2017. Organic complexation in the geosphere for SR PSU. SKBdoc 1577134 ver 1.0, Svensk Kärnbränslehantering AB.

Crawford J, 2018. Technical Note – K_d values for oxyanions in SR-PSU. Updated K_d recommendations for Mo-93 and Se-79. Kemakta Konsult AB. SKBdoc 1689868 ver 1.0, Svensk Kärnbränslehantering AB.

Cronstrand P, 2005. Assessment of uncertainty intervals for sorption coefficients. SFR-1 uppföljning av SAFE. SKB R-05-75, Svensk Kärnbränslehantering AB.

Cronstrand P, 2007. Modelling the long-time stability of the engineered barriers of SFR with respect to climate changes. SKB R-07-51, Svensk Kärnbränslehantering AB.

Cronstrand P, 2014. Evolution of pH in SFR 1. SKB R-14-01, Svensk Kärnbränslehantering AB.

Cronstrand P, 2016. Long-term performance of the bentonite barrier in the SFR silo. SKB TR-15-08, Svensk Kärnbränslehantering AB.

Cronstrand P, Hassanzadeh M, Hed G, 2011. Metodik för bedömning av långsiktig funktion hos betongbarriär. SFR. AE-NCC 11-013, Vattenfall AB. (In Swedish.)

Dario M, Molera M, Allard B, 2004. Effect of organic ligands on the sorption of europium on TiO_2 and cement at high pH. SKB TR-04-04, Svensk Kärnbränslehantering AB.

Daoud W Z, Renken K J, 1999. Laboratory measurements of the radon gas diffusion coefficient for a fractured concrete sample and radon gas barrier systems. Proceedings of the International Radon Symposium (AARST), Las Vegas, NV, 1999, 14.0–14.12.

Diomidis N, 2014. Scientific basis for the production of gas due to corrosion in a deep geological repository. Arbeitsbericht NAB 14-21, Nagra, Switzerland.

Dmitriev P P, Konstantinov I O, Krasnov N N, 1967. Determination of the Mo93 half-life from the yields of nuclear reactions. Yadernaya Fizika 6, 209; also published in Soviet Journal of Nuclear Physics 6, 153 (1968).

Duro L, Grivé M, Domènech C, Roman-Ross G, Bruno J, 2012. Assessment of the evolution of the redox conditions in SFR 1. SKB TR-12-12, Svensk Kärnbränslehantering AB.

Dverstorp B, Sundström B, 2003. SSI:s och SKI:s granskning av SKB:s uppdaterade slutlig säkerhetsrapport för SFR 1. Granskningsrapport. SSI Rapport 2003:21, Swedish Radiation Protection Authority, SKI Rapport 2003:37, Swedish Nuclear Power Inspectorate. (In Swedish.)

Dzombak D A, Morel F M M, 1990. Surface complexation modelling: hydrous ferric oxide. New York: Wiley.

Ecke H, Hansson N, 2012. Determination of carbonate content in concrete from 1BMA. Report U 12-82, Vattenfall Research & Development AB. SKBdoc 1377831 ver 2.0, Svensk Kärnbränslehantering AB.

Elfwing M, Mårtensson P, Pettersson A, 2015. Rapport över aktuell status för 1BMA i SFR1. SKBdoc 1440875 ver 2.0, Svensk Kärnbränslehantering AB. (In Swedish.)

Elfwing M, Lundin M, von Schenck H, 2017. Vidareutvecklad utformning av förvarsutrymmet 2BMA i utbyggd del av SFR. SKBdoc 1569813 ver 1.0, Svensk Kärnbränslehantering AB. (In Swedish.)

Elfwing M, von Schenck H, Åstrand P-G, 2018. Uppdaterad analys av strålsäkerheten efter förslutning för 1BMA i SFR1. SKBdoc 1686798 ver 1.0, Svensk Kärnbränslehantering AB. (In Swedish.)

Emrén A T, 1983. Theoretical calculation of swelling properties of ion-exchange resins. KEFYDA Konsult AB.

Ericsson K, Klingstedt G, 1987. Svällningsegenskaper hos radioaktiva jonbytarmassor från Forsmarksverket. Rapport 87041, The Swedish Cement and Concrete Research Institute (CBI). (In Swedish.)

Eriksen T E, Jansson M, 1996. Diffusion of I^-, Cs^+ and Sr^{2+} in compacted bentonite. Anion exclusion and surface diffusion. SKB TR 96-16, Svensk Kärnbränslehantering AB.

Eschrich H, 1980. Properties of long-term behaviour of bitumen and radioactive waste-bitumen mixtures. SKBF/KBS TR 80-14, Svensk Kärnbränsleförsörjning AB.

Fanger G, Skagius K, Wiborgh M, 2001. Project SAFE. Complexing agents in SFR. SKB R-01-04, Svensk Kärnbränslehantering AB.

Firestone R B, Baglin C M (ed), Chu S Y F (ed), 1998. Table of isotopes: 1998 update. 8th ed. New York: Wiley.

Gaucher E, Tournassat C, Nowak C, 2005. Modelling the geochemical evolution of the multi-barrier system of the Silo of the SFR repository. Final report. SKB R-05-80, Svensk Kärnbränslehantering AB.

Gerard B, Pijaudier-Cabot G, Laborderie C, 1998. Coupled diffusion-damage modelling and the implications on failure due to strain localisation. International Journal of Solids and Structures 35, 4107–4120.

Giffaut E, Grivé M, Blanc P, Vieillard P, Colàs E, Gailhanou H, Gaboreau S, Marty N, Madé B, Duro L, 2014. Andra thermodynamic database for performance assessment: ThermoChimie. Applied Geochemistry 49, 225–236.

Gimeno M J, Auqué L F, Gómez J B, Acero P, 2011. Site investigation SFR. Water–rock interaction and mixing modeling in the SFR. SKB P-11-25, Svensk Kärnbränslehantering AB.

Glaus M A, Frick S, Rossé R, Van Loon L R, 2010. Comparative study of tracer diffusion of HTO, $^{22}Na^{+}$ and $^{36}Cl^{-}$ in compacted kaolinite, illite and montmorillonite. Geochimica et Cosmochimica Acta 74, 1999–2010.

Goldberg S, Glaubig R A, 1988. Anion sorption on a calcareous, montmorillonitic soil-selenium. Soil Science Society of America Journal 52, 954–958.

Goldberg S, Forster H S, Godfrey C L, 1996. Molybdenum adsorption on oxides, clay minerals, and soils. Soil Science Society of America Journal 60, 425–432.

Goldberg S, Johnston C T, Suarez D L, Lesch S M, 2007. Mechanism of molybdenum adsorption on soils and soil minerals evaluated using vibrational spectroscopy and surface complexation modeling. In Barnett M, Kent D (eds). Adsorption of metals by geomedia II: variables, mechanisms, and model applications. Amsterdam: Elsevier. (Developments in Earth & Environmental Sciences 7), 235–266.

Goutelard F, Charles Y, 2004. Etude de l'effet de la température et de la viscosité de l'eau sur les paramètres de la diffusion dans les l'argilites du Callovo-Oxfordien et la bentonite. Rapport Andra C.NT.PSTR.04.009; data presented in Andra 2005.

Gorgeon L, 1994. Contribution à la modélisation physico-chimique de rétention de radioéléments à vie longue par des matériaux argileux. PhD thesis. Université Paris VI.

Grambow B, Fattahi M, Montavon G, Moisan C, Giffaut E, 2006. Sorption of Cs, Ni, Pb, Eu(III), Am(III), Cm, Ac(III), Tc(IV), Th, Zr, and U(IV) on MX 80 bentonite: an experimental approach to assess model uncertainty. Radiochimica Acta 94, 627–636.

Grolander S, 2013. Biosphere parameters used in radionuclide transport modelling and dose calculations in SR-PSU. SKB R-13-18, Svensk Kärnbränslehantering AB.

Grütter A, von Gunten H R, Rössler E, Keil R, 1994. Sorption of nickel and cobalt on a size-fraction of unconsolidated glaciofluvial deposits and on clay minerals. Radiochimica Acta 65, 181–187.

Haas P, Gartenmann P, Golser R, Kutschera W, Suter M, Synal H-A, Wagner M J M, Wild E, Winkler G, 1996. A new half-life measurement of the long-lived fission product ^{126}Sn. Nuclear Instruments and Methods in Physics Research Section B: Beam Interactions with Materials and Atoms 114, 131–137.

Hakanen M, Ervanne H, Puukko E, 2014. Safety case for the disposal of spent nuclear fuel at Olkiluoto. Radionuclide migration parameters for the geosphere. Posiva 2012-41, Posiva Oy, Finland.

Harbottle G, 1970. The half-lives of two long-lived nuclear isomers, ^{108m}Ag and $^{192m2}Ir$, and of ^{137}Cs and ^{204}Tl. Radiochimica Acta 13, 132–134.

He M, Jiang S, Jiang S, Chen Q, Qin J, Wu S, Dong Y, Zhao Z, 2000. Measurement of ^{79}Se and ^{64}Cu with PXAMS. Nuclear Instruments and Methods in Physics Research B 172, 177–181.

He M, Jiang S, Jiang S, Diao L, Wu S, Li Ch, 2002. Measurement of the half-life of ^{79}Se with PX-AMS. Nuclear Instruments and Methods in Physics Research B 194, 393–398.

Hejll A, Hassanzadeh M, Hed G, 2012. Sprickor i BMA:s betongbarriär – Inspektion och orsak. Rapport AE-NCC 12-004, Vattenfall AB. SKBdoc 1430853 ver 1.0, Svensk Kärnbränslehantering AB. (In Swedish.)

Hedström S, 2019. Steel corrosion in SFR by waste type and vault without solubility or transport limitations. SKBdoc 1858222 ver 1.0, Svensk Kärnbränslehantering AB.

Hedström S, 2020. Utvärdering av komplexbildande tri- och tetraminer i rostskyddsfärg. SKBdoc 1892917 ver 1.0, Svensk Kärnbränslehantering AB. (In Swedish.)

Hellman H, 2017. Ändrad anläggningsutformning vid övergång till segmenterade reaktortankar. SKBdoc 1581334 ver 1.0, Svensk Kärnbränslehantering AB. (In Swedish.)

Helmer R G, Browne E, Bé M-M, 2002. International decay data evaluation project. Journal of Nuclear Science and Technology, Supplement 2, 455–458.

Holgersson S, Albinsson Y, Allard B, Borén, H, Pavasars I, Engkvist I, 1998. Effects of glucoisosaccharinate on Cs, Ni, Pm, and Th sorption onto, and diffusion into cement. Radiochimica Acta 82, 393–398.

Holmén J G, 1997. On the flow of groundwater in closed tunnels. Generic hydrogeological modelling of nuclear waste repository, SFL 3-5. SKB TR 97-10, Svensk Kärnbränslehantering AB.

Holmén J G, 2005. SFR-1. Inverse modelling of inflow to tunnels and propagation of estimated uncertainties to predictive stages. SKB R-05-74, Svensk Kärnbränslehantering AB.

Holmén J, 2007. SFR inverse modelling Part 2. Uncertainty factors of predicted flow in deposition tunnels and uncertainty in distribution of flow paths from deposition tunnels. SKB R-07-61, Svensk Kärnbränslehantering AB.

Holmén J G, Stigsson M, 2001a. Modelling of future hydrogeological conditions at SFR. SKB R-01-02, Svensk Kärnbränslehantering AB.

Holmén J G, Stigsson M, 2001b. Details of predicted flow in deposition tunnels at SFR, Forsmark. SKB R-01-21, Svensk Kärnbränslehantering AB.

Höglund L O, 1992. Some notes on ettringite formation in cementitious materials; Influence of hydration and thermodynamic constraints for durability. Cement and Concrete Research 22, 217–228.

Höglund L O, 2001. Project SAFE. Modelling of long-term concrete degradation processes in the Swedish SFR repository. SKB R-01-08, Svensk Kärnbränslehantering AB.

Höglund L O, 2014. The impact of concrete degradation on the BMA barrier functions. SKB R-13-40, Svensk Kärnbränslehantering AB.

Höglund L O, 2018. pH-utveckling i bergssal BRT. SKBdoc 1608409 ver 2.0, Svensk Kärnbränslehantering AB. (In Swedish.)

Höglund L O, 2019. pH evolution in 2BMA – Assumptions, data and modelling results. Kemakta Konsult AB, 2019-06-20. SKBdoc 1698794 ver 1.0, Svensk Kärnbränslehantering AB.

Höglund L O, Bengtsson A, 1991. Some chemical and physical processes related to the long-term performance of the SFR repository. SKB SFR 91-06, Svensk Kärnbränslehantering AB.

ICRP, 1983. Radionuclide transformations: energy and intensity of emissions. Oxford: Pergamon (ICRP Publication 38; Annals of the ICRP 11–13).

ICRP, 2008. Nuclear decay data for dosimetric calculations. Amsterdam: Elsevier. (ICRP Publication 107; Annals of the ICRP 38(3)).

Ikeda T, Amaya T, 1998. Model development of chemical evolution in repository. Vol.II. Acquisition of nuclide migration data in near-field. Technical Report PNC ZJ 1281 98–03, Power Reactor and Nuclear Development Corporation, Japan.

IPCC, 2013. Climate change 2013: the physical science basis: summary for policymakers. Contribution of Working Group I to the Fifth Assessment Report of the Intergovernmental Panel on Climate Change. Available at: http://www.ipcc.ch

Irisawa K, Meguro Y, 2017. Swelling pressure and leaching behaviors of synthetic bituminized waste products with various salt contents under a constant-volume condition. Journal of Nuclear Science and Technology 54, 365–372.

Irisawa K, Ohsone O, Meguro Y, 2014. Effects of salt content on leaching properties of synthetic bituminized wastes. Journal of Nuclear Science and Technology 51, 323–331.

Jacobsen S, Gjørv O E, 1987. Hydraulisk konduktivitet i SFR silobetong. SKB Projekt SFR Teknisk PM 45, Svensk Kärnbränslehantering AB. (In Norwegian.)

Jan Y-L, Wang T-H, Li M-H, Tsai S-C, Wei Y-Y, Hsu C-N, Teng S-P, 2007. Evaluating adsorption ability of granite to radioselenium by chemical sequential extraction. Journal of Radioanalytical and Nuclear Chemistry 273, 299–306.

Jan Y-L, Wang T-H, Li M-H, Tsai S-C, Wei Y-Y, Teng S-P, 2008. Adsorption of Se species on crushed granite: A direct linkage with its internal iron-related minerals. Applied Radiation and Isotopes 66, 14–23.

Jensen V, Karnland O, Hedström M, 2017. Swelling capacity and swelling pressure of ion-exchange resins at SFR. Clay Technology AB. SKBdoc 1667888 ver 1.0, Svensk Kärnbränslehantering AB.

Jiang S, Guo J, Jiang S, Li Ch, Cui A, He M, Wu S, Li S, 1997. Determination of the half-life of ^{79}Se with the accelerator mass spectrometry technique. Nuclear Instruments and Methods in Physics Research B 123, 405–409.

Jiang S, He M, Diao L, Guo J, Wu S, 2001. Remeasurement of the half-life of ^{79}Se with the projectile x-ray detection method. Chinese Physics Letters 18, 746–749.

Johansson E, 2017. Kemirapport AP TD PSU15-16-025 Volymexpansion och lakningsexperiment åt PSU-1504. SKBdoc 1603429 ver 1.0, Svensk Kärnbränslehantering AB. (In Swedish.)

Jörg G, Bühnemann R, Hollas S, Kivel N, Kossert K, Van Winckel S, Gostomski C L, 2010. Preparation of radiochemically pure ^{79}Se and highly precise determination of its half-life. Applied Radiation and Isotopes 68, 2339–2351.

Kajan I, Heinitz S, Kossert K, Sprung P, Dressler R, Schumann D, 2021. First direct determination of the ^{93}Mo half-life. Scientific Reports 11, 19788. doi:10.1038/s41598-021-99253-5

Kaplan D, Robers K, Coates J, Siegfried M, Serkitz S, 2008. Saltstone and concrete interactions with radionuclides: sorption (K_d), desorption, and reduction capacity measurements. Report SRNS-STI-2008-00045, Savannah River National Laboratory, Aiken, South Carolina.

Keith-Roach M, Shahkarami P, 2021. Organic materials with the potential for complexation in the SFR, the final repository for short-lived radioactive waste. Investigation of new acceptance criteria. SKB R-21-03, Svensk Kärnbränslehantering AB.

Keith-Roach M, Lindgren M, Källström K, 2014. Assessment of complexing agent concentrations in SFR. SKB R-14-03, Svensk Kärnbränslehantering AB.

Keith-Roach M, Lindgren M, Källström K, 2021. Assessment of complexing agent concentrations for the post-closure safety assessment in PSAR SFR. SKB R-20-04, Svensk Kärnbränslehantering AB.

Khan S A, Rehman R, Khan M A, 1995. Adsorption of chromium (III), chromium (VI) and silver (I) on bentonite. Waste Management 15, 271–282.

Kummert R, Stumm W, 1980. The surface complexation of organic acids on hydrous γ-Al_2O_3. Journal of Colloid and Interface Science 75, 373–385.

Kursten B, Smalios E, Azkarate I, Werme L, Smart N R, Santarini G, 2004. COBECOMA State-of-the-art document on the COrrosion BEhaviour of COntainer Materials. Contract FIKW-CT-20014-20138, Final report, European Commission.

Laaksoharju M, Gurban I, Skårman, 1998. Summary of hydrochemical conditions at Aberg, Beberg and Ceberg. SKB TR-98-03, Svensk Kärnbränslehantering AB.

Lagerblad B, Rogers P, Vogt C, Mårtensson P, 2017. Utveckling av konstruktionsbetong till kassunerna i 2BMA. SKB R-17-21, Svensk Kärnbränslehantering AB. (In Swedish.)

Lagerlund J, 2020. Mätning av hydraulisk konduktivitet för tvättad makadam, 16/32 mm. VRD – R50:2020, Vattenfall AB. SKBdoc 1910987 ver 1.0, Svensk Kärnbränslehantering AB. (In Swedish.)

Lagerlund J, 2022. Hydraulisk konduktivitet i grovkorniga jordmaterial. Rapport 2022:849, Energiforsk. (In Swedish.)

Le Feunteun S, Diat O, Guillermo A, Poulesquen A, Podor R, 2011. NMR 1D-imaging of water infiltration into mesoporous matrices. Magnetic Resonance Imaging 29, 443–455.

Li X, Puhakka E, Liu L, Zhang W, Ikonen J, Lindberg A, Siitari-Kauppi M, 2020. Multi-site surface complexation modelling of Se(IV) sorption on biotite. Chemical Geology 533, 119433. doi:10.1016/j.chemgeo.2019.119433

Liang D, Jiang S, Xiao-Bo W, Dong K J, Shao-Yong W, Xu-Ran Y, Xiao-Ming W, Xiao-Xi L, Qing-Liang X, Ming H, 2014. Measurement of the half-life of ^{79}Se with accelerator mass spectrometry. Chinese Physics C 38, 106204. doi:10.1088/1674-1137/38/10/106204.

Lindgren M, Pettersson M, Karlsson S, Moreno L, 2001. Project SAFE. Radionuclide release and dose from the SFR repository. SKB R-01-18, Svensk Kärnbränslehantering AB.

Lu Y, Garboczi E, Bentz D, Davis J, 2012. Modeling chloride transport in cracked concrete: a 3-D image-based microstructure simulation. In Proceedings of COMSOL Conference 2012, Boston, MA, 3–5 October 2012. Available at: http://www.nist.gov/customcf/get_pdf.cfm?pub_id=912153

Luna M, Arcos D, Duro L, 2006. Effects of grouting, shotcreting and concrete leachates on backfill geochemistry. SKB R-06-107, Svensk Kärnbränslehantering AB.

Löfgren M, Sidborn M, 2018. Modelling of bounding corrosion rates of reactor pressure vessels in SFR due to earth currents. SKB R-16-14, Svensk Kärnbränslehantering AB.

Mariën A, Mokni N, Valcke E, Olivella S, Smets S, Li X, 2013. Osmosis-induced water uptake by Eurobitum bituminized radioactive waste and pressure development in constant volume conditions. Journal of Nuclear Materials 432, 348–365.

Marques Fernandes M, Baeyens B, Bradbury M H, 2008. The influence of carbonate complexation on lanthanide/actinide sorption on montmorillonite. Radiochimica Acta 96, 691–697.

Matsuda M, Nishi T, Chino K, Kikuchi M, 1992. Solidification of spent ion exchange resin using new cementious material, (I). Swelling pressure of ion exchange resin. Journal of Nuclear Science and Technology 29, 883–889.

Mattigod S V, Bovaird C C, Wellman D M, Skinner D J, Cordova E A, Wood M I, 2009. Effect of concrete waste form properties on radionuclide migration. PNNL-18745, Pacific Northwest National Laboratory, Richland, Washington.

McNaught A D, Wilkinson A, 1997. Compendium of chemical terminology: IUPAC recommendations. 2nd ed. Oxford: Blackwell Science. XML on-line corrected version available at: http://goldbook.iupac.org

Melot G, Dangla P, Granet S, M'Jahad S, Champenois J B, Poulesquen A, 2020. Chemo-hydro-mechanical analysis of bituminized waste swelling due to water uptake: experimental and model comparisons. Journal of Nuclear Materials 536, 152165. doi:10.1016/j.jnucmat.2020.152165

Missana T, Alonso U, García-Gutiérrez M, 2009. Experimental study and modeling of selenite sorption onto illite and smectite clays. Journal of Colloid and Interface Science 334, 132–138.

Missana T, García-Gutiérrez M, Mingarro M, Alonso U, 2019. Selenite retention and cation co-adsorption effects under alkaline conditions generated by cementitious materials: the case of C-S-H phases. ACS Omega 4, 13418–13425.

Mokni N, Olivella S, Valcke E, Mariën A, Smets S, Li X, 2011. Deformation and flow driven by osmotic processes in porous materials: application to bituminised waste materials. Transport in Porous Media 86, 635–662.

Molera M, Eriksen T, 2002. Diffusion of $^{22}Na^{+}$, $^{85}Sr^{2+}$, $^{134}Cs^{+}$ and $^{57}Co^{2+}$ in bentonite clay compacted to different densities: experiments and modeling. Radiochimica Acta 90, 753–760.

Montavon G, Guo Z, Lützenkirchen J, Alhajji E, Kedziorek M A M, Bourg A C M, Grambow B, 2009. Interaction of selenite with MX-80 bentonite: effect of minor phases, pH, selenite loading, solution composition and compaction. Colloids and Surfaces A: Physicochemical and Engineering Aspects 332, 71–77.

Moreno L, Neretnieks I, 2013. Impact of gas generation on radionuclide release – comparison between results for new and old data. SKB P-13-40, Svensk Kärnbränslehantering AB.

Moreno L, Skagius K, Södergren S, Wiborgh M, 2001. Project SAFE. Gas related processes in SFR. SKB R-01-11, Svensk Kärnbränslehantering AB.

Motta M M, Miranda C F, 1989. Molybdate adsorption on kaolinite, montmorillonite and illite: constant capacitance modelling. Soil Science Society of America Journal 53, 380–385.

Mu S, De Schutter G, Ma B-G, 2013. Non-steady state chloride diffusion in concrete with different crack densities. Materials and Structures 46, 123–133.

Muurinen A, Penttilä-Hiltunen P, Rantanen J, 1987. Diffusion mechanisms of strontium and caesium in compacted sodium bentonite. In Bates J K, Seefeldt W B (eds). Scientific basis for nuclear waste management X: symposium held in Boston, Massachusetts, USA, 1–4 December 1986. (Materials Research Society Symposium Proceedings 84), 803–812.

Mårtensson P, 2014. He-läcksökning av sprickor i betongkonstruktionen i 1BMA. SKBdoc 1452199 ver 1.0, Svensk Kärnbränslehantering AB. (In Swedish.)

Mårtensson P, 2017. Hållfasthetsegenskaper hos betongkonstruktionerna i 1–2BMA under de första 20 000 åren efter förslutning, SKBdoc 1577237 ver 1.0, Svensk Kärnbränslehantering AB. (In Swedish.)

Mårtensson P, Vogt C, 2019. Concrete caissons for 2BMA. Large scale test of design and material. SKB TR-18-12, Svensk Kärnbränslehantering AB.

Mårtensson P, Vogt C, 2020. Concrete caissons for 2BMA. Large scale test of design, material and construction method. SKB TR-20-09, Svensk Kärnbränslehantering AB.

Mårtensson P, Luterkort D, Nyblad B, Wimelius H, Pettersson A, Aghili B, Andolfsson T, 2022. SFR Förslutningsplan. SKBdoc 1358612 ver 4.0, Svensk Kärnbränslehantering AB. (In Swedish.)

NEA, 2005. NEA Sorption Project. Phase II: Interpretation and prediction of radionuclide sorption onto substrates relevant for radioactive waste disposal using thermodynamic sorption models. Paris: OECD/NEA.

NEA, 2012. NEA Sorption Project. Phase III: Thermodynamic sorption modelling in support of radioactive waste disposal safety cases. a guideline document. Paris: OECD/NEA.

Nilsson A-C, Högfeldt E, Muhammed M, Wingefors S, 1988. On the swelling of ion exchange resins used in the Swedish nuclear power plants. SKI TR 1988:1, Swedish Nuclear Power Inspectorate.

Nilsson A-C, Tullborg E-L, Smellie J, Gimeno M J, Gómez J B, Auqué L F, Sandström B, Pedersen K, 2011. SFR site investigation. Bedrock hydrogeochemistry. SKB R-11-06, Svensk Kärnbränslehantering AB.

Nishiizumi K, Gensho R, Honda M, 1981. Half-life of ^{59}Ni. Radiochimica Acta 29, 113–116.

Noshita N, Nishi T, Yoshida T, Fujihara H, Saito N, Tanaka S, 2001. Categorization of cement hydrates by radionuclide sorption mechanism. In Hart K P, Lumpkin G R (eds). Scientific basis for nuclear waste management XXIV: symposium held in Sydney, Australia, 27–31 August 2000. Warrendale, PA: Materials Research Society. (Materials Research Society Symposium Proceedings 663), 115–121.

Ochs M, Talerico C, 2004. SR-Can. Data and uncertainty assessment. Migration parameters for the bentonite buffer in the KBS-3 concept. SKB TR-04-18, Svensk Kärnbränslehantering AB.

Ochs M, Talerico C, Lothenbach B, Giffaut E, 2003. Systematic trends and empirical modelling of lead uptake by cements and cement minerals. In Finch R J, Bullen D B (eds). Scientific basis for nuclear waste management XXVI. Warrendale, PA: Materials Research Society. (Materials Research Society Symposium Proceedings 757), 693–698.

Ochs M, Vielle-Petit L, Wang L, Mallants D, Leterme B, 2011. Additional sorption parameters for the cementitious barriers of a near-surface repository. NIROND-TR 2010–06 E, ONDRAF/NIRAS, Belgium.

Ochs M, Mallants D, Wang L, 2016. Radionuclide and metal sorption on cement and concrete. Cham: Springer International Publishing.

Oda C, Ikeda T, Shibata M, 1999. Experimental studies for sorption behavior of tin on bentonite and rocks, and diffusion behavior of tin in compacted bentonite. JNC TN8400 99-073, Japan Nuclear Cycle Development Institute.

Odén M, Follin S, Öhman J, Vidstrand P, 2014. SR-PSU Bedrock hydrogeology. Groundwater flow modelling methodology, setup and results. SKB R-13-25, Svensk Kärnbränslehantering AB.

Olsson D, 2016. 1BMA – utredning kring gas och svällning. SKBdoc 1535025 ver 1.0, Svensk Kärnbränslehantering AB. (In Swedish.)

Olsson D, 2017. Silo – utredning kring gas och svällning. SKBdoc 1535026 ver 1.0, Svensk Kärnbränslehantering AB. (In Swedish.)

Pabalan R T, Turner D R, 1997. Uranium(6+) sorption on montmorillonite: experimental and surface complexation modeling study. Aquatic Geochemistry 2, 203–226.

Pettersson M, Elert M, 2001. Characterisation of bituminised waste in SFR 1. SKB R-01-26, Svensk Kärnbränslehantering AB.

Pointeau I, 2000. Étude mécanistique et modélisation de la rétention de radionucleides par les silicates de calcium hydrates (CSH) des ciments. PhD thesis. University of Reims, France. (In French.)

Pointeau I, Coreau N, Reiller P, 2002. Étude expérimentale et modélisation de la rétention de $^{14}CO_3$ par les matériaux constituant le béton dans le cadre d'un entreposage de barres graphite UNGG. Note Technique CEA. NT DPC/SCPA 02-046, CEA. (In French.)

Pointeau I, Reiller P, Macé N, Landesman C, Coreau N, 2006. Measurement and modelling of the surface potential evolution of hydrated cement pastes as a function of degradation. Journal of Colloid and Interface Science 300, 33–44.

Pointeau I, Coreau N, Reiller P E, 2008. Uptake of anionic radionuclides onto degraded cement pastes and competing effect of organic ligands. Radiochimica Acta 96, 367–374.

Polettini A, Pomi R, Sirini P, 2002. Fractional factorial design to investigate the influence of heavy metals and anions on acid neutralization behavior of cement-based products. Environmental Science & Technology 36, 1584–1591.

Pomiès M-P, Lequeux N, Boch P, 2001. Speciation of cadmium in cement: Part I. Cd^{2+} uptake by C-S-H. Cement and Concrete Research, 31, 563–569.

Pusch R, Cederström M, 1987. Material- och byggnadskontroll av bentonitbarriärer i SFR, Forsmark. SKB SFR 87-08, Svensk Kärnbränslehantering AB. (In Swedish.)

Rabung T, Pierret M C, Bauer A, Geckeis H, Bradbury M H, Baeyens B, 2005. Sorption of Eu(III)/Cm(III) on Ca-montmorillonite and Na-illite. Part 1: Batch sorption and time-resolved laser fluorescence spectroscopy experiments. Geochimica et Cosmochimica Acta 69, 5393–5402.

Riggare P, Johansson C, 2001. Project SAFE. Low and intermediate level waste in SFR-1. Reference Waste Inventory. SKB R-01-03, Svensk Kärnbränslehantering AB.

Rosdahl J, 2022. Cementhalt för kringgjutningsbruk i 1BRT. SKBdoc 1955764 ver 1.0, Svensk Kärnbränslehantering AB. (In Swedish.)

Rühm W, Schneck B, Knie K, Korschinek G, Zerle L, Nolte E, Weselka D, Vonach H, 1994. A new half-life determination of ^{59}Ni. Planetary and Space Science 42, 227–230.

Sato H, 1998. Data setting for effective diffusion coefficients (De) of nuclides in the buffer for reference case in performance assessments of the geological disposal of high-level radioactive waste (I). PNC Technical Report TN8410 98–097, Power Reactor and Nuclear Fuel Development Corporation, Japan.

Savage D, Stenhouse, M, 2002. SFR 1 vault database. SKI Report 02:53, Swedish Nuclear Power Inspectorate.

Schenk R, 1988. Untersuchungen über die Wasserstoffbildung durch Eisenkorrosion unter Endlagerbedingungen. Nagra NTB 86-24, Nagra, Switzerland.

Schrader H, 2004. Half-life measurements with ionization chambers – a study of systematic effects and results. Applied Radiation and Isotopes 60, 317–323.

Schötzig U, Schrader H, Debertin K, 1992. Precision measurements of radioactive decay data. In Qaim S M (ed). Nuclear data for science and technology. Berlin: Springer, 562–564.

SFS 1984:3. Lag om kärnteknisk verksamhet (Nuclear Activities Act). Stockholm: Ministry of the Environment. (In Swedish.)

SFS 1998:808. Miljöbalk (Environmental Code). Stockholm: Ministry of the Environment. (In Swedish.)

Shibutani T, Yui M, Yoshikawa H, 1994. Sorption mechanism of Pu, Am and Se on sodiumbentonite. In Barkatt A, Van Konynenburg R A (eds). Scientific basis for nuclear waste management XVII: symposium held in Boston, Massachusetts, USA, 29 November – 3 December. Pittsburgh, PA: Materials Research Society. (Materials Research Society Symposium Proceedings 333), 725–730.

Shugart H A, Browne E, Norman E B, 2018. Half-lives of ^{101}Rh^{g} and ^{108}Ag^{m}. Applied Radiation and Isotopes 136, 101–103.

Simpson J P, Weber J, 1988. Hydrogen evolution from corrosion in nuclear waste repositories. In Proceedings of UK Corrosion ’88 with EUROCORR, Brighton, 3–5 October 1988. Birmingham: Institution of Corrosion Science and Technology, 33–46.

Simpson J P, Schenk R, Knecht B, 1985. Corrosion rate of unalloyed steels and cast irons in reducing granitic groundwaters and chloride solutions. In Werme L O (ed). Scientific basis for nuclear waste management IX: symposium held in Stockholm, Sweden, 9–11 September 1985. Pittsburgh, PA: Materials Research Society. (Materials Research Society Symposium Proceedings 50), 429–436.

SKB, 2014. Svar på Föreläggande om redovisning rörande betydelsen av jordströmmar vid SFR. SKBdoc 1434594 ver 1.0, Svensk Kärnbränslehantering AB. (In Swedish.)

SKB R-01-14. SKB 2001. Project SAFE. Compilation of data for radionuclide transport analysis. Svensk Kärnbränslehantering AB.

SKB R-08-130. SKB 2008. Safety analysis SFR 1. Long-term safety. Svensk Kärnbränslehantering AB.

SKB R-15-15. SKB 2015. Low and intermediate level waste in SFR. Reference inventory for waste 2013. Svensk Kärnbränslehantering AB.

SKB R-18-07. SKB 2019. Låg- och medelaktivt avfall i SFR. Referensinvetarium för avfall 2016. Svensk Kärnbränslehantering AB. (In Swedish.)

SKB R-23-01. SKB 2023. Assessment activities and input data for the post-closure safety assessment in PSAR SFR. Svensk Kärnbränslehantering AB.

SKB TR-06-25. SKB 2006. Data report for the safety assessment SR-Can. Svensk Kärnbränslehantering AB.

SKB TR-10-47. SKB 2010. Buffer, backfill and closure process report for the safety assessment SR-Site. Svensk Kärnbränslehantering AB.

SKB TR-10-50. SKB 2010. Radionuclide transport report for the safety assessment SR-Site. Svensk Kärnbränslehantering AB.

SKB TR-10-52. SKB 2010. Data report for the safety assessment SR-Site. Svensk Kärnbränslehantering AB.

SKB TR-11-04. SKB 2013. Site description of the SFR area at Forsmark at completion of the site investigation phase. SDM-PSU Forsmark. Svensk Kärnbränslehantering AB.

SKB TR-13-05. SKB 2014. Climate and climate-related issues for the safety assessment SR-PSU. Svensk Kärnbränslehantering AB.

SKB TR-14-01. SKB 2015. Safety analysis for SFR. Long-term safety. Main report for the safety assessment SR-PSU. Revised edition. Svensk Kärnbränslehantering AB.

SKB TR-14-09. SKB 2015. Radionuclide transport report for the safety assessment SR-PSU. Revised edition. Svensk Kärnbränslehantering AB.

SKB TR-14-10. SKB 2014. Data report for the safety assessment SR-PSU. Svensk Kärnbränslehantering AB.

Smart N R, Hoch A R, 2010. A survey of steel and zircaloy corrosion data for use in the SMOGG gas generation model. Report to the NDA RWMD. SA/ENV-0841, Issue 3, Serco, UK.

Smart N R, Blackwood D J, Marsh G P, Naish C C, O'Brien T M, Rance A P, Thomas M I, 2004. The anaerobic corrosion of carbon and stainless steels in simulated cementitious repository environments: a summary review of Nirex research. AEAT/ERRA-0313, AEAT Technology, UK.

Snellman M, Valkiainen M (eds), 1985. Long-term properties of bitumenised waste products. Nordic Liaison Committee for Atomic Energy (NKA).

Snellman M, Valkiainen M, Airola C, Bonnevie-Svendsen M, Brodersen K, Forsström H, Wingefors S, 1986. Long-term behavior of bituminized waste, Waste Management '86 Proceedings of the Symposium on Waste Management at Tucson, Arizona, March 2–6, 1986. American Nuclear Society. Vol 3, 501–507.

SSM, 2019. Granskningsrapport – Utbyggnad och fortsatt drift av SFR. Report 2019:18, Swedish Radiation Safety Authority. (In Swedish.)

Suzuki S, Sato H, Ishidera T, Fujii N, 2004. Study on anisotropy of effective diffusion coefficient and activation energy for deuterated water in compacted sodium bentonite. Journal of Contaminant Hydrology 68, 23–37.

Svensk byggtjänst, 2017. Betonghandbok. Material Del I. Delmaterial samt färsk och hårdnande betong. 3rd ed. Solna: Svensk byggtjänst. (In Swedish.)

Swanton S W, Baston G M N, Smart N R, 2015. D 2.1 State of the art review of steel corrosion and C14 release, EURATOM Program FP7/2207-2013, European Commission.

Tachi Y, Shibutani T, Nishikawa Y, Shinozaki T, 1999. Sorption behavior of selenium on bentonite and granodiorite under reducing conditions. JNC TN8410 94-395, Japan Nuclear Cycle Development Institute.

Tasi A, 2018. Solubility, redox and sorption behavior of plutonium in the presence of α-D-isosaccharinic acid and cement under reducing, alkaline conditions. PhD thesis. Karlsruhe Institute of Technology, Germany.

Taylor H F W, 1990. Cement chemistry. London: Academic Press.

Tertre E, Berger G, Castet S, Loubet M, Giffaut E, 2005. Experimental sorption of Ni^{2+}, Cs^{+} and Ln^{3+} onto a montmorillonite up to 150 °C. Geochimica et Cosmochimica Acta 69, 4937–4948.

Thomson G, Miller A, Smith G, Jackson D, 2008. Radionuclide release calculations for SAR-08. SKB R-08-14, Svensk Kärnbränslehantering AB.

Tiller K G, Hodgson J F, 1960. The specific sorption of cobalt and zinc by layer silicates. Clays and Clay Minerals 9, 393–403.

Tits J, Wieland E, Dobler J-P, Kunz D, 2004. The uptake of strontium by calcium silicate hydrates under high pH conditions: an experimental approach to distinguish adsorption from co-precipitation processes. In Oversby V M, Werme L O (eds). Scientific basis for nuclear waste management XXVII: symposium held in Kalmar, Sweden, 15–19 June 2003. Warrendale, PA: Materials Research Society. (Materials Research Society Symposium Proceedings 807), 689–694.

Tits J, Fujita T, Harfouche M, Dähn R, Tsukamoto M, Wieland E, 2014. Radionuclide uptake by calcium silicate hydrates: Case studies with Th(IV) and U(VI): PSI Bericht 14-03, Paul Scherrer Institut, Switzerland.

Turner D R, Pabalan R T, Bertetti F P, 1998. Neptunium(V) sorption on montmorillonite: an experimental and surface complexation modeling study. Clays and Clay Minerals 46, 259–269.

Ulrich H J, Degueldre C, 1993. The sorption of ^{210}Pb, ^{210}Bi and ^{210}Po on montmorillonite: a study with emphasis on reversibility aspects and on the radioactive decay of adsorbed nuclides. Radiochimica Acta 62, 81–90.

US DOE, 2009. Review of mechanistic understanding and modeling and uncertainty analysis methods for predicting cementitious barrier performance. Cementitious Barriers Partnership. CBP-TR-2009-002, Rev.0, U.S. Department of Energy.

Valcke E, Mariën A, Smets S, Li X, Mokni N, Olivella S, Sillen X, 2010. Osmosis-induced swelling by Eurobitum bituminized radioactive waste in constant total stress conditions. Journal of Nuclear Materials 406, 304–316.

Valkiainen M, Vuorinen U, 1985. Properties of bituminzation product from Olkiluoto power plant. Report YJT-85-24, Nuclear Waste Commission of Finnish Power Companies.

Valkiainen M, Vuorinen U, 1989. Long-term properties of TVO's bituminized resins. Report YJT-89-06, Nuclear Waste Commission of Finnish Power Companies.

Van Loon L R, Glaus M A, 1998. Experimental and theoretical studies on alkaline degradation of cellulose and its impact on the sorption of radionuclides. Nagra NTB 97-04, Nagra, Switzerland.

Villar M V, Gutiérrez M G, Barrios B C, Álvarez C G, Martínez R I, Martín P L, Missana T, Mingarro M, Morejón J, Olmeda J, Idiart A, 2019. Experimental study of the transport properties of different concrete mixes. SKB P-19-10, Svensk Kärnbränslehantering AB.

Vidstrand P, Follin S, Selroos J-O, Näslund J-O, Rhén I, 2013. Modeling of groundwater flow at depth in crystalline rock beneath a moving ice-sheet margin, exemplified by the Fennoscandian Shield, Sweden. Hydrogeology Journal 21, 239–255.

Vidstrand P, Follin S, Selroos J-O, Näslund J-O, 2014. Groundwater flow modelling of periods with periglacial and glacial conditions for the safety assessment of the proposed high-level nuclear waste repository site at Forsmark, Sweden. Hydrogeology Journal 21, 1251–1267.

Volchek K, Miah M Y, Kuang W, DeMaleki Z, Tezel F H, 2011. Adsorption of cesium on cement mortar from aqueous solutions. Journal of Hazardous Materials 194, 331–337.

Vonach H, Hille M, Hille P, 1969. Bestimmung der Halbwertszeit von ^{108m}Ag über (n, 2n) – Querschnitte des Silbers. Zeitschrift für Physik 227, 381–390. (In German.)

von Schenck H, Bultmark F, 2014. Effekt av bitumensvällning i silo och BMA. SKB R-13-12, Svensk Kärnbränslehantering AB. (In Swedish.)

Wallner A, Knie K, Faestermann T, Korschinek G, Kutschera W, Rochow W, Rugel G, Vonach H, 2008. Study of the ^{60}Ni(n, 2n)^{59}Ni reaction from threshold to 20 MeV and the half-life of ^{59}Ni. In Proceedings of the International Conference on Nuclear Data for Science and Technology 2007. doi:10.1051/ndata:07628

Wang L, Martens E, Jacques D, de Cannière P, Berry J, Mallants D, 2009. Review of sorption values for the cementitious near field of a near-surface radioactive waste disposal facility. NIROND TR 2008-23E, ONDRAF/NIRAS, Belgium.

Weast R C, 1985. CRC Handbook of chemistry and physics: a ready-reference book of chemical and physical data. 65th ed. Cleveland, OH: CRC Press.

Widestrand H, Byegård J, Nilsson K, Höglund S, Gustafsson E, Kronberg M, 2010a. Long Term Sorption Diffusion Experiment (LTDE-SD). Performance of main in situ experiment and results from water phase measurements. SKB R-10-67, Svensk Kärnbränslehantering AB.

Widestrand H, Byegård J, Selnert E, Skålberg M, Höglund S, Gustafsson E, 2010b. Long Term Sorption Diffusion Experiment (LTDE-SD). Supporting laboratory program – Sorption diffusion experiments and rock material characterisation. With supplement of adsorption studies on intact rock samples from the Forsmark and Laxemar site investigations. SKB R-10-66, Svensk Kärnbränslehantering AB.

Wieland E, 2014. Sorption Data Base for the Cementitious Near Field of L/ILW and ILW Repositories for Provisional Safety Analyses for SGT-E2. NAGRA Technical Report 14-08, Nagra, Switzerland.

Wieland E, Van Loon L R, 2002. Cementitious near-field sorption data base for performance assessment of an ILW repository in Opalinus Clay. Nagra NTB 02-20, Nagra, Switzerland.

Wieland E, Tits J, Ulrich A, Bradbury M H, 2006. Experimental evidence for solubility limitation of the aqueous Ni(II) concentration and isotopic exchange of ^{63}Ni in cementitious systems. Radiochimica Acta 94, 29–36.

Wieland E, Tits J, Kunz D, Dähn R, 2008. Strontium uptake by cementitious materials. Environmental Science and Technology 42, 403–409. Available at: https://doi.org/10.1021/es071227y

Wimelius H, 2021. Kostnadsuppskattning och beräkning av mantimmar för betongförstärknings-arbeten 1BMA. NCC Infrastructure. SKBdoc 1953615 ver 1.0, Svensk Kärnbränslehantering AB. (In Swedish.)

Wold S, 2003. On diffusion of organic colloids in compacted bentonite. PhD thesis. Royal Institute of Technology, Stockholm, Sweden.

Yoon I-S, 2012. Chloride penetration through cracks in high performance concrete and surface treatment system for crack healing. Advances in Materials Science and Engineering 2012, 294571. doi:10.1155/2012/294571

Yu J-W, Neretnieks I, 1997. Diffusion and sorption properties of radionuclides in compacted bentonite. SKB TR 97-12, Svensk Kärnbränslehantering AB.

Yu R, Guo J, Cui A, Tang P, Li D, Liu D, 1995. Measurement of the half-life of ^{79}Se using a radiochemical method. Journal of Radioanalytical and Nuclear Chemistry 196, 165–170.

Yui M, Azuma J, Shibata M, 1999. JNC thermodynamic database for performance assessment of high-level radioactive waste disposal system. JNC Technical Report TN8400 99-070, Japan Nuclear Cycle Development Institute.

Zang S, Guo J, Cui A, Li D, Liu D, 1996. Measurement of the half life of ^{126}Sn using a radiochemical method. Journal of Radioanalytical and Nuclear Chemistry 212, 93–99.

Zhang J, Lounis Z, 2006. Sensitivity analysis of simplified diffusion-based corrosion initiation model of concrete structures exposed to chlorides. Cement and Concrete Research 36, 1312–1323.

Zhou W, Kozak M W, Xu S, Stenhouse M, 2009. Review and Assessment of SFR 1 long-term safety analyses. Report MSCI-2818-3 Rev 3.1.

Öhman J, Odén M, 2018. SR-PSU (PSAR) Bedrock hydrogeology. TD18 – Temperate climate conditions. SKB P-18-02, Svensk Kärnbränslehantering AB.

Öhman J, Follin S, Odén M, 2014. SR-PSU Hydrogeological modelling. TD11 – Temperate climate conditions. SKB P-14-04, Svensk Kärnbränslehantering AB.

Appendix A

Terms and abbreviations

Terms and abbreviations used in this report are explained in Table A-1.

Table A-1. Explanations of terms and abbreviations used in this report.

Term or abbreviation	Description
1–2BTF	Vaults for concrete tanks in SFR1.
1BLA	Vault for low-level waste in SFR1.
1BMA	Vault for intermediate-level waste in SFR1.
1BRT	Vault for reactor pressure vessels in SFR3.
1D	One-dimensional.
2–5BLA	Vaults for low-level waste in SFR3.
2BMA	Vault for intermediate-level waste in SFR3.
AD	Anno Domini.
AMBER	Assisted Model Building with Energy Refinement, a compartmental computer code.
Annual dose	Assessment endpoint calculated as the annual effective dose to an adult, where the annual effective dose is defined as the effective dose from external exposure in a year, plus the committed effective dose from intakes of radionuclides in that year.
Assessment team	The group of persons responsible for performing the safety assessment. The team judge the material delivered by the data supplier and recommend data for use in the assessment.
Barrier	In the safety assessment context, a barrier is a physical feature, engineered or natural, which in one or several ways contributes to the containment and retention or prevention of dispersion of radioactive substances, either directly or indirectly by protecting other barriers.
Barrier function	In the safety assessment context, a barrier function is a role by means of which the barrier contributes to post-closure safety.
Basin	In the terminology used in this safety assessment for the drainage area of a biosphere object (cf below) minus the drainage area of any upstream object. When the basin is below sea level, the basin is identical to the biosphere object.
Best estimate	A single value for a parameter, describing a property or a process, used in deterministic calculations. Best estimates are typically derived from site and/or literature data and often correspond to mean values of the underpinning datasets.
Biosphere object	A part of the landscape that will potentially receive radionuclides released from the repository, directly or indirectly via other biosphere objects.
Bulk density	The bulk density of a porous medium is defined as the mass of the solid particles that make up the medium divided by the total volume they occupy. The total volume includes particle volume, inter-particle void volume and internal pore volume.
Climate domain	A climatically determined environment with a specific set of characteristic processes of importance for post-closure safety.
Climate variant	A climate development used in describing the range of possible future climate developments that may influence post-closure safety.
Clab	Central interim storage facility for spent nuclear fuel in Simpevarp, Sweden.
COMSOL Multiphysics	Commercial software for finite element analysis, solver and multi-physics simulation.
Conceptual model	A qualitative description of a physical system, including important processes and components and interactions between these components.
Crushed rock	Mechanically crushed rock material with varying grain size distribution and hydraulic properties. The selected grain size distribution is dependent on the required properties. See also macadam.
CSH	Calcium silicate hydrates.
Customer	The terms customer and supplier come from standard quality assurance terminology. The customer is a person or group that represent the assessment team. The customer defines the requested data delivery.
DarcyTools	A computer code developed by SKB for simulation of flow and transport in porous and/or fractured media.
Data uncertainty	Uncertainties concerning all quantitative input data, that is parameter values, used in the assessment.
DFN	Discrete fracture network.
EDTA	Ethylenediaminetetraacetic acid, a complexing agent.

Table A-1. Continued.

Term or abbreviation	Description
Exposure	The act or condition of being subject to irradiation (not to be used as a synonym for dose, which is a measure of the effects of exposure).
FARF31	Semi-analytical computer code for modelling of radionuclide transport in the geosphere.
FEP	Features, events and processes.
GEKO/QI	Product name of bentonite used in the silo.
Geosphere	The bedrock, including groundwater, surrounding the repository, bounded above by the surface system.
GIA	Glacial isostatic adjustment.
HCP	Hydrated cement paste.
IAEA	International Atomic Energy Agency.
ICRP	International Commission on Radiological Protection.
Initial state	The expected conditions (state) of the repository and its environs at closure of the repository.
Intermediate-level waste	Radioactive waste that requires final disposal in a geological repository and shielding during handling. Cooling of the waste is not required.
ISA	Isosaccharinate, a complexing agent that is a cellulose degradation product.
ISO	International Organization for Standardization.
KBS-3	Method developed by SKB for final disposal of spent nuclear fuel.
L/ILW	Low- and intermediate-level waste.
Long-lived radionuclide	In the safety assessment context, radionuclides with a half-life exceeding 31 years.
Low-level waste	Radioactive waste that requires final disposal in a geological repository. Shielding during handling and cooling are not required.
Macadam	Crushed rock sieved in fractions 2–65 mm. Macadam has no or very little fine material (grain size < 2 mm). The fraction is given as intervals, for example “Macadam 16-32” is crushed rock comprising the fraction 16–32 mm.
Modelling uncertainty	Uncertainties arising from a necessarily imperfect understanding of the nature of processes involved in repository evolution which leads to imperfect conceptual models. The mathematical representation of conceptual models and imprecision in the numerical solution of mathematical models are other sources of uncertainty which fall into this category.
MX-80	A product name of bentonite clay.
NEA	OECD Nuclear Energy Agency.
Near-field	Typically used for the model domain representing the repository, which may contain part of the nearby bedrock to obtain boundary conditions.
NTA	Nitrilotriacetic acid, a complexing agent.
OPC	Ordinary Portland Cement.
Packaging	The outer container, such as a mould, drum or ISO-container, protecting the waste form (synonymous with Waste packaging).
PDF	Probability density function.
PHAST	Computer code used, for example, for concrete degradation calculations and geochemical evolution in the geosphere.
PHREEQC	Computer code used for geochemical modelling.
PSAR	Preliminary Safety Analysis Report.
PSAR SFR	Preliminary Safety Analysis Report for the extended SFR.
PSU	Programme SFR extension.
QA	Quality assurance.
Relative sea level	The vertical position of the sea relative to land, as measured in the reference height system RH 2000. The relative sea level is determined by the net effect of eustasy and isostasy.
Repository	The disposed waste packages, the engineered barriers and other repository structures.
Repository system	The repository, the bedrock and the biosphere surrounding the repository. Synonymous with repository and its environs.
Risk	Refers in the post-closure safety assessment to the radiological risk, defined as the product of the probability of receiving a radiation dose and the harmful effects of that radiation dose.
SAFE	Post-closure safety assessment for SFR1 reported to the regulatory authorities in 2001.
Safety analysis	In the context of the present safety assessment, the distinction is generally not viewed as important and therefore safety analysis and safety assessment are used interchangeably. However, if the distinction is important, safety analysis should be used as a documented process for the study of safety and safety assessment should be used as a documented process for the evaluation of safety.

Table A-1. Continued.

Term or abbreviation	Description
Safety assessment	The safety assessment is the systematic process periodically carried out throughout the lifetime of the repository to ensure that all the relevant safety requirements are met and entails evaluating the performance of the repository system and quantifying its potential radiological impact on human health and the environment. The safety assessment corresponds to the term safety analysis in the Swedish Radiation Safety Authority's regulations.
Safety function	A role through which a repository component contributes to post-closure safety
Safety function indicator	A measurable or calculable property of a repository component that indicates the extent to which a safety function is fulfilled.
SAR	Safety Analysis Report.
SAR-08	Post-closure safety assessment for SFR1 reported to the regulatory authorities in 2008.
Scenario	A description of a potential evolution of the repository and its environs, given an initial state and specified external conditions and their development and how the protective capability of the repository is affected.
SFL	Final repository for long-lived radioactive waste.
SFR	Final repository for short-lived radioactive waste at Forsmark.
SFR1	The existing part of SFR.
SFR3	The extension part of SFR.
Shoreline displacement	The movement of the shoreline, that is the variation in time of the spatial location of the shoreline.
Shoreline regression	Migration of the coastline away from the land as the relative sea level decreases, which in turn increases the extent of the land area.
Silo	Cylindrical vault for intermediate-level waste (part of SFR1).
SKB	Swedish Nuclear Fuel and Waste Management Company.
SKBdoc	Internal document management system at SKB.
SKI	Swedish Nuclear Power Inspectorate. SKI and SSI were merged into SSM in July 2008.
Sorption coefficient	Element-specific sorption coefficient, defined as the ratio between the elemental concentrations in the solid and liquid phases.
SR-Can	Preliminary post-closure safety assessment for the planned spent nuclear fuel repository, published in 2006.
SR-PSU	Post-closure safety assessment that was a reference to the F-PSAR (First Preliminary Safety Analysis Report) for the extended SFR, reported to the regulatory authority in 2014.
SRF	Sorption Reduction Factor (due to complexing agents).
SR-Site	Post-closure safety assessment for a spent nuclear fuel repository in Forsmark, reported to the regulatory authority in 2011.
SSI	Swedish Radiation Protection Authority. SSI and SKI were merged into SSM in July 2008.
SSM	Swedish Radiation Safety Authority.
Supplier	The terms customer and supplier come from standard quality assurance terminology. The supplier is an expert working at, or on behalf of, SKB. The supplier qualifies the data according to the methodology described in Chapter 2.
Surface system	In the safety assessment context, refers to the part of the repository system that is above the geosphere, with all its abiotic and biotic processes and features, as well as humans and human behaviour. Synonymous with Biosphere system.
System component	A physical component of the repository system; a sub-system.
WAC	Waste acceptance criteria.
Waste domain	Part of waste vaults where waste is placed (inside the engineered barriers).
Waste form	Waste in its physical and chemical form after treatment and/or conditioning.
Waste package	The waste (form) and its packaging.
Waste packaging	The outer container, such as a mould, drum or ISO-container, protecting the waste form (synonymous with Packaging).
Waste stream	The pathway of a specific waste, from its origin through to its disposal in a defined waste type.
Waste type	SKB's systematic classification of wastes according to a developed code system.
Waste type description	Safety report for a waste type. The waste type description contains, among other things, information about the waste, waste packaging, treatment of the waste and where the waste is to be disposed.
Waste vault	Part of repository where waste is disposed.

Arkitektkopia AB, Bromma, 2023

SKB is responsible for managing spent nuclear fuel and radioactive waste produced by the Swedish nuclear power plants such that man and the environment are protected in the near and distant future.

skb.se